

PHYSICAL MODELLING OF INNOVATIVE SINGLE ROW ENLARGED PILE HEAD BREAKWATER

Thesis

**Submitted in partial fulfilment of the requirements for the degree of
DOCTOR OF PHILOSOPHY**

by

PRAVEEN SUVARNA S



**DEPARTMENT OF WATER RESOURCES AND OCEAN ENGINEERING
NATIONAL INSTITUTE OF TECHNOLOGY KARNATAKA,
SURATHKAL, MANGALURU - 575 025**

September 2022

PHYSICAL MODELLING OF INNOVATIVE SINGLE ROW ENLARGED PILE HEAD BREAKWATER

Thesis

**Submitted in partial fulfilment of the requirements for the degree of
DOCTOR OF PHILOSOPHY**

by

PRAVEEN SUVARNA S

(Reg. No.: 177020AM502)

Under the Guidance of

Dr. PRUTHVIRAJ U.

Prof. KIRAN G. SHIRLAL



**DEPARTMENT OF WATER RESOURCES AND OCEAN ENGINEERING
NATIONAL INSTITUTE OF TECHNOLOGY KARNATAKA,
SURATHKAL, MANGALURU - 575 025**

September 2022

DECLARATION

By the Ph.D. Research Scholar

I hereby *declare* that the Research Thesis entitled “**Physical Modelling of Innovative Single Row Enlarged Pile Head Breakwater**” which is being submitted to the **National Institute of Technology Karnataka, Surathkal** in partial fulfilment of the requirements for the award of the Degree of **Doctor of Philosophy** in **Department of Water Resources and Ocean Engineering** is a *bonafide report of the research work* carried out by me. The material contained in this Research Thesis has not been submitted to any University or Institution for the award of any degree.



177020AM502, PRAVEEN SUVARNA S.

(Register Number, Name & Signature of the Research Scholar)

Department of Water Resources and Ocean Engineering

Place: NITK-Surathkal

Date: 16-08-2022

CERTIFICATE

This is to *certify* that the Research Thesis entitled “**Physical Modelling of Innovative Single Row Enlarged Pile Head Breakwater**” submitted by **Praveen Suvarna S** (Register Number: 177020AM502) as the record of the research work carried out by him, is *accepted as the Research Thesis submission* in partial fulfilment of the requirements for the award of degree of **Doctor of Philosophy**.

Pruthviraj U. 16/09/2022
Dr. Pruthviraj U.
(Research Guide)

16/09/2022

Prof. Kiran G. Shirlal
(Research Guide)



16/09/2022
(Chairman – DRPC)

Chairman (DRPC)
Dept. of Water Resources & Ocean Engineering

**DEPARTMENT OF WATER RESOURCES AND OCEAN ENGINEERING
NATIONAL INSTITUTE OF TECHNOLOGY KARNATAKA,
SURATHKAL, MANGALURU - 575 025**

ACKNOWLEDGMENT

With a deep sense of gratitude, I express my heartfelt thanks to Dr. Pruthviraj U. and Prof. Kiran G. Shirlal, Research Guides, Department of Water Resources and Ocean Engineering, NITK, Surathkal. Their logical and tactical suggestions have been very valuable and encouraging during the development of this research. I acknowledge, the time spent in the discussions with my supervisors regarding the completion of this research work. Their moral support and critical guidance have been priceless and have given me an invaluable opportunity to publish my research work in international journals and conferences, which is a matter of great pride and satisfaction to me.

I express my heartfelt gratitude to my Research Progress Assessment Committee (RPAC) members, Prof. K. S. Babu Narayan and Dr. Vadivuchezhian K., for their valuable suggestions for the betterment of this research work. I am thankful to Prof. B. M. Dodamani, Head of the Department and Prof. Amai Mahesha and Prof. Amba Shetty, former Head of the Department, for granting me the permission to utilise the laboratory and departmental facilities for the completion of this work. I thank all the faculty members of the Department of Water Resources and Ocean Engineering for their support.

I would like to express my gratitude to Prof. Udaykumar R. Yaragatti, Director (In-charge) and Prof. Karanam Uma Maheshwar Rao, former Director, NITK Surathkal for granting me the permission to use the institutional infrastructure facilities.

I express my heartfelt gratitude to the authors of all those research publications which have been referred to in this thesis work. I also recognise the efforts and time dedicated by all the reviewers for their insightful suggestions on shaping current desertion work.

I am greatly indebted to Prof. Subba Rao and Dr. Manu for their encouragement and granting permission to use the data acquisition system during laboratory work. I express my regards to Prof. K. V. Gangadharan for their kind support during the progress of the research work. I express my gratitude to Prof. Hans Bihs and Dr. Arun Kamath from the

Department of Civil and Environmental Engineering, Norwegian University of Science and Technology (NTNU), Norway for the help rendered in numerical modelling. I also gratefully acknowledge the computational resources provided by the Centre for System Design (CSD), NITK Surathkal and NTNU, Norway, for numerical modelling work.

Nothing great was ever accomplished alone. I would like to thank my co-research scholar Arunakumar H. S. for all the discussions, support, and encouragement. I gratefully acknowledge the support and all help rendered by my other research scholars: Yathish H., Mallikarjun S. B., Sandesh, Vishwanath Mane, Tom Elias, and Saketh Shetty; Postgraduate students: Shery Mathew, Shashank K., Zaid M. Sayyad, Vooha Challagulla, Preetham G., Patchava Mahendra Naidu, Ramayanam Balaji and Jishnulal K. I also convey my regards to Mr. Manjunath T.L. and Mr. Lingappa N.C. for their moral support and encouragement.

I sincerely acknowledge the help and support rendered by the department staff Mr. Seetharam, Mr. Anil Kumar, Mr. Ananda Devadiga, Mr. Gopalakrishna and all the staff of the Department and CSD. I also thank Mr. Balakrishna for his encouragement in solving the computer snags during my research.

I also sincerely thank the present and former Principal, Executive Director, HOD and all staff members of the Civil Engineering Department of P. A. College of Engineering, for their cooperation.

Finally, I wish to express gratitude, love and affection to my beloved family member, Father Sri. Shanthappa M., Mother Smt. Geetha S., my Wife, Dr. Shilpashri, my Daughter Namya, Brother Prashanth and his family, Sister Prathibha and her family and all my friends and relatives for their encouragement, moral support and all their big and small sacrifices during the course of this research. I also bow down to the Almighty in making this thesis a reality.

ABSTRACT

Breakwaters are constructed to dissipate the wave energy and safeguard the coast, coastline infrastructures and communities from the destructive wave forces. Conventional type breakwaters are massive structures and suitable for the coastal sites where complete protection from the waves is essential. An environmentally friendly structure constructed for the protection of the coast without spoiling the aesthetics and advantages of a natural beach is always a better option. One such structure is the pile breakwater. Conventional pile breakwater is a non-gravity type breakwater consisting of closely placed single or multiple rows of circular or rectangular piles. The pile breakwater is generally constructed as an emergent structure. In pile breakwaters, the wave energy dissipation occurs due to wave structure interaction associated with turbulence, eddy formation and vortex shedding. For small recreational harbours or fisheries harbours and at locations where large littoral drift or onshore-offshore sediment movement exist, unconventional types of breakwaters like floating breakwater or piled breakwaters are highly preferred. Pile breakwaters are constructed and have been working successfully in many places like Auckland harbour in New Zealand, suspended breakwater in North-Western coast of Egypt, steel pipe breakwaters constructed in Asaka port at Japan, concrete pile breakwater at Pass Christian, Mississippi, USA and pile row breakwaters at Langkawi, Malaysia. An economical, eco-friendly and efficient breakwater system is vital for coastal protection and harbour tranquillity. In this regard, various researchers have been working to develop appropriate solutions to encounter site-specific challenges. With this viewpoint, the concept of enlarged pile head breakwater is developed.

The wave energy is more concentrated at the surface and reduces gradually depthwise. On this basis, providing a larger area of the structure at the surface level may result in increased wave structure interaction inducing larger wave attenuation. Hence, the concept of structure enlargement at the surface and perforation is comprehended for the advancement of enlarged pile head breakwater. The enlarged portion is termed as pile head and the portion below is denoted as a trunk.

In the present study, wave transmission, reflection and energy dissipation of the single row enlarged pile head breakwater are examined experimentally in a 1:30 scaled model. The experimental models are subjected to monochromatic wave heights ranging from 0.06 m to 0.16 m and wave period 1.4 s to 2 s, which in actual conditions corresponds to wave heights and wave periods of 1.8 m to 4.8 m and 7 s to 11 s, respectively.

Initially, the experiments are conducted on non-perforated enlarged pile head breakwater to optimize the relative pile head spacing and depth of water. The effect of relative pile head diameter and height on wave transmission (K_t), reflection (K_r) and dissipation (K_d) characteristics are studied comprehensively. With the decrease in relative spacing between the piles from 0.9 to 0.2, a maximum of 19.75% reduction in K_t is obtained for the case of $D/H_{\max} = 0.6$ with $Y/H_{\max} = 1.0$ at 0.3 m water depth. It is observed that with an increase in the depth of water, K_t increases and K_r and K_d decreases. For 25% to 33.33% increase in water depth, K_t increases by an average of 4% to 6%, K_r decreases by 17% to 19% and K_d decreases by 7% to 8%. An increase in D/H_{\max} from 0.4 to 0.6 and Y/H_{\max} from 0.5 to 1.0 decreases the K_t and increases K_r and K_d . The enlarged pile head breakwater structure with the structural configuration of $b/D = 0.2$, $D/H_{\max} = 0.6$ and $Y/H_{\max} = 1.0$, has least value of K_t (0.62). Using the present experimental data, a hybrid theoretical solution is developed and validated with the available theoretical solutions. The proposed hybrid equation predicts encouragingly better transmission, reflection and dissipation coefficient than the existing solutions. Moreover, the results predicted by the proposed hybrid equation are in good agreement with the conventional pile breakwater model.

In the second stage, on fixing the relative pile spacing and depth of water, investigations are continued on perforated enlarged pile head breakwater. The study focused on improving the hydraulic efficiency of enlarged pile head breakwater by incorporating perforations on the pile head. Effect of percentage distribution of perforations (pa), size of perforations (S) and percentage of perforations (P) on K_t , K_r , and K_d are investigated. Results indicate that the pore size highly dominates the wave attenuation than considering the increasing percentage of perforations with the small size of the pore. Perforations effectively reduce the K_t by about 10% to 18%

compared to that of non-perforated pile head breakwater. Hydraulic efficiency of enlarged pile head breakwater is optimum when $D/H_{\max} = 0.6$, $Y/H_{\max} = 1.0$, $b/D = 0.2$, $S = 0.25D$, $p_a = 75\%$ and $P = 22.5\%$ at 0.3 m water depth. For the quick estimate of hydraulic coefficients, a hybrid theoretical solution developed for non-perforated pile head breakwater is modified to suite for the perforated pile head breakwater. The proposed hybrid equation for the perforated pile breakwater predicts more reliable K_t , K_r and K_d values. The performance of the proposed breakwater is also compared with similar types of breakwaters. A smallest K_t of about 0.58 is obtained for the enlarged perforated pile breakwater structure with the structural configuration of $b/D = 0.2$, $D/H_{\max} = 0.6$, $Y/H_{\max} = 1.0$, $S = 0.25D$, $p_a = 75\%$ and $P = 22.5$ along with $K_r = 0.36$ and $K_d = 0.73$.

The best performing configurations for non-perforated ($D/H_{\max} = 0.6$, $Y/H_{\max} = 1.0$ and $b/D = 0.2$) and perforated ($D/H_{\max} = 0.6$, $Y/H_{\max} = 1.0$, $b/D=0.2$, $S = 0.25D$, $p_a = 75\%$ and $P = 22.5$) structures as obtained from the present experimental work are numerically modelled using open source CFD software REEF3D. The results of K_t , K_r and K_d obtained from the REEF3D are in line with the experimental and theoretical data. REEF3D underpredicts K_t by about 1% to 3%, overpredicts K_r by 4% to 11% and variation of K_d is about 1% with reference to the experimental results. From the analysis, it is concluded that the REEF3D numerical model can be used for estimating the hydraulic performance of the enlarged pile head breakwater.

Keywords: Coastline protection, pile breakwater, non-perforated enlarged pile head, perforated enlarged pile head, numerical modelling, REEF3D, wave transmission, wave reflection, energy dissipation.

CONTENTS

ABSTRACT	i
CONTENTS	iv
LIST OF FIGURES	ix
LIST OF TABLES	xv
NOMENCLATURE	xvii
CHAPTER 1	
INTRODUCTION	1
1.1 GENERAL	1
1.2 EROSION ALONG DAKSHINA KANNADA COAST	2
1.3 PILE STRUCTURE TO COMBAT EROSION	2
1.4 WAVE ATTENUATION MECHANISM OF PILE STRUCTURE	7
1.5 ORGANIZATION OF THE THESIS	10
CHAPTER 2	
BACKGROUND AND LITERATURE REVIEW	13
2.1 GENERAL	13
2.2 EXPERIMENTAL STUDIES ON PILE BREAKWATER	15
2.3 HYBRID THEORETICAL MODEL	34
2.3.1 Theoretical background	35
2.4 NUMERICAL MODELLING	38
2.5 SUMMARY OF LITERATURE REVIEW	42
2.6 KNOWLEDGE GAP	42
2.7 PROBLEM FORMULATION	43
2.8 OBJECTIVES	43
CHAPTER 3	
EXPERIMENTAL INVESTIGATIONS	45
3.1 GENERAL	45
3.2 DIMENSIONAL ANALYSIS	45
3.2.1 Predominant variables and their dimensions	46
3.2.2 Details of dimensional analysis	47
3.3 SIMILITUDE CRITERIA AND MODEL SCALE SELECTION	49

3.4	LABORATORY AND SCALE EFFECTS IN SHORT WAVE MODEL	51
3.4.1	Laboratory effects	51
3.4.2	Scale effects	51
3.5	DESIGN CONDITIONS	52
3.6	EXPERIMENTAL SETUP	53
3.6.1	Details of wave flume	53
3.6.2	Data acquisition system	54
3.6.3	Calibration of test facilities	54
3.6.3.1	Wave flume	54
3.6.3.2	Wave probes	55
3.7	ENLARGED PILE HEAD BREAKWATER MODEL	56
3.7.1	Pile trunk	56
3.7.2	Non-perforated pile head	58
3.7.3	Perforated pile head	58
3.8	RANGE OF EXPERIMENTAL VARIABLES	61
3.9	MODIFICATION OF HYBRID THEORETICAL EQUATIONS	62
3.9.1	For non-perforated enlarged pile head breakwater	62
3.9.2	For perforated enlarged pile head breakwater	63
3.9.3	Quantitative assessment of hybrid theoretical equations	63
3.10	REEF3D NUMERICAL MODELLING	64
3.10.1	Free surface	65
3.10.2	Reconstruction of free surface	66
3.10.3	Validation of wave generation and testing	66
3.10.4	Grid and time step convergence tests	66
3.10.5	Non-uniform grid	72
3.10.6	Numerical evaluation of enlarged pile head breakwater	72
3.11	PHYSICS OF THE EXPERIMENT	74
3.12	WAVE-STRUCTURE INTERACTION IN NUMERICAL MODEL	83
3.13	METHODOLOGY	88
3.14	TEST CONDITIONS	90
3.15	TEST PROCEDURE	91
3.16	SOURCES OF ERRORS AND PRECAUTIONS EXERCISED	92

3.17	UNCERTAINTY ANALYSIS	93
3.18	PHOTOS OF EXPERIMENTAL SET-UP AND MODELS	93
CHAPTER 4		
INVESTIGATION ON HYDRAULIC PERFORMANCE OF NON-PERFORATED ENLARGED PILE HEAD BREAKWATER		97
4.1	EFFECT OF INCIDENT WAVE STEEPNESS	97
4.2	INFLUENCE OF RELATIVE PILE SPACING	97
4.2.1	On wave transmission	97
4.2.2	On wave reflection	100
4.2.3	On wave energy dissipation	103
4.3	IMPACT OF VARYING PILE HEAD CHARACTERISTICS	106
4.3.1	Influence of pile head diameter on	107
4.3.1.1	Wave transmission	107
4.3.1.2	Wave reflection	109
4.3.1.3	Wave Energy dissipation	110
4.3.2	Influence of pile head height on	112
4.3.2.1	Wave transmission	112
4.3.2.2	Wave reflection	113
4.3.2.3	Wave energy dissipation	114
4.4	EFFECT OF VARYING RELATIVE SUBMERGENCE OF PILE HEAD AND DEPTH OF WATER	115
4.4.1	On wave transmission	115
4.4.2	On wave reflection	116
4.4.3	On wave energy dissipation	116
4.5	VALIDATION OF MODIFIED HYBRID THEORETICAL EQUATION FOR NON-PERFORATED PILE BREAKWATERS	119
4.5.1	Enlarged pile head breakwater	119
4.5.2	Conventional circular pile breakwater	122
4.6	VALIDATION OF NON-PERFORATED ENLARGED PILE HEAD BREAKWATER USING REEF3D	124
4.7	COMPARISON OF NON-PERFORATED ENLARGED PILE BREAKWATER PERFORMANCE WITH OTHER RESEARCH WORKS	126

4.8	CONCLUSIONS ON NON-PERFORATED PILE HEAD BREAKWATER	128
CHAPTER 5		
INVESTIGATION ON PERFORATED ENLARGED PILE HEAD BREAKWATER		131
5.1	RESULTS AND DISCUSSION ON PERFORATED ENLARGED PILE HEAD BREAKWATER	131
5.2	EFFECT OF WAVE STEEPNESS	131
5.3	INFLUENCE OF PERFORATIONS ON THE PERFORMANCE CHARACTERISTICS	132
5.3.1	Effect of distribution of perforation around the pile head when diameter of pile head is 0.064 m on	132
5.3.1.1	Wave transmission	132
5.3.1.2	Wave reflection	134
5.3.1.3	Wave Energy dissipation	136
5.3.2	Effect of relative pore size when diameter of pile head is 0.064 m on	138
5.3.2.1	Wave transmission	138
5.3.2.2	Wave reflection	140
5.3.2.3	Wave energy dissipation	141
5.3.3	Effect of distribution of perforation around the pile head when diameter of pile head is 0.096 m on	142
5.3.3.1	Wave transmission	142
5.3.3.2	Wave reflection	143
5.3.3.3	Wave energy dissipation	143
5.3.4	Effect of relative pore size when diameter of pile head is 0.096 m on	144
5.3.4.1	Wave transmission	144
5.3.4.2	Wave reflection	145
5.3.4.3	Wave energy dissipation	146
5.4	COMPARISON OF PERFORATED AND NON-PERFORATED ENLARGED PILE HEAD BREAKWATER	146
5.4.1	Wave transmission	146
5.4.2	Wave reflection	147

5.4.3	Wave energy dissipation	148
5.5	PERFORMANCE EVALUATION OF THE BEST MODEL UNDER TIDE	148
5.6	VALIDATION OF MODIFIED HYBRID THEORETICAL EQUATION FOR PERFORATED PILE BREAKWATERS	151
5.6.1	Enlarged pile head breakwater	151
5.6.2	Conventional circular pile breakwater	152
5.7	VALIDATION OF PERFORATED ENLARGED PILE HEAD BREAKWATER USING REEF3D	154
5.7.1	Comparison of numerical results with the experimental and theoretical data	154
5.7.2	Effect of perforations	155
5.8	COMPARISON OF HYDRAULIC PERFORMANCE OF PERFORATED ENLARGED PILE BREAKWATER WITH OTHER RESEARCH WORKS	157
5.9	CONCLUSIONS ON PERFORATED ENLARGED PILE HEAD BREAKWATER	159
CHAPTER 6		
SUMMARY AND CONCLUSIONS		163
6.1	BACKGROUND	163
6.2	GENERAL CONCLUSIONS	164
6.3	CONCLUSIONS ON NON-PERFORATED ENLARGED PILE HEAD BREAKWATER	165
6.4	CONCLUSIONS ON PERFORATED ENLARGED PILE HEAD BREAKWATER	166
6.5	SUMMARY OF CONCLUSIONS	167
6.6	SCOPE FOR FURTHER RESEARCH	168
APPENDIX I: REYNOLDS NUMBER		169
APPENDIX II: UNCERTAINTY ANALYSIS		171
REFERENCES		177
PUBLICATIONS		190
RESUME		191

LIST OF FIGURES

Fig. No.	Title	Page No
Fig. 1.1	Dakshina Kannada coast	2
Fig. 1.2	Row of pile breakwater at Langkawi, Malaysia (Reedijk and Muttray 2009)	6
Fig. 1.3	Row of pile breakwater at Pasir Panjang, Singapore (Liu et al. 2011)	6
Fig. 1.4	Flow behind a cylinder for various Re (Davidson 2015)	9
Fig. 1.5	Formation of vortex when wave crest passing over the structure (Liu et al. 2011)	9
Fig. 1.6	Typical cascade of energy from larger eddies to smaller eddies (Davidson 2015)	10
Fig. 2.1	description for porous structure (Kondo and Toma 1972)	16
Fig. 2.2	Concept of pile breakwater defined by Hutchinson and Raudkivi (1984)	17
Fig. 2.3	Concept double screen breakwater Gardner et al. (1986)	18
Fig. 2.4	Typical arrangement of suspended pipe breakwater (Mani and Jayakumar 1995)	20
Fig. 2.5	Details of perforated pile breakwater (Rao et al. 1999)	21
Fig. 2.6	Details of perforated pipe breakwater (Rao and Rao 2001)	22
Fig. 2.7	Schematic view of T-type breakwater (Neelamani and Rajendran 2002)	23
Fig. 2.8	Schematic view of U-type breakwater (Günaydin and Kabdaşlı 2004)	23
Fig. 2.9	Lee side view of pile supported vertical wall breakwater (Suh et al. 2006)	25
Fig. 2.10	Wave interaction with closely spaced rectangular cylinders (Huang 2007)	25
Fig. 2.11	Typical arrangement of wave screen breakwater (Krishnakumar et al. 2010)	26
Fig. 2.12	Horizontal slotted pile-supported breakwater Rageh and Koraim (2010)	27
Fig. 2.13	Model view of double porous curtain wall breakwater (Elsharnouby et al. 2012)	29
Fig. 2.14	Typical arrangement of C shaped screen type breakwater (Koraim et al. 2014)	30
Fig. 2.15	Details of arc and horizontal plate breakwater (Wang et al. 2016)	31

Fig. 2.16 View of pile rock breakwater (Le Xuan et al. 2020)	32
Fig. 2.17 Pile breakwater model (Yagci et al. 2006)	33
Fig. 2.18 Schematic sketch of the pile-supported breakwater (Ramnarayan et al. 2020)	34
Fig. 2.19 Typical arrangement of enlarged pile head breakwater	35
Fig. 3.1 Schematic diagram of the experimental setup	54
Fig. 3.2 View of enlarged pile head structure model and dimensions of the enlarged head	57
Fig. 3.3 A typical arrangement of the structure at different water depths	57
Fig. 3.4 Arrangement of perforations on the pile head of $D = 0.064$ m	58
Fig. 3.5 Arrangement of perforations on pile head of $D = 0.096$ m	59
Fig. 3.6 Typical arrangement of distribution of perforations (pa) around the pile head	60
Fig. 3.7 Wave profile for grid size $dx = 0.08$ m with CFL = 0.1	68
Fig. 3.8 Wave profile for grid size $dx = 0.04$ m with CFL = 0.1	68
Fig. 3.9 Wave profile for grid size $dx = 0.02$ m with CFL = 0.1	69
Fig. 3.10 Wave profile for grid size $dx = 0.01$ m with CFL = 0.1	69
Fig. 3.11 Wave profile for CFL = 0.4 and grid size $dx = 0.02$ m	70
Fig. 3.12 Wave profile for CFL = 0.2 and grid size $dx = 0.02$ m	70
Fig. 3.13 Wave profile for CFL = 0.1 and grid size $dx = 0.02$ m	71
Fig. 3.14 Wave profile for CFL = 0.05 and grid size $dx = 0.02$ m	71
Fig. 3.15 Typical representation of non-uniform grid in numerical wave tank	72
Fig. 3.16 Detailed view of numerical wave tank	73
Fig. 3.17 REEF3D non-perforated and perforated enlarged pile head breakwater model	73
Fig. 3.18 Interaction of wave with non-perforated pile head breakwater	75
Fig. 3.19 Snapshot of wave interaction with the non-perforated pile head breakwater of $D/H_{\max} = 0.6$, $Y/H_{\max} = 1.0$ and at 0.3 m depth of water	76
Fig. 3.20 Interaction of wave with perforated pile head breakwater with $S = 0.25D$ and $P = 22.5$	77
Fig. 3.21 Wave approaching perforated pile head for $D = 0.064$ m, $Y = 0.16$ m and $S = 0.15D$	78

Fig. 3.22 Wave approaching perforated pile head for $D = 0.096$ m, $Y = 0.16$ m and $S = 0.25D$	78
Fig. 3.23 Snapshot of wave interaction with the perforated pile head breakwater of $D/H_{\max} = 0.6$, $Y/H_{\max} = 1.0$, $b/D = 0.2$, $S = 0.25D$, $p_a = 75\%$ and $P = 22.5$ at 0.3 m depth of water	81
Fig. 3.24 Reflection of the wave from perforated pile head breakwater with $S = 0.25D$ and $P = 22.5$	81
Fig. 3.25 A typical wave interaction under crest with perforated pile head for $D = 0.096$ m, $Y = 0.16$ m and $S = 0.25D$	82
Fig. 3.26 A typical wave interaction under trough with perforated pile head for $D = 0.096$ m, $Y = 0.16$ m and $S = 0.25D$	82
Fig. 3.27 Wave interaction with enlarged pile head in NWT	83
Fig. 3.28 Wave interaction with a non-perforated enlarged pile breakwater	83
Fig. 3.29 Wave interaction with a perforated enlarged pile breakwater	84
Fig. 3.30 Wave interaction with a perforated enlarged pile breakwater	85
Fig. 3.31 View of water flowing back (towards seaside) under wave trough from the perforated of enlarged pile head	86
Fig. 3.32 Formation of vortex behind pile head under wave crest in REFF3D	87
Fig. 3.33 Formation of vortex behind pile head under wave trough in REFF3D	87
Fig. 3.34 Flow chart of methodology	89
Fig. 3.35 Data acquisition system	93
Fig. 3.36 View of wave flume with wave probes for data acquisition	94
Fig. 3.37 Wave generation system (clockwise from top left: inverter drive, motor, flap type wave paddle and wave filter)	94
Fig. 3.38 View of the wave flume (from generation side)	95
Fig. 4.1 Graphs of K_t versus H_i/gT^2 for varying ratios of b/D , D/H_{\max} and Y/H_{\max} at a water depth of 0.30 m	98
Fig. 4.2 Graphs of K_t versus H_i/gT^2 for varying ratios of b/D , D/H_{\max} and Y/H_{\max} at a water depth of 0.40 m	99
Fig. 4.3 Graphs of K_t versus H_i/gT^2 for varying ratios of b/D , D/H_{\max} and Y/H_{\max} at a water depth of 0.50 m	100

Fig. 4.4 Graphs of K_r versus H_i/gT^2 for varying ratios of b/D , D/H_{max} and Y/H_{max} at a water depth of 0.30 m	101
Fig. 4.5 Graphs of K_r versus H_i/gT^2 for varying ratios of b/D , D/H_{max} and Y/H_{max} at a water depth of 0.40 m	102
Fig. 4.6 Graphs of K_r versus H_i/gT^2 for varying ratios of b/D , D/H_{max} and Y/H_{max} at a water depth of 0.50 m	103
Fig. 4.7 Graphs of K_d versus H_i/gT^2 for varying ratios of b/D , D/H_{max} and Y/H_{max} at a water depth of 0.30 m	104
Fig. 4.8 Graphs of K_d versus H_i/gT^2 for varying ratios of b/D , D/H_{max} and Y/H_{max} at a water depth of 0.40 m	105
Fig. 4.9 Graphs of K_d versus H_i/gT^2 for varying ratios of b/D , D/H_{max} and Y/H_{max} at a water depth of 0.50 m	106
Fig. 4.10 Variation of K_t with H_i/gT^2 when $b/D = 0.2$ for different h , D/H_{max} and Y/H_{max}	108
Fig. 4.11 Variation of K_r with H_i/gT^2 when $b/D = 0.2$ for different h , D/H_{max} and Y/H_{max}	110
Fig. 4.12 Variation of K_d with H_i/gT^2 when $b/D = 0.2$ for different h , D/H_{max} and Y/H_{max}	111
Fig. 4.13 Variation of K_t with H_i/gT^2 when $b/D = 0.2$ and $D/H_{max} = 0.6$ for different h , and Y/H_{max}	112
Fig. 4.14 Variation of K_r with H_i/gT^2 when $b/D = 0.2$ and $D/H_{max} = 0.6$ for different h , and Y/H_{max}	113
Fig. 4.15 Variation of K_d with H_i/gT^2 when $b/D = 0.2$ and $D/H_{max} = 0.6$ for different h , and Y/H_{max}	114
Fig. 4.16 Variation of K_t with H_i/gT^2 for various h and Z when $b/D = 0.2$	115
Fig. 4.17 Variation of K_r with H_i/gT^2 for various h and Z when $b/D = 0.2$	116
Fig. 4.18 Variation of K_d with H_i/gT^2 for various h and Z when $b/D = 0.2$	117
Fig. 4.19 Comparison of theoretical K_t , K_r and K_d with the measured values	120
Fig. 4.20 Comparison of theoretical K_t , K_r and K_d with Rao (1999) data	122
Fig. 4.21 Validation of non-perforated pile head breakwater REEF3D results with experimental and theoretical values	125

Fig. 4.22 Comparison of K_t , K_r and K_d with different single row pile breakwater models	127
Fig. 5.1 Graphs of K_t versus H_i/gT^2 for various percentage of p_a , $D/H_{max} = 0.4$, $S = 0.1D$ and $0.15D$ at a water depth of 0.30 m	133
Fig. 5.2 Graphs of K_t versus H_i/gT^2 for various percentage of p_a , $D/H_{max} = 0.4$, $S = 0.2D$ and $0.25D$ at a water depth of 0.30 m	134
Fig. 5.3 Graphs of K_r versus H_i/gT^2 for various percentage of p_a , $D/H_{max} = 0.4$, $S = 0.1D$ and $0.15D$ at a water depth of 0.30 m	135
Fig. 5.4 Graphs of K_r versus H_i/gT^2 for various percentage of p_a , $D/H_{max} = 0.4$, $S = 0.2D$ and $0.25D$ at a water depth of 0.30 m	136
Fig. 5.5 Graphs of K_d versus H_i/gT^2 for various percentage of p_a with $D/H_{max} = 0.4$, $S = 0.1D$ and $S = 0.15D$ at a water depth of 0.30 m	137
Fig. 5.6 Graphs of K_d versus H_i/gT^2 for various percentage of p_a with $D/H_{max} = 0.4$, $S = 0.2D$ and $0.25D$ at a water depth of 0.30 m	138
Fig. 5.7 Graphs of K_t versus H_i/gT^2 for $D/H_{max} = 0.4$ for various P and S at 0.3 m water depth	139
Fig. 5.8 Graphs of K_r versus H_i/gT^2 for $D/H_{max} = 0.4$ with various percentage of perforation and pore size at 0.3 m water depth	140
Fig. 5.9 Graphs of K_d versus H_i/gT^2 for $D/H_{max} = 0.4$ with various P and S at 0.3 m water depth	141
Fig. 5.10 Graphs of K_t versus H_i/gT^2 for various p_a , $D/H_{max} = 0.6$, $S = 0.2D$ and $0.25D$ at a water depth of 0.30 m	142
Fig. 5.11 Graphs of K_r versus H_i/gT^2 for various p_a , $D/H_{max} = 0.6$, $S = 0.2D$ and $0.25D$ at a water depth of 0.30 m	143
Fig. 5.12 Graphs of K_d versus H_i/gT^2 for various p_a , $D/H_{max} = 0.6$, $S = 0.2D$ and $0.25D$ at a water depth of 0.30 m	144
Fig. 5.13 Graphs of K_t versus H_i/gT^2 for $D/H_{max} = 0.6$, various percentage of perforations and pore size at 0.3 m water depth	145
Fig. 5.14 Graphs of K_r versus H_i/gT^2 for $D/H_{max} = 0.6$, with various P , p_a and S at 0.3 m water depth	145
Fig. 5.15 Graphs of K_d versus H_i/gT^2 for $D/H_{max} = 0.6$, with various P , p_a and S at 0.3 m water depth	146

Fig. 5.16 Effect of perforations on K_t for $D/H_{\max} = 0.4$ and 0.6 at 0.3 m water depth	147
Fig. 5.17 Effect of perforations on K_r for $D/H_{\max} = 0.4$ and 0.6 at 0.3 m water depth	147
Fig. 5.18 Effect of perforations on K_d for $D/H_{\max} = 0.4$ and 0.6 at 0.3 m water depth	148
Fig. 5.19 Effect of water level variations on K_t , K_r and K_d for non-perforated pile head breakwater	149
Fig. 5.20 Effect of water level variations on K_t , K_r and K_d for perforated pile head breakwater	150
Fig. 5.21 Comparison of theoretical K_t , K_r and K_d with measured values	152
Fig. 5.22 Comparison of theoretical K_t , K_r and K_d with Rao (1999) data	153
Fig. 5.23 Validation of perforated pile head breakwater REEF3D results with experimental and theoretical values	155
Fig. 5.24 Effect of perforations on K_t , K_r and K_d for $D/H_{\max} = 0.6$ at 0.3 m water depth	156
Fig. 5.25 Comparison of K_t , K_r and K_d with different single row pile breakwater models	158

LIST OF TABLES

Table No.	Title	Page No.
Table 3.1	Predominant variables and their dimensions	46
Table 3.2	Wave parameters of prototype and model	50
Table 3.3	Calibrated values of wave flume for 0.3 m depth of water	55
Table 3.4	Calibrated values of wave flume for 0.4 m depth of water	55
Table 3.5	Calibrated values of wave flume for 0.5 m depth of water	55
Table 3.6	Structural dimensions of prototype and model	56
Table 3.7	Details on S, p_a and for $D = 0.064$ m dia. pile head	60
Table 3.8	Details on S, p_a and P for $D = 0.096$ m dia. pile head	61
Table 3.9	Experimental variables for non-perforated pile head	61
Table 3.10	Experimental variables for perforated pile head	62
Table 3.11	Amplitude error with RMSE value for various grid size and CFL number	71
Table 3.12	Structural configuration considered for enlarged pile head breakwater	74
Table 4.1	The projected area of the whole structure at 0.3 m water depth	108
Table 4.2	Percentage variation of K_t , K_r and K_d with water depth for $b/D = 0.2$, $Y/H_{max} = 0.5$ and $D/H_{max} = 0.4$	117
Table 4.3	Percentage change in K_t , K_r and K_d with water depth for $b/D = 0.2$, $Y/H_{max} = 1.0$ and $D/H_{max} = 0.4$	118
Table 4.4	Percentage change in K_t , K_r and K_d with water depth for $b/D = 0.2$, $Y/H_{max} = 0.5$ and $D/H_{max} = 0.6$	118
Table 4.5	Percentage change in K_t , K_r and K_d with water depth for $b/D = 0.2$, $Y/H_{max} = 1.0$ and $D/H_{max} = 0.6$	118
Table 4.6	Variation coefficient (R^2) value obtained for different equations for the present experimental data	121
Table 4.7	Scatter index (SI) value obtained for different equations for the present experimental data	121
Table 4.8	Relative root mean square error (RrmsE) value obtained for different equations for the present experimental data	121

Table 4.9 Experimental parameters, as cited by Rao (1999)	123
Table 4.10 Variation coefficient (R^2) value obtained for different equations for Rao (1999) experimental data	123
Table 4.11 Scatter index (SI) value obtained for different equations for Rao (1999) experimental data	123
Table 4.12 Relative root mean square error (RrmsE) value as obtained for different equations for Rao (1999) experimental data	124
Table 4.13 Quantitative assessment of error using S.I., RrmsE and R^2 indexes	125
Table 4.14 Test conditions as indicated by the various authors	126
Table 5.1 An average percentage variation in K_t , K_r and K_d with change in water depth	151
Table 5.2 Experimental parameters of perforated pile breakwater (Rao, 1999).	152
Table 5.3 Quantitative assessment of error using S.I., RrmsE and R^2 indexes.	153
Table 5.4 Quantitative assessment of error using S.I., RrmsE and R^2 indexes	154
Table 5.5 Test conditions as indicated by the various authors	157

NOMENCLATURE

2A	Centre to centre spacing between pile heads in a row	p	Pressure
b	Clear spacing between pile head in a row	pa	Distribution of perforations
C	Blockage coefficient	P	Percentage of perforations
C_c	Contraction coefficient	Re	Real part of a complex value
D	Diameter of pile head	S	Size of perforations
D_t	Diameter of pile trunk	T	Wave period
E_d	Energy of dissipated waves	u	Velocity away from the pile
E_i	Energy of incident waves	u_0	Velocity at the gap of piles
E_r	Energy of reflected waves	Y	Height of pile head
E_t	Energy of transmitted waves	Z	Relative submergence of pile head
f	Head loss coefficient	β	Linearised friction coefficient
g	Acceleration due to gravity	γ	Friction coefficient
h	Depth of water	ρ	Density of water
H_i	Incident wave height	Φ	Velocity potential function
H_{max}	Maximum wave height	l	Length of the jet flowing through the gap between the piles
H_r	Reflected wave height	θ	Angle of wave attack
H_t	Transmitted wave height	ω	Angular frequency
k	Wave number.	ϵ	Porosity
K_d	Energy dissipation coefficient	$\bar{\epsilon}$	Spatial variation of porosity
K_r	Reflection coefficient	ν	Kinematic viscosity
K_t	Transmission coefficient	ν_t	Eddy viscosity
L	Wavelength		

CHAPTER 1

INTRODUCTION

1.1 GENERAL

A region separating the sea and the land is termed as the 'coast' and this acts as an interface between the two bodies. As mankind chooses to concentrate his activities along the coast, a close relationship has been maintained by them with the sea for centuries. Further, due to rapid urbanization, industrialization and developmental activities, there has been high pressure along coastal regions to facilitate trade and commerce meeting the demand of the industry and the population. The objectives of coastal engineering are to provide perspectives for sustainable development of the vulnerable coastal zone facing disaster scenarios as well as to meet the demands of the civilization and preservation of nature.

The Indian coastline is about 7516.6 km long, 5422.6 km spread along the mainland and around 2094 km along the coast of the archipelago of Andaman and Nicobar, and Lakshadweep. The coastline comprises a myriad of coastal features such as headlands, promontories, rocky shores, sandy spits, barrier beaches, open beaches, embayment, estuaries, inlets, bays, marshy land and islands etc. According to the naval hydrographic charts, the Indian mainland consists of nearly 43% sandy beaches, 11% rocky coasts with cliffs and 46% mudflats and marshy coasts.

Advancement and retreat of the shoreline along the Indian coast are seasonal. Some of the beaches regain their original profiles by March/April. Fifty percent of the beaches that do not regain their original shape over an annual cycle undergo net erosion. According to the National Centre for Coastal Research (Kankara et al 2018), in the last 26 years (1990 to 2016), about 34% of the coastline in India is affected by erosion. In Karnataka, 22% (70.02 km) of the coastal line has been eroded. Whereas Dakshina Kannada (D. K.) and Udupi coasts are eroded by about 45.33% and 36%, respectively.

1.2 EROSION ALONG DAKSHINA KANNADA COAST

Dakshina Kannada (D. K) coast as shown in Fig. 1.1, is situated along the west coast of India lies between Talapadi ($12^{\circ} 45' 30''$ N, $74^{\circ}52'$ E) in the south and Mulki ($13^{\circ}5' 30''$ N, $74^{\circ}47' 30''$ E) in the north covering a distance of about 46 km.

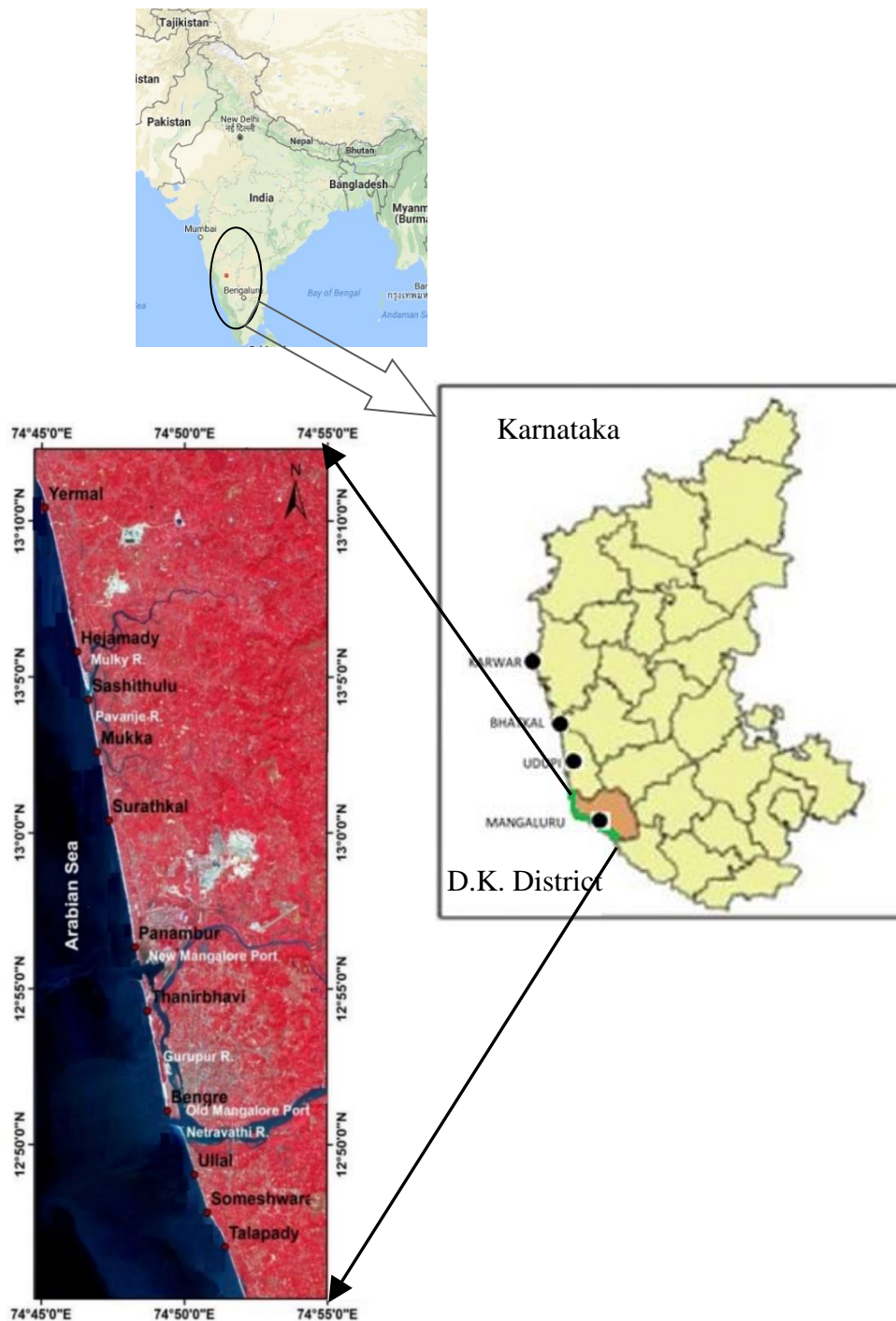


Fig. 1.1 Dakshina Kannada coast

The rivers in the D. K. district originate in the Western Ghats, flow westward and take almost a right angle bend near the coast and then flow either northward or southward close to and parallel to the coast before joining the Arabian Sea. It is observed that two or more rivers confluence before they discharge into the Arabian Sea. The D.K region receives waves predominantly from the southwest, west and northwest. The waves are more than 1.0 m during the monsoon season, with a maximum wave height of 4.0 m and wave periods of 9 s to 10 s were typically observed. The single largest wave recorded was about 5.4 m. Waves during non-monsoon months are generally less than 1.0 m in height (KREC Study Team 1994).

Coastal erosion and accretion are complex processes that depend upon many factors like geological, wave, tide, currents, sea-level rise, wave refraction and energy concentration under the wind, wave and tidal currents; beach dynamics within a sediment/littoral cell; and human activities along the coast. With increasing sea level that influences the local water depth, the higher waves with increased energy can play a significant role in sediment transport mechanism along the coastal belt. Thus, the coast starts to adjust to the new sea level to maintain a dynamic equilibrium.

Erosion at the site is mainly because of one or a combination of the above causes and it is important to find which one or combination of these is responsible for the coastal erosion along the D.K coast. On the Karnataka coast with negligible littoral drift, the erosions reported, particularly on the open coasts cannot be due to interception of littoral drift, which causes erosion on the downdrift side (KREC Study Team 1994). With reference to the Karnataka coast, there is a relative sea-level fall as a result of the upwarping of land at a faster rate than the global sea-level rise (Subrahmanya and Rao 1991). Sea level changes cannot be the cause of any erosion on the Karnataka coast at present. Sand mining from the beaches is prohibited and if it occurs illegally, the magnitudes of such mining activity on the D.K coast are small and unlikely to cause erosion. According to John (1988) and KREC Study Team (1994), the concentration of wave energy due to wave refraction is the main reason for the coastal erosion along Dakshina Kannada coast.

Coastal erosion in any region needs to be addressed judiciously. If not, that can threaten the settlements and economic interests of the region. The three basic options available to mitigate the sea erosion (Griggs et al. 1991 and Tilmans et al. 1993) are:

i) Nourishment: the soft measure of restoring the beach by artificially feeding the sand to the beach.

ii) Armouring: the hard measure of protecting the beach by constructing a protective structure like bulkheads, revetment, sea wall, groynes or an offshore breakwater.

iii) No action: Retreat, withdrawal beyond the active coastal zone.

Among the three basic options, the best option is the retreat as envisaged in Coastal Regulation Zone Notification (2019) because most solutions require substantial investment. If no life, inexpensive structures and only undeveloped lands are in danger, then retreat is the better option. Sometimes, relocation of endangered structures is less expensive than investing in shore protection. As per the Coastal Regulation Zone Notification (2019), the Government of India has declared the coastal stretch up to 500 m on the landward side from the High Tideline as Coastal Regulation Zone (CRZ) and has put severe restrictions on the developmental activities in this zone.

The next best possibility is the artificial beach nourishment. This method offers a smart solution for the place, where the erosion is mainly due to a scarcity of longshore sediment transport. Even though this solution method is very expensive, it is often preferred as it is the most environmentally friendly.

Hard measures such as offshore breakwaters, groynes and seawalls are not suitable as the littoral drift is not the reason for erosion along the west coast of India (KREC Study Team, 1994). Also, seawalls are vast and may indulge the natural magnificence of the beaches. Offshore detached breakwaters create shadow areas on the shoreward side, resulting in sand entrapment just behind the breakwater and beach developments with salient. Hence, submerged breakwaters may be a better alternative. But the construction of offshore breakwaters is costlier, difficult, and interferes with the movement of the onshore-offshore sediment (Rao and Rao 2001).

1.3 PILE STRUCTURE TO COMBAT EROSION

An environmentally friendly structure constructed to protect the coast without spoiling the beauty of the natural beach may be a better option. One such structure is the pile breakwater. The pile breakwater structure effectively reduces the wave energy due to turbulence resulting from wave-structure interaction and less reflection. Pile breakwater allows the incoming waves to pass through the gaps therefore, on-shore, offshore sediment movement is not affected. Due to certain advantages of pile structures, a detailed study on the performance of pile breakwater is undoubtedly valuable for finding an alternative solution for coastal erosion. Various researchers (Bovin 1964; Koraim et al. 2014; Mani and Jayakumar 1995; Rao 1999, 2002b; Van Weele and Herbich 1972) have investigated perforated and non-perforated piles and concluded that these types of pile breakwaters are better than conventional types where full protection from the waves is not required.

Due to the uniqueness of pile breakwater over the conventional rubble mound breakwater, pile breakwaters are constructed worldwide. A steel pipe breakwater of 2 m in diameter and spaced at 0.05 m between the adjacent pipe was constructed in the year 1966 at Japan in the Port of Osaka (Nagai 1966). Concrete pile breakwater of 1.4 m in diameter and spaced at 0.152 m was built at Pass Christian, Mississippi, USA (Herbich 1990). Pile breakwater constructed (1995) at Langkawi, Malaysia, for beach development is shown in Fig. 1.2. The constructed pile breakwater is even effective in reducing the effect of Tsunami waves (Reedijk and Muttray 2009). Fig. 1.3 shows another example of pile breakwater constructed at Pasir Panjang, Singapore (Liu et al. 2011). Similarly, pile breakwater was also constructed in Hanstholm, Denmark and Marsa el Brega in Libya (Sundar and Rao 2002)



Fig. 1.2 Row of pile breakwater at Langkawi, Malaysia (Reedijk and Muttray 2009)



Fig. 1.3 Row of pile breakwater at Pasir Panjang, Singapore (Liu et al. 2011)

The wave energy is more concentrated at the surface and reduces gradually depth wise. On this basis, providing a larger area of the structure at the surface level may result in more wave-structure interaction inducing larger wave attenuation. Hence, the concept of structure enlargement at the surface and perforation is comprehended for the

advancement of enlarged pile head breakwater. In a pile breakwater, the wave energy dissipation occurs due to wave-structure interaction associated with turbulence, eddy formation, and vortex shedding. Energy dissipation characteristics of non-perforated pile breakwater can be increased with perforations (Huang et al. 2011; Kondo and Toma 1972; Rao et al. 2002b; Rao and Rao 1999, 2001) due to increased wave-structure interaction, turbulence, eddy formation and vortex shedding. Hence, the concept of perforation is utilised and investigated through the present study.

In this research work, an investigation to study the hydraulic performance of innovative pile breakwaters is presented. A portion of pile near the free surface of water is enlarged and is termed as pile head and the portion below is denoted as a trunk. At the top, the pile area is increased to have a significant part of the structure in contact with the waves, while the trunk portion consists of a regular pile. This increased pile head area is further optimised with perforations to increase its efficiency. The hydraulic performance of perforated enlarged pile head breakwater is examined through physical experiments and the result are verified using REEF3D software.

1.4 WAVE ATTENUATION MECHANISM OF PILE STRUCTURE

It is important to understand the mechanism by which wave energy gets dissipated due to pile breakwater. In general, it can be said that in a pile type breakwater, the wave energy dissipation occurs due to wave-structure interaction associated with turbulence, eddy formation, and vortex shedding. Wave interaction with the structure is a complex phenomenon (Park et al. 2000). Study indicates that in the absence of currents under monochromatic waves, wave energy dissipation due to pile breakwater (slotted or perforated) takes place by means of the following mechanism (Hildebrandt and Sriram 2014; Huang et al. 2011; Kakuno and Liu 1993; Liu et al. 2011; Park et al. 2000; Rao et al. 1999; Suh et al. 2006, 2011).

- Flow separations
- Inertia resistance
- Contraction
- Wave reflection
- Turbulence

- Vortex shedding

Wave approaching the pile structure encounters flow separation along the front and behind portion of the structure, resulting in dissipation of wave energy. In the theoretical analysis, the same is accommodated in the form of linearized dissipation coefficients. The energy losses due to the inertia resistance is termed theoretically in the form of blockage coefficient. In the gap between the piles, the flow gets contracted, resulting in energy loss due to contraction. The effect of contraction is theoretically defined by the head loss coefficient. When the wave interacts with the pile structure, part of it gets reflected, resulting loss of energy due to reflection. The flow in relation with the wave motion is turbulent in nature. Hence, in the case of turbulent flow, inertia force is more than the viscous force, which results in vortex formation behind the pile structure (Davidson 2015). A typical flow behind the cylinder for various Reynolds numbers (Re) is shown in Fig. 1.4. The formation of turbulence and vortex for circular pile under a monochromatic wave is shown in Fig. 1.5.

As shown in Fig. 1.5, the vortex formation may take place behind or in front of the pile structure, depending on the wave crest and trough position. The vortex generally forms, behind the structure during wave crest, whereas, in front of the structure under the wave trough. In the process of turbulence dissipation, the energy from the larger eddies gets transferred by breaking into smaller vortices, as shown in Fig. 1.6. The process of breaking into smaller vortices will continue till the inertia force dominates. On equalization of the inertial and viscous force ($Re \approx 1$), a breaking process of eddies will cease, and viscosity will absorb the remaining energy (Davidson 2015).

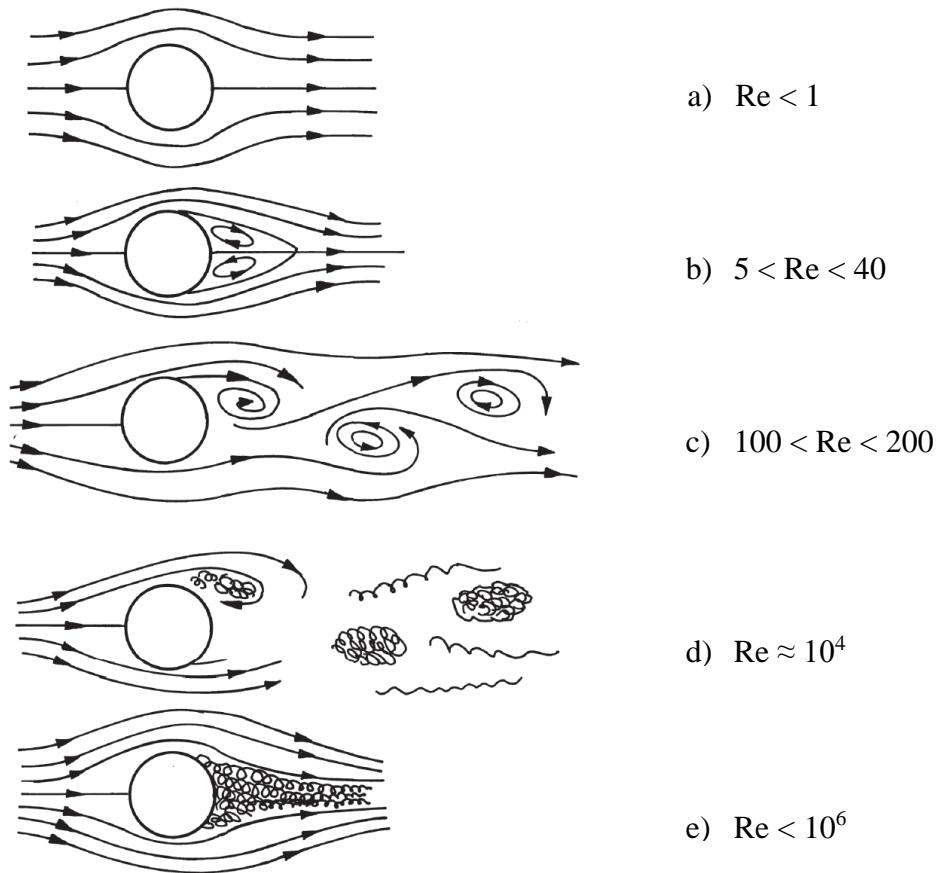


Fig. 1.4 Flow behind a cylinder for various Re (Davidson 2015)

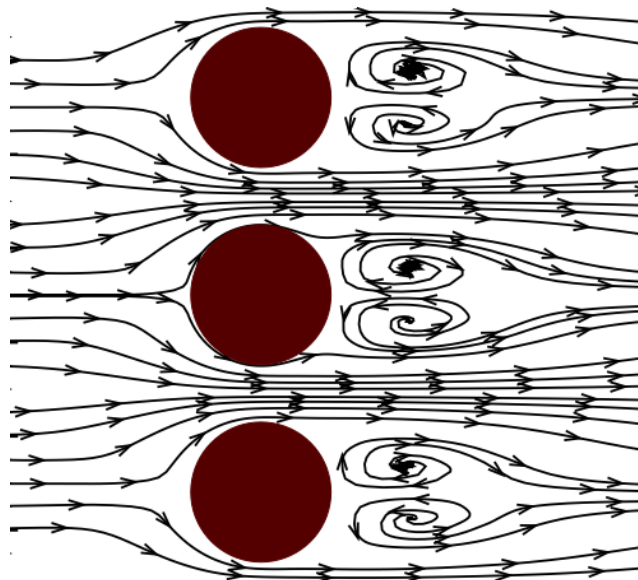
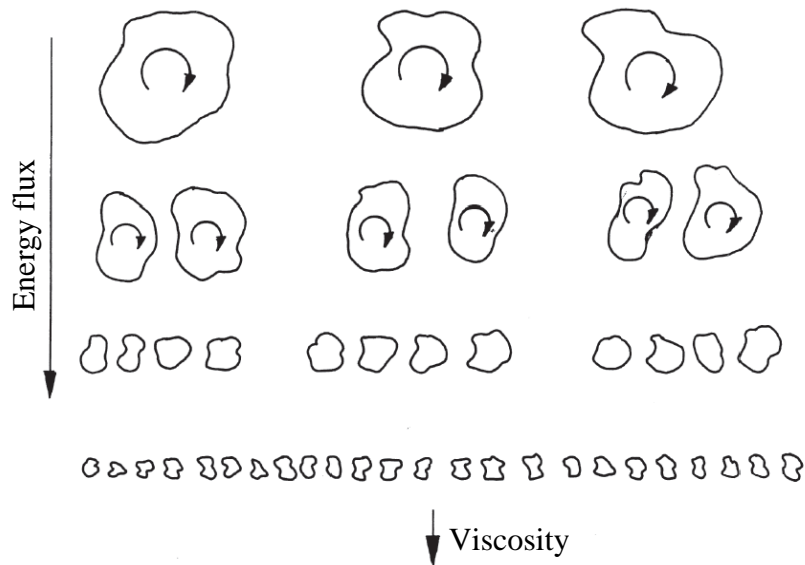


Fig. 1.5 Formation of vortex when wave crest passing over the structure (Liu et al. 2011)



**Fig. 1.6 Typical cascade of energy from larger eddies to smaller eddies
(Davidson 2015)**

1.5 ORGANIZATION OF THE THESIS

The present thesis report is organized into 6 chapters. An introduction, importance and wave attenuation by pile structure is described in Chapter 1. The chapter also highlights the need for pile breakwater, wave attenuation mechanism and organization of the thesis.

Chapter 2 deals more specifically with the wave climatic conditions and sea erosion along the D.K. coast, an outline of the present state of knowledge on pile breakwater and pile-supported breakwaters, the background of the hybrid theoretical equation, research problem formulation and the objectives of the current study.

The details of the experimental investigation, such as dimensional analysis, similitude criteria, model scale selection, design conditions, test model, range of experimental parameters and experimental set-up, are explained in Chapter 3. This chapter also discusses the development of modified hybrid theoretical equations and numerical modelling along with the physics of the experiments and wave-structure interactions.

Investigation on the hydraulic performance of non-perforated enlarged pile head breakwater to investigate the influence of relative pile spacing, the impact of varying pile head characteristics and depth of water under various wave climatic conditions are discussed in Chapter 4. This chapter also describes the validation of non-perforated enlarged pile head breakwater results using a modified hybrid theoretical equation and numerical modelling. The best configuration of non-perforated enlarged pile head breakwater obtained from the physical test is compared with the other similar type of non-perforated breakwaters.

Chapter 5 explains the results obtained for perforated enlarged pile head breakwater. This chapter describes the effect of the distribution of perforations, size of perforations and percentage of perforations on the hydraulic performance of the breakwater. The experimental results are validated using the present hybrid theoretical equation and REEF3D model. The performance of non-perforated and perforated structures are compared to arrive at the best performing model. Further, the hydraulic efficiency of the best performing model is compared with the other studies on similar types of breakwaters.

The summary of the present research work and its conclusions find their place in the final Chapter 6.

BACKGROUND AND LITERATURE REVIEW

2.1 GENERAL

A study conducted by Karnataka Engineering Research Station (1989), on the beach erosion problem at Ullal (shown in Fig. 1.1) concluded that the materials from the deeper zones were removed and deposited on the foreshore, thereby forming a berm during pre-monsoon and post-monsoon period. During monsoons, the same material was eroded and deposited in deeper zones. During monsoon season, the beach slopes were generally steep and relatively flat during the non-monsoon season indicating that beach width has an annual seasonal oscillation exhibiting dynamic equilibrium.

Chandramohan et al. (1994) conducted a field study between Bhatkal to Ullal from June 1989 to 1990. It was concluded that the southwest monsoon dominated the study region from June to September. According to the ship's observed data, the swells predominantly vary between 1 m and 3.5 m from June to September and 0.5 m and 1m from October to January. The period of swell waves falls between 5 s and 8 s during June to September and between 5 s to 12 s during October to May. From June to August, the monsoon wave predominantly approaches the coast from the southwest and northwest sector. The tides in this region are characterized by a mixed type, mostly semi-diurnal type. Based on the predicted tidal range for New Mangalore Port, the average tidal range is about 0.25 m to 1.54 m. The Beach profile study indicates the influence of seasonal erosion and accretion. It was observed that during the NE monsoon period, the longshore current direction was predominantly North, and during the SW monsoon and fair weather period, it was southward.

KREC Study Team (1994) conducted a study on coastal erosion along the Dakshina Kannada coast. It was reported that the SW monsoon generally reaches Mangaluru around the first week of June and withdraws by the end of June, mid-September or the first week of October. After August, a reverse series of changes occur in the predominant wind direction accompanied by a decrease in the strength, leading to the

NE monsoon and October and November being quiet. By mid-November, the NE wind regularly blows from the North and by mid-December from the South.

In the monsoon season, waves are more than 1 m along the coast, while the wave heights are less than 1 m during the non-monsoon season and the wave periods show wide variation with the presence of long-period waves. Predominant deep-water wave direction in monsoon is SW, W and NW. These waves become almost parallel to the coast due to refraction as they are near to the shoreline. Tides are semidiurnal with a mean tidal range of 1.2 m and a spring tidal range of 1.8 m. The ocean currents off the D. K. coast during the months, February to September were generally towards the South. From the beach profile studies carried out along the D. K. coast, KREC study team (1994) concluded that beaches along D. K coast were in the state of dynamic equilibrium. It was also reported that net erosion tendency was observed at Ullal. The study team concluded that littoral drift along the study area was negligibly small. Some of the evidence given by them are, however, had there been a large scale littoral drift, and there would have been a case of, maximum accretion of sea borne sediments on the north of the northern New Mangalore Port Trust (NMPT) breakwater and matching erosion on the southern part. Also, the analysis of the siltation at the entrance channel of NMPT and the changes in the coastline adjacent to the breakwaters at NMPT indicated that the littoral drift in the study area was negligibly small.

Sea sledge survey along the D. K. Coast during 1995 and 1996 conducted by Dattatri et al. (1997) revealed that the pre-monsoon and post-monsoon profiles were almost the same. This indicated that the pre-monsoon profiles had regained their profiles during post-monsoon, i.e., the pre-monsoon and post-monsoon profiles closely followed each other. The material eroded during the monsoon was recovered during the post-monsoon period. From this, it was concluded that there was no net erosion or deposition, although there were changes during the monsoon. Hence, the portion of the beach considered in the study was in a state of dynamic equilibrium. From the study, it was found that littoral drift was negligible along the Mangaluru coast

Based on the beach profile and sediment trend matrix investigations done by Rao and Pramod (2003) and Rao et al. (2001, 2002a, 2003, 2004), it was concluded that the

sediment movement along D. K. coast was seasonal and there was no net littoral drift along with it. Further, studies carried out by Rao (2002) and Rao et al. (2006) revealed that the direction of sediment movement got reversed along D. K. coast seasonally. Rao (2002) also observed that littoral drift will not pose any problem in the coasts of D. K. district.

Rao et al. (2007) concluded that beaches at Ullal and Bengre were generally in dynamic equilibrium, though at Ullal, there was net erosion of small magnitude. A bathymetry survey conducted indicated that the seabed at Ullal was steeper than that at Bengre. The main cause of erosion in the study area was a direct wave attack on the beach and typical circulatory currents.

Shetty et al. (2015) conducted shoreline change analysis of Mangaluru coast using topo maps of 1967 and multi-temporal satellite images using Remote Sensing and GIS techniques. The study indicated that the breakwaters at New Mangalore Port and the mouth of Nethravathi-Gurupur estuary had contributed substantially to shoreline modification. Construction of seawalls had resulted in the shifting of erosion sites to the downdrift (southern) side. Ullal spit was subjected to severe erosion.

2.2 EXPERIMENTAL STUDIES ON PILE BREAKWATER

Gravity-type breakwaters using rubble-mound or vertical caissons have been constructed and used widely to protect harbour facilities from rough seas. The construction of the conventional breakwaters requires a huge amount of material, especially when built-in deeper waters. Often, they block littoral drift and cause severe erosion or accretion on neighbouring beaches. In addition, they may prevent the circulation of water, thus deteriorating the water quality within the harbour. In order to resolve these problems, permeable or perforated type structures have been introduced, especially for small craft harbours. Pile type breakwaters are one such permeable, environmentally friendly structures that do not spoil the aesthetic beauty of the beaches and protect the coast from erosion. The experimental studies by earlier researchers are discussed in the following section.

Bovin (1964) conducted experiments on the slotted vertical wall breakwater. The study revealed that the total void ratio on the seaward side is more vital than the individual perforation characteristics. It was identified that the shape of the opening had a diminutive impact on the effectiveness of the porous structure.

Hayashi et al. (1966) developed a theory for calculating transmission coefficient and wave force on the closely spaced piles and compared with the experimental results. It was concluded that the transmission coefficient (K_t) predicted by the equation is in good agreement with the experimental results and thus, the equation may be used for engineering design purposes.

Hayashi et al. (1968) modified a theory developed by Hayashi et al. (1966) on the assumption that the waves near the breakwater are shallow-water waves of small amplitude. It was observed that the transmission coefficient increased with an increase in relative clear spacing between the piles and suggested that the pile breakwaters could protect the shoreline from beach erosion.

Kondo and Toma (1972) worked on the hydraulic characteristics of an idealized porous structure, as shown in Fig. 2.1 on K_t and K_r . The experiments concluded that the K_t decreases with an increase in relative thickness of the structure (B/L), where B is the thickness of porous structure and L is the wavelength.

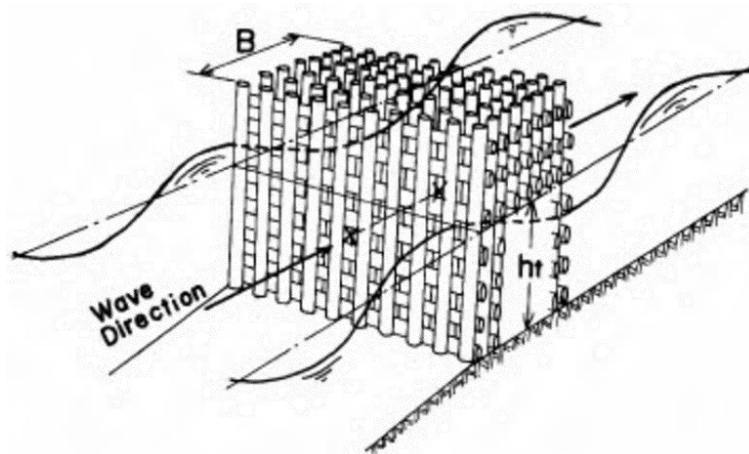


Fig. 2.1 description for porous structure (Kondo and Toma 1972)

Van Weele and Herbich (1972) observed that the reflection coefficient reduces to a larger extent with increased relative clear spacing (i.e. b/D , where, b is the clear spacing between the pile rows and D is the outer diameter of pile). It was reported that, according to Morrison's work, the interference effect of two rows of piles was negligible for spacings greater than 1.5 times the pile diameter. It was concluded that staggering of piles decreases K_t marginally.

An integral equation was proposed by Hagiwara (1984) for estimating K_t and K_r of upright structures. Various factors associated with wave and structural conditions relating to wave dissipating characteristics were investigated. The theoretical results were in line with the experimental data. It was reported that, relative chamber width (defined as the ratio of spacing between the walls to the wavelength) and the opening ratios place an vital role in reducing K_t and K_r .

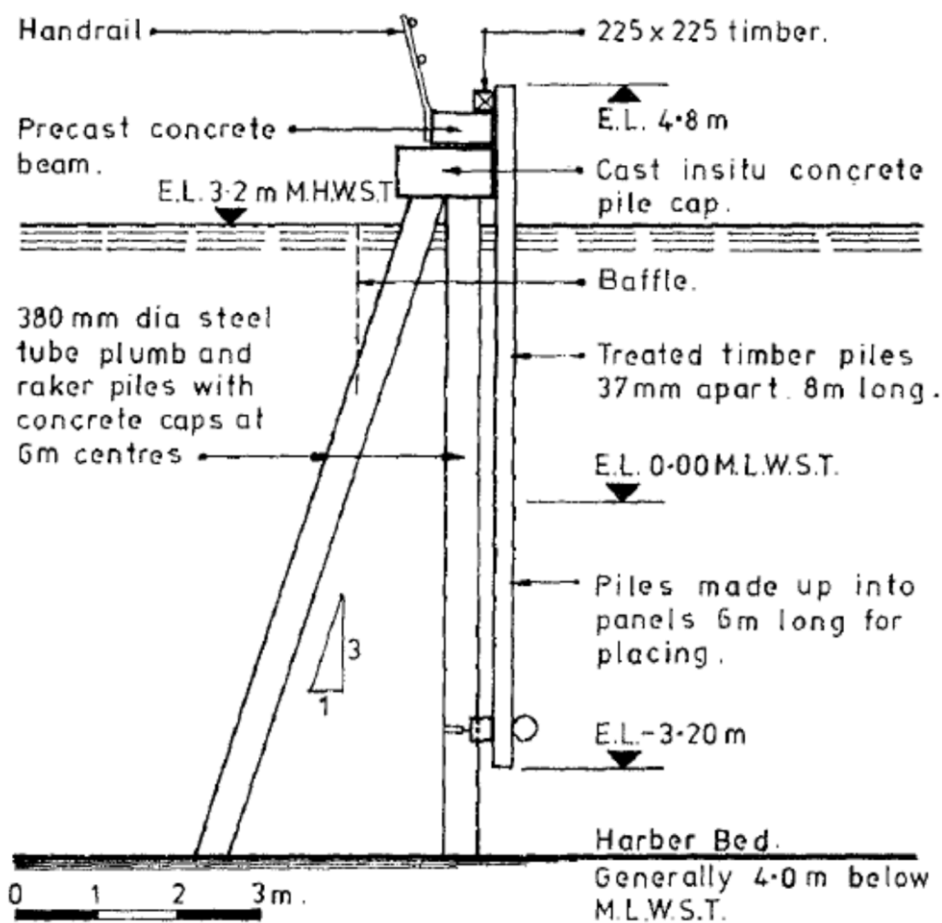


Fig. 2.2 Concept of pile breakwater defined by Hutchinson and Raudkivi (1984)

Pile breakwater with treated pine piles supported on an orthodox plumb and raker structure was tested by Hutchinson and Raudkivi (1984). The treated timber piles were 8 m long and 300 mm in diameter at 37 mm apart, as shown in Fig. 2.2. The plumb and raker piles were made of 380 mm diameter steel tube and provided at 6 m centre to centre. A wave flume model (scale 1:12) test revealed that a 50% reduction of wave height could be achieved with timber piles of 300 mm diameter spaced at 37 mm. It was reported that no maintenance work was carried out for the 12 years after the construction of breakwaters and thus provided satisfactory shelter to 485 marina boats.

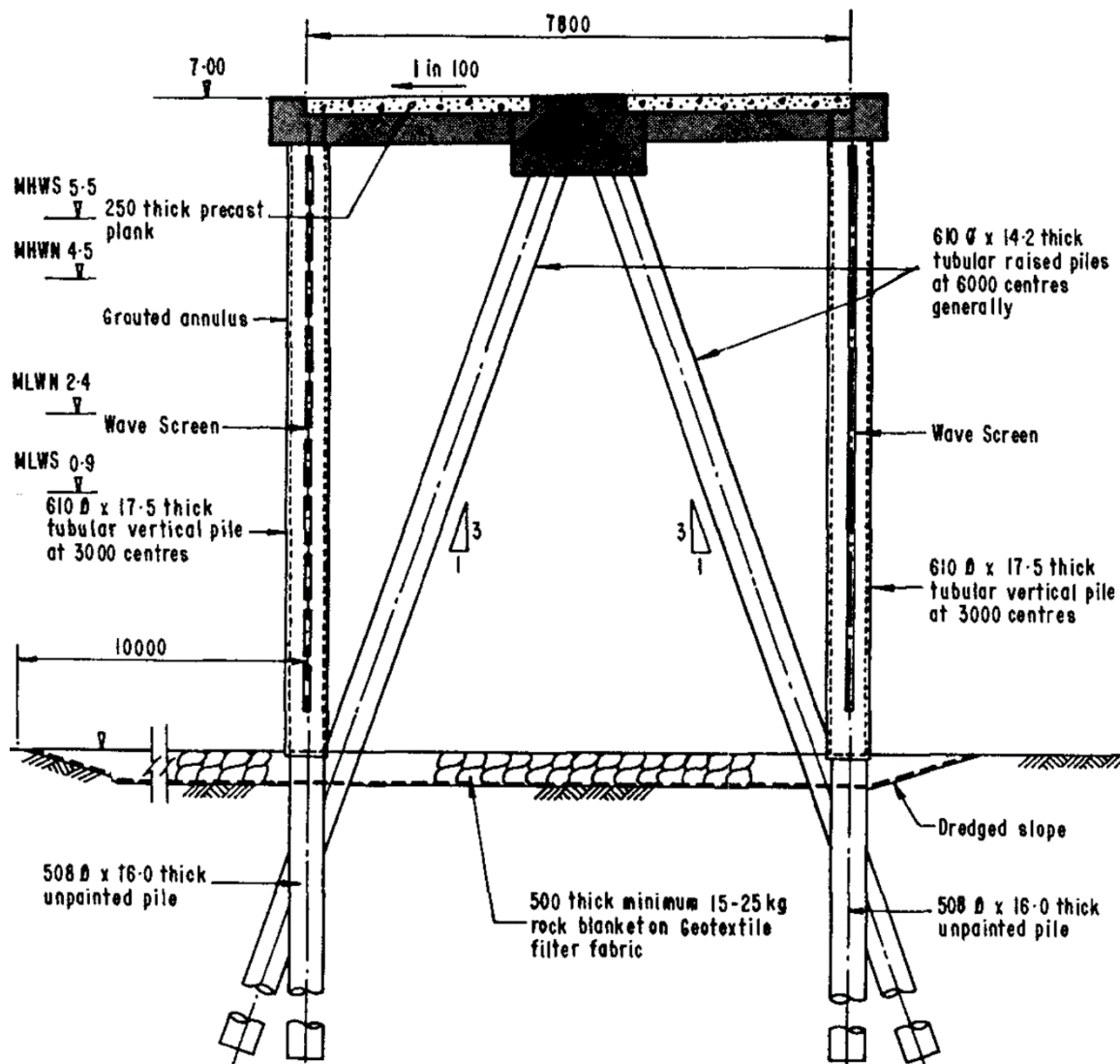


Fig. 2.3 Concept double screen breakwater Gardner et al. (1986)

Based on the model test results, a double screen slotted breakwater was proposed for the marina at Plymouth, England, by Gardner et al. (1986). The schematic section of the model is shown in Fig. 2.3. It was reported that the wave reflection from the breakwater was not affecting the navigation in the shipping channel.

Truitt and Herbich (1987) performed model studies for random wave transmission through pile breakwaters. The test was conducted for several cases with respect to different pile spacings and pile diameters. Hayashi et al. (1968) formulae were used to predict the transmission for model study and reached a good agreement with experimental results. Investigations were also carried out to know the influence of wave height and depth of water on wave transmission. It was stated that the model wave parameters were important variables on wave transmission, but breakwater geometry had an essential role in the transmission. It was concluded that more research is required on transmission through pile breakwaters in order to understand the influence of wave transmission.

Herbich and Douglas (1988) conducted a study on double row pile breakwaters and compared the results with single row pile breakwaters. The comparison showed that utilising the second row reduced the wave transmission up to 15% for relative pile spacing of $b/D = 0.2$ (where b is the spacing between piles, D is the pile diameter) and up to 10% for relative pile spacing $b/D = 0.1$. The effect of wave height, wave period, and water depth on the wave transmission was also investigated. It was observed that wave transmission increased for increasing water depth to wave height ratio (h/H) and increasing wave period (T), and wave transmission decreased with increasing wave steepness (H/L).

The wave transmission under monochromatic and random waves through a single row of pile breakwater was studied by Herbich (1990). The experimental results with random waves indicated that the relationship developed for monochromatic waves might be applicable to random waves. The study reported that the K_t under monochromatic waves increased with the wave period (T). The study also reported that for a 10% gap ratio, addition of the second row of piles reduced K_t by 5% to 10%.

Kakuno and Liu (1993) studied the dispersion of the waves passing through single row vertical cylinders. They have developed a theoretical method to solve the scattering effect of piles on water waves by modelling the flows near the piles. For the study, rectangular and circular piles were used. It was stated that the research conducted was reliable to limited cases and required further investigations on different cross-sections and wave characteristics.

Mani and Jayakumar (1995) conducted a study on wave transmission by single row suspended pipe breakwater, as shown in Fig. 2.4. The test was conducted with the spacing to diameter ratio of $b/D = 0.11$ to 1.0 and Y/h ($Y =$ draft of the pipe; $h =$ depth of water) ranging from 0.26 to 0.56 . It was observed that for relative clear spacing (b/D) of 0.22 , relative depth of submergence (Y/h) of 0.46 and wave steepness of (H_i/gT^2) 0.008 , a transmission coefficient of 0.5 could be achieved. The performance and cost of conventionally adopted pile breakwater (involving a row of closely spaced piles driven on the seabed) were compared with the suspended pipe breakwater. The comparison revealed that the present system could reduce the investment by about 40% to conventional pile breakwater for the same wave attenuation capacity.

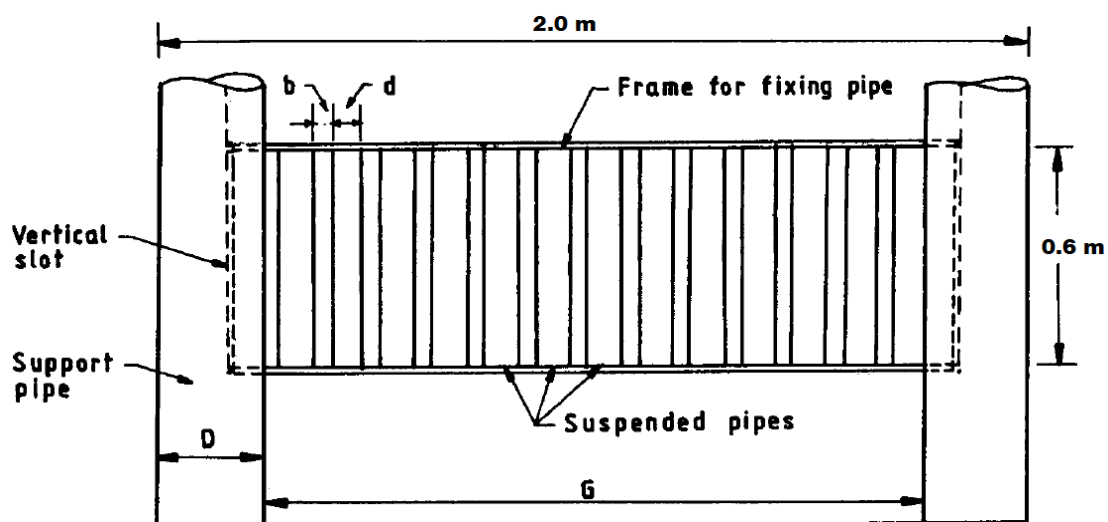


Fig. 2.4 Typical arrangement of suspended pipe breakwater (Mani and Jayakumar 1995)

Laboratory investigations on wave reflection characteristics of suspended perforated pipe breakwater were carried out by Rao and Rao (1999). From the investigations, it

was found that as the Y/h increased, the reflection also increased. Water depth had an insignificant effect on K_r . K_r increased as incident wave steepness increased. For perforated pipes, the size of the pipe had a negligible effect on K_r and the wave period alone did not directly influence the reflection.

Rao et al. (1999) conducted an experimental investigation on two rows of perforated and non-perforated piles to study their wave transmission characteristics. The typical arrangement of perforated pile breakwater considered for the study is shown in Fig. 2.5. It was reported that K_t decreased from 0.9 to 0.75, with increased incident wave steepness (H_i/gT^2) from 0.0006 to 0.01. It can be envisaged that for the change in B/D ratio (relative clear spacing between the pile rows) from 2 to 0.5 there is no significant change in K_t . 50% reduction in relative clear spacing between the piles (b/D) had decreased K_t by 7 to 10% only. Staggering of piles and depth of water has an insignificant influence on transmission coefficient for both perforated and non-perforated piles. It was observed that K_t decreased about 5% more than the pile without perforation (pile with 6.25% perforation) and a maximum of 10% at $b/D = 0.5$ and lower wave steepness ($H_i/gT^2 = 0.0006$).

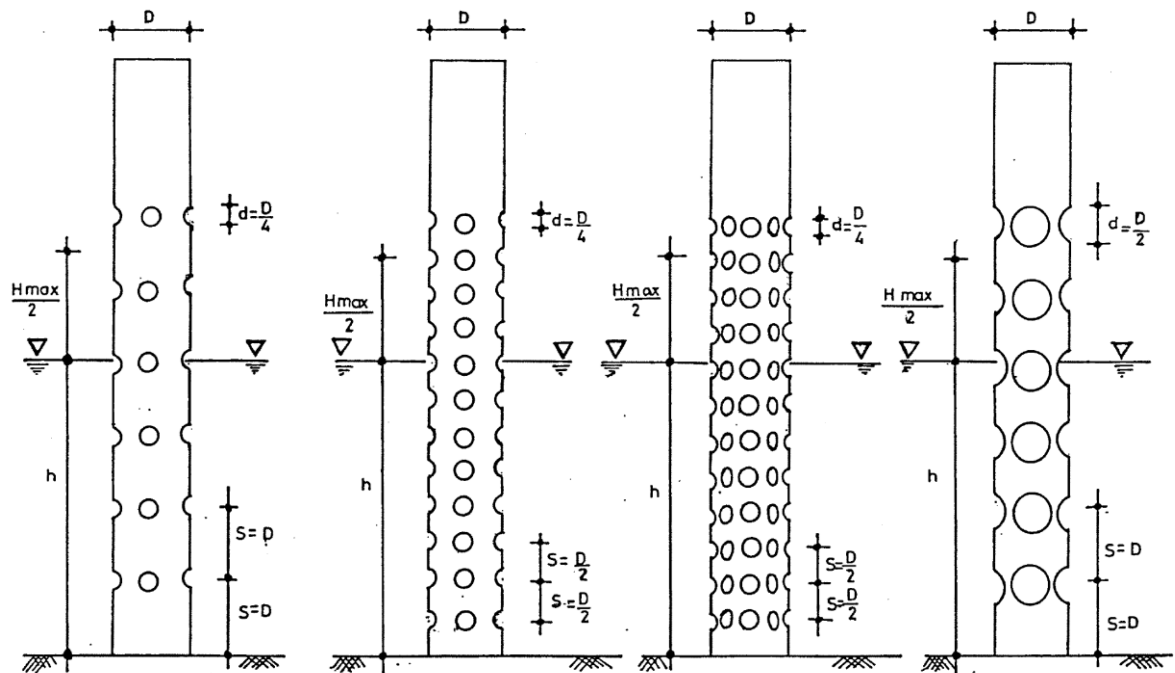


Fig. 2.5 Details of perforated pile breakwater (Rao et al. 1999)

Physical model studies were conducted on suspended perforated hollow cylinders pipes (Fig. 2.6), with a relative clear spacing of 0.15 (Rao and Rao 2001). The study focuses on the effect of incident wave steepness, the relative depth of submergence, size of pipes, percentage of perforations, size of perforations and depth of water on wave attenuation. From the investigations, it was found that as the depth of submergence increased K_t decreased. But beyond 50% of the depth of submergence, the decrease in K_t was negligible. It was also noted that K_t decreased as incident wave steepness increased. For perforated pipes, the size of the pipe had a marginal effect on transmitted wave characteristics. Perforated pipes with 25% of perforations were found to attenuate about 10% to 14% more wave energy than non-perforated pipes. The size of perforations did not have a significant effect on transmission for the same area of perforations.

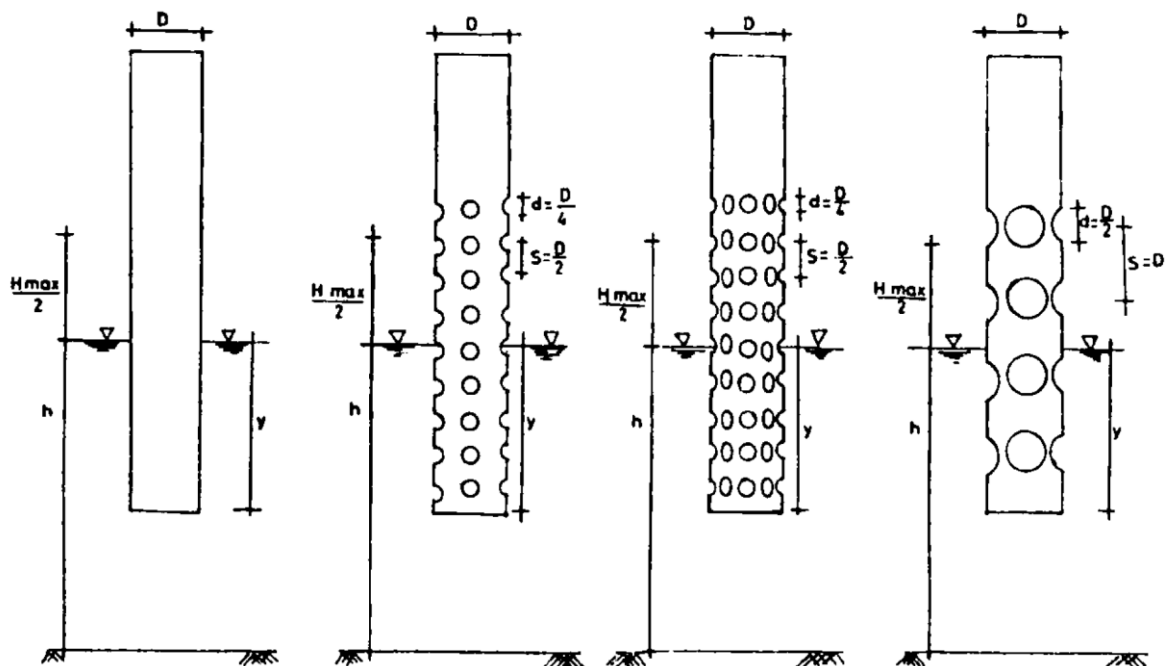


Fig. 2.6 Details of perforated pipe breakwater (Rao and Rao 2001)

Neelamani and Rajendran (2002) carried out an experimental investigation on partially submerged T-type breakwater (Fig. 2.7) under monochromatic and random wave conditions. It was concluded that T-type breakwater was best suited near deep water conditions. A comparison with the monochromatic and random wave conditions showed that the performance of T-type 20% better under random waves. When the T-

type breakwater was immersed about 7% of total water depth, the obtained value of K_t was less than 0.35 under normal and high wave energy input. Their study reported that the conceptual breakwater design was about 65% effective in dissipating the incident wave energy.

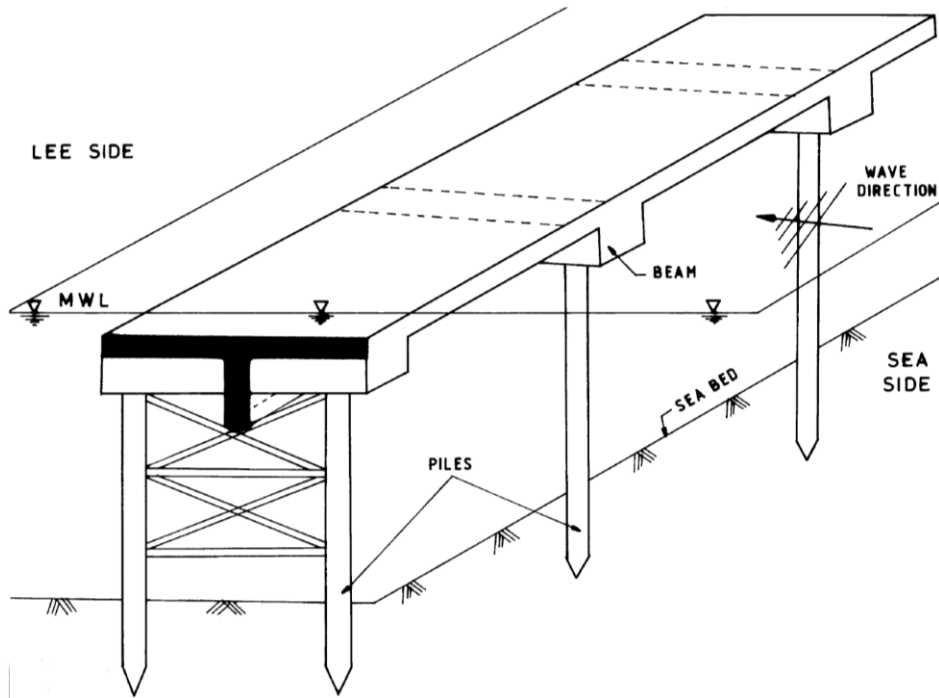


Fig. 2.7 Schematic view of T-type breakwater (Neelamani and Rajendran 2002)

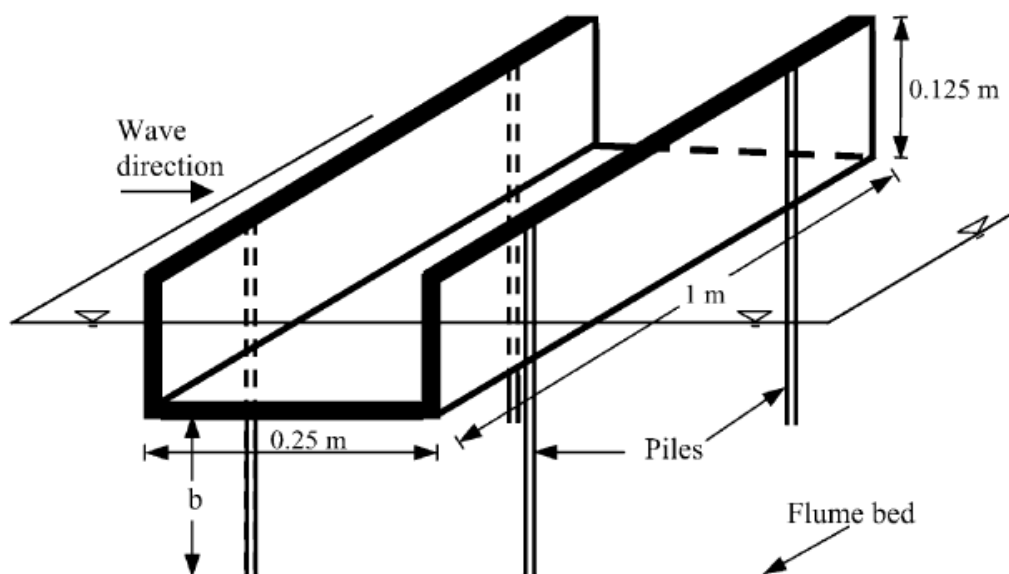


Fig. 2.8 Schematic view of U-type breakwater (Günaydin and Kabdaşlı 2004)

Günaydin and Kabdaşlı (2004) conducted experimental work on pile-supported perforated U-type breakwater under monochromatic and random wave conditions. The concept view of the breakwater is shown in Fig. 2.8. Results indicated that in general, K_t decrease with an increase in depth of immersion. The performance of the breakwater in random wave conditions was more (10% to 30%) than that of monochromatic wave conditions. Under the monochromatic wave conditions, the perforated U-type breakwater has showed an average of 12% decrease in K_t , 18% decrease in K_r , and 4% increase in K_d compared with the non-perforated model. But in the case of monochromatic wave conditions, 4% decreases in K_t , 20% decreases in K_r and 4% increase in K_d was observed.

Analytical and experimental studies on single and two rows of pile-supported skirt breakwater were conducted by (Laju et al. 2005, 2011). The performance of double skirt breakwater was better (15% to 20%) than single skirt breakwater in attenuating the waves. The results showed that the wave transmissibility was dependent on the maximum submergence of either the front or rear skirt, whereas, the reflection was found to depend on the submergence of the front skirt. The study recommended a relative spacing (B/h , where B was spacing between pile rows and h was water depth) equal to 1 for better performance. It was reported that the numerical solutions proposed were well matching with the experimental results.

Mani (2009) conducted numerical and experimental investigations on the performance of zigzag porous screen breakwater. Zigzag porous screen breakwater can attenuate incident waves by 50% for $H_i/gT^2 > 0.008$, and the results observed are not different from that of pile-supported pipe breakwater (Mani and Jayakumar 1995).

Laboratory experiments on pile-supported vertical wall breakwater were carried out by Suh et al. (2006) under monochromatic and random wave climates. The concept breakwater is shown in Fig. 2.9. The experiments were conducted for a constant spacing of piles with a varying draft of the upper vertical wall such that the height of the wall provided was enough to prevent overtopping. Results indicated that with an increase in the draft of the upper vertical wall, the transmission coefficient decreased, and the reflection coefficient increased. Hence, smaller K_t and larger K_r were normal and more

likely to occur in pile-supported vertical wall breakwaters than compared with the curtain wall or pile breakwaters. The mathematical model developed by Suh et al. (2006) was modified by Suh et al. (2007) to suit circular pile breakwaters. Results indicated that with increased porosity between the piles, K_t increased, and K_r decreased.



Fig. 2.9 Lee side view of pile supported vertical wall breakwater (Suh et al. 2006)

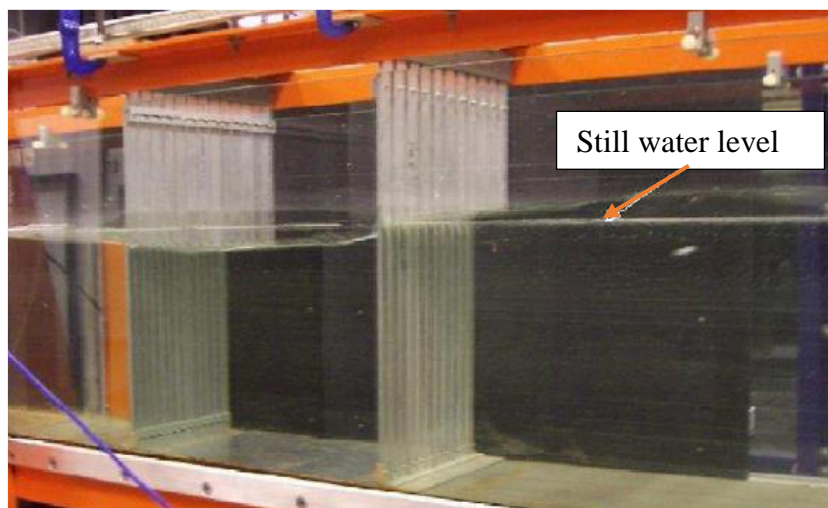


Fig. 2.10 Wave interaction with closely spaced rectangular cylinders (Huang 2007)

Huang (2007) conducted experimental work on closely spaced rectangular piles with one and two rows of configurations (Fig. 2.10). The study reported that with an increase

in wave height, K_t decreased, and K_r increased. In the case of double row configuration, K_t was insignificantly affected by the width of the chamber (spacing between the piles). Huang (2007) also developed a linear wave solution for the preliminary design of single or double slotted breakwaters.

A comprehensive experimental work was conducted on slotted wave screen breakwater made of circular elements of diameter 0.05 m and spaced at 0.015 m apart. The experiments are carried on monochromatic wave conditions with single and double layer configurations. The typical configuration of the wave screen is as shown in Fig. 2.11. From the experiments conducted on single layer screen breakwater, Krishnakumar et al. (2010) concluded that K_t increases with the decrease in relative depth of submergence due to decrease in blockage effect of wave screen. For h/L of 0.18 to 0.6 range of increase in K_t is found to be 10% to 15%. At the same time, K_r decreased with the decrease in relative depth of submergence in the range of 30% to 60%.

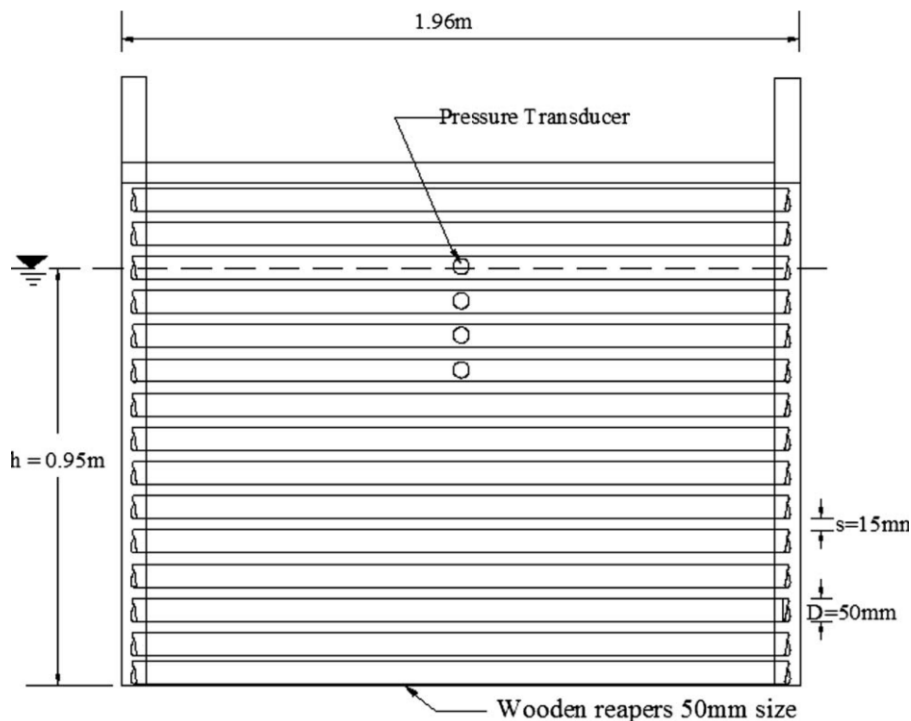


Fig. 2.11 Typical arrangement of wave screen breakwater (Krishnakumar et al. 2010)

An experimental and theoretical study on the hydraulic performance of horizontally slotted pile-supported breakwater under monochromatic wave conditions was undertaken by Rageh and Koraim (2010). The concept breakwater is shown in Fig. 2.12. The study concentrated on finding the effect of structural parameters (draft of upper part of the structure and porosity of lower part) under different wave climates. It was concluded that with an increase in upper draft and decrease in lower part porosity, K_t decreased while K_r flowed the opposite trend. For the relative wavelength (h/L) of 0.3, relative upper draft greater (Y/h) than 0.5 with lower part porosity less than 0.5, the model gives K_t less than 0.5 and K_r greater 0.5. It was also noted that the model could dissipate more than 50% of incident wave energy for the relative wavelength in the range of 0.25 to 0.35.

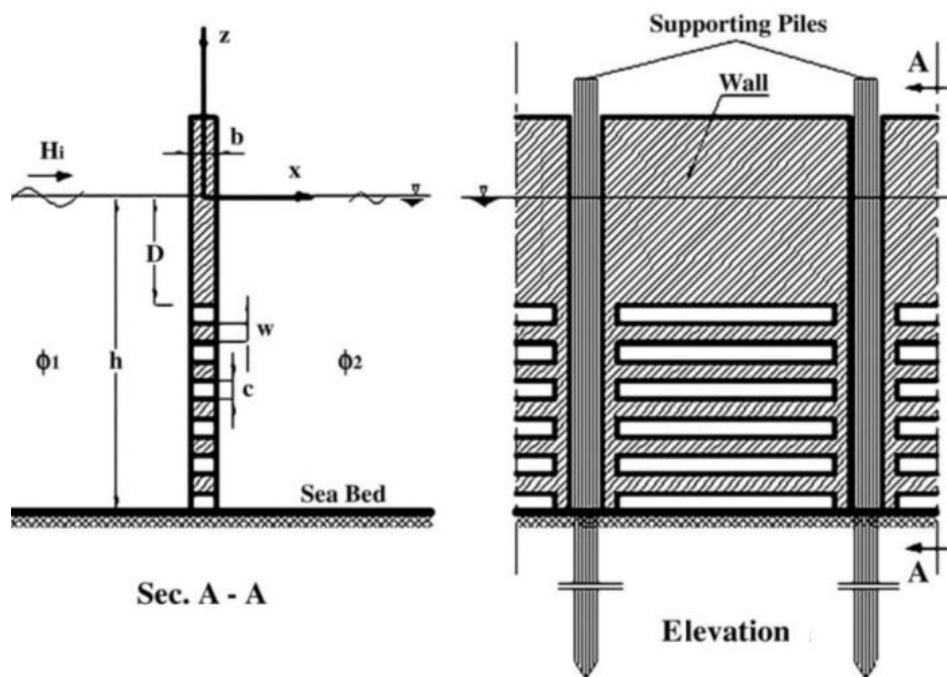


Fig. 2.12 Horizontal slotted pile-supported breakwater Rageh and Koraim (2010)

Zhu (2011, 2013) worked on the analytical method to study the interaction of monochromatic plane waves with a row of rectangular piles and compared the results obtained from laboratory experiments conducted by other authors (Hagiwara 1984; Isaacson et al. 1998a; Kakuno et al. 1996; Kakuno and Liu 1993). It was concluded that the present model provided adequate estimations of the coefficients of transmission, reflection and total energy loss coefficients (or dissipation coefficients, K_d) and wave

forces. Also showed that the K_t decreased with increased wave frequency and the net wave force increased with increased wave frequency.

Suh et al. (2011) proposed a new (hybrid) solution developed by Kim (1998) for single row vertical slotted barriers with square piles. New solutions were proposed based on the fundamental fluid mechanics and empirical formulas in a hybrid form. It was stated that the suggested solutions in the literature to predict the wave transmission underestimate the wave transmission for lower wave steepness ranges. Comparison between experimental results on K_t and K_r with that obtained values from the hybrid solutions showed that results are in concurrence with the experimental data. It was concluded that the hybrid method could also be applied to the circular pile breakwaters.

A two-row perforated double ring pile type breakwater was conceptualised by Anuar and Sidek (2012). Experiments conducted revealed that, as h/L increased from 0.1 to 0.35 at constant porosity of 0.0625, K_t decreased from 0.9 to 0.6 at 0.35 m depth of water (h) and 0.3 to 0.25 at 0.19 m depth of water. The height of the structure considered for the experiments was 0.25 m, thus indicating fully submerged condition had higher wave transmissions than the partially submerged ($h \leq 0.27$ m). It was shown that as the perforation increased from 0.0625 to 0.48, wave transmission increased from 0.29 to 0.69 with in a H_i/L range between 0.012 and 0.026. Hence, the K_t increased in the order of 30% to 35%. With increased number of rows from one to two, K_t decreased by 15% to 20% at H_i/L , ranging between 0.015 to 0.02. Similarly, with an increased number of rows from two to three, K_t decreased by 7% to 10% at a similar range of H_i/L . Hence, proving an increase in the rows of piles had little effect on wave transmission.

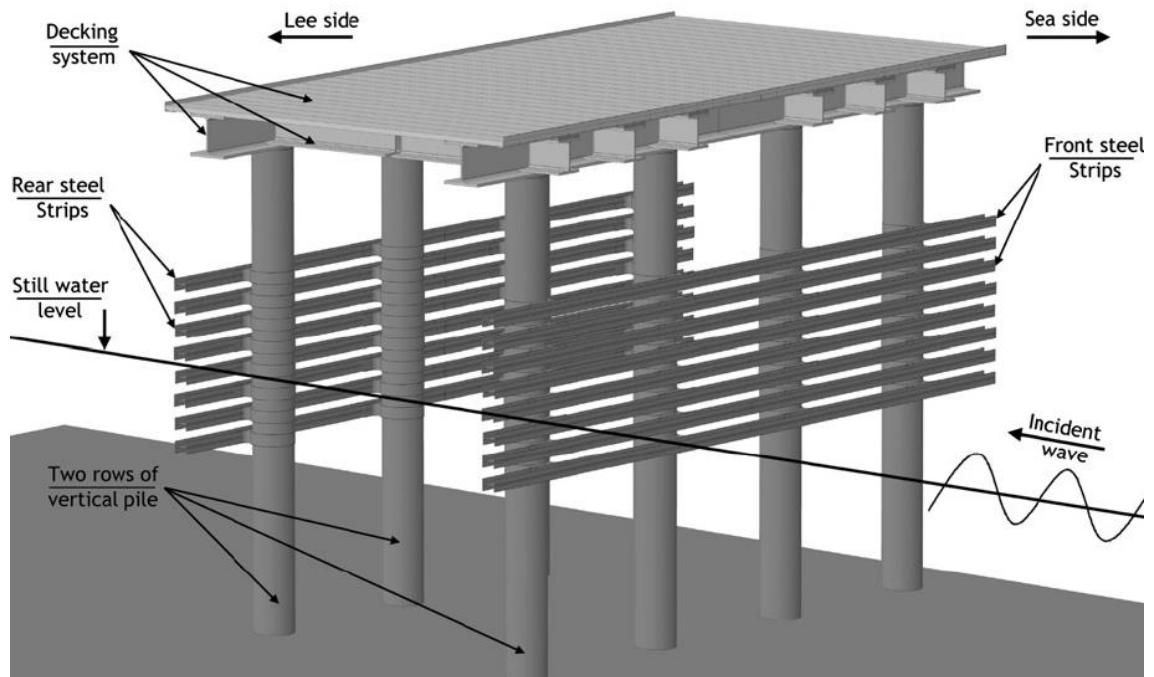


Fig. 2.13 Model view of double porous curtain wall breakwater (Elsharnouby et al. 2012)

Elsharnouby et al. (2012) proposed a double porous curtain wall breakwater made of horizontal steel plate attached to the pile (refer Fig. 2.13) for North-Western Coast of Egypt. The suitability of the proposed breakwater is analysed using a Flow-3D numerical model for the actual wave and bathymetry condition of the region. Results showed that the proposed model could protect the shoreline without any adverse effects.

Theoretical and experimental model studies were conducted to assess the performance of double rows of piles with suspended horizontal C-shaped bar (refer Fig. 2.14) under monochromatic waves. The influence of the ratio of water depth to the wavelength (h/L), pile diameter to the water depth (D/h) and row distance to the water depth (B/h) was investigated by Koraim et al. (2014). The theoretical model over predicted the K_t and under predicted the K_r with an accuracy of $\pm 10\%$ to that of experimental results. As the porosity of the C shaped bar (ϵ_s) increased from 0 to 0.5, K_t increased to 0.5 from 0.2 and the reflection coefficient decreased from 0.76 to 0.52.

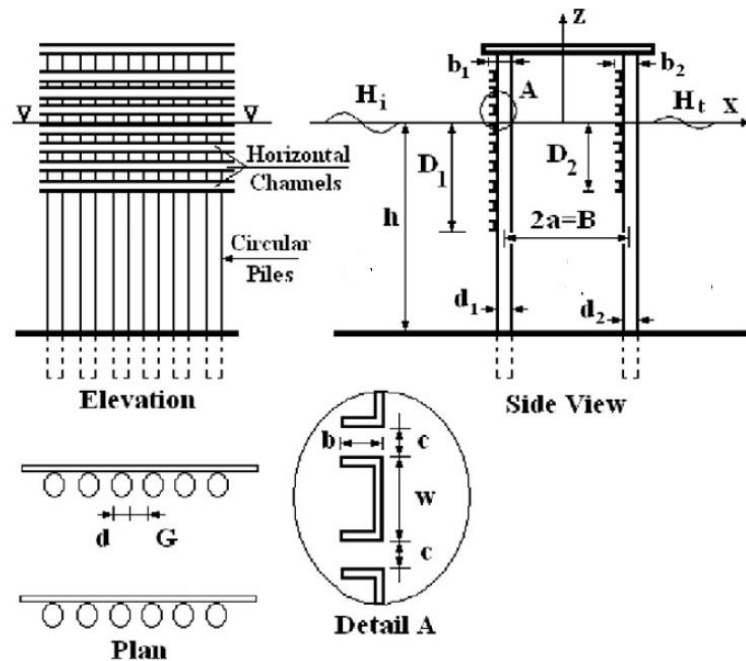


Fig. 2.14 Typical arrangement of C shaped screen type breakwater (Koraim et al. 2014)

From the graph presented in the literature (Koraim et al. 2014), it can be envisaged that, for increased value of d/h (0.078 to 0.156) K_t value decreased from 0.6 to 0.4 and K_r followed the reverse trend (i.e. from 0.4 to 0.6) when tested for $\epsilon_s = 0.5$, $Y/h = 0.5$, $B/h = 1.25$ and $D/h = 0.125$. The increased relative span between the two rows of piles (B/h) from 0.63 to 1.88, as observed from the graph presented in the literature, had no effect on K_t . But K_t decreased from 0.9 to 0.44 with increased h/L (0.08 to 0.35) and K_r showed erratic variation, which exhibited many peaks and troughs at different values of h/L depending on B/h .

Koraim (2014) conducted experimental and theoretical studies to appraise the hydraulic performance of single rows of piles with suspended horizontal L-shaped bars under normal monochromatic waves. The investigation focused on finding the effect of wavelength, L-shaped bars part draft (D), porosity, a clear distance of supporting pile and diameter on hydrodynamic characteristics. Also developed the theoretical model based on an Eigen Function, Expansion Method and a Least Square Technique to study the hydrodynamic performance of breakwater. The K_t and K_r calculated by the theoretical model were in line with the experimental results with a maximum error of $\pm 10\%$ when the upper and lower friction factors are $f_U = 1.25$ and $f_L = 0.75$. For the test

condition of $c/w = 1$, $b/d = 1$, $d/h = 0.06$ and $f_U = 1.25$, K_t decreased from 1 to 0.7 for increased h/L (0.08 to 0.518) and D/h (0.1 to 1). Effect of L shaped bar porosity (c/w) and pile spacing ratio (G/d) were tested by keeping $D/h = 0.5$, $b/d = 1$, $d/h = 0.06$ and $f_U = 1.25$. Results showed c/w had a little to no effect on K_t at h/L is 0.05 to 0.4, but when $h/L = 0.5$, K_t increased from 0.52 to 0.72 for $c/w = 0$ to 1, while K_r decreased to 0.4 from 0.5. K_t increased from 0.5 to 0.85 at $h/L = 0.5$ for increased b/d (0.33 to 5) at $h/L = 0.5$.

Wave damping performance of the pile-supported arc and horizontal plate type breakwater is assessed through physical experiments under monochromatic wave conditions. The typical arrangement of the breakwater is shown in Fig. 2.15. Wang et al. (2016) confirmed that the performance of arc plate type breakwater is better than the horizontal type of breakwater. The K_t of arc type plate breakwater decreases by about 15% to 50% and K_r by 5% to 60% to horizontal type plate breakwater. The study also stated that relative width, height, gap and amount of arc in the plate are the important parameter influencing the K_t and K_r .

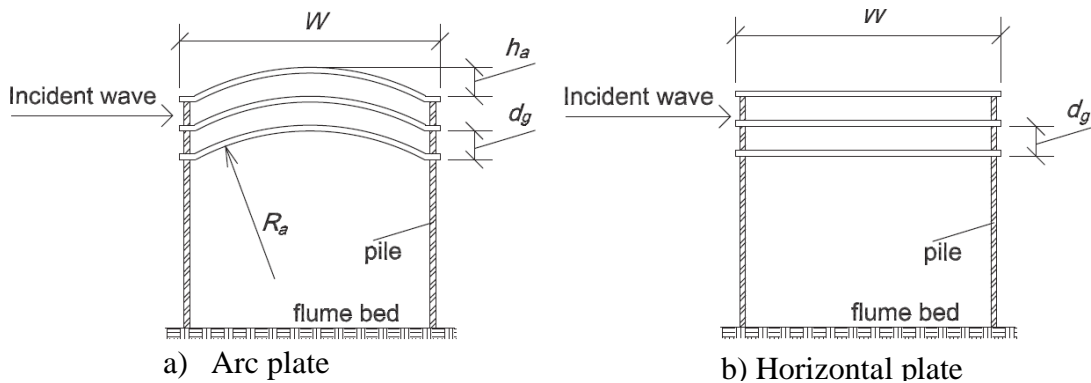


Fig. 2.15 Details of arc and horizontal plate breakwater (Wang et al. 2016)

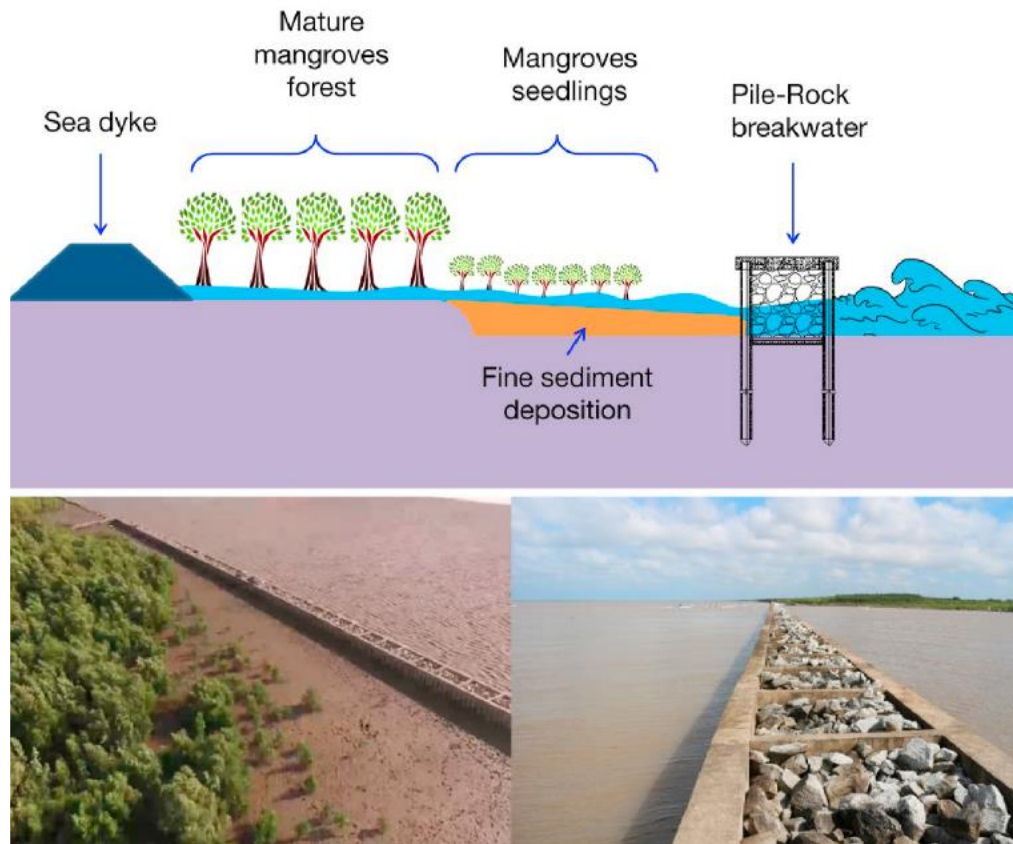


Fig. 2.16 View of pile rock breakwater (Le Xuan et al. 2020)

Pile-rock breakwater (PRBW) was constructed to protect the coast along of Mekong Delta in southern Vietnam. The efficiency of PRBWs was tested by a physical model studies and the performance was verified through field study. It was reported that the results of the experimental investigation matched well with the field observation made. The concept of the breakwater is shown in Fig. 2.16. Le Xuan et al. (2020) reported that even after a decade of installation, PRBWs showed a significant performance in reducing the impact of waves to protect and rejuvenate the mangroves forest. PRBW has a small transmission coefficient (K_t) in the range of 0.3 to 0.4 and reflection is noticeably high ($K_r = 0.45$ to 0.6). It was also stated that PRBWs have more advantages than the conventional type of breakwater due to their increased potential to combat erosion and stability.

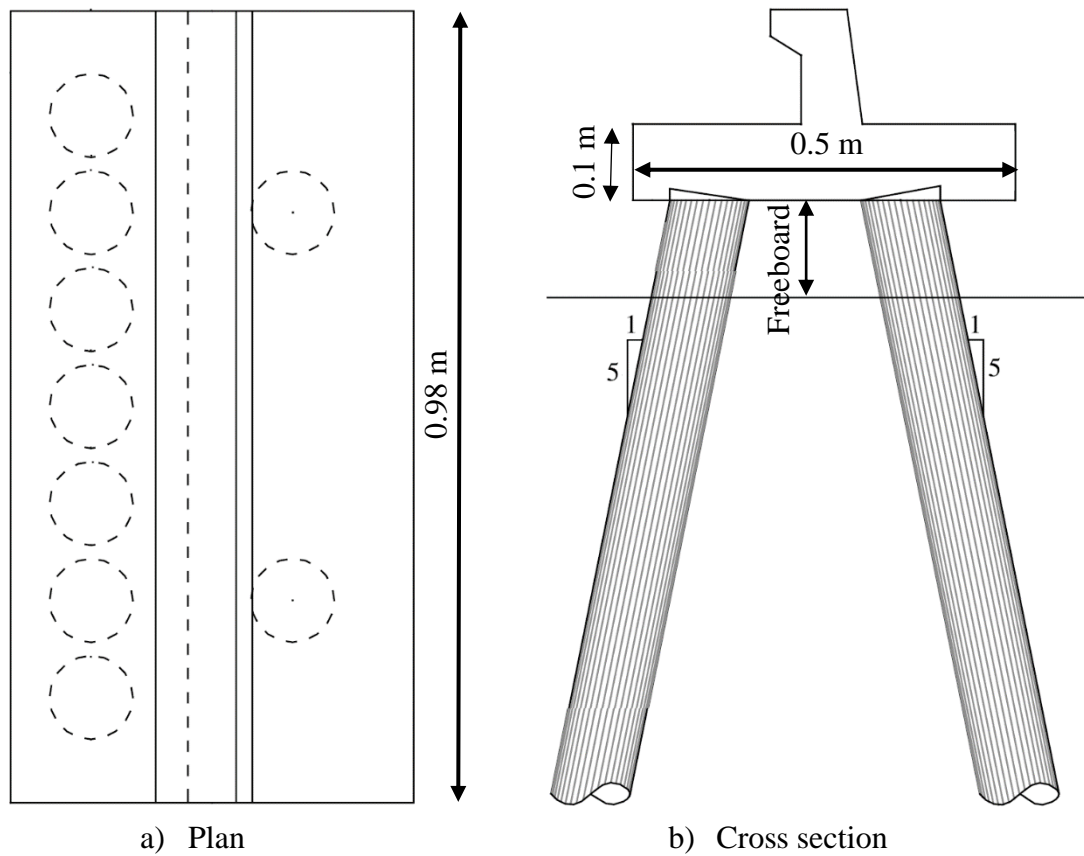


Fig. 2.17 Pile breakwater model (Yagci et al. 2006)

Pile type breakwaters have been constructed worldwide due to their unique preference over the conventional rubble bound breakwater. Yagci et al. (2006) proposed a closely spaced racker pile breakwater in two rows, as shown in Fig. 2.17. The experimental investigation as conducted by Yagci et al. (2006) was extended by Mojtahedi et al. (2020) by replacing circular-shaped piles with square-shaped piles under monochromatic and random wave conditions. Mojtahedi et al. (2020) first conducted experiments on rectangular shape monopiles to optimize the shape and orientations and extended the same to model pile breakwater. The study concluded that K_r increased by about 7% to 30% for the change in the shape of pile from circular to square cross-section.

Ramnarayan et al. (2020) investigated the hydrodynamic characteristics of pile-supported breakwaters (PSB) (refer Fig. 2.18) under the monochromatic waves. Vertical face type (VW), Galveston wall Shape (GS) and Circular-cum Parabola Shape (CPS) profile were selected for the investigation. Pile breakwater with GS showed the

least K_t value (0.04 to 0.53) and K_r (0.17 to 0.72) than the other two models. Hence it was confirmed that, among the considered models, CPS's hydrodynamics characteristics stands higher due to the least K_t and K_r with high energy dissipation coefficient ($K_d = 0.7$ to 0.95).

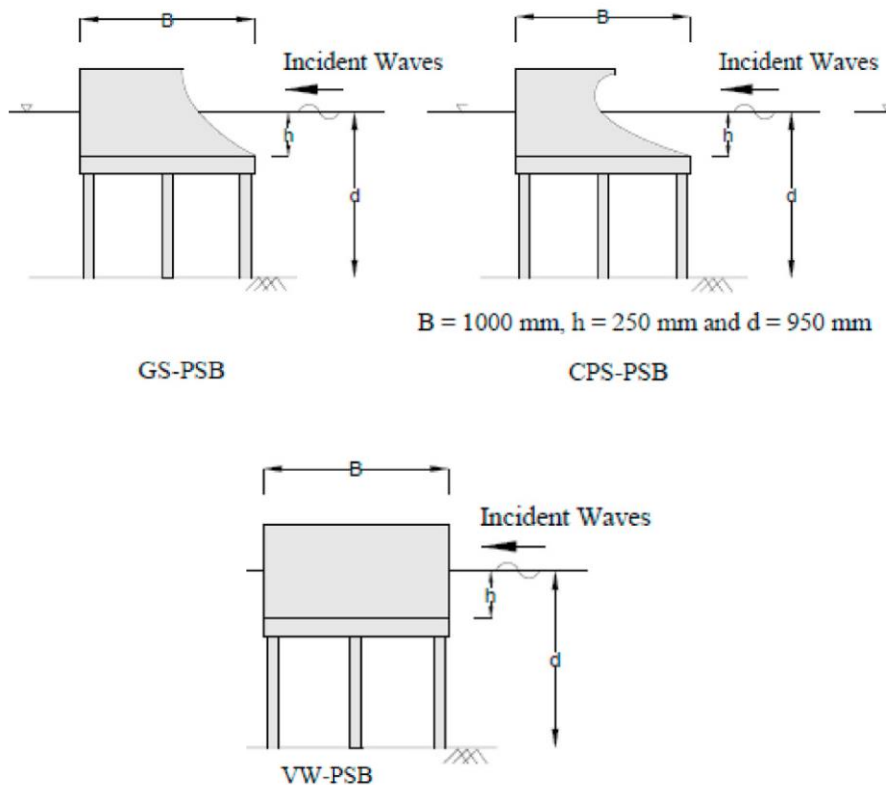


Fig. 2.18 Schematic sketch of the pile-supported breakwater (Ramnarayan et al. 2020)

2.3 HYBRID THEORETICAL MODEL

Various researchers developed theoretical solutions for computing the hydraulic performance of regular non-perforated pile breakwater (Mei 1989; Kakuno and Liu 1993; Park et al. 2000; Suh et al. 2011, 2002) are explained below. In the present study, a hybrid solution developed by Suh et al. (2011) for the non-perforated pile is improved by reconstructing the empirical coefficient and validating the same based on the current experimental data. The potential of the modified hybrid solution for non-perforated conventional pile breakwater is also verified by using Rao (1999) experimental data.

It is noted that introducing the perforations will increase the hydraulic efficiency of the pile breakwater (Rao and Rao 2001, 1999; Terrett et al. 1968). The literature review indicated that no theoretical or hybrid equations are available to predict the hydraulic efficiency of perforated enlarged pile breakwater. Hence, in the present study, an attempt is made to develop an hybrid equation to predict the coefficient of K_t , K_r and K_d for perforated pile breakwater.

2.3.1 Theoretical background

The typical arrangement of enlarged pile head breakwater is shown in Fig. 2.19 in which, h is the still water depth, $2A$ is the centre to centre distance between the pile heads, b is the clear spacing between the pile heads, D is the diameter of the pile head and Y is the height of the pile head.

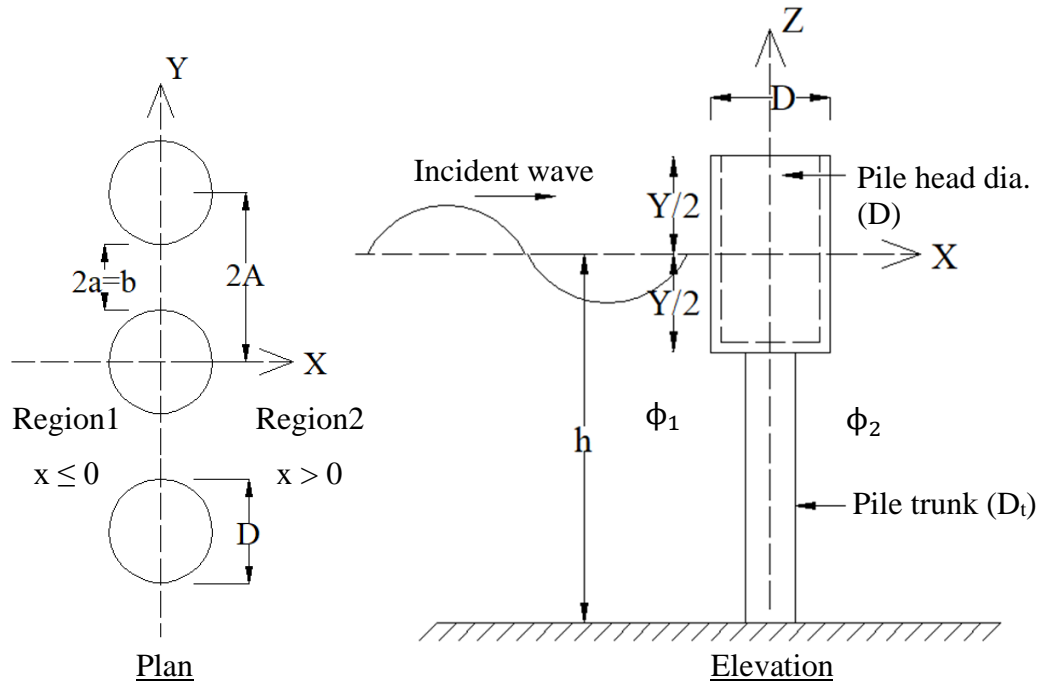


Fig. 2.19 Typical arrangement of enlarged pile head breakwater

For the monochromatic wave propagating over a constant water depth, the velocity potential function $\phi(x, y, z, t)$ for incompressible and irrotational flow motion can be expressed as (Isaacson et al. 1998; Suh et al. 2006, 2011)

$$\phi_n(x, y, z, t) = \text{Re} \left\{ -\frac{igH_i}{2\omega} \phi(x, y) \left(\frac{\cosh[k(h+z)]e^{-i\omega t}}{\cosh(kh)} \right) \right\}, \quad n = 1, 2 \quad (2.1)$$

Where $n = 1, 2$ refer to the wave region 1 and 2 respectively, Re symbolises the real part of a complex value, $i = \sqrt{-1}$, g is the gravitational acceleration, ω is the angular frequency and k is wave number.

Boundary conditions:

$$\frac{\partial \phi_n}{\partial z} = 0, \text{ at } z = -h \text{ (at seabed) } n = 1, 2 \quad (2.2)$$

$$\frac{\partial \phi_n}{\partial z} = \frac{\omega}{g} \phi_n, \text{ at } z = 0 \text{ (at free surface)} \quad (2.3)$$

$$\frac{\partial \phi_1}{\partial x} = \frac{\partial \phi_2}{\partial x}, \text{ at } x = 0 \text{ (at pile)} \quad (2.4)$$

Considering wave propagating in region two as shown in Fig. 2.19, the solution for $\phi_n(x)$ in each region may be constructed as (Park et al. 2000; Suh et al. 2006, 2011)

$$\phi_1(x) = e^{ikx} + K_r e^{-ikx} \quad x \leq 0 \quad (2.5)$$

$$\phi_2(x) = K_t e^{ikx} \quad x > 0 \quad (2.6)$$

Dynamic equations for pressure are obtained by applying moment conservation in the vicinity of the cylindrical gap to a controlled volume and expressed as

$$\frac{p_2}{\rho} - \frac{p_1}{\rho} + \frac{f}{2} u|u| + \int_1 \frac{\partial u}{\partial t} dl = 0 \quad \text{at } x = 0 \quad (2.7)$$

Where p_1 and p_2 are the pressure in the region 1 and 2 respectively and u is the velocity away from the pile.

$$u = \epsilon u_0 \quad (2.8)$$

u_0 is the velocity at the gap of piles and f is the head loss coefficient. For circular pile, f is evaluated as (Park et al. 2000)

$$f = \left(\frac{1}{\bar{\epsilon} C_c} - 1 \right)^2 \quad (2.9)$$

Spatial variation of porosity is calculated as $\bar{\epsilon}$

$$\bar{\epsilon} = \frac{1}{D} \int_{-\frac{D}{2}}^{\frac{D}{2}} \frac{dx}{[r(x)]^2} \quad (2.10)$$

$$r(x) = 1 - \frac{\sqrt{\left(\frac{D}{2}\right)^2 - x^2}}{\frac{D}{2} + a} \quad (2.11)$$

Contraction coefficient (C_c) is calculated empirically as per Mei (1989)

$$C_c = 0.6 + 0.4\epsilon^2 \quad (2.12)$$

Where,

$$\epsilon \text{ is the porosity} = \frac{a}{A} \quad \text{at } x = 0 \quad (2.13)$$

In Eq. (2.7), l is the length of the jet flowing through the gap between the piles and represents the inertial resistance at the barrier. This parameter is calculated as per Suh et al., (2002).

$$l = 2C \quad (2.14)$$

As per Kakuno and Liu (1993), blockage coefficient (C) for circular piles is obtained as

$$C = \frac{\pi}{2} A(1-\epsilon)^2 \frac{1}{1-\xi} \quad (2.15)$$

$$\xi = \frac{\pi^2}{12} (1-\epsilon)^2 \quad (2.16)$$

Expressing, $p = \rho \left(\frac{\delta\phi_n}{\delta t} \right)$ dynamic wave pressure and $u = -\frac{\partial\phi}{\partial x}$ and linearising the nonlinear energy dissipation term in Eq. (2.7) by $\frac{f}{2} u|u| = \beta u$.

Rewriting the Eq. (2.7) (Suh et al. 2002)

$$\phi_2 = \phi_1 + \left(\frac{i\beta}{\omega} + 1 \right) \frac{\partial\phi}{\partial x} \quad \text{at } x = 0 \quad (2.17)$$

Expressing the coefficient of transmission and reflection as

$$K_r = a_0 + ib_0 \quad (2.18)$$

$$K_t = c_0 + id_0 \quad (2.19)$$

The equation for transmission and reflection coefficient is obtained by substituting Eq. (2.18) and Eq. (2.19) in Eq. (2.5) and Eq. (2.6) respectively and applying matching conditions as per Eq. (2.4) and Eq. (2.17) (Park et al. 2000; Suh et al. 2011).

$$K_r = \frac{R(R+2)+Q^2}{(R+2)^2+Q^2} - i \frac{2Q}{(R+2)^2+Q^2} \quad (2.20)$$

$$K_t = \frac{2(R+2)}{(R+2)^2+Q^2} + i \frac{2Q}{(R+2)^2+Q^2} \quad (2.21)$$

Where $Q = lK$ and $R = \frac{\beta K}{\omega}$.

As per Suh et al. (2011) hybrid solution, the value of β (Linearised friction coefficient) is obtained as

$$\beta = \frac{\omega D \gamma}{\epsilon} \quad (2.22)$$

Where γ is the friction coefficient and is calculated empirically as given by Suh et al. (2011)

$$\gamma = 0.0584 \left(\frac{\epsilon b}{h} \right)^{-0.7} \quad (2.23)$$

2.4 NUMERICAL MODELLING

Afshar (2010) worked on numerical wave generation using OpenFOAM® software. For the wave generation relaxation technique was used. The experiments suggested that the outgoing waves got absorbed efficiently when the damping relaxation zone was at least three wavelengths, and one wavelength extension was sufficient for the wave generating zone. The study also showed that grid resolution was highly dependent on the wave steepness. The steeper the wave, the higher was the number of grids required per wavelength.

Numerical investigation of the interactions between solitary wave and pile breakwaters using Bhatnagar–Gross–Krook (BGK) based methods were undertaken by Liu et al. (2011). The K_t and K_r as obtained numerically were compared with the experimental data, which yielded no variation when the ratio of wave height to water depth was small (i.e. $H/h < 0.20$). As this ratio exceeded the value of 0.20, the numerical model underpredicted the K_t by 20% to 25%, whereas, K_r overestimated by 50%. The numerical and experimental results indicated that the transmission of solitary waves decreased by 22% to 16%, and reflection increased by 60% with a 13.33% reduction in gaps between the adjacent cylinders. It was also observed that both K_t and K_r were not very sensitive to the variation in wave height.

A good alternative to physical modelling in civil engineering was explored by Kamath (2012), through the testing of numerical wave tank features of the open-source Computational Fluid Dynamics (CFD) package REEF3D. Two tasks were set to achieve the objectives. First, validation of the numerical wave tank and test its performance under different numerical and wave parameters. Second to use the wave tank to calculate wave forces on a structure and validate the numerical solution. This work was limited to calculating a simple case of non-breaking wave forces on a single cylindrical pile in a rectangular wave field. Running more complex cases would require more time in terms of man-hours for coding and testing of package and computational time to carry out the numerical experiment. The validation of the numerical wave tank was carried out by comparing the numerical results generated with the analytical values obtained using wave theory. Various parameters such as grid cell density, time step

size, numerical beach width, relaxation methods for wave generation and absorption and discretization schemes were tested. In addition, the performance of the wave tank at different amplitudes and wave types was observed. Wave force calculated by the model were compared with the theoretical value obtained by using the Morison equation. Results indicated that for the coarse grid (grid size 0.05 m) and for the fine grid (0.025 m), 25% and 30% deviations were obtained with reference to the theoretical value.

Wroniszewski et al. (2014) used OpenFOAM® to solve the Navier-Stokes equation to simulate solitary wave propagation and runup on beaches. The Navier-Stokes solvers are based on finite volume discretization and free surface capturing techniques, where a solid body immersed in the field is based on the volume of fluid method. Alternatively, the presence of such a body can be modelled with source terms in the governing equations, as in the immersed boundary method. Such methods largely reduce the meshing effort in cases involving complex geometries and give good prospects for simulations of moving bodies.

Numerical simulation to determine the wave force on a row of cylinders using open-source CFD model REEF3D was attempted by Kamath et al. (2015). REEF3D was used to simulate the interaction of low steepness linear waves and high steepness 5th-order Stokes waves with a single cylinder and linear arrays of two, three, four and five large cylinders. From the study, it was concluded that the diffraction effects were stronger for incident waves of higher steepness, resulting in significantly lower forces on the downstream cylinders in comparison to the incident wave of lower steepness. It was observed that wave force on the first cylinder increased to $1.25F_0$ (where F_0 is the wave force on the cylinder without any downstream cylinder) with one downstream cylinder, it increased to $1.53F_0$ with the addition of four downstream cylinders. This indicated that the wave force on the first cylinder in the array increased with the increased number of downstream cylinders, but the rate of increment was reduced with every additional downstream cylinder. The computed wave force on the 5th cylinder was observed to be $0.57F_0$ and hence, experienced the least force in the cylinder array.

Aggarwal et al. (2016), conducted a numerical study on wave forces on a large vertical circular cylinder subjected to random waves. In the study, JONSWAP spectrum was used to generate random waves. The wave force calculated numerically was compared with the theoretical forces, calculated using the MacCamy-Fuchs equation and Morison equation. It was stated that for the higher wave steepness MacCamy-Fuchs theory over predicts the magnitude of wave forces approximately by 9%. It was observed that the variation in the wave force calculated by numerical wave tank in comparison with theoretical wave force is less than 1.5%.

The performance of different wave generation and absorption methods available in the CFD based REEF3D software is evaluated by Miquel et al. (2018). REEF3D solves the Reynolds-averaged Navier–Stokes (RANS) equations to simulate two-phase flow problems. The free surface is computed using the level set method (LSM) and $k-\omega$ model is employed for turbulence modelling. The different methods available in the REEF3D for generating and absorbing the waves are relaxation, Dirichlet and active wave absorption. The wave reflections without any structures in the Numerical Wave Tank (NWT) were studied for six different types of incident waves considering, linear, second and fifth-order Stokes waves, solitary waves, cnoidal waves and random waves. Further, Wave breaking over a sloping bed, wave forces on a vertical cylinder, influence of the reflections on the wave breaking location and the wave forces on the cylinder were investigated. Comparison with another open-source CFD code OpenFOAM® was also carried out based on published results by Higuera et al. (2013). Overall, the active wave absorption method was found to be more efficient for long waves, whereas, the relaxation method performed better for shorter waves. The relaxation method-based numerical beach generally resulted in lower reflected waves in the NWT for most simulated cases. The comparably better performance of the relaxation method comes at the cost of higher computational requirements due to the relaxation zones that have to be included in the domain.

Aggarwal et al. (2018) investigated the capability of the REEF3D software on free surface reconstruction by using theoretical and experimental data. The free surface was reconstructed by spectrally decomposing the irregular wave train as a summation of the harmonic components in coupling with the Dirichlet inlet boundary condition at wave

generation. The applicability of the proposed approach to generate irregular waves by reconstructing the free surface was investigated for different coastal and ocean engineering problems. The wave parameters such as amplitude, wave frequency and wave phases were modelled with good accuracy in the time domain. The proposed approach on irregular wave generation was also employed to model steep irregular waves in deep water. Further, the irregular wave forces on a monopile were also investigated and found that the amplitudes and phases of the wave force signal under irregular waves were accurately modelled in the time domain. The proposed approach on reproducing the free surface elevation numerically using REEF3D provided accurate results for all the benchmark cases studied.

The numerical performance of the different wave modelling techniques in the REEF3D software is analysed by Wang et al. (2020) to educate the choice of wave models for different coastal engineering scenarios. The different techniques available are the Fully Nonlinear Potential Flow (FNPF) model, Computational Fluid Dynamic (CFD) model and non-hydrostatic shallow water model (SFLOW). CFD model solves the incompressible Navier–Stokes equations with a RANS turbulence model. SFLOW model reduces the computational costs significantly by solving the depth-averaged shallow water equations with a non-hydrostatic extension based on a quadratic vertical pressure profile. Whereas, FNPF solves the Laplace equation with the fully nonlinear boundary conditions. The performances of the different modules were validated and compared using several benchmark cases such as simple wave propagation, two-dimensional wave breaking over a mild slope, three-dimensional wave breaking over a flat-tipped reef and wave propagation over a submerged bar. The comparison of results for monochromatic waves indicates that all three approaches are capable of computing the wave propagation. The submerged bar case showed high accuracy with CFD and FNPF models, whereas, the SFLOW model failed due to its theoretical limitations. The two-dimensional wave breaking case revealed that all three models were able to represent wave energy dissipation accurately during the breaking of a wave. For the case of the three-dimensional wave breaking, the CFD model perfectly mimicked the physics of wave propagation, including the complex overturning of the wave during the breaking process with high computational time.

2.5 SUMMARY OF LITERATURE REVIEW

From the literature review, it can be concluded that a decrease in relative wave height and increase in relative clear spacing of piles increase K_t and decrease K_r . An increase in wave steepness decreases K_t and increases K_r and K_d . The relative depth of water and diameter of the pile had little or no effect on the wave transmission. From the past experiments conducted by various authors (Anuar and Sidek 2012; Herbich 1990; Rao and Rao 1999; Van Weele and Herbich 1972) it can be stated that the increase in rows of pile will increase the wave attenuation by 10%, and hence, increasing number of rows of piles to a large number does not improve the wave attenuation considerably. The staggered arrangement of piles has a marginal effect on wave transmission. Perforated piles have a better wave energy attenuation capacity of about 10% more than non-perforated piles.

The wave parameters such as, relative wave height (h/H_i), incident wave steepness (H_i/gT^2) and relative depth of water (h/gT^2), and structural parameters like, number of pile rows, arrangement of pile rows, relative clear spacing between the piles (b/D), relative clear spacing of pile rows (B/D), relative depth of submergence (y/h) and porosity of the structure are the important factors influence the wave transmission and reflection characteristics of pile breakwaters.

2.6 KNOWLEDGE GAP

Since after the conceptualization of pile breakwater, a series of investigations based on experimental, theoretical and numerical approach were conducted to assess the hydraulic performance of pile breakwaters. New concepts were developed like perforated piles, vertical slotted barriers and pile-supported screen breakwaters to enhance the hydraulic efficiency of the pile breakwater. From the literature review, it was found that no physical or numerical studies were carried out to evaluate the hydraulic performance of pile breakwater with an increased area at the top of the pile. In this context, the present study aims to bridge the existing knowledge gap that is achieved through experimental and numerical investigations by proposing innovative pile breakwaters.

2.7 PROBLEM FORMULATION

In the pile breakwater, the mechanism by which the energy dissipation takes place is by the kinematics in wave motion interfered by the pile structure across the waves inducing turbulence and loss of energy. By increasing the turbulence, more energy can be dissipated, which lead to the findings of perforated pile breakwaters.

Increasing the turbulence is the main concept behind the development of enlarged pile section in the vicinity of water surface. The present study proposes to have a pile-supported structure with an increasing area near the surface called pile head. The size of the structure is increased to have a larger area of the structure to be in contact with waves. Thus, the pile breakwater is split into two parts, namely pile head and trunk. The trunk part is solid without perforations and the head portion is hollow and open at the top. The present study intends to add knowledge on the pile type breakwater by conducting physical model tests on the proposed concept of enlarged pile head breakwater.

2.8 OBJECTIVES

The objectives of the physical model investigations of the hydraulic performance of a single row of enlarged pile head breakwater are to:

1. Study the influence of varying spacing, height and diameter of the pile head under assumed wave climate.
2. Evaluate the effect of perforations on the pile head for their varying distribution, size and percentage.
3. Determine the optimum configuration.
4. Validate the optimum configuration employing REEF3D numerical model.

EXPERIMENTAL INVESTIGATIONS

3.1 GENERAL

In general, the laboratory studies are termed as physical model studies because they represent the actual physical system (Hughes 1993). The best data would be the data collected through field investigations, but the field data are prone to many natural variables and are usually expensive. Physical and numerical models have better control over the structure and test parameters than that of field investigations (Kamphuis 1991). In comparison, the data collected from experiments will be economical and facilitate quicker data collection, simpler than natural, can be easily analysed and interpreted.

Investigations on the proposed concept of the breakwater are primarily achieved by the traditional techniques of laboratory experiments. The two-dimensional wave flume available in the Marine Structures laboratory of the Department of Water Resources and Ocean Engineering, NITK Surathkal, is used to conduct the experimental studies. The experimental set up along with the equipment used for the investigation are explained in this chapter. The experimental procedure and the method of data collection are also enumerated.

3.2 DIMENSIONAL ANALYSIS

Dimensions and dimensional units play a vital part in every measurement of a physical property. Dimensional analysis is a well-articulated procedure to combine the physical variables into dimensionless parameters and to reduce the number of variables to be considered (Langhaar 1951). Problems involving fluid motions are quite complex in nature. Representing the intricate flow phenomenon responsible for energy dissipation by mathematical equations is quite complicated. In such cases, one has to rely on experimental investigations and investigation results are more useful when related using dimensionless parameters. The dimensional analysis is carried out to find out the relationship between different variables of the phenomena to be investigated.

Following two methods are generally/widely used for dimensional analysis.

1. Rayleigh's method
2. Buckingham's π -theorem

The Rayleigh's methods become more arduous if the number of variables is more than the fundamental dimensions. But Buckingham's π -theorem overcomes such difficulties. For modelling of any physical phenomena, it is important to identify the relevant variables and then relating these variables by means of known physical laws. Buckingham's π -theorem describes how many physically meaningful equations involving n variables can be rewritten into $(n - r)$ dimensionless terms. Where, n is the number variables and r is the number of fundamental dimensions used. The three fundamental dimensions are length (L), mass (M) and time (T).

3.2.1 Predominant variables and their dimensions

For the present investigation, the following predominant variables are considered for dimensional analysis.

Table 3.1 Predominant variables and their dimensions

Predominant variables		Dimensions
Wave parameters	Incident wave height (H_i)	[L]
	Transmitted wave height (H_t)	[L]
	Reflected wave height (H_r)	[L]
	Dissipated wave height (H_d)	[L]
	Maximum wave height (H_{max})	[L]
	Water depth (h)	[L]
	Wave period (T)	[T]
	Wavelength (L)	[L]
	Wave celerity (C) or water particle velocity (u, v and w)	[LT ⁻¹]
Structure parameters	Diameter of pile head (D)	[L]
	The diameter of the pile trunk (D_t)	[L]

	Clear spacing of piles in a row (b)	[L]
	Centre to centre distance between the pile heads (2A)	[L]
	Size of perforation (S)	[L]
	Percentage of perforations (P)	[1]
	Height of pile head (Y)	[L]
Fluid parameters	Mass density (ρ)	[ML ⁻³]
	Dynamic viscosity (μ)	[ML ⁻¹ T ⁻¹]
External parameters	Acceleration due to gravity (g)	[LT ⁻²]

3.2.2 Details of dimensional analysis

For deep water wave conditions, L and T are related by the equation,

$$L_0 = \frac{gT^2}{2\pi} \quad (3.1)$$

Where L_0 is the deep-water wavelength. The term gT^2 is incorporated in the Eq. (3.1) to represent the wavelength L. Because if L is utilised directly, it would be for specific depth. The parameter gT^2 is independent on depth of water and hence, represents the deep water characteristics. Thus, depending on the local bathymetry, which may be altered effectively to shallow water conditions.

The wave transmission coefficient (K_t) is obtained by using Eq. (3.2)

$$K_t = \frac{H_t}{H_i} \quad (3.2)$$

The wave reflection coefficient (K_r) is obtained by using equation

$$K_r = \frac{H_r}{H_i} \quad (3.3)$$

The reflected wave heights (H_r) are decomposed by a method proposed by Isaacson (1991). Wave energy dissipation equation is obtained by considering energy

equilibrium conditions as per Hagiwara (1984), Isaacson et al. (1998), Koraim et al. (2014) and Suh et al. (2006) and is given by,

$$E_t + E_r + E_d = E_i \quad (3.4)$$

$$E_d = E_i - (E_t + E_r) \quad (3.5)$$

Where, $E_i = \frac{\rho g H_i^2}{8}$, $E_r = \frac{\rho g H_r^2}{8}$, $E_t = \frac{\rho g H_t^2}{8}$ and $E_d = \frac{\rho g H_d^2}{8}$; Substituting in Eq. (3.5) and divided by E_i

$$\frac{H_d^2}{H_i^2} = \frac{H_i^2}{H_i^2} - \left(\frac{H_t^2}{H_i^2} + \frac{H_r^2}{H_i^2} \right) \quad (3.6)$$

$$K_d = \sqrt{1 - (K_t^2 + K_r^2)} \quad (3.7)$$

By using Eq. (3.7), the energy dissipation coefficient (K_d) is calculated.

By applying Buckingham's π -theorem following equation of the forms are obtained for transmission coefficient (K_t), reflection coefficient (K_r) and dissipation coefficient (K_d).

$$K_t = f_1 \left(\frac{H_t}{H_i}, \frac{H_i}{gT^2}, \frac{b}{D}, \frac{D}{H_{\max}}, P, \rho a, \frac{S}{D}, \frac{Y}{h}, \frac{Y}{H_{\max}} \right) \quad (3.8)$$

$$K_r = f_2 \left(\frac{H_r}{H_i}, \frac{H_i}{gT^2}, \frac{b}{D}, \frac{D}{H_{\max}}, P, \rho a, \frac{S}{D}, \frac{Y}{h}, \frac{Y}{H_{\max}} \right) \quad (3.9)$$

$$K_d = f_3 \left(\frac{H_d}{H_i}, \frac{H_i}{gT^2}, \frac{b}{D}, \frac{D}{H_{\max}}, P, \rho a, \frac{S}{D}, \frac{Y}{h}, \frac{Y}{H_{\max}} \right) \quad (3.10)$$

Where,

$\frac{H_t}{H_i}$ is transmission coefficient, K_t

$\frac{H_r}{H_i}$ is reflection coefficient, K_r

$\frac{H_d}{H_i}$ is dissipation coefficient, K_d

$\frac{H_i}{gT^2}$ is incident wave steepness

$\frac{b}{D}$ is relative clear spacing of pile heads

P is percentage of perforations, defined as the ratio of total area of perforations to the surface area of pile head

$\frac{S}{D}$ is relative size of perforations or relative pore size

pa is distribution of perforations around pile head

$\frac{Y}{h}$ is relative submergence of pile head which is denoted by Z

3.3 SIMILITUDE CRITERIA AND MODEL SCALE SELECTION

Providing mitigation measures to coastal engineering problems is a complicated task. The process normally involves a complex wave structure interaction. Hence, such problems are typically addressed by combining large-scale field studies with mathematical and numerical modelling. The mathematical models ingeniously predict the complicated wave-structure interactions; they are certainly simplified using some empirical coefficients drawn by limited input data. Physical model studies predict the behaviour of a physical phenomenon, both quantitatively and qualitatively (Hughes 1993). The idea behind all physical models is that the physical model behaves identically to that of the prototype for the intended purpose. Physical model studies allow imitating of intricate physical phenomena in abridged laboratory environments. It is important to validate the physical model to emulate physical phenomena in laboratory studies. Thus, the validated model will abet to fetch the information required for the design of the prototype and thus avoid costly mistakes.

The similitude is accomplished when a majority of factors influencing reactions are in accordance with the prototype and model. The factors which are not in accordance with the prototype throughout the model domain are so small that they are insignificant to the process (Hughes 1993). Model similitude can be achieved by,

- Calibration
- Dimensional analysis
- Differential equation
- Scale series

The calibration method is time consuming and more suitable for movable bed models. Differential equations method is not suitable because the wave-structure interaction is not clearly understood. Scale series is largely used to ascertain the scaling criteria for a complex phenomenon and has to be careful in analysing the results from the model tests and generalizing the same to prototype. For the present study, the method of dimensional analysis is adopted to achieve the similitude condition. Incorrect ratios of forces between the prototype and model lead to scale effects, whereas imperfect prototype reproduction in the model with respect to geometry, wave climate, recording and data analysis method will be the model effects (Burcharth and Andersen 2009). The present study deals with the surface waves, and hence, Froude scaling law is used for the scaling. In the prototype, the gravity effect is predominant for wave motion studies. Froude similitude is preferable when the flow velocity is reasonably small, flow is turbulent and surface tension is minimum. Nearly 90% of the coastal engineering or hydraulic flow problems are scaled according to Froude's Law (Hughes 1993).

Using the non-dimensional parameters, the similitude between the prototype and model is accomplished. The range of non-dimensional parameters should be the same for the prototype and model. For the current work, wave climate off Mangaluru coast is considered. In the present study, wave steepness (H_i/gT^2) is a non-dimensional parameter considered to achieve the similitude criteria. The same is shown in Table 3.2. Using the two-dimensional wave flume available for the present study, monochromatic waves of heights and periods ranging from 0.03 m to 0.24 m and 1 s to 3 s respectively can be produced. A 1:30 geometrically similar model scale is selected for the present experimental investigations. The equivalent of 1:30 geometric model that is scaled up to real field conditions.

Table 3.2 Wave parameters of prototype and model

Wave parameters	T (s)	H_i (m)	H_i/gT²
Prototype	5.48 to 16.43	0.9 to 7.2	0.00034 to 0.02446
Model	1.0 to 3.0	0.03 to 0.24	0.00034 to 0.02446

3.4 LABORATORY AND SCALE EFFECTS IN SHORT WAVE MODEL

Wave motion can be separated into short and long waves based on wave period in nature. A wave with a wave period from 1 s to 20 s is termed as short period waves and wave period ranging between few minutes to several hours is designated as long period waves. The short wave model is used to study wind waves and swell effects on coastal structures, beaches and navigations. The laboratory and scale effects are the two most important factors affecting the scale model results (Hughes 1993).

3.4.1 Laboratory effects

The laboratory effects in the short-wave model are primarily related to physical constraints of boundaries on the flow, unintentional nonlinear effects (brought by using the mechanical means of wave) and simplification of prototype forcing conditions (such as representing prototype wave conditions as unidirectional). In a two-dimensional wave tank, the generated waves propagate towards the far end structure or beach. These waves are reflected towards the generation zone as it happens in the open sea. In open sea, reflected waves continue out to open sea whereas, this results in laboratory effects in wave tanks. These laboratory effects can be dealt with in a number of ways (Hughes 1993).

- By conducting the experiments in a series of wave bursts, with each burst of waves ending before re-reflected waves can again reach the testing section of the wave flume.
- By implementing active wave absorption method at the wave board to detect and absorb unwanted reflected wave energy.
- By using energy dissipating beaches.

For the present study experiments are conducted in a series of wave bursts and energy dissipating beaches are used to delt the laboratory effects.

3.4.2 Scale effects

The scale effects in short wave models result from the scaling assumption that gravity is the dominant physical force balancing the inertial forces. Hence, the model based on

Froude scaling incorrectly scales other physical forces of viscosity, elasticity, surface tension, etc., believing that these forces contribute little to the physical processes. The model scaled according to Froude's criterion, the non-similitude of viscous and surface tension forces can lead to scale effects involving wave transformation, wave energy dissipation and wave breaking. Some of the scale effects are wave reflection, wave transmission, viscosity and friction, surface tension, wave breaking, use of fresh water in wave tank, air compression effects etc. According to Hudson (1975), as quoted by US Army Corps of Engineering (1984), the scale effect will be negligible if $Re > 3 \times 10^5$. To minimise the scale effects and to generate a high Reynolds number ($Re > 3 \times 10^4$), it is preferred to conduct the model test on a scale varying from 1:10 to 1:50 (Hughes 1993). Generally, Reynolds numbers above 1×10^4 are in the range of turbulent flow where the viscous force becomes independent of Reynolds number.

Viscous dissipation will be dominant within the structure at $20 < Re < 2 \times 10^3$; whereas strong turbulent dissipation would be expected at $Re > 2 \times 10^3$ (Teh and Venugopal 2013; Hughes 1993). For many years, it has been considered that no modelling error will arise as long as armour unit, Reynolds number is greater than 3×10^4 . However, Owen and Briggs (1986) stated that the model studies conducted with different scales and comparison with recorded damage suggest that Re can be as low as 8×10^3 or even 3×10^3 before any significant error rise. Similarly, researchers like, Jensen and Klinting (1983) as stated by Hughes (1993), Teh and Venugopal (2013) and Sheng et al. (2014) showed Re can be as low as possible (2×10^3 to 1.9×10^4). For the current experiments conducted, Re is in the range of 8×10^3 to 3×10^4 , which is more than the required range of Re to satisfy the flow to be turbulent and hence, viscous effect is neglected. Calculation of Reynolds number for the present study is presented in Appendix I.

3.5 DESIGN CONDITIONS

The wave climates off Mangaluru coast, recorded by KREC study team (1994), are considered for the present investigations. The single largest wave height recorded off Mangaluru coast during the monsoon is about 5.4 m. However, the KREC team suggested considering a design wave height of 4.8 m for the Mangaluru coast. During monsoon, the predominant wave period is in the range of 8 s to 11 s. Wave height barely

exceeds 1 m during fair weather season and wave periods up to 15 s are occasionally observed. The tides at Mangaluru are mixed semi-diurnal type with a range of ± 1.68 m (tidal variation with respect to mean sea level). Hence, for the enlarged pile head breakwater model design, monochromatic waves of heights in the range of 1.8 m to 4.8 m and a wave period of 8 s to 11 s are simulated. The present verification considers the normal wave attack ($\theta = 90^\circ$), which is the worst condition for any coastal structure wherein the complete structure confronts the incident waves and therefore proved to give conservative results (Jeya et al. 2021; Whillock and Price 1976). The experimental results under monochromatic wave conditions would give conservative results than the irregular waves (Ergin and Pora 1971; Neelamani and Rajendran 2002; Neelamani and Vedagiri 2002).

3.6 EXPERIMENTAL SETUP

The physical model study of enlarged pile head breakwater under monochromatic waves was conducted in a two-dimensional wave flume available at Marine Structures Laboratory of Water Resources and Ocean Engineering Department, National Institute of Technology Karnataka, Surathkal. The facilities employed for the investigations are briefly explained in the following sections.

3.6.1 Details of wave flume

The two-dimensional wave flume has dimensions of 50 m \times 0.71 m \times 1.1 m. It has a 42 m long, smooth concrete bed. About 25 m length of the flume is provided with glass panels on one side to facilitate the observations and photography. It has a 6.3 m long, 1.5 m wide and 1.4 m deep chamber at one end where the hinged bottom flap generates waves. The flap is controlled by an induction motor of 11 kW, 1420 rpm. This motor is regulated by an inverter drive, 0 – 50 Hz rotating with a speed range of 0 – 1550 rpm. Monochromatic waves of 0.06 m to 0.24 m heights and wave period of 1 s to 3 s, in a maximum water depth of up to 0.70 m, can be generated with this facility. Fig. 3.1 gives a schematic diagram of the experimental setup.

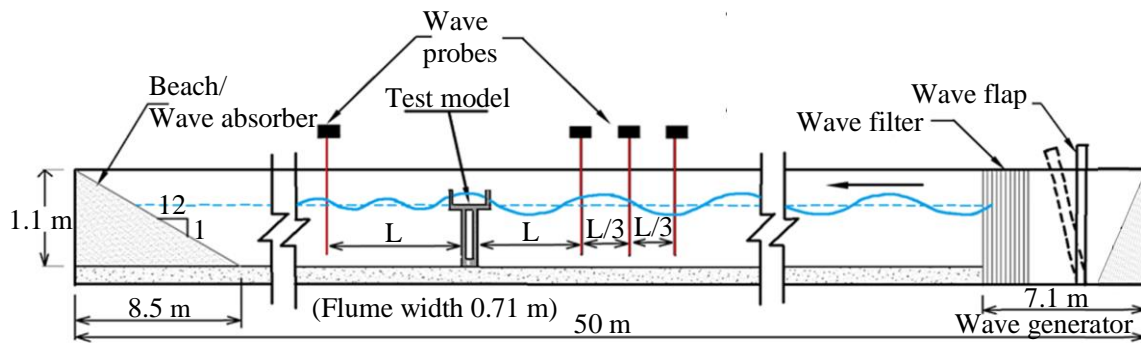


Fig. 3.1 Schematic diagram of the experimental setup

3.6.2 Data acquisition system

Computer data acquisition systems with capacitance type wave probes and amplification units are used to record the water surface elevations. The variation of capacitance between water and the copper conductor is a measure of wave height. The circuit inside the electronic unit senses this variation. These digital voltage signals are converted into wave data using the software provided by EMCON (Environmental Measurements and Controls), Cochin, Kerala, India.

3.6.3 Calibration of test facilities

Accuracy of the data collection is ensured by calibration of the experimental setup and instruments. The calibration process of wave flume and wave probe is illustrated in the following sections.

3.6.3.1 Wave flume

The relationship between eccentricity and wave height; and inverter frequency and wave period for a particular depth of water is assessed. The wave height generated in the wave flume is directly proportional to the eccentricity of the wave board and the frequency of the inverter is inversely proportional to the wave period. The inverter drive is used to generate the preferred wave period by altering the frequency. Changing the eccentricity of a bar chain on the flywheel generates desired wave height for a certain wave period. For the present experiments, three depths of water (0.3 m, 0.4 m and 0.5 m) are considered. The incident wave height (H_i) ranges from 0.06 m to 0.16 m with wave periods (T) from 1.4 s to 2.0 s generated. Table 3.3 to Table 3.5 shows the

calibrated values of the eccentricity of the wave board for the various wave heights, wave periods and depths of water.

Table 3.3 Calibrated values of wave flume for 0.3 m depth of water

Wave period (s) \ Wave height (m)	0.06	0.08	0.10	0.12	0.14	0.16
2	8.3	11.4	13.8	16.6	18	WB
1.6	6.7	8.8	11.2	13.2	WB	WB
1.4	6.2	8.3	10.1	WB	WB	WB

Table 3.4 Calibrated values of wave flume for 0.4 m depth of water

Wave period (s) \ Wave height (m)	0.06	0.08	0.10	0.12	0.14	0.16
2	6.5	9	11.2	14	16	WB
1.6	6	7.5	9.3	11.2	13.6	WB
1.4	5.1	6.3	8	9.5	11	WB

Table 3.5 Calibrated values of wave flume for 0.5 m depth of water

Wave period (s) \ Wave height (m)	0.06	0.08	0.10	0.12	0.14	0.16
2	5.5	7.5	9.7	11.3	12	14
1.6	5	6	7.4	8.8	9.6	10.8
1.4	5.2	6.2	7.8	8.9	9.8	10.5

3.6.3.2 Wave probes

The wave probes work on the principle of electrical conductance. The primary output is in the form of voltage which varies from 0 to 5 V. The embedded software in the wave recording system converts it to water level variations. The manufacturer initially calibrated the probes. However, the output is expected to show minor variations depending on the salinity and temperature of water used in the flume. Hence, the probes are subjected to static immersion tests and the relationship between the water level and the output voltage is determined and recorded. The probes are calibrated by lowering

and raising the probe in a known depth of immersion and recording the variations in corresponding voltages. The probes are calibrated every day before and after the experiments, and corrections are incorporated into the data. Silica gel is applied to the probes to reduce the effect of surface tension.

3.7 ENLARGED PILE HEAD BREAKWATER MODEL

Considering the existing facilities of the two-dimensional wave flume at NITK Surathkal, the enlarged pile head breakwater and the wave parameters are modelled with the largest possible scale of 1:30. The selected scale is within the range of scales (1:10 to 1:50) recommended by Hughes (1993) for the short-wave hydrodynamic models. The wave parameters and the model are simulated with the application of Froude's law. The Reynolds number of flow in the present study is in the range of 8×10^3 to 3×10^4 . The effects of the model scale and the viscosity are not significant if the Reynolds number is above 2×10^3 (Hughes 1993; Teh and Venugopal (2013) and Sheng et al. (2014)). The investigation is conducted for different depth of water (h) and by varying the wave heights (H) and wave periods (T). The pile structure consists of a pile head and trunk, whose dimensions are listed in Table 3.6.

Table 3.6 Structural dimensions of prototype and model

Structural Parameters	Prototype		Model	
	Diameter (m)	Height (m)	Diameter (m) (D)	Height (m) (Y)
Pile Trunk	1.2	Vary with water depth	0.04	Vary with water depth
Pile Head	1.92 and 2.88	2.4 and 4.8	0.064 and 0.096	0.08 and 0.16

3.7.1 Pile trunk

Pile trunk is the lower portion of enlarged pile head breakwater which will be solid and rigid. The trunk portion is made up of PVC pipes of 0.04 m diameter infilled with concrete. The pile trunk supports the pile head and is attached to a metal plate of 0.012 m thick. This configuration makes the enlarged pile head breakwater rigid. The typical arrangement of pile head breakwater is as shown in Fig. 3.2. Depending on the depth of water level and height of pile head, height of the pile trunk is varied so that the water

level is at the centre of the pile head. The arrangement of the pile head breakwater for different water depths is shown in Fig. 3.3.

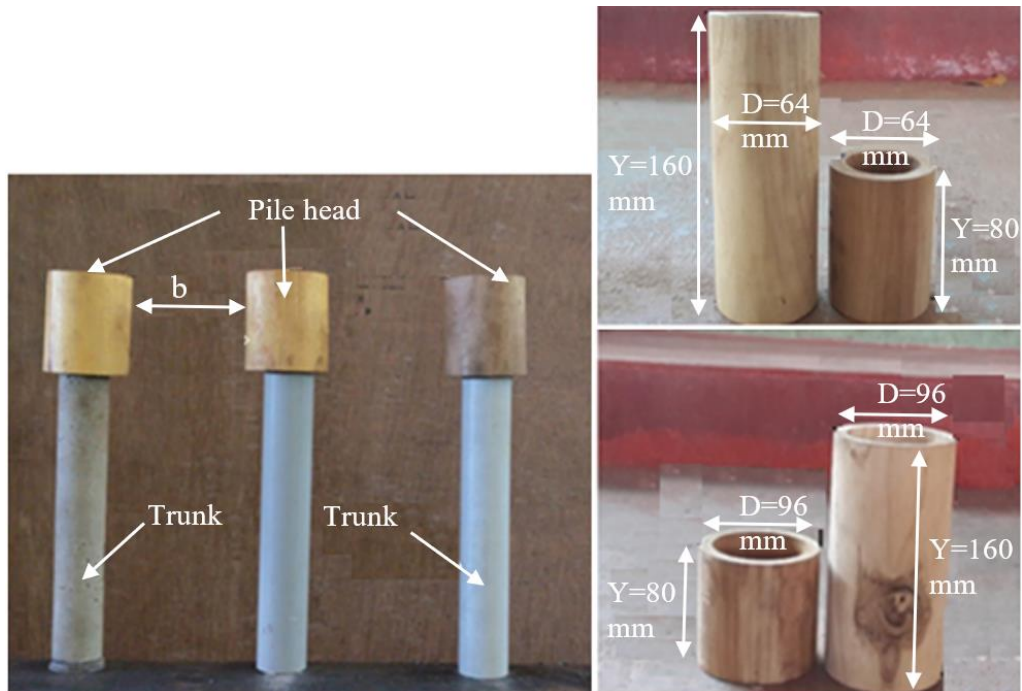


Fig. 3.2 View of enlarged pile head structure model and dimensions of the enlarged head

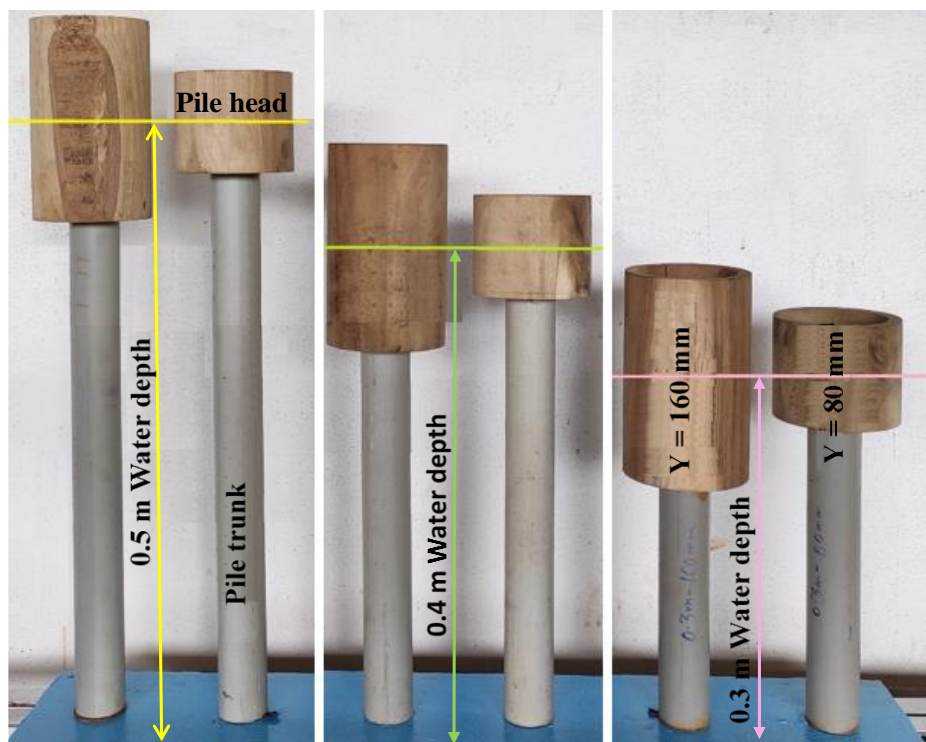
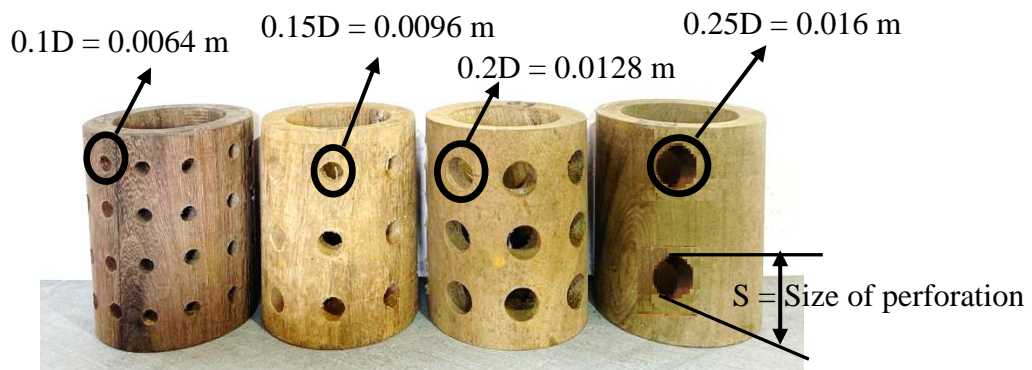


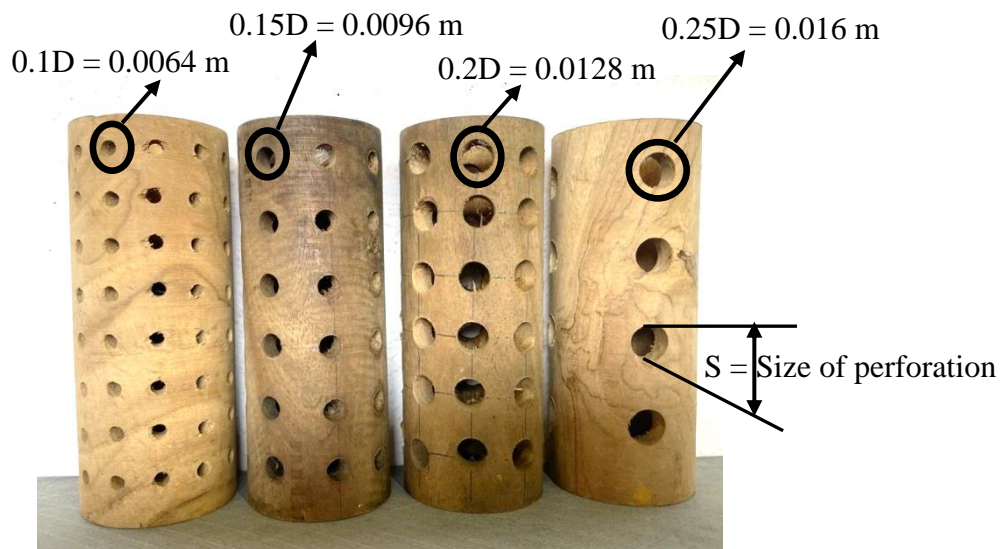
Fig. 3.3 A typical arrangement of the structure at different water depths

3.7.2 Non-perforated pile head

Pile head is the top portion of enlarged pile head breakwater, which is shown in Fig. 3.2 and Fig. 3.3. The head portion of the structure is made of wood and is open at the top with 0.01m wall thickness. For the present study, the height (Y) and diameter (D) of the pile head are varied from 0.080 m to 0.160 m and 0.064 m to 0.096 m, respectively.



a) Y = 0.080 m



b) Y = 0.160 m

Fig. 3.4 Arrangement of perforations on the pile head of D = 0.064 m

3.7.3 Perforated pile head

In the study framework, perforations are provided in relation to the diameter of the enlarged pile head (D). The structural parameter related to the perforated pile head is

as depicted in Table 3.10. Fig. 3.4 and Fig. 3.5 illustrate the arrangement of the perforations on the pile head.

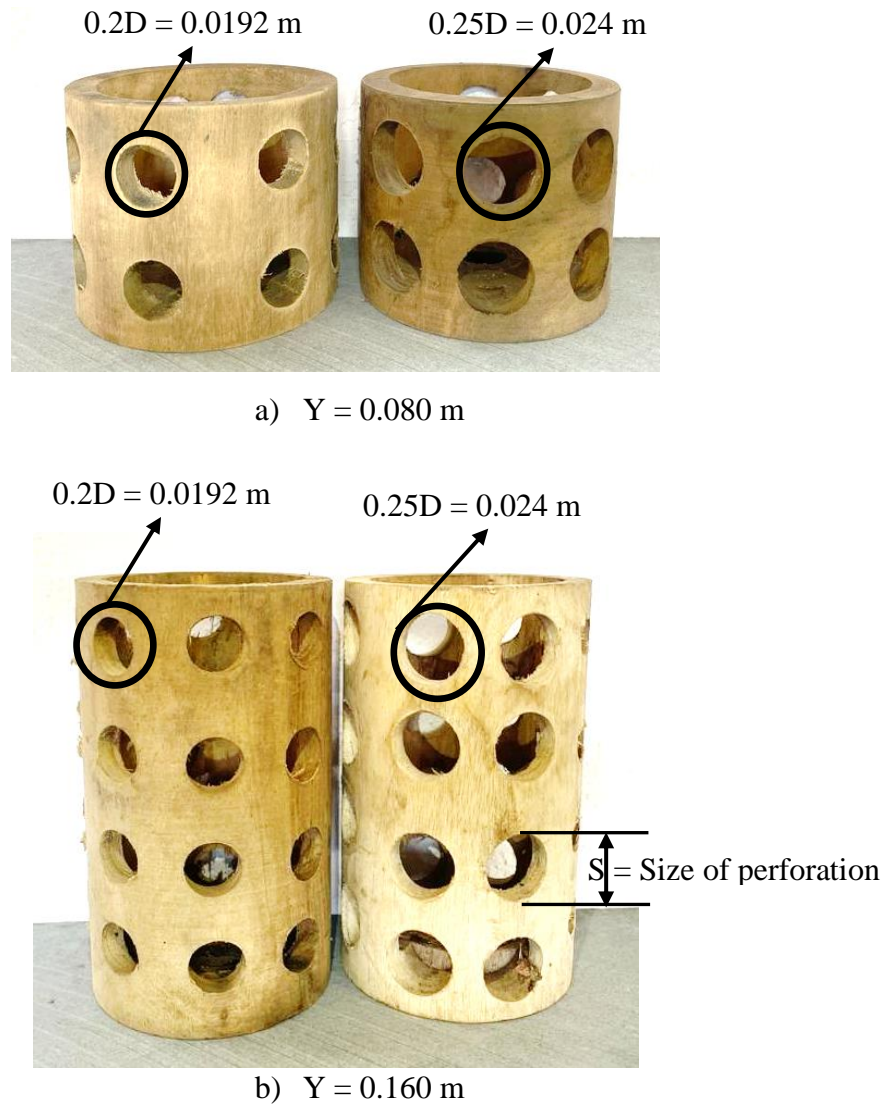


Fig. 3.5 Arrangement of perforations on pile head of $D = 0.096$ m

The effect of percentage distribution of perforations (p_a) around the pile head is studied by increasing p_a in a stage of 25%, 50%, 75% and 100%. Fig. 3.6 shows the plan view of the typical distribution of perforations (p_a) around the pile head. Table 3.7 and Table 3.8 show the details of S , p_a and P considered for the study. The percentage of perforation (P) is defined as the ratio of the total area of perforations to the surface area of the pile head.

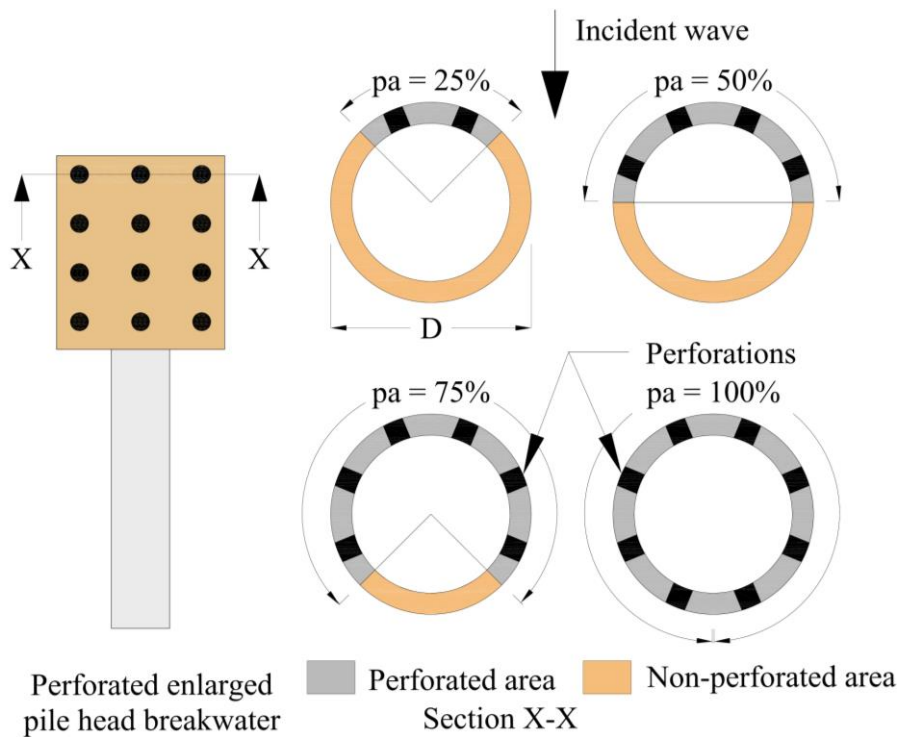


Fig. 3.6 Typical arrangement of distribution of perforations (pa) around the pile head

Table 3.7 Details on S, pa and for D = 0.064 m dia. pile head

S/D	S	No. of pores		P	pa
		Y = 80 mm	Y = 160 mm		
0.10	6.4	12	12	2.40	25
0.10	6.4	24	24	4.80	50
0.10	6.4	36	36	7.20	75
0.15	9.6	6	6	2.70	25
0.15	9.6	12	12	5.40	50
0.15	9.6	18	18	8.10	75
0.20	12.8	12	12	9.60	50
0.20	12.8	18	18	14.40	75
0.20	12.8	24	24	19.20	100
0.25	16	4	4	5.00	50
0.25	16	6	6	7.50	75
0.25	16	8	8	10.00	100

Table 3.8 Details on S, pa and P for D = 0.096 m dia. pile head

S/D	S	No. of pores		P	pa
		Y = 80 mm	Y = 160 mm		
	mm			%	%
0.20	19.2	8	8	9.6	50
0.20	19.2	12	12	14.4	75
0.20	19.2	16	16	19.2	100
0.25	24	8	8	15	50
0.25	24	12	12	22.5	75
0.25	24	16	16	30	100

3.8 RANGE OF EXPERIMENTAL VARIABLES

In any experimental studies on the breakwater, the range of experimental variables is to be designated at the earlier stage. The parameters related to the wave conditions and structure are portrayed in Table 3.9 and Table 3.10.

Table 3.9 Experimental variables for non-perforated pile head

Variables	Expression	Parameter Range	
Diameter of pile head (m)	D	0.064	0.096
Relative pile head diameter	D/H _{max}	0.4	0.6
Diameter of the pile trunk (m)	D _t	0.04	
Height of pile head (m)	Y	0.08	0.16
Relative pile head height	Y/H _{max}	0.5	1.0
Relative spacing between the piles head in a row	b/D	0.2, 0.4, 0.8, 1.2	0.2, 0.4, 0.6, 0.9
Wave period (s)	T	1.4, 1.6, 1.8, 2.0	
Incident wave height (m)	H _i	0.06, 0.08, 0.10, 0.12, 0.14	
Water Depth (m)	h	0.3, 0.4, 0.5	
Relative submergence of pile head	Z = (Y/2)/h	8 %, 10%, 13.333%, 16%, 20%, 26.667 %	
Angle of the wave attack	θ	90°	
Incident wave steepness	H _i / gT ²	0.0015 to 0.0062	

Table 3.10 Experimental variables for perforated pile head

Variables	Expression	Parameter Range	
Diameter of pile head (m)	D	0.064	0.096
Relative pile head diameter	D/H _{max}	0.4	0.6
Diameter of the pile trunk (m)	D _t	0.04	
Height of pile head (m)	Y	0.08	0.16
Relative pile head height	Y/H _{max}	0.5	1.0
Relative spacing between the piles head in a row	b/D	0.2	0.2
Wave period (s)	T	1.4, 1.6, 1.8, 2.0	
Incident wave height (m)	H _i	0.06, 0.08, 0.10, 0.12, 0.14, 0.16	
Depth of water (m)	h	0.3	
Relative submergence of pile head	Z = (Y/2)/h	13.333%, 26.667 %	
Relative size of perforations or relative pore size	S/D	0.1, 0.15, 0.2, 0.25	
Size of perforations or pore size (m)	S	0.0064, 0.0096, 0.0128, 0.016, 0.0096, 0.0144, 0.0192, 0.024	
Percentage of perforations (%)	P	2.4, 2.7, 4.8, 5.0, 5.4, 7.2, 7.5, 8.1, 9.6, 10.0, 14.4, 19.2 10.0, 10.8, 14.4, 15.0, 22.5, 30.0	
Distribution of perforations around pile head	p _a	25%, 50%, 75%, 100%	
Angle of the wave attack	θ	90°	
Incident wave steepness	H _i / gT ²	0.0015 to 0.0052	

3.9 MODIFICATION OF HYBRID THEORETICAL EQUATIONS

3.9.1 For non-perforated enlarged pile head breakwater

As a part of the present research, an attempt is made to derive an independent solution by modifying the empirically calculated γ parameter as defined by Suh et al. (2011), elaborately discussed and presented in section 2.5.1.

The empirically reformed γ equation using the current set of experimental data is given by,

$$\gamma = 1.569 \left(\frac{\bar{\epsilon} \left(\frac{H_i}{h} \right) f \left(\frac{Y}{2h} \right)}{\bar{\epsilon} \bar{\epsilon}} \right)^{0.433} \quad (3.11)$$

For regular pile breakwater, the Eq. (3.11) is modified by considering the value of $\frac{Y}{2h} =$

1. Then the Eq. (3.11) for regular pile breakwater becomes,

$$\gamma = 1.569 \left(\frac{\bar{\epsilon} \left(\frac{H_i}{h} \right) f}{\bar{\epsilon} \bar{\epsilon}} \right)^{0.433} \quad (3.12)$$

3.9.2 For perforated enlarged pile head breakwater

The theoretical equation available for the non-perforated pile breakwater is inadequate for perforated pile as the perforated pile has better hydraulic efficiency. In the present study, K_t and K_r for perforated pile breakwater are predicted by introducing γ_P .

Where,

$$\gamma_P = \gamma - X_R \quad (3.13)$$

X_R is the reduction factor for perforation and is defined as

$$X_R = X_P + \frac{6.391 \times 10^{-4}}{(S-0.0181)} + \frac{H_i}{h} \quad (3.14)$$

In which S = size of perforation (m), and

$$X_P = 0.0117P' + \frac{0.027}{(P'-3.24)} + \frac{0.0282}{(6.79-P')} - \frac{0.0473}{(P'-10.12)} \quad (3.15)$$

$$P' = \frac{100}{P}$$

Where, P is the percentage of perforation.

For conventional type pile breakwater, only the absolute value of X_R is considered.

The value of γ is obtained using Eq. (3.11) or Eq. (3.12) depending on the enlarged pile head or conventional pile breakwater.

3.9.3 Quantitative assessment of hybrid theoretical equations

It is vital to measure the prediction errors to quantify the accuracy in the theoretical calculation of hydraulic coefficients. For the present analysis, widely used three methods (Komen et al. 1994; Nam et al. 2017; Rattanapitikon 2007; Salmon et al. 2015) namely, Scatter Index (S.I.), Relative Root Mean Square Error (RrmsE) and coefficient

of determination (R^2) are used to express the error in the prediction. S.I., RrmsE and R^2 are calculated as per the equation given below.

$$S. I. = \frac{\sqrt{\frac{\sum_{i=1}^N (K_{obs} - K_{cal})^2}{N}}}{\bar{K}_{obs}} \quad (3.16)$$

$$RrmsE = \sqrt{\frac{\sum_{i=1}^N (K_{obs} - K_{cal})^2}{\sum_{i=1}^N (K_{obs})^2}} 100 \quad (3.17)$$

$$R^2 = \frac{[N(\sum_{i=1}^N K_{obs} K_{cal}) - \sum_{i=1}^N K_{obs} \sum_{i=1}^N K_{cal}]^2}{[N(\sum_{i=1}^N K_{obs}^2) - (\sum_{i=1}^N K_{obs})^2][N(\sum_{i=1}^N K_{cal}^2) - (\sum_{i=1}^N K_{cal})^2]} \quad (3.18)$$

Where, K stands for K_t , K_r , K_d

obs = Observed value (Flume)

cal = Calculated value (Equation)

N = Number of data

The scatter index and RrmsE are considered to be the primary measure of model accuracy since both the index consists of random and systematic errors of the predictions. The coefficient of determination indicates how well the predicted value is correlated with the experiment or observed data (Komen et al. 1994; Nam et al. 2017; Rattanapitikon 2007; Salmon et al. 2015). As per the literature review, predicted model results could be acceptable if the errors associated are less, and preferably not more than 20%.

3.10 REEF3D NUMERICAL MODELLING

An open-source CFD software, REEF3D (Bihs et al. 2016), developed by the Norwegian University of Science and Technology (NTNU), Norway, is used in the present study for numerical modelling of enlarged pile head breakwater. The REEF3D is widely used for investigating coastal problems such as wave breaking (Aggarwal et al. 2019; Bihs et al. 2016, 2019), wave-structure interaction (Bihs et al. 2017; Kamath et al. 2015a, 2016), seabed scouring (Ahmad et al. 2019), floating structures (Bihs and Kamath 2017), porous structures (Martin and Bihs 2021; Sasikumar et al. 2020) and aquaculture structures (Martin et al. 2020).

REEF3D solves the flow problems using Reynolds-Averaged Navier-Stokes (RANS) equations.

$$\frac{\partial u_i}{\partial x_i} = 0 \quad (3.19)$$

$$\frac{\partial u_i}{\partial t} + U_j \frac{\partial u_i}{\partial x_j} = -\frac{1}{\rho} \frac{\partial p}{\partial x_i} + \frac{\partial}{\partial x_j} \left[(v + v_t) \left(\frac{\partial u_i}{\partial x_j} + \frac{\partial u_j}{\partial x_i} \right) \right] + g_i \quad (3.20)$$

Where u_i is the averaged velocity over time t , ρ is the density of water, v is the kinematic viscosity, v_t is the eddy viscosity, p is the pressure and g is the acceleration due to gravity.

The pressure terms in the RANS equation is solved by the projection method proposed by Chorin (1968). BiCGStab algorithm (Van Der Vorst 1992) is applied to solve the Poisson equation for pressure. $k-\omega$ model presented by Wilcox (1994) is applied for turbulence modelling in which k and ω denotes turbulent kinetic energy and specific turbulence dissipation rate, respectively. The fifth-order weighted essentially non-oscillatory (WENO) scheme developed by Jiang and Shu (1996) is employed to discretise the convection terms of the RANS equation. Time discretization is achieved through the third-order TVD Runge–Kutta scheme (Shu and Osher 1988). REEF3D uses Courant-Friedrichs-Lewy (CFL) criterion, which determines the optimal time steps to maintain the numerical stability throughout the simulation. MPI (Message Passing Interface) is used for parallel computation between multiples cores to maximise the numerical model's efficiency. A non-uniform grid based on a Cartesian system is used in the present work wherein which ghost cell immersed boundary method takes care of the complex geometries.

3.10.1 Free surface

The free surface between the air and water is differentiated based on a level set method in accordance with Osher and Sethian (1988). The level set function is reinitialized after each iteration as per the procedure stated by Peng et al. (1999) by means of a partial differential equation. The level set function (ϕ) gives the shortest distance from the interface between two fluid domains. The phases are distinguished based on the sign of level set function, which is given by,

$$\Phi(\vec{x}, t) \begin{cases} > 0 \text{ if } \vec{x} \text{ is in phase 1} \\ = 0 \text{ if } \vec{x} \text{ is in interphase} \\ < 0 \text{ if } \vec{x} \text{ is in phase 2} \end{cases} \quad (3.21)$$

3.10.2 Reconstruction of free surface

In REEF3D, the waves can be reconstructed (Aggarwal et al. 2018) using the time-domain data of free surface elevation based on the spectral decomposition technique. To simulate the wave parameters with more accuracy, the free surface elevation is regenerated in the numerical wave tank using the time-domain data of wave elevation. The reconstruction of free surface elevation is based on the coupling between Dirichlet inlet boundary conditions and input wave characteristics. Aggarwal et al. (2018) explored the capability of the REEF3D on free surface reconstruction using both the theoretical and experimental input waves. The study was conducted on random waves against few benchmark cases (wave breaking over the submerged bar, deep water wave generation and wave-structure interaction with monopole) and proved that the REEF3D is efficient in free surface reconstruction.

3.10.3 Validation of wave generation and testing

The validation of wave generation is carried out in a two-dimensional (2D) Numerical Wave Tank (NWT) without placing the structure. The width of the 2D tank is kept as one cell size with symmetry boundary conditions on the side walls. For the accuracy and validation of the numerical model, the wave surface in the numerical model is generated using the time domain data as measured using wave probes from the experimental works.

3.10.4 Grid and time step convergence tests

The grid density is one of the important factors that can affect the numerical results and is defined as the number of grid cells per wavelength. Smaller grid size (dx) results in a greater number of cells per wavelength and provides better solutions with a higher computational time. Hence, it is important to arrive at an optimal grid size to ensure accurate numerical results and to check not being too expensive with regard to computation time consumed. The quality of wave generation is checked for the wave height of 0.06 m and wave period of 2.0 s for various grid sizes as shown in Fig. 3.7 to

Fig. 3.10. The grid optimization test is conducted on four different size of grid ($dx = 0.08$ m, 0.04 m, 0.02 m and 0.01 m) by fixing CFL number to 0.1 .

Fig. 3.7 to Fig. 3.10. show the wave elevation compared with the experimental results and Table 3.11 presents the Root Mean Square Error RMSE values between the experimental and numerically reconstructed wave surface elevations. It is clearly noticed from the grid size study that reducing the grid size from 0.08 m to 0.04 m resulted in a better wave generation with reduced RMSE values. The wave elevation profile (Fig. 3.9) matches the input data for the grid size of 0.02 m. Further reducing the grid size from 0.02 to 0.01 m has shown (Fig. 3.10) a negligible improvement and also the RMSE values are converging for the grid sizes of 0.02 m and 0.01 m. Hence, it is evident that the grid size of 0.02 is good enough for accurate wave generation with a maximum RMSE of 0.0020 m. Therefore, $dx = 0.02$ m is fixed for further studying the influence of CFL number on wave generation.

The time step is another important factor that has to be considered to obtain the best numerical solution. In the present study, the CFL number is used to study the effect of time step size on the results obtained. The CFL numbers considered are 0.4 , 0.2 , 0.1 and 0.05 as shown in Fig. 3.11 to Fig. 3.14 and the errors associated are listed in Table 3.11. From Fig. 3.11 it can be observed that not only the wave amplitude is dampened but also the waveform is irregular with multiple peaks in some points. This effect is reduced with the reduction in the CFL number pointing to the importance of maintaining a suitably low time step to obtain a good solution. A CFL number of 0.1 appears to be the optimum one, increasing which affects the wave quality whereas, reducing the same has shown a negligible effect. From the above study, it is clear that simulating the waves with a CFL number of 0.1 with a grid size lesser than or equal to 0.02 m results in accurate reconstruction of the free surface of waves.

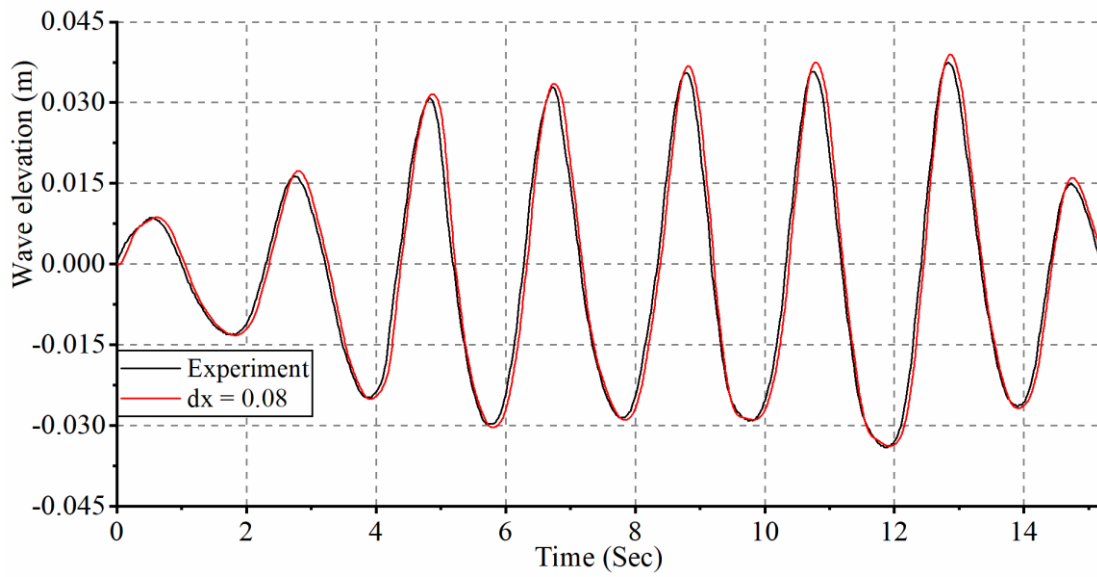


Fig. 3.7 Wave profile for grid size $dx = 0.08$ m with $CFL = 0.1$

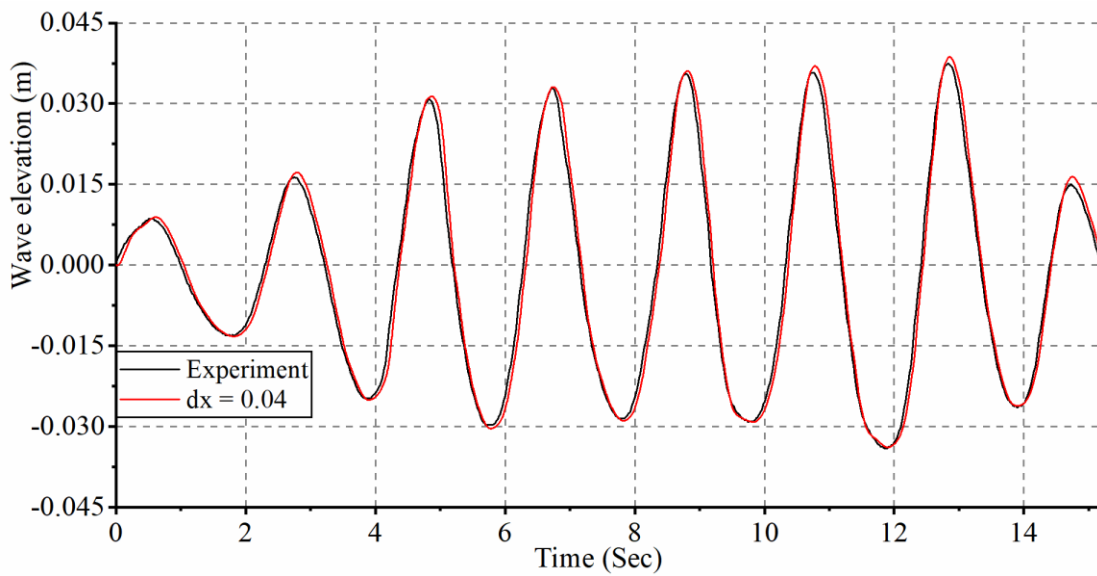


Fig. 3.8 Wave profile for grid size $dx = 0.04$ m with $CFL = 0.1$

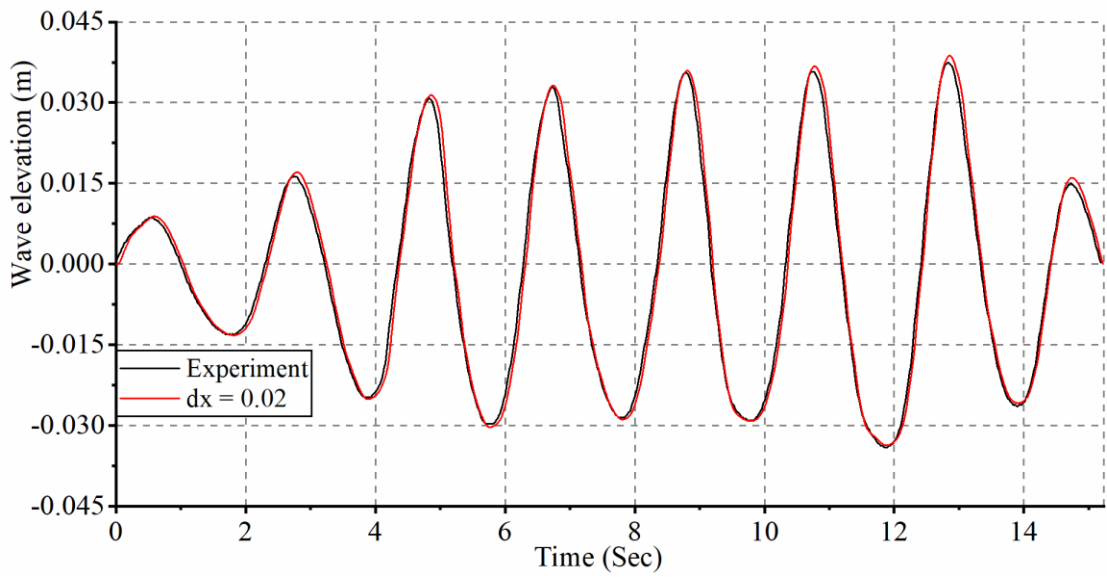


Fig. 3.9 Wave profile for grid size $dx = 0.02$ m with $CFL = 0.1$

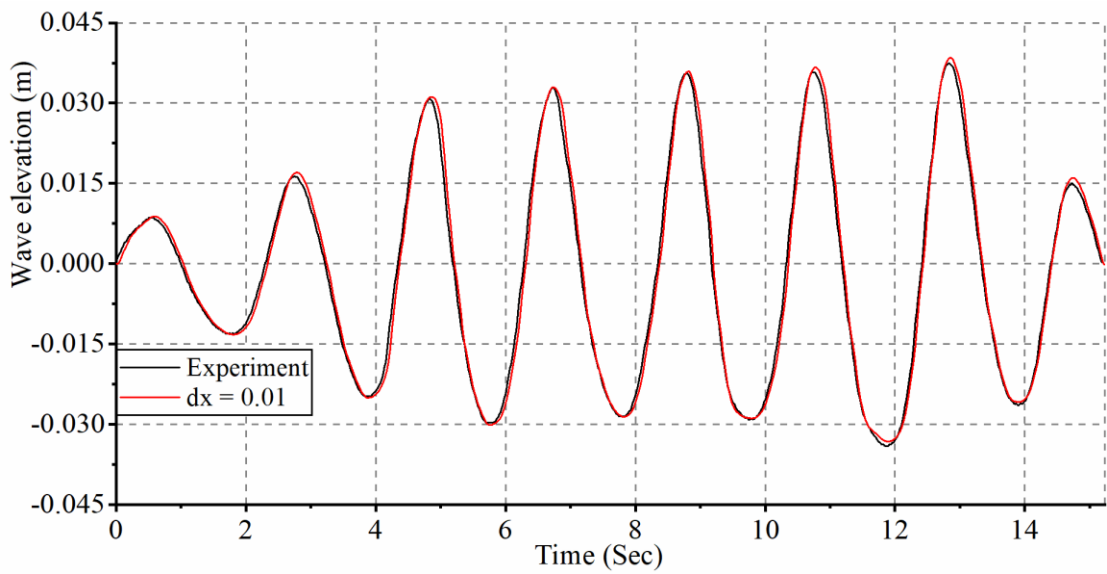


Fig. 3.10 Wave profile for grid size $dx = 0.01$ m with $CFL = 0.1$

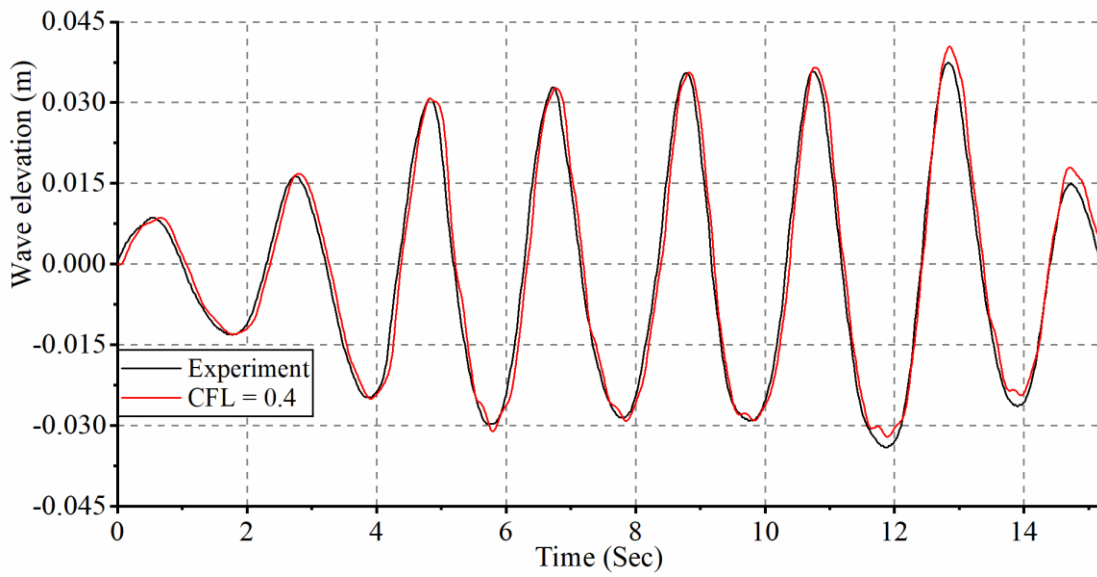


Fig. 3.11 Wave profile for CFL = 0.4 and grid size dx = 0.02 m

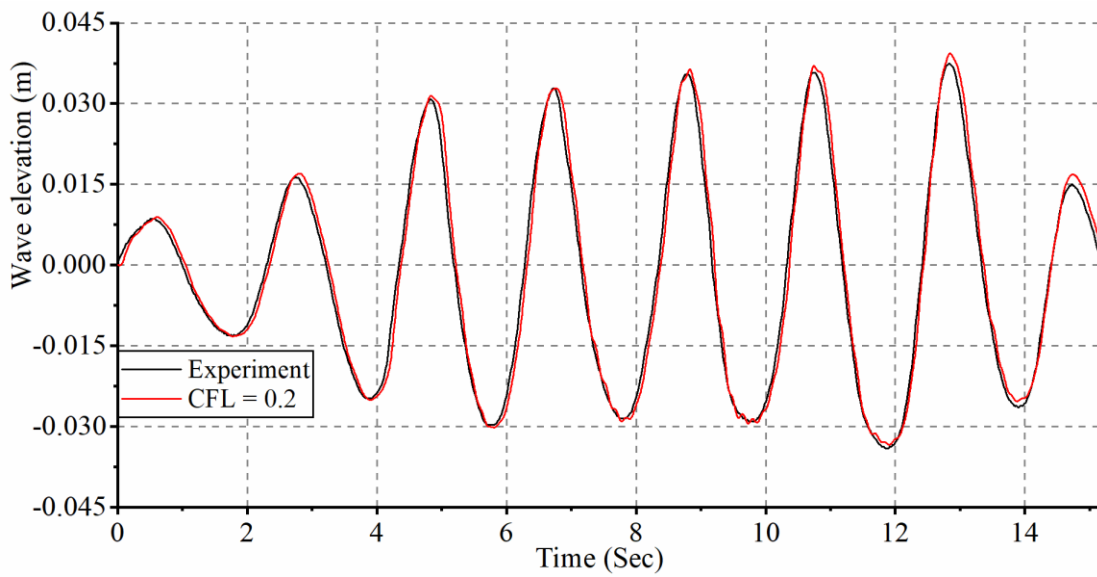


Fig. 3.12 Wave profile for CFL = 0.2 and grid size dx = 0.02 m

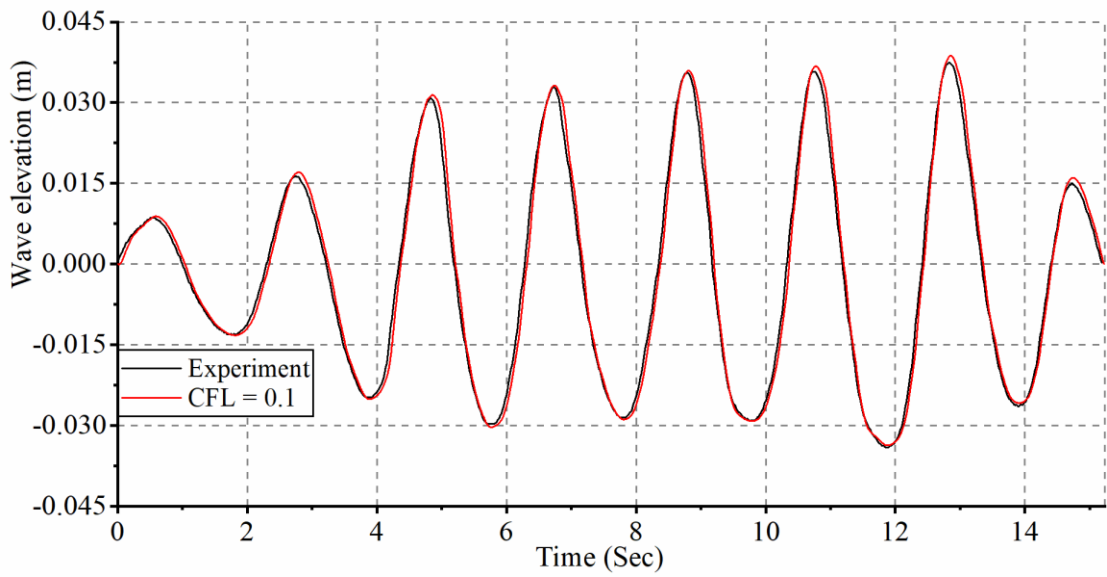


Fig. 3.13 Wave profile for CFL = 0.1 and grid size dx = 0.02 m

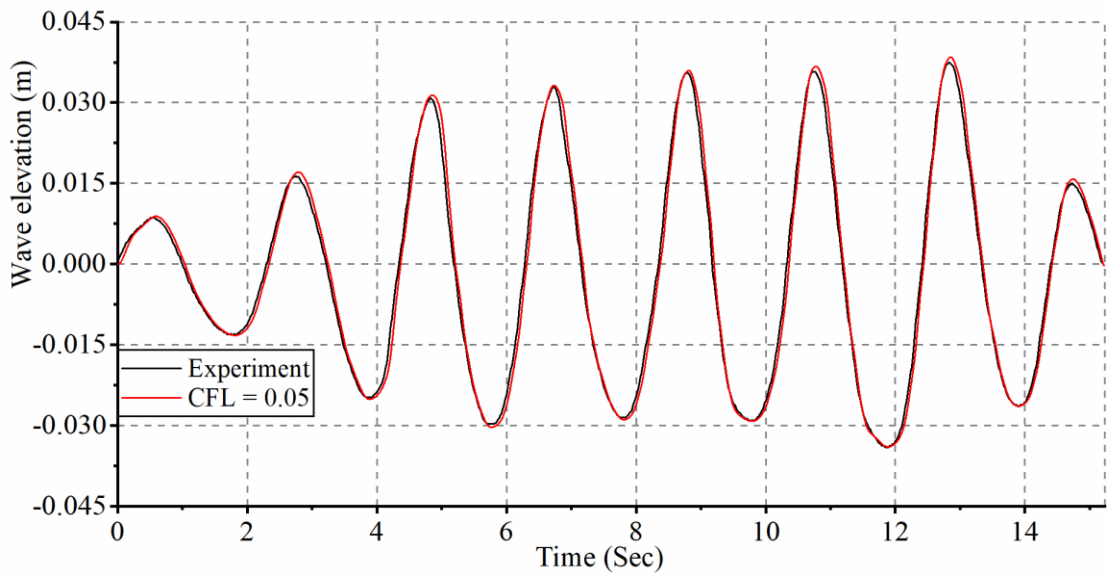


Fig. 3.14 Wave profile for CFL = 0.05 and grid size dx = 0.02 m

Table 3.11 Amplitude error with RMSE value for various grid size and CFL number

T (s)	H (m)	Grid study		CFL study	
		dx (m)	RMSE (m)	CFL No.	RMSE (m)
2.0	0.06	0.08	0.0033	0.40	0.0025
		0.04	0.0021	0.20	0.0025
		0.02	0.0020	0.10	0.0023
		0.01	0.0018	0.05	0.0023

3.10.5 Non-uniform grid

For simulating the enlarged pile head breakwater, a non-uniform grid is used in x-direction where a coarser grid size of 0.02 m is maintained at the generation and absorption zone. To define the enlarged pile head breakwater structure properly, a grid size of 0.004 m is used at the structure. The grid sizes are varied gradually from 0.02 m to 0.004 m, as shown in Fig. 3.15. At the same time, a uniform grid size of 0.004 m is kept in the y-direction and 0.004 m in the z-direction.

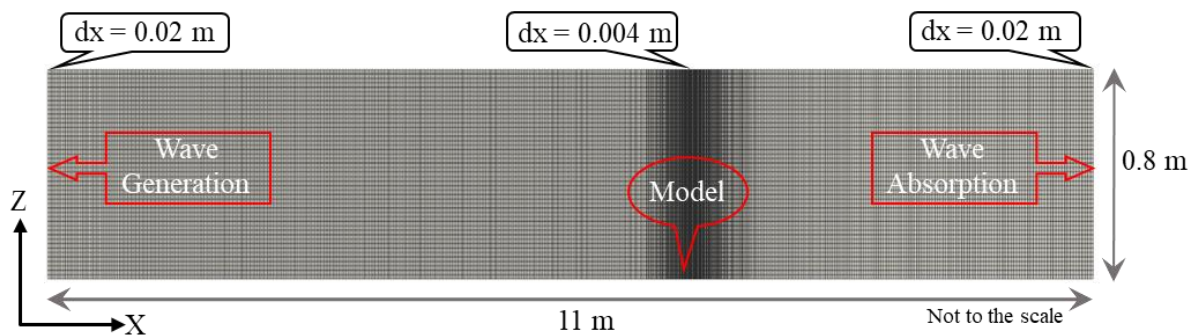


Fig. 3.15 Typical representation of non-uniform grid in numerical wave tank

3.10.6 Numerical evaluation of enlarged pile head breakwater

The numerical investigation on performance characteristics of enlarged pile head breakwater is carried out by simulating the structure in NWT. The NWT dimensions are reduced compared to the experimental tank to save computational time. The length of the NWT is reduced to 11 m based on the minimum length requirement to calculate K_t and K_r as per Isaacson (1991) method. The width of the tank is reduced by half with a symmetric plane boundary condition applied at one side of the wall, and wall boundary conditions are enforced on the other side of the wall and bottom of the tank. The waves are generated at one end using the Dirichlet inlet boundary condition. Active beach method is adopted at the opposite end to dampen the generated waves, which requires no additional tank length. The top side of the NWT is applied with symmetry plane boundary. The details of the boundary condition of NWT is presented in Fig. 3.16. To simulate the structural and wave parameters, 1:30 scale (same as physical model studies) is followed. Numerical model of enlarged pile head is initially created in AutoCAD then transferred to REEF3D in the STL (Standard Triangle Language) format. A typical numerical model of enlarged pile head is shown in Fig. 3.17.

The performance of enlarged pile head breakwater is investigated using REEF3D under the conditions of the monochromatic wave. For validating and testing the performance of enlarged pile breakwater in REEF3D, only the best performing case (non-perforated and perforated) as obtained by the physical model study is considered. Structural configuration considered for non-perforated and perforated cases is shown in Table 3.12.

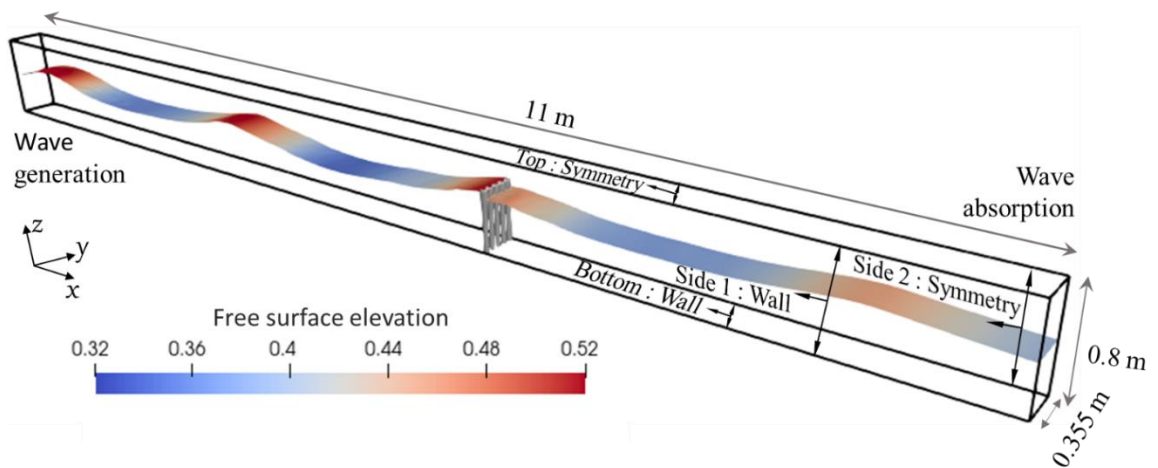


Fig. 3.16 Detailed view of numerical wave tank

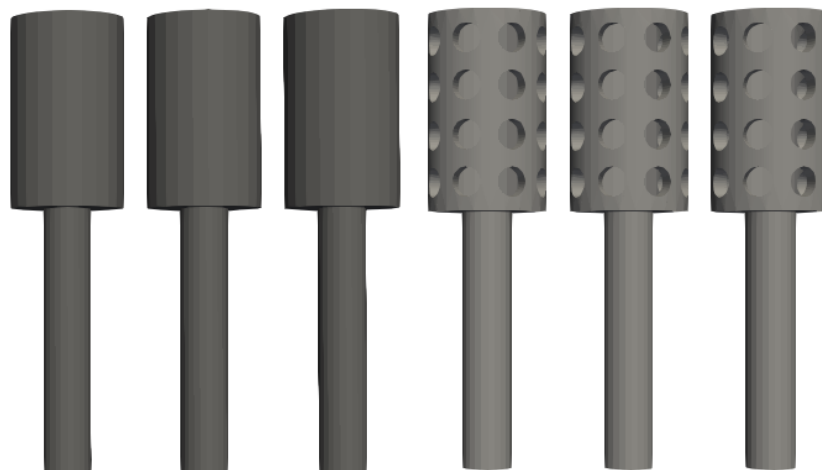


Fig. 3.17 REEF3D non-perforated and perforated enlarged pile head breakwater model

**Table 3.12 Structural configuration considered for enlarged pile head
breakwater**

Configurations	b/D	D/H_{max}	Y/H_{max}	S	pa	P	h (m)
Non-perforated	0.2	0.6	1.0	-	-	-	0.3
Perforated	0.2	0.6	1.0	0.25D	75%	22.5	0.3

3.11 PHYSICS OF THE EXPERIMENT

An idea of introducing the enlarged pile head breakwater in place of conventional pile breakwater is its effectiveness in increasing the hydraulic efficiency. The mechanism of wave energy dissipation in conventional pile breakwater is explained in section 1.4. In addition to the listed wave energy dissipation mechanism, a provision of central hollow part in the non-perforated enlarged pile breakwater results in a unique wave-structure interaction resulting in improved hydraulic efficiency (as shown in Fig. 3.18). When the wave crest overtops the pile head, some portion of wave crest may fall into the central hollow portion of the pile head and come out to the surface with a burst by losing a part of its energy. The central hollow part of the enlarged pile head increases the wave-structure interaction and turbulence, resulting in enhanced energy dissipation and, thus, increased hydraulic efficiency over the conventional pile breakwater. A detailed snapshot of wave-structure interaction with non-perforated pile head breakwater is shown in Fig. 3.19. Providing perforations over the pile head on the sea sides further increase the efficiency of this structure due to increased wave-structure interaction (as shown in Fig. 3.20). It is observed that K_t decreases with the increasing size of perforations and the size of perforations highly dominates than the percentage of perforations. The probable reason for the same is that the smaller size of perforations is ineffective in wave separation and does not facilitate effective wave passing. Hence, the wave interaction with the pile head of smaller perforations ($S < 0.15D$) is nearly similar to that of the non-perforated pile head structure.

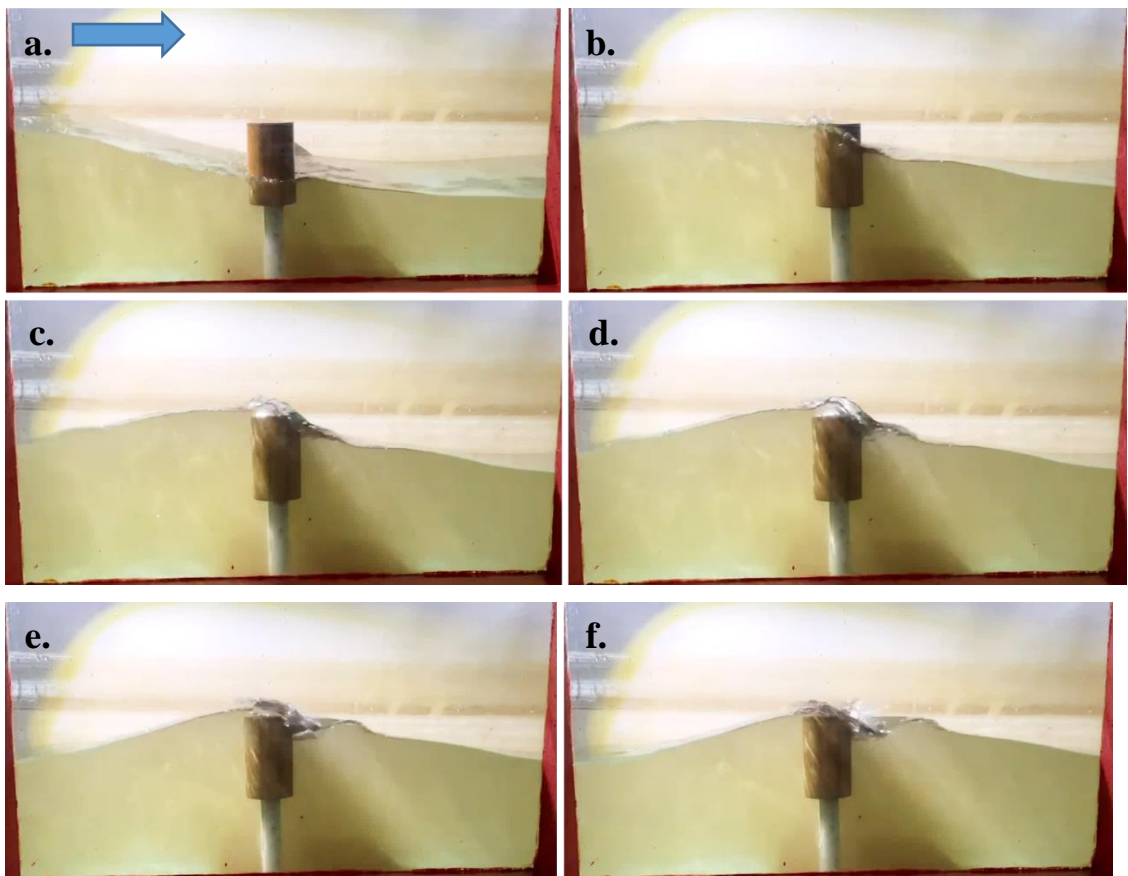


a) $D/H_{\max} = 0.6$, $Y/H_{\max} = 0.5$, $b/D = 0.2$



b) $D/H_{\max} = 0.6$, $Y/H_{\max} = 1.0$, $b/D = 0.2$

Fig. 3.18 Interaction of wave with non-perforated pile head breakwater



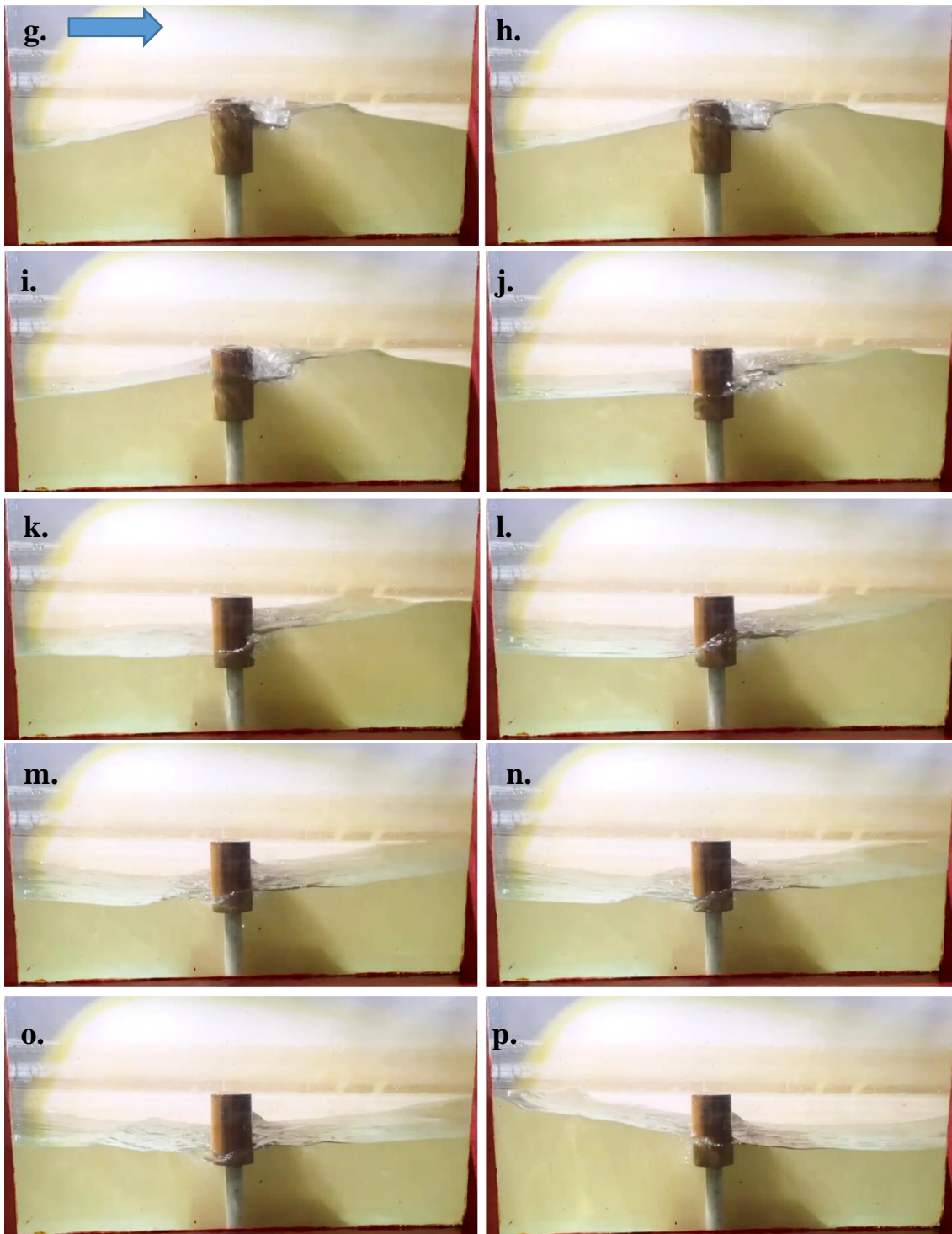


Fig. 3.19 Snapshot of wave interaction with the non-perforated pile head breakwater of $D/H_{\max} = 0.6$, $Y/H_{\max} = 1.0$ and at 0.3 m depth of water



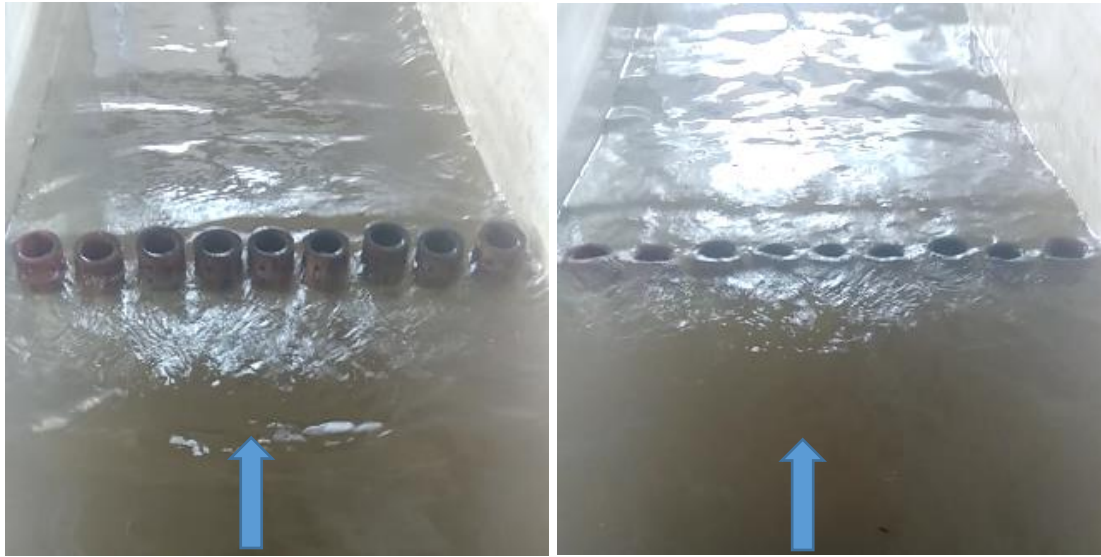
a) $D/H_{\max} = 0.6$, $Y/H_{\max} = 0.5$, $b/D = 0.2$



b) $D/H_{\max} = 0.6$, $Y/H_{\max} = 1.0$, $b/D = 0.2$

Fig. 3.20 Interaction of wave with perforated pile head breakwater with $S = 0.25D$ and $P = 22.5$

Fig. 3.21 describes the wave approaching and falling into the pile head portion with $S = 0.15D$. With an increase in the size of perforations, the perforations are effective in wave separation, and a certain percentage of waves can pass through these perforations, as shown in Fig. 3.22. In the case of a pile head with a larger size of perforations, the water level inside the pile head increases in line with the approaching wave crest. When the wave crest is at the pile head, the wave crest falls into the central hollow portion and interacts with the wave entered through the perforations resulting in increased turbulence.



a) Wave crest approaching pile head b) Wave crest plunging into hollow portion

Fig. 3.21 Wave approaching perforated pile head for $D = 0.064$ m, $Y = 0.16$ m and $S = 0.15D$

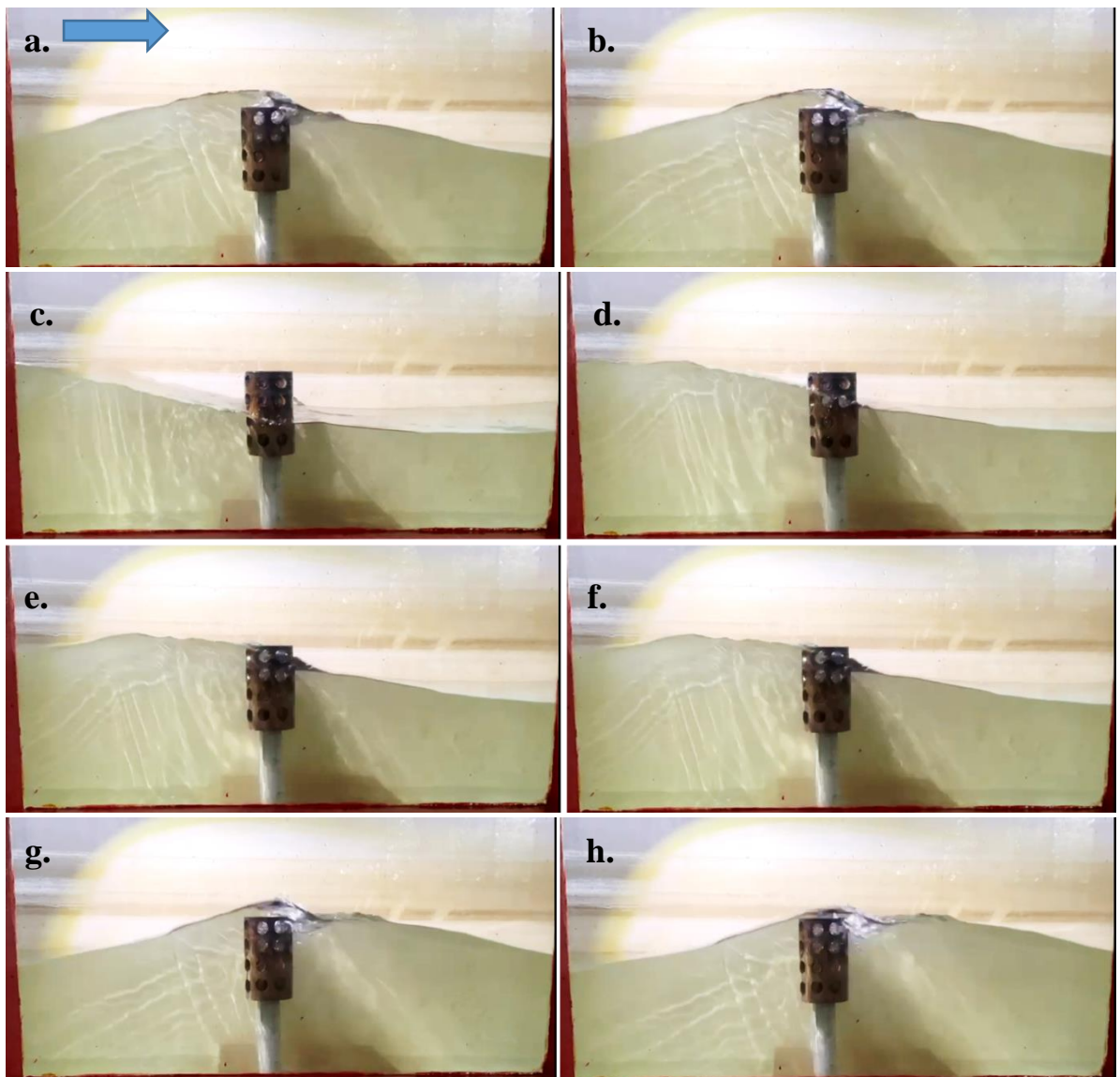


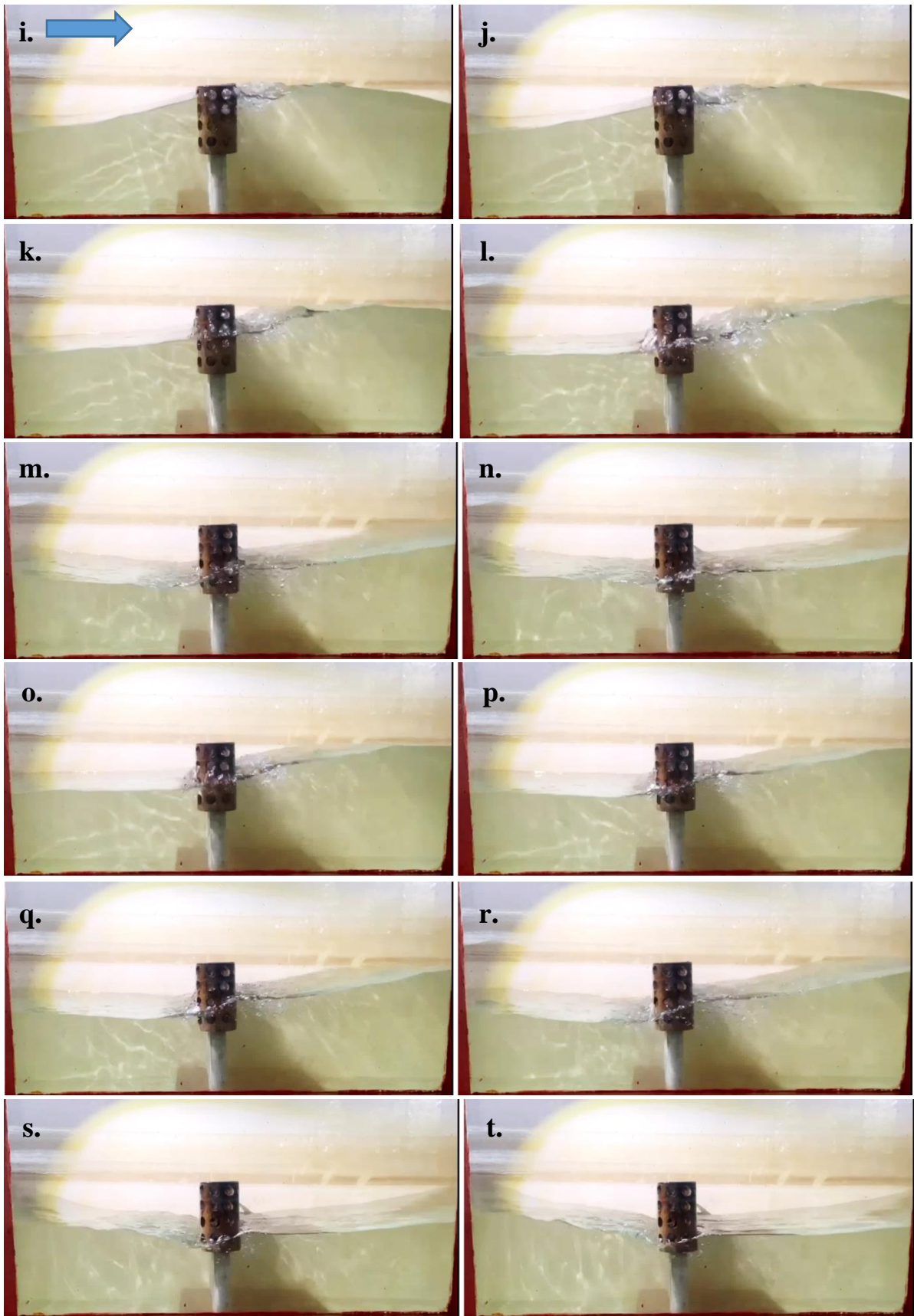
a) Wave crest approaching pile head b) Wave crest plunging into hollow portion

Fig. 3.22 Wave approaching perforated pile head for $D = 0.096$ m, $Y = 0.16$ m and $S = 0.25D$

Hence, it results in increased energy dissipation and hydraulic efficiency over the non-perforated pile head breakwater. A detailed snapshot of the wave-structure interaction

is depicted in Fig. 3.23. It is noted that the perforated pile head has more reflection than the non-perforated pile head breakwater. A probable reason for this phenomenon could be due to the additional reflection caused by the water coming out of the pores towards the seaside when the wave crest passes the structure. The same is as illustrated in Fig. 3.24. Typical wave interaction with pile head under wave crest and trough for $D = 0.096$ m, $Y = 0.16$ m and $S = 0.25D$ are shown in Fig. 3.25 and Fig. 3.26, respectively.





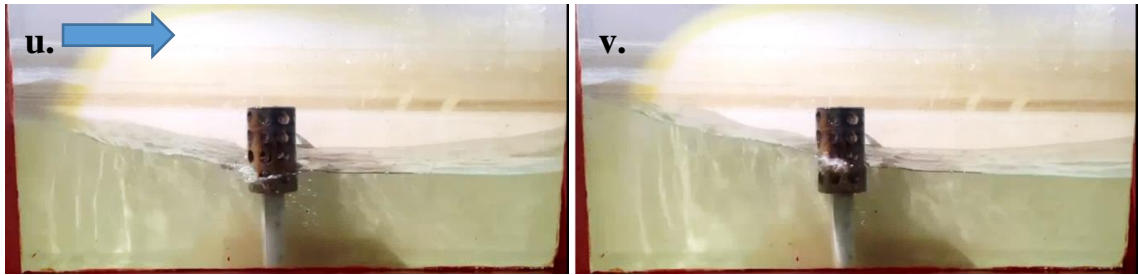


Fig. 3.23 Snapshot of wave interaction with the perforated pile head breakwater of $D/H_{\max} = 0.6$, $Y/H_{\max} = 1.0$, $b/D = 0.2$, $S = 0.25D$, $p_a = 75\%$ and $P = 22.5$ at 0.3 m depth of water



a) $D/H_{\max} = 0.6$, $Y/H_{\max} = 0.5$, $b/D = 0.2$ b) $D/H_{\max} = 0.6$, $Y/H_{\max} = 1.0$, $b/D = 0.2$

Fig. 3.24 Reflection of the wave from perforated pile head breakwater with $S = 0.25D$ and $P = 22.5$

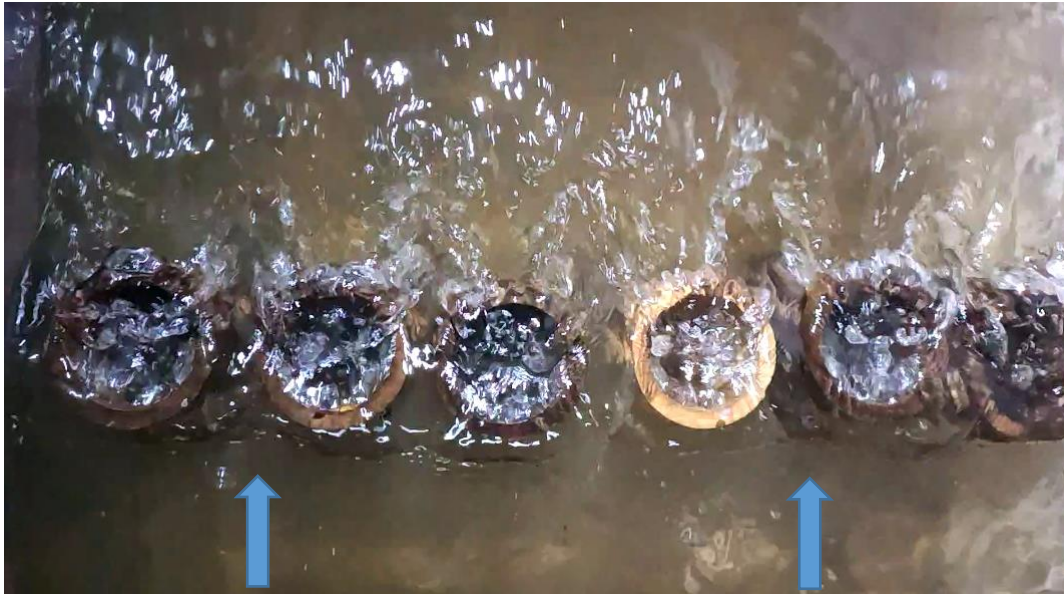


Fig. 3.25 A typical wave interaction under crest with perforated pile head for $D = 0.096$ m, $Y = 0.16$ m and $S = 0.25D$

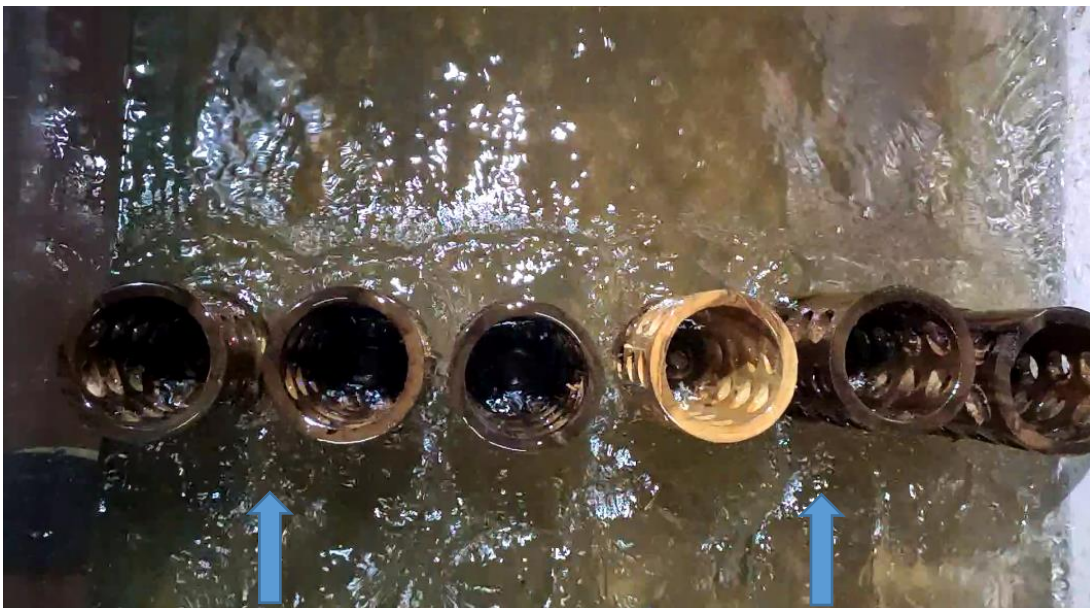


Fig. 3.26 A typical wave interaction under trough with perforated pile head for $D = 0.096$ m, $Y = 0.16$ m and $S = 0.25D$

3.12 WAVE-STRUCTURE INTERACTION IN NUMERICAL MODEL

In numerical modelling, it is possible to visualise the wave-structure interactions, similar to that of physical model studies. A complete view of NWT with wave interaction is shown Fig. 3.27. A detailed view of wave interaction with the enlarged pile head breakwater in the numerical and physical models are compared in Fig. 3.28 to Fig. 3.31.

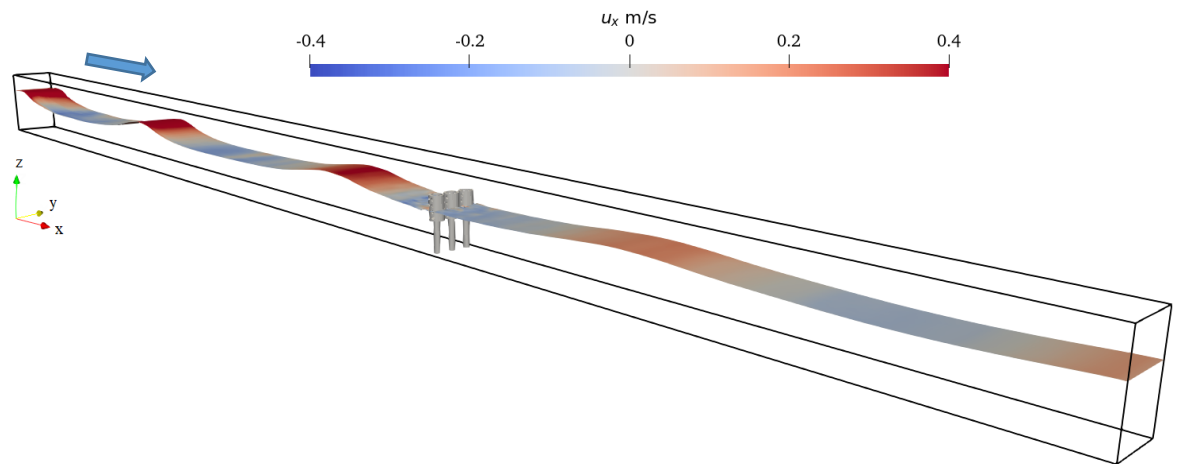


Fig. 3.27 Wave interaction with enlarged pile head in NWT

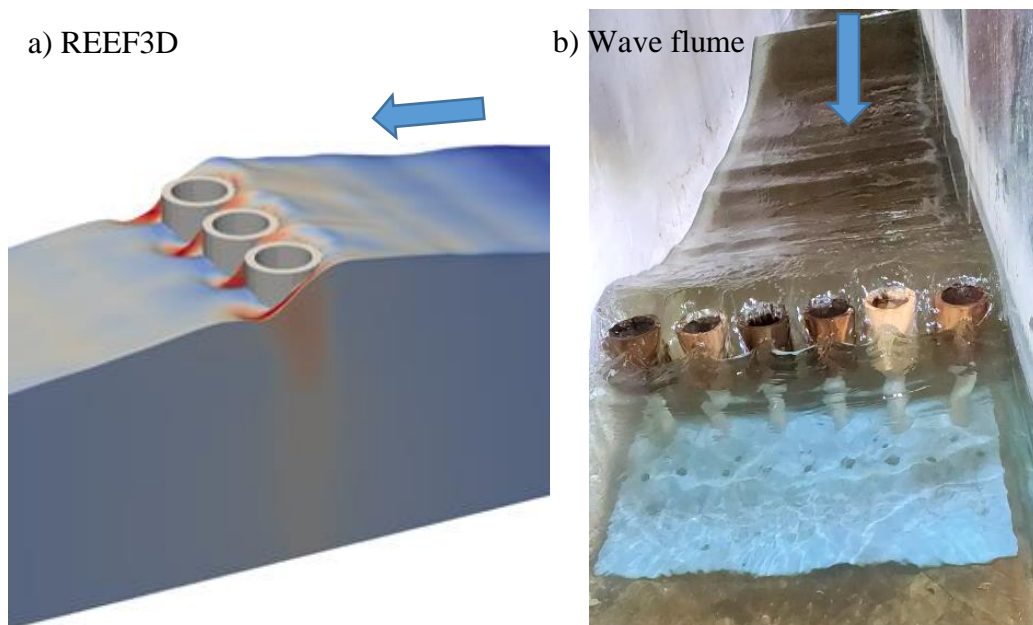


Fig. 3.28 Wave interaction with a non-perforated enlarged pile breakwater

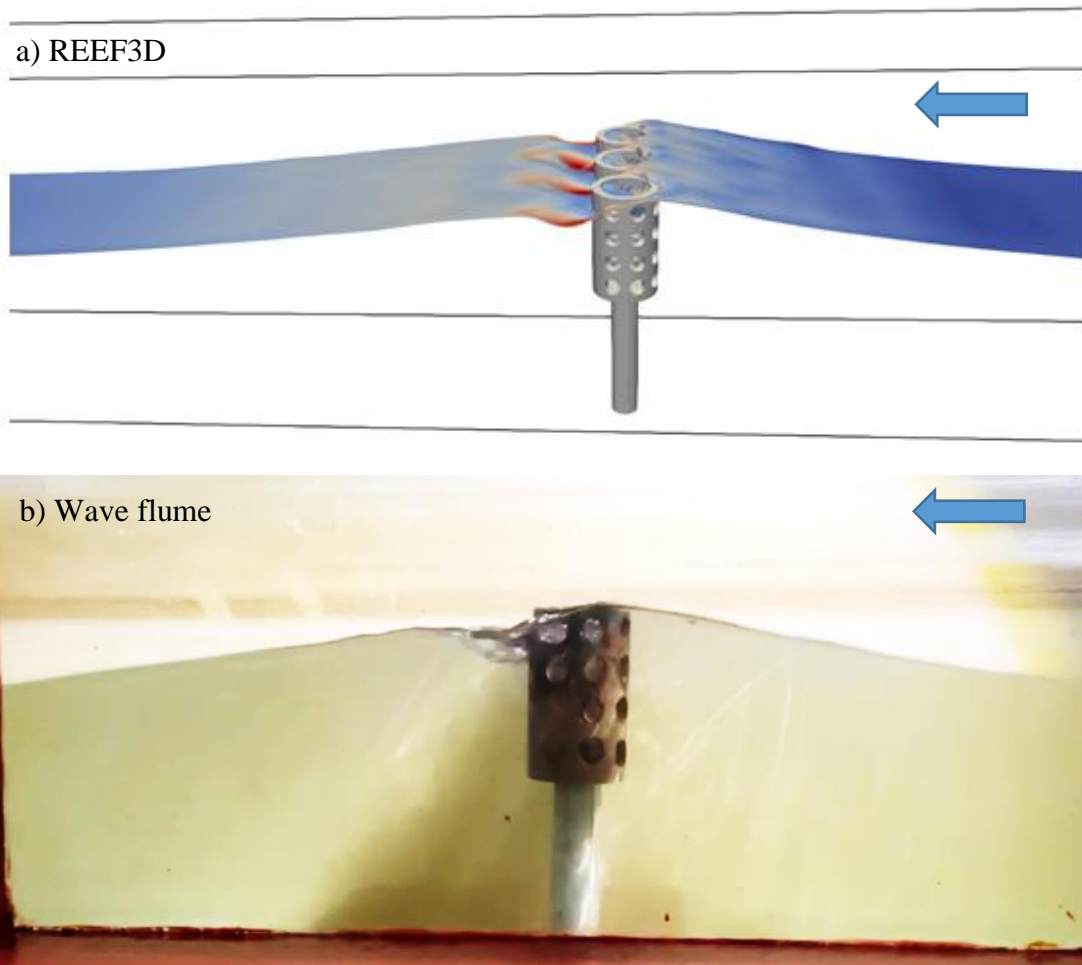
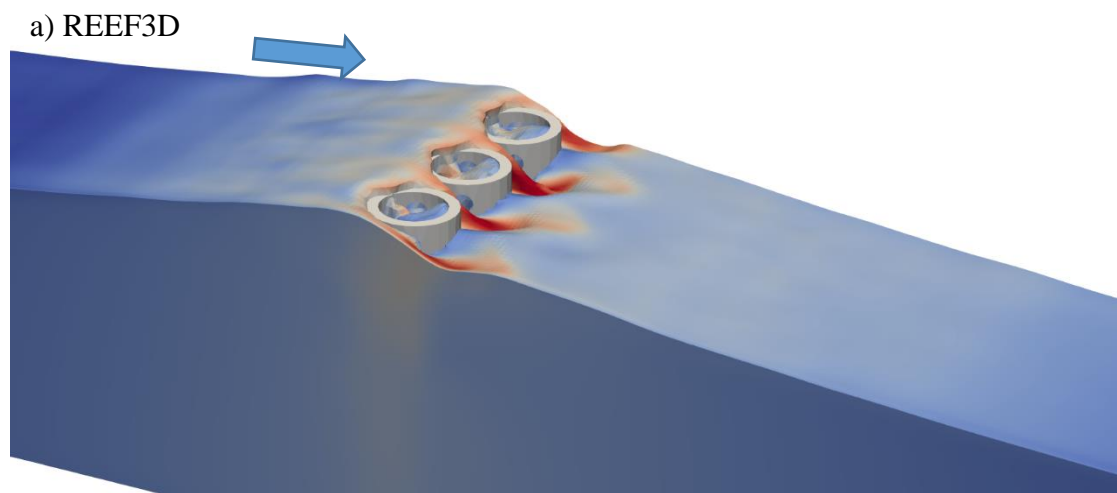


Fig. 3.29 Wave interaction with a perforated enlarged pile breakwater

Fig. 3.28 to Fig. 3.31 demonstrates the wave-structure interactions in the experimental and numerical modelling. The wave-structure interaction in the numerical modelling well resembles the physical observations. Fig. 3.30 shows the water entering through the perforations ($0.25D$), and Fig. 3.31 clearly shows how the water flows back through the perforation under the wave trough towards the seaside.



b) Wave flume

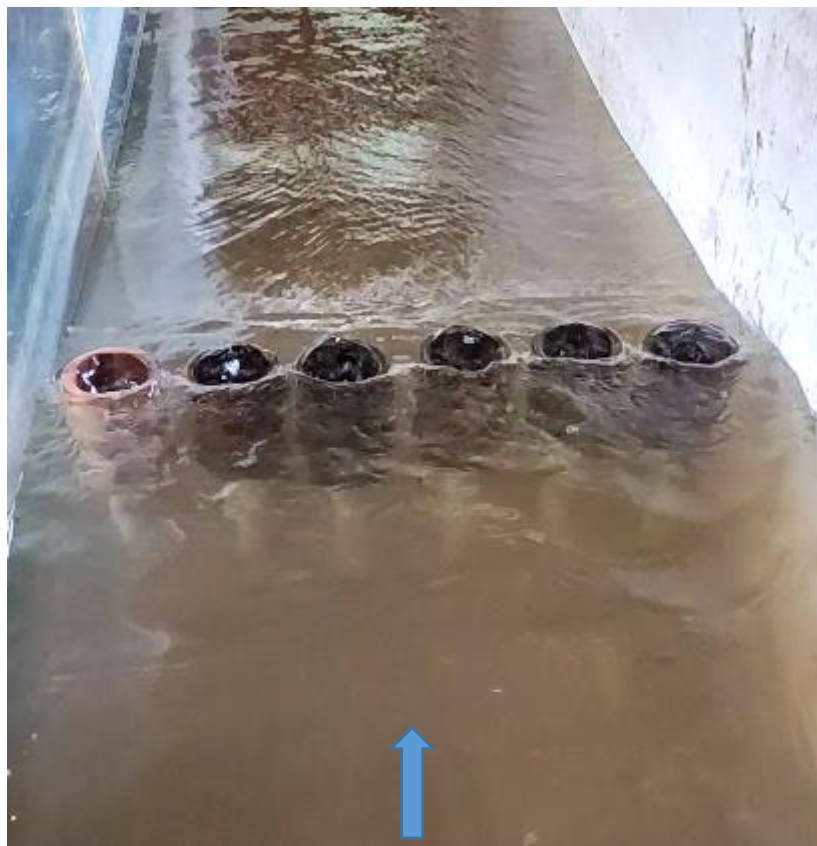
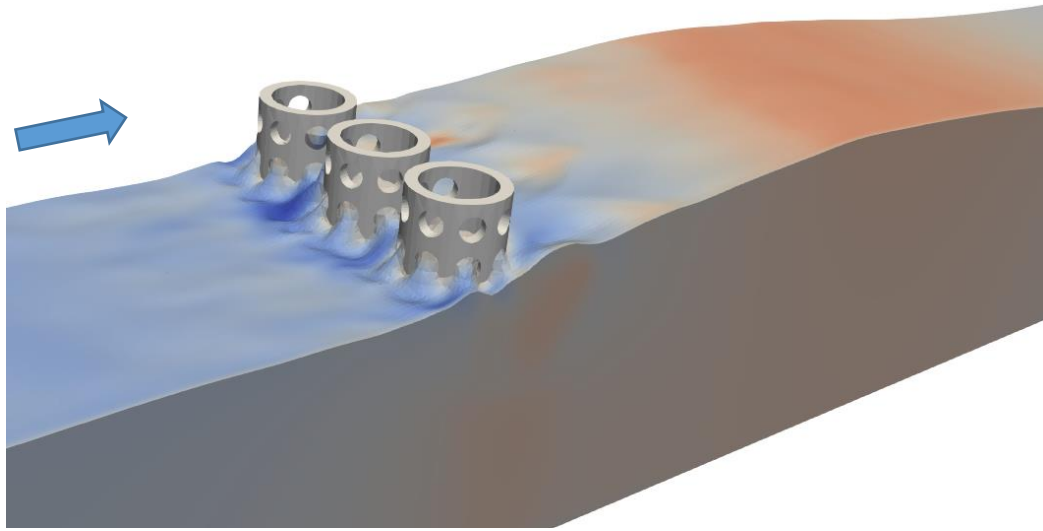


Fig. 3.30 Wave interaction with a perforated enlarged pile breakwater

a) REEF3D



b) Wave flume



Fig. 3.31 View of water flowing back (towards seaside) under wave trough from the perforated of enlarged pile head

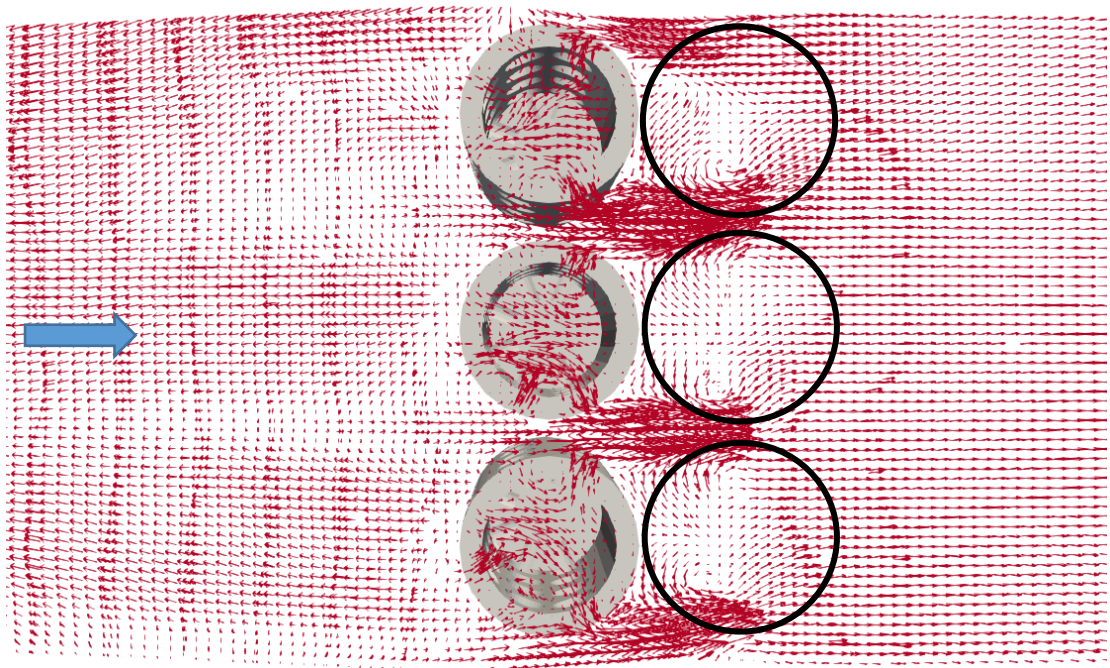


Fig. 3.32 Formation of vortex behind pile head under wave crest in REFF3D

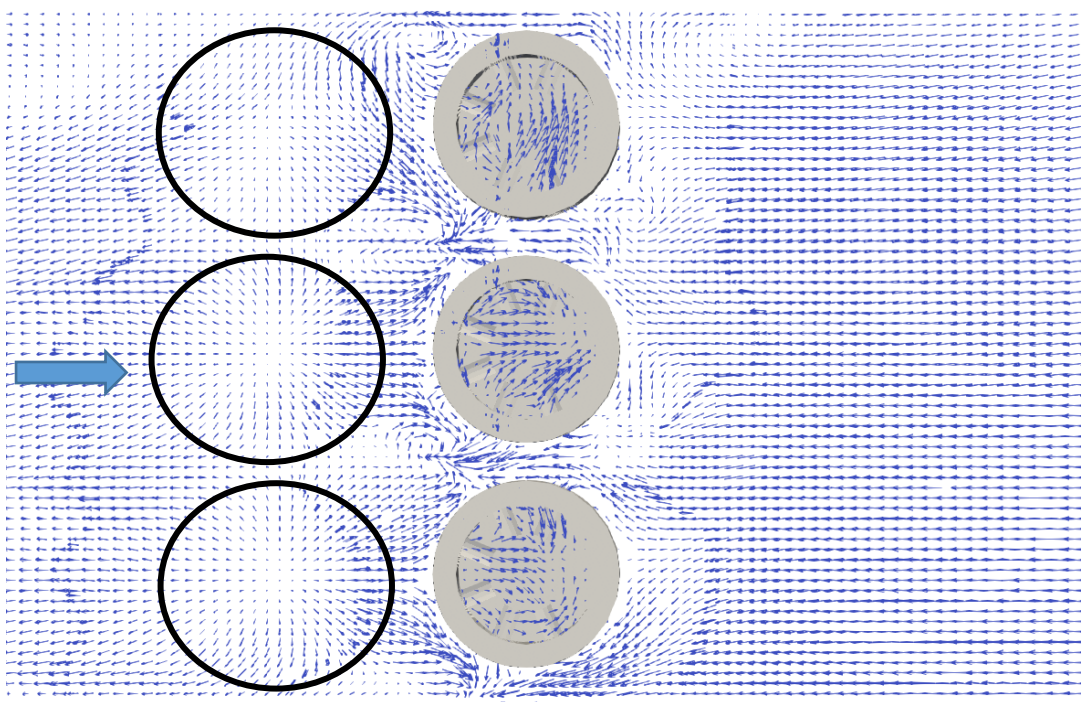


Fig. 3.33 Formation of vortex behind pile head under wave trough in REFF3D

It was stated that in the case of pile structure, wave energy is dissipated due to wave-structure interaction associated with inertia resistance, contraction, wave reflection,

turbulence and vortex shedding. The formation of vortex is believed to be shifting from seaside to lee side depending on wave crest and trough. The formation of vortex can be visualized by enabling the particle flow pattern in the REEF3D numerical model. Fig. 3.32 and Fig. 3.33 show the formation of vortex behind and in front of the structure under wave crest and trough respectively. Results are plotted for the structural configuration of $b/D = 0.2$, $D/H_{\max} = 0.6$, $Y/H_{\max} = 1.0$, $S = 0.25D$, $p_a = 75\%$ and $P = 22.5$. The concept of formation of the vortex resembles, as explained in section 1.4.

3.13 METHODOLOGY

The methodology adopted for the present research work is explained in this chapter and the flow chart of the methodology is presented in Fig. 3.34.

Literature survey:

Literature survey is the foundation of any research work to know what works have been accomplished and what technologies or methodologies have been evolved in the past, what development have been taken place till date and the current state of the art of technology in the area of research.

Problem formulation:

Interaction between wave and pile structure is a very complex phenomenon and review of the literature showed that there is no research done so far on wave attenuation due to enlarged pile head breakwater structure. The proposed concept of the breakwater is intended to bridge the knowledge gap by investigating this new type of breakwater using physical model study and also to explore the application of numerical model technologies to it.

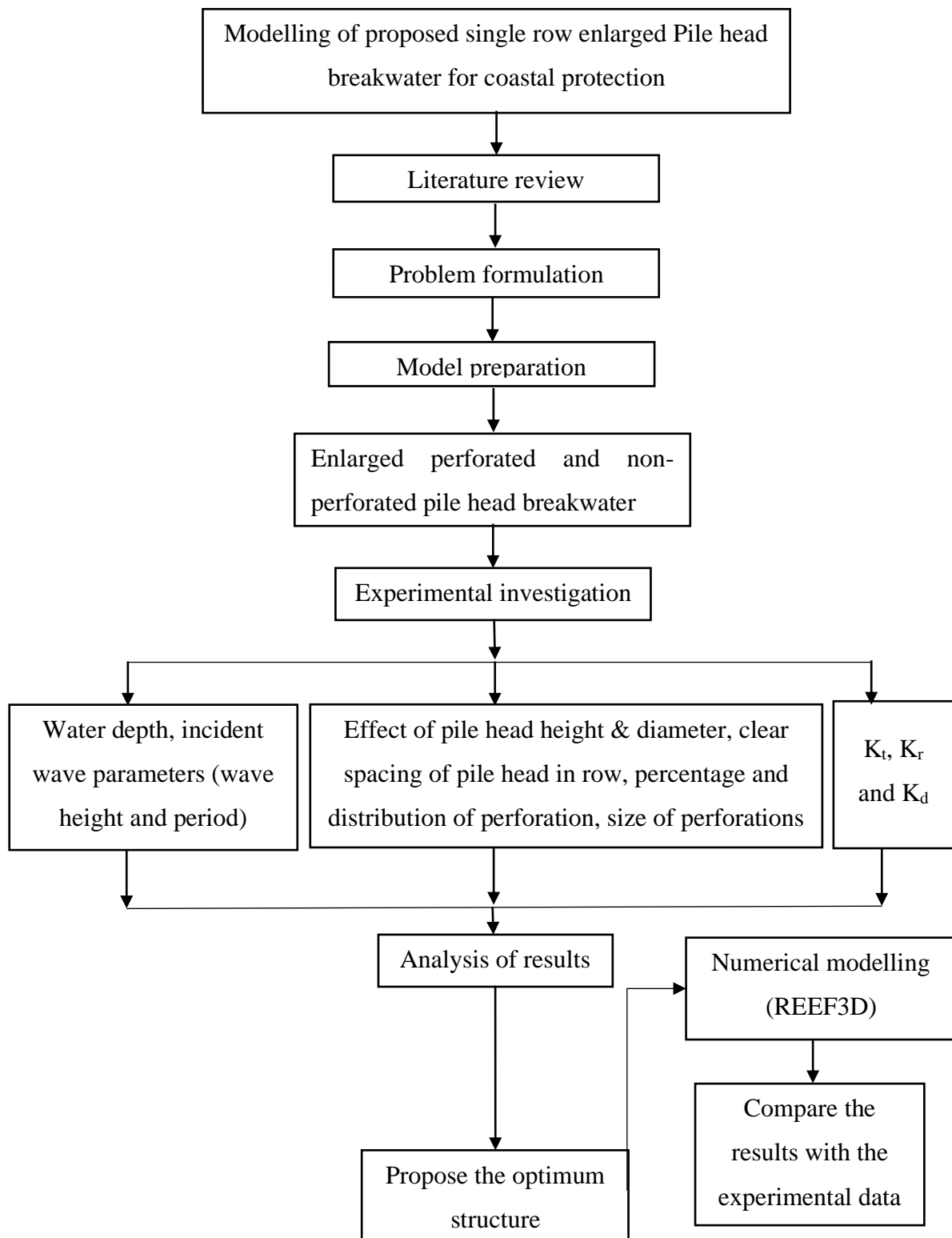


Fig. 3.34 Flow chart of methodology

Physical modelling:

The main objectives of the current study are to explore the hydraulic performance of the innovative enlarged pile head breakwater structure with and without perforations. Froude scaling is adopted for the modelling of the perforated structure, which allows for the correct facsimile of gravitational and fluid inertial forces. In the present study, 1:30 scaled dimension is used to describe the model dimensions and the wave climate. The proposed model is subjected to monochromatic waves of varying wave heights and wave periods generated in different water depths. The influence of the proposed perforated and non-perforated enlarged pile head breakwater model on K_t , K_r and K_d are studied.

Numerical modelling:

Numerical models are simulated for the proposed breakwater in open-source software REEF3D and results are compared with those obtained from the physical model study.

Experimental technique:

Series of experiments are conducted in a two-dimensional wave flume and the performance of the structure was tested by generating monochromatic waves. The wave elevation data is collected using the capacitance type wave probes to determine incident, reflected and transmitted wave heights for varying test conditions.

Analysis of results:

The performance and configuration of enlarged pile head (with and without perforations) breakwater subjected to varying wave climate is analysed and an attempt is made to evolve an optimised breakwater model.

3.14 TEST CONDITIONS

To design safe and economical structures, the model test conditions must be designed and operated judiciously. The current experimental studies are carried under the following test conditions:

- The seabed is fixed and hence, it is assumed that the movement of sediments does not interfere with wave motion and does not affect the model performance.
- Waves generated are in a short burst of five waves.

- The waves generated in each burst are periodic and monochromatic.
- Brief intervals are provided between wave burst to ensure reflected waves does not interfere with the incident waves.
- Secondary waves produced are insignificant for the test.
- The density difference between freshwater and seawater is not considered.
- The pile structure is rigid and fixed at the bed.

3.15 TEST PROCEDURE

The wave flume is cleaned and filled with potable water to the determined depth. Experiments are conducted on a single row of piles. Before conducting the experiments, the wave flume is calibrated for the considered combinations of wave heights and wave periods. Capacitance type wave probes are installed to measure the water surface elevation. The probes are also calibrated every time before and at the end of the experiments. As suggested by Isaacson (1991), wave height measurement with three probes method is used for calculating the wave reflection. Three probes are installed before the model (on the seaward side) to measure the incident and reflected wave heights as illustrated in Fig. 3.1. The spacing between the probes in the seaward side is adjusted to one-third of the wavelength (L) to ensure accuracy of wave reflections (Goda and Suzuki 1976; Isaacson 1991). Transmitted wave heights (H_t) are recorded from a probe placed at a distance L from the model towards the lee side. In the current investigation, experiments are conducted for 0.3 m, 0.4 m and 0.5 m water depths. For all the considered depth of water, the pile head is fixed in such a manner that the water level is at the centre of the pile head. The schematic arrangement of the pile head breakwater for different water depth is shown in Fig. 3.3. The height of the pile head, pile diameter and pile trunk are varied with respect to the maximum wave height (H_{max}). For the current study maximum wave height of 4.8 m as suggested by KREC study team (1994) is considered which is equal to 0.16 m in model.

Waves are generated in a burst of five at a time to avoid reflections. The models are tested for wave heights ranging from 0.06 m to 0.16 m and wave periods of 1.4 to 2 s. The water surface elevation from the probe is recorded by wave recorder and using EMCON software. The generated wave heights are analysed to study the wave-

structure interaction in the form of K_t , K_r and K_d . The water surface elevation measured by probes is observed manually by fixing strips of graphs to one side of the flume as a cross-check.

3.16 SOURCES OF ERRORS AND PRECAUTIONS EXERCISED

The following are the sources of errors identified in the experimental studies.

- Liner dimensions error: The model is built with a linear dimension accuracy of up to 1.0 mm. This may contribute an error ranging from 0.2 to 0.3%.
- Error in wave height measurement: Errors resulting from wave height measurement are minimised (<0.2 %) using probes having the least count of ± 0.10 mm.
- Error due to change in water level: This error occurs due to the improper desired water level in the flume.

The following criteria was adopted to minimise the errors in the present study:

- As per the standard procedure, the model is constructed with the largest possible model scale of 1:30.
- To ensure the repeatability of the experimentation, each test case is investigated thrice, and it is noted that the relative error ranges between -5 to +5%.
- Error due to change in water level is minimised by monitoring and maintaining the desired water level within ± 2 mm by refilling.
- Calibration of the flume and wave probes are undertaken without the model placement and before the commencement of experiments. The wave heights employed in the test runs are obtained during calibration. This prevents the losses due to wave interference with flume sidewalls and bed and eliminates these error sources.
- Waves are generated in a burst of five waves, and a sufficient time gap is given between wave bursts to diffuse the wave energy

3.17 UNCERTAINTY ANALYSIS

Uncertainty is an estimate of experimental error. It describes the degree of goodness of a measurement or experimentally determined result. With the help of uncertainty analysis, it is possible to conduct experiments in a scientific manner and predict the accuracy of the result (Misra, 2001). Experimental error sources should be identified and the error (δ) should be determined from manufactures brochures, from calibration and conducting simple experiments respectively. The distribution of uncertainty between precision and bias is arbitrary. The confidence interval gives an estimated range of values, which is likely to include an unknown population parameter. The estimated range is calculated from a given set of observations. The 95% confidence interval limits must always be estimated and this concept of confidence level is fundamental to uncertainty analysis (Misra, 2001). The details of the uncertainty analysis are explained in Appendix II.

3.18 PHOTOS OF EXPERIMENTAL SET-UP AND MODELS

The snapshots showing details of data acquisition system is shown in Fig. 3.35 and Fig. 3.36. The Fig. 3.37 show the wave generation system used in the present investigation.



Fig. 3.35 Data acquisition system



Fig. 3.36 View of wave flume with wave probes for data acquisition



Fig. 3.37 Wave generation system (clockwise from top left: inverter drive, motor, flap type wave paddle and wave filter)

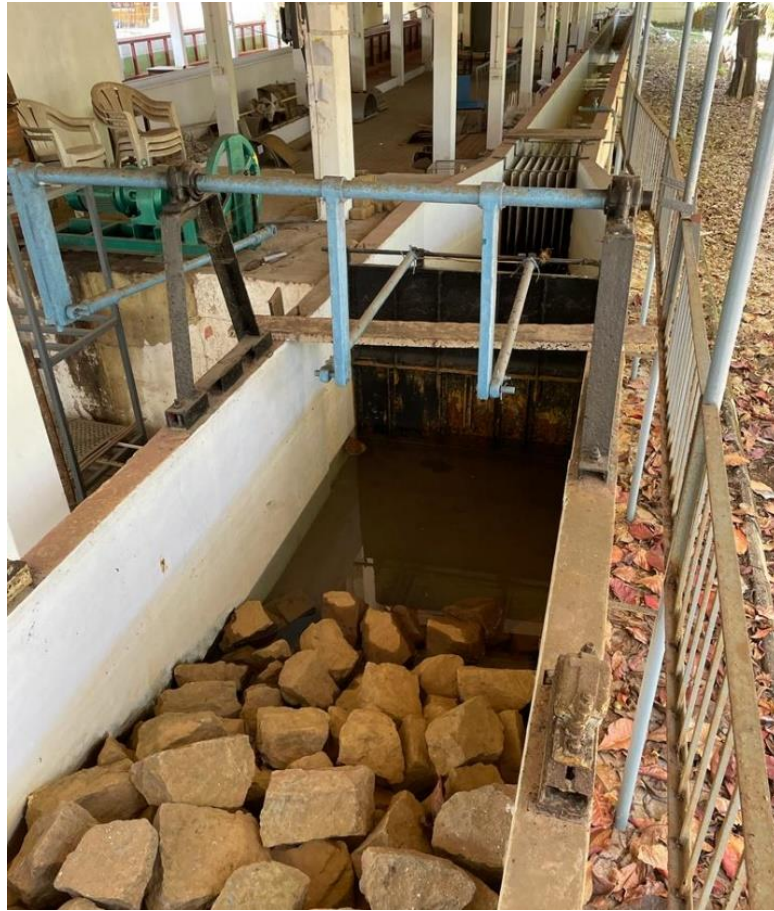


Fig. 3.38 View of the wave flume (from generation side)

INVESTIGATION ON HYDRAULIC PERFORMANCE OF NON-PERFORATED ENLARGED PILE HEAD BREAKWATER

The experimental results are presented in graphical form by considering the non-dimensional parameters. The results are analysed by considering various parameters such as incident wave steepness (H_i/gT^2), relative spacing between the piles (b/D), depth of water (h), diameter (D) and height of pile head (Y) on wave transmission (K_t), reflection (K_r) and energy dissipation (K_d). As observed from the scatter plots (Fig. 4.1 to Fig. 4.6), the wave-structure interaction is not consistent enough to exhibit a perfect correlation with wave parameters. Therefore, best fit lines are shown for better visualisations.

4.1 EFFECT OF INCIDENT WAVE STEEPNESS

The transmission coefficient is plotted against the incident wave steepness (H_i/gT^2), as shown in Fig. 4.1 to Fig. 4.3, for the different relative spacing between piles and varying depths of water. It is observed that irrespective of the depth of water and relative pile spacing, the transmission coefficient decreases with increasing incident wave steepness. Increase in H_i/gT^2 from 0.002 to 0.005 results in 5% to 18% reduction in K_t , 10% to 45% increase in K_r and 5% to 39% increase in K_d . This behaviour is because steeper waves are more likely to break and dissipate energy and hence, the transmission reduces. This type of behaviour is similar to the findings of other types of pile breakwaters as reported by Koraim et al. (2014), Mani and Jayakumar (1995), Rao and Rao (2001, 1999) and Van Weele and Herbich (1972).

4.2 INFLUENCE OF RELATIVE PILE SPACING

4.2.1 On wave transmission

To understand the influence of relative pile spacing (b/D) on K_t , graphs are plotted for K_t versus H_i/gT^2 with b/D as a third variable. Fig. 4.1 to Fig. 4.3 show that, as the b/D decreases from 1.2 to 0.2, the transmission coefficient decreases for all the wave steepness considered in the present study.

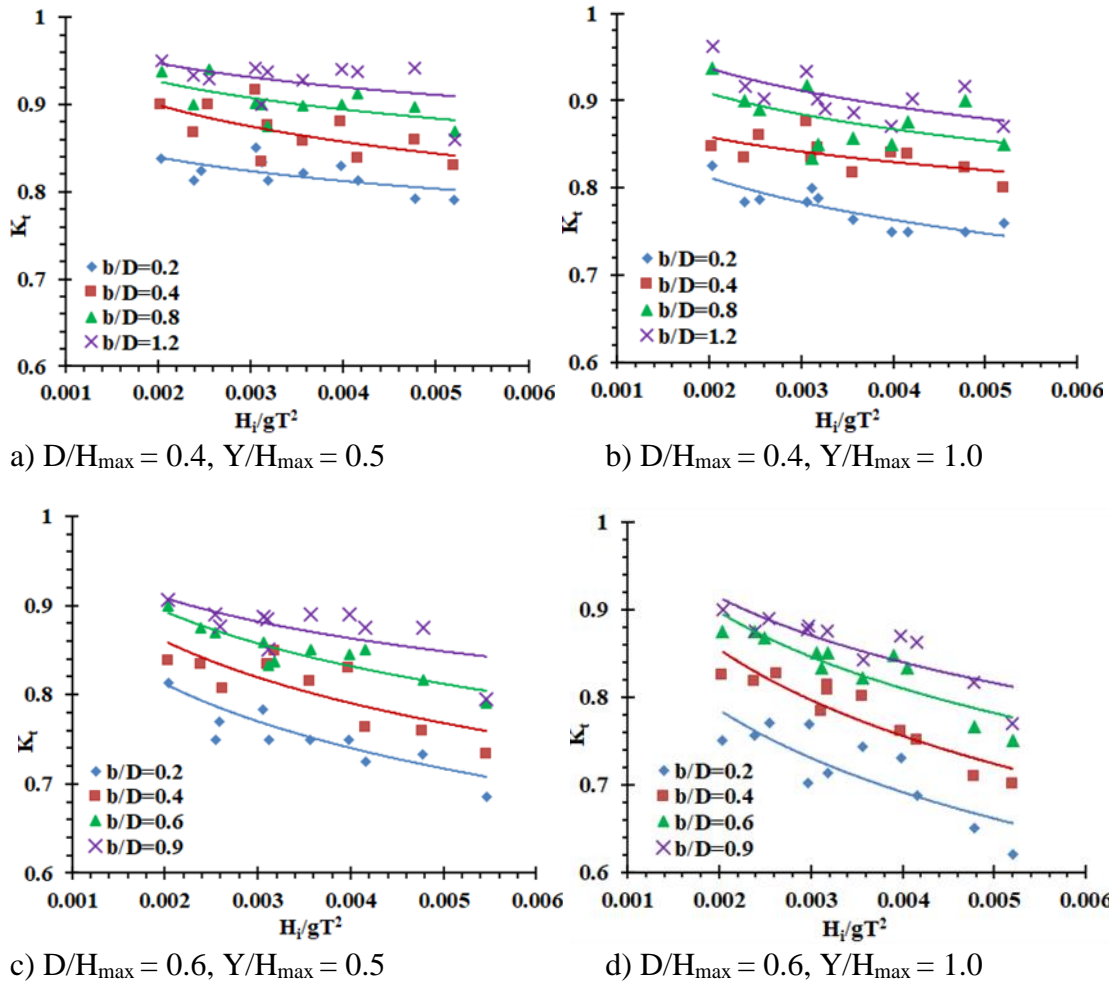
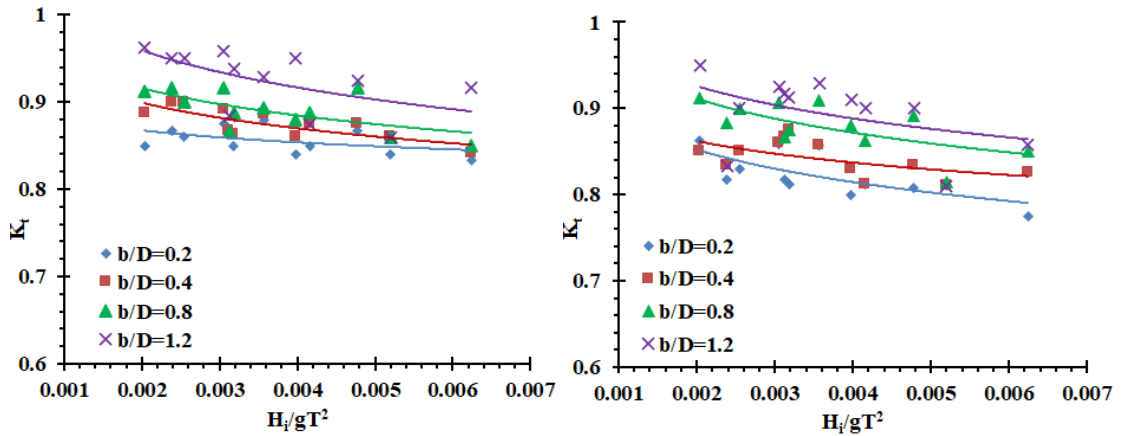


Fig. 4.1 Graphs of K_t versus H_i/gT^2 for varying ratios of b/D , D/H_{max} and Y/H_{max} at a water depth of 0.30 m

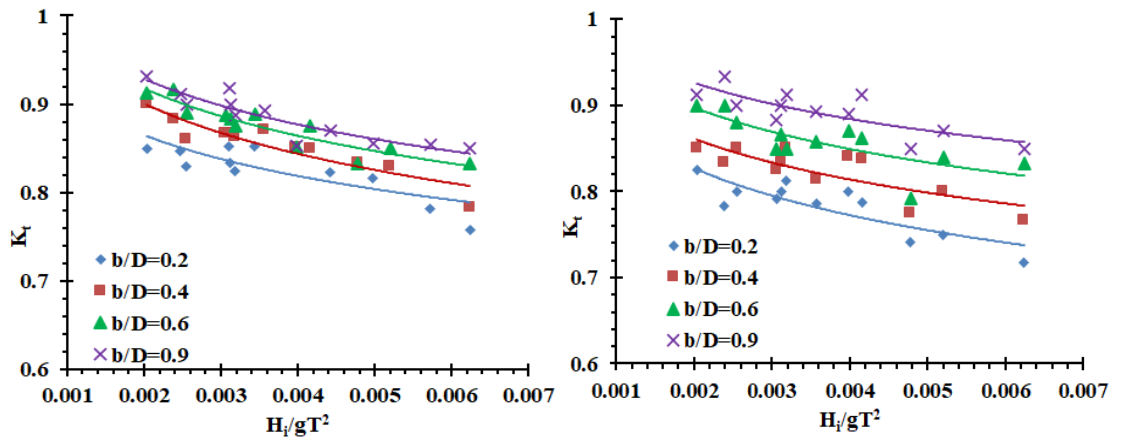
From Fig. 4.1 (a), Fig. 4.2 (a) and Fig. 4.3 (a), for pile head of diameter 0.064 m ($D/H_{max} = 0.4$) and head height 0.08 m ($Y/H_{max} = 0.5$) with b/D decreasing from 1.2 to 0.2, value of K_t decreases from 0.975 to 0.8375 (14.1%) and 0.91 to 0.79 (13.18%) at lower wave steepness (0.0021) and higher wave steepness (0.0052) respectively. From Fig. 4.1 (b), Fig. 4.2 (b) and Fig. 4.3 (b), for diameter of pile head 0.064 m ($D/H_{max} = 0.4$) and height 0.16 m ($Y/H_{max} = 1.0$) with decreasing b/D from 1.2 to 0.2, K_t value decreases to 0.825 from 0.97 (14.94%) and 0.76 from 0.9 (15.55%) at lower wave steepness and higher wave steepness respectively. Effect of b/D when $D/H_{max} = 0.6$ with $Y/H_{max} = 0.5$ and 1.0 is shown in Fig. 4.1 (c and d), Fig. 4.2 (c and d) and Fig. 4.3 (c and d). The trend observed are similar to the case of $D/H_{max} = 0.4$ with $Y/H_{max} = 0.5$ and 1.0, A maximum reduction in K_t is noticeable for the case when of $D/H_{max} = 0.6$

and $Y/H_{\max} = 1.0$. For this case a maximum of 27.73% reduction in K_t is observed when b/D changes from 0.9 to 0.2 at higher wave steepness. Above analysis shows that $b/D = 0.2$ is the optimum relative spacing for the enlarged pile breakwater.



a) $D/H_{\max} = 0.4, Y/H_{\max} = 0.5$

b) $D/H_{\max} = 0.4, Y/H_{\max} = 1.0$



c) $D/H_{\max} = 0.6, Y/H_{\max} = 0.5$

d) $D/H_{\max} = 0.6, Y/H_{\max} = 1.0$

Fig. 4.2 Graphs of K_t versus H_i/gT^2 for varying ratios of b/D , D/H_{\max} and Y/H_{\max} at a water depth of 0.40 m

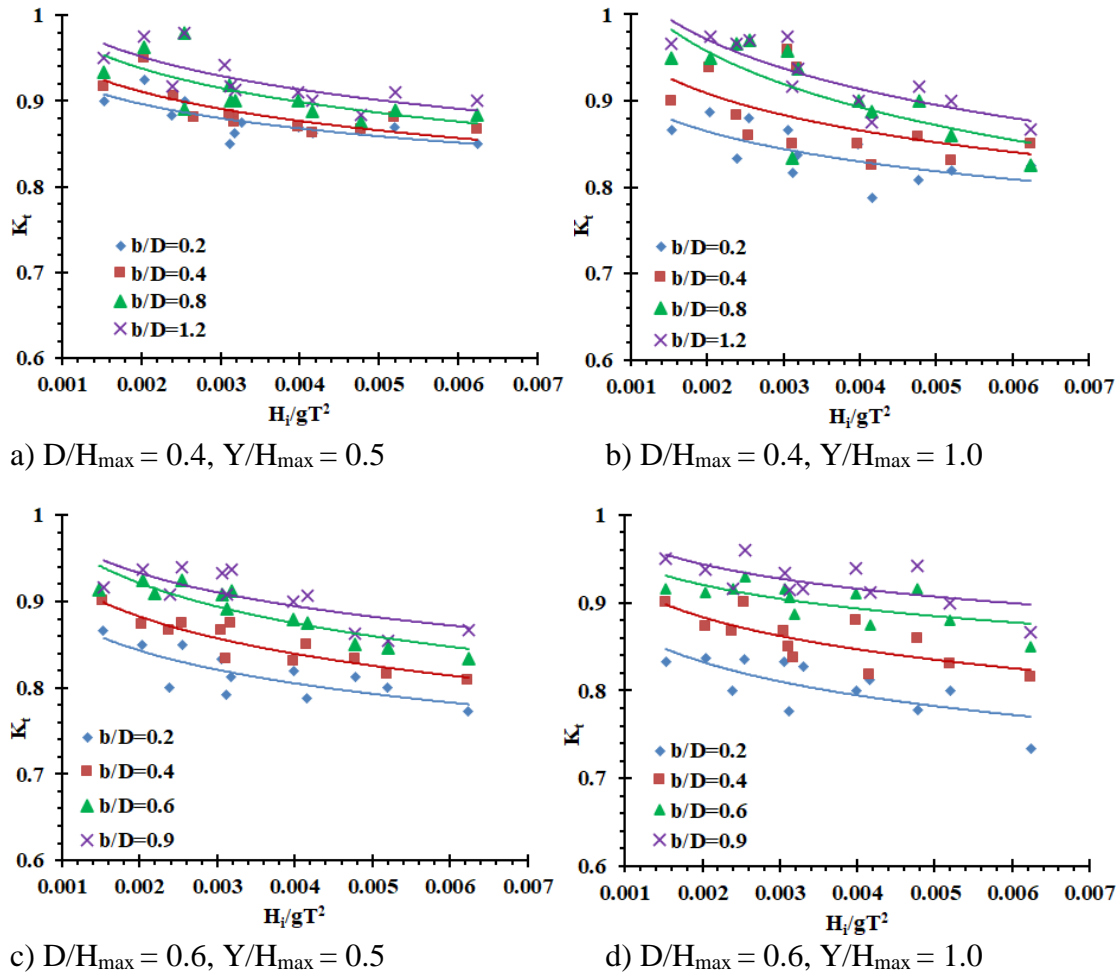
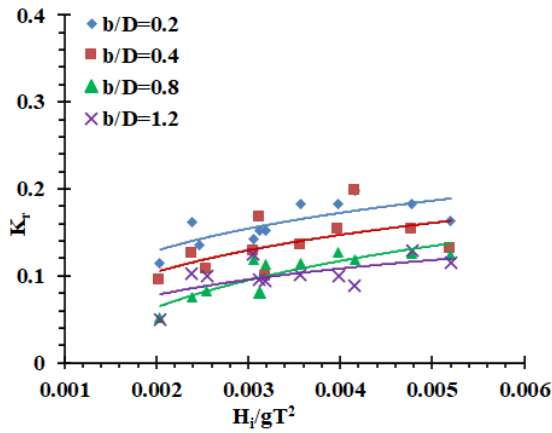


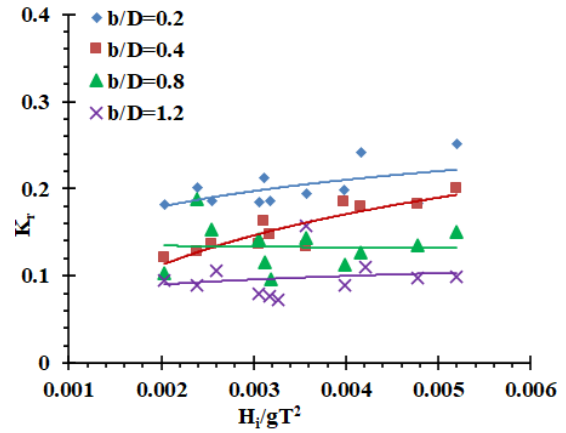
Fig. 4.3 Graphs of K_r versus H_i/gT^2 for varying ratios of b/D , D/H_{\max} and Y/H_{\max} at a water depth of 0.50 m

4.2.2 On wave reflection

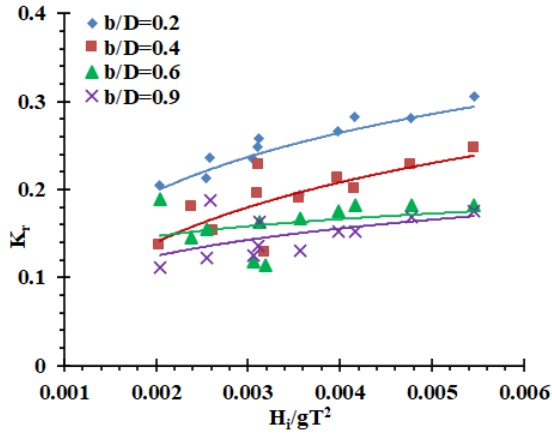
Variation of reflection coefficient (K_r) for changing depths of water are shown in Fig. 4.4, Fig. 4.5 and Fig. 4.6 with changing b/D . The trend observed is opposite to that of K_t , hence decrease in b/D , K_r increases. Maximum reflection is observed for the case when $D/H_{\max} = 0.6$, $Y/H_{\max} = 1.0$, $b/D = 0.2$ at a depth of water of 0.3 m. For the same case a maximum change of K_r from 0.17 to 0.34 (100%) is observed at higher wave steepness and 0.12 to 0.24 at lower wave steepness when b/D changes from 0.9 to 0.2.



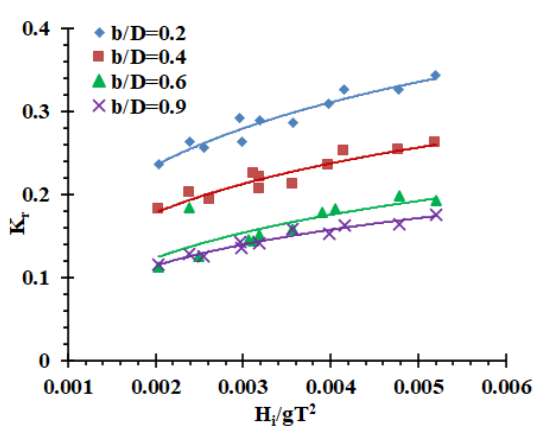
a) $D/H_{\max} = 0.4, Y/H_{\max} = 0.5$



b) $D/H_{\max} = 0.4, Y/H_{\max} = 1.0$

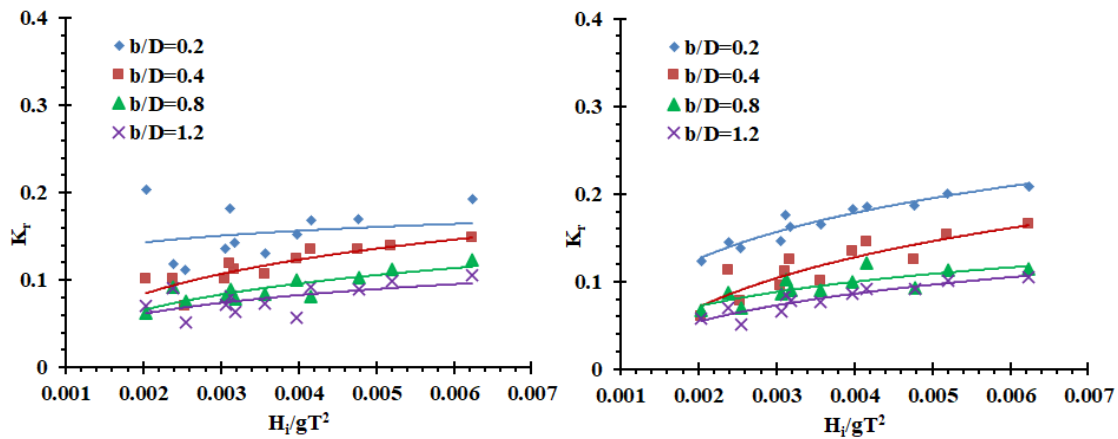


c) $D/H_{\max} = 0.6, Y/H_{\max} = 0.5$



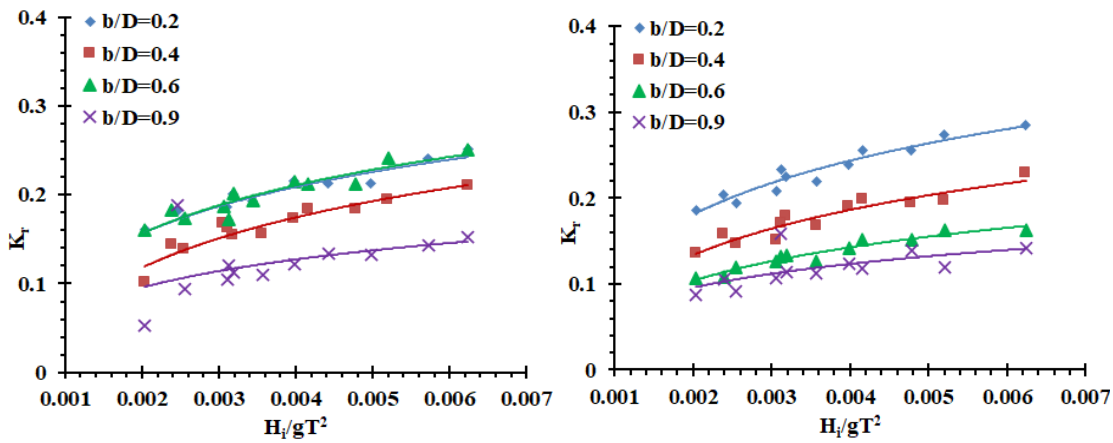
d) $D/H_{\max} = 0.6, Y/H_{\max} = 1.0$

Fig. 4.4 Graphs of K_r versus H_i/gT^2 for varying ratios of b/D , D/H_{\max} and Y/H_{\max} at a water depth of 0.30 m



a) $D/H_{\max} = 0.4$, $Y/H_{\max} = 0.5$

b) $D/H_{\max} = 0.4$, $Y/H_{\max} = 1.0$



c) $D/H_{\max} = 0.6$, $Y/H_{\max} = 0.5$

d) $D/H_{\max} = 0.6$, $Y/H_{\max} = 1.0$

Fig. 4.5 Graphs of K_r versus H_i/gT^2 for varying ratios of b/D , D/H_{\max} and Y/H_{\max} at a water depth of 0.40 m

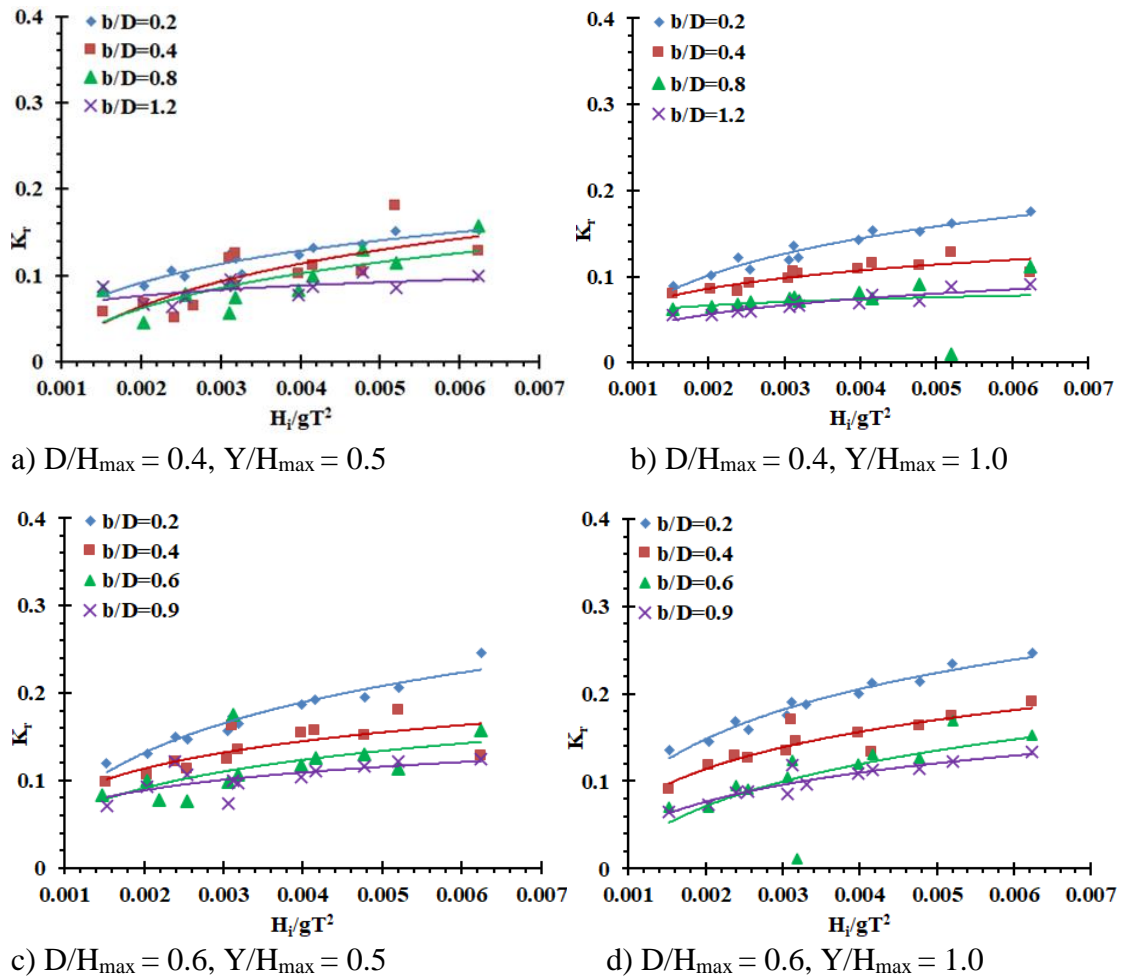


Fig. 4.6 Graphs of K_r versus H_i/gT^2 for varying ratios of b/D , D/H_{max} and Y/H_{max} at a water depth of 0.50 m

4.2.3 On wave energy dissipation

Variation of energy dissipation coefficient (K_d) with b/D for changing depths of water are shown in Fig. 4.7, Fig. 4.8 and Fig. 4.9. The trend observed are opposite to that of K_t and in line with K_r , hence decrease in b/D , K_d increases. Maximum K_d is observed for the case when $D/H_{max} = 0.6, Y/H_{max} = 1.0, b/D = 0.2$ at 0.3 m depth of water. For the same case, change in b/D from 0.9 to 0.2 results in an increase of K_d from 0.4 to 0.58 (45%) at lower wave steepness and 0.55 to 0.67 (21.8%) at higher wave steepness.

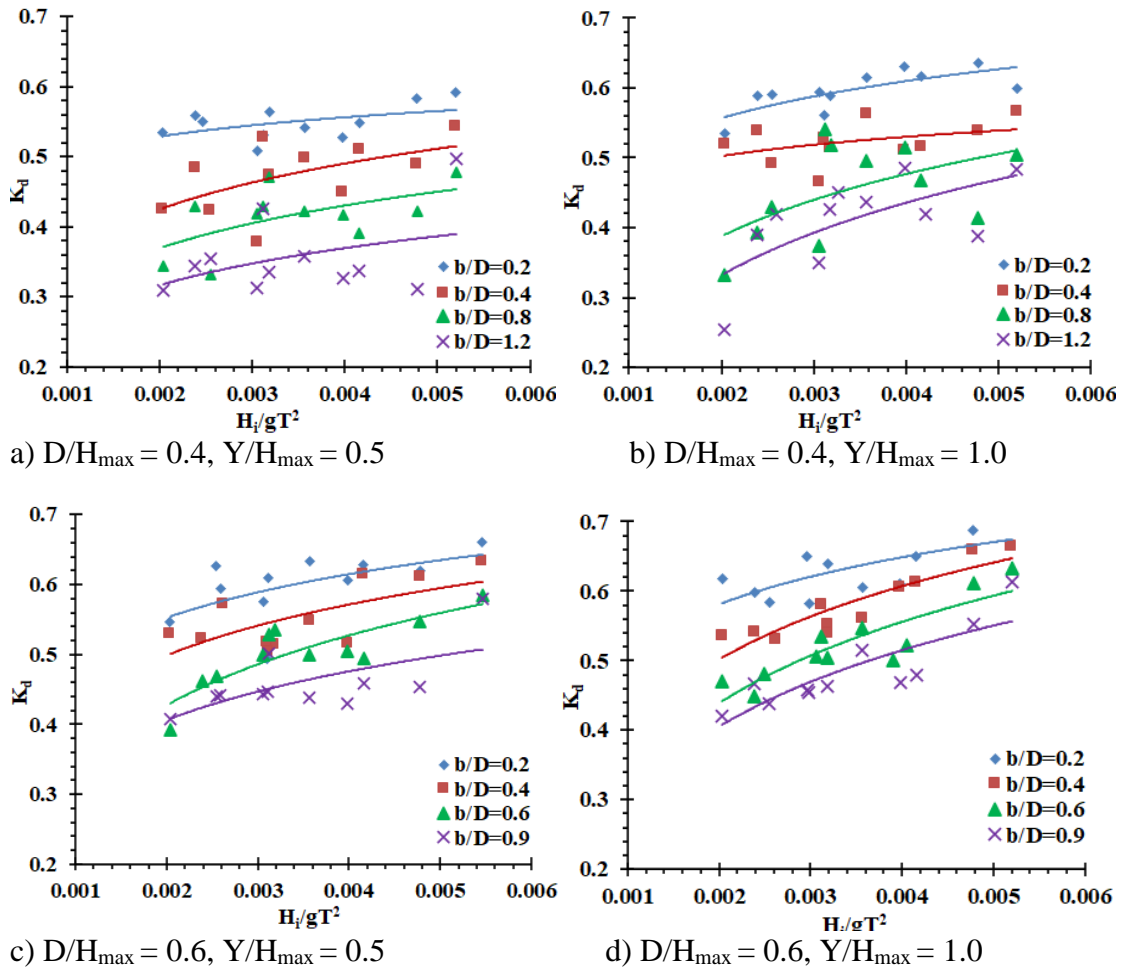


Fig. 4.7 Graphs of K_d versus H_i/gT^2 for varying ratios of b/D , D/H_{\max} and Y/H_{\max} at a water depth of 0.30 m

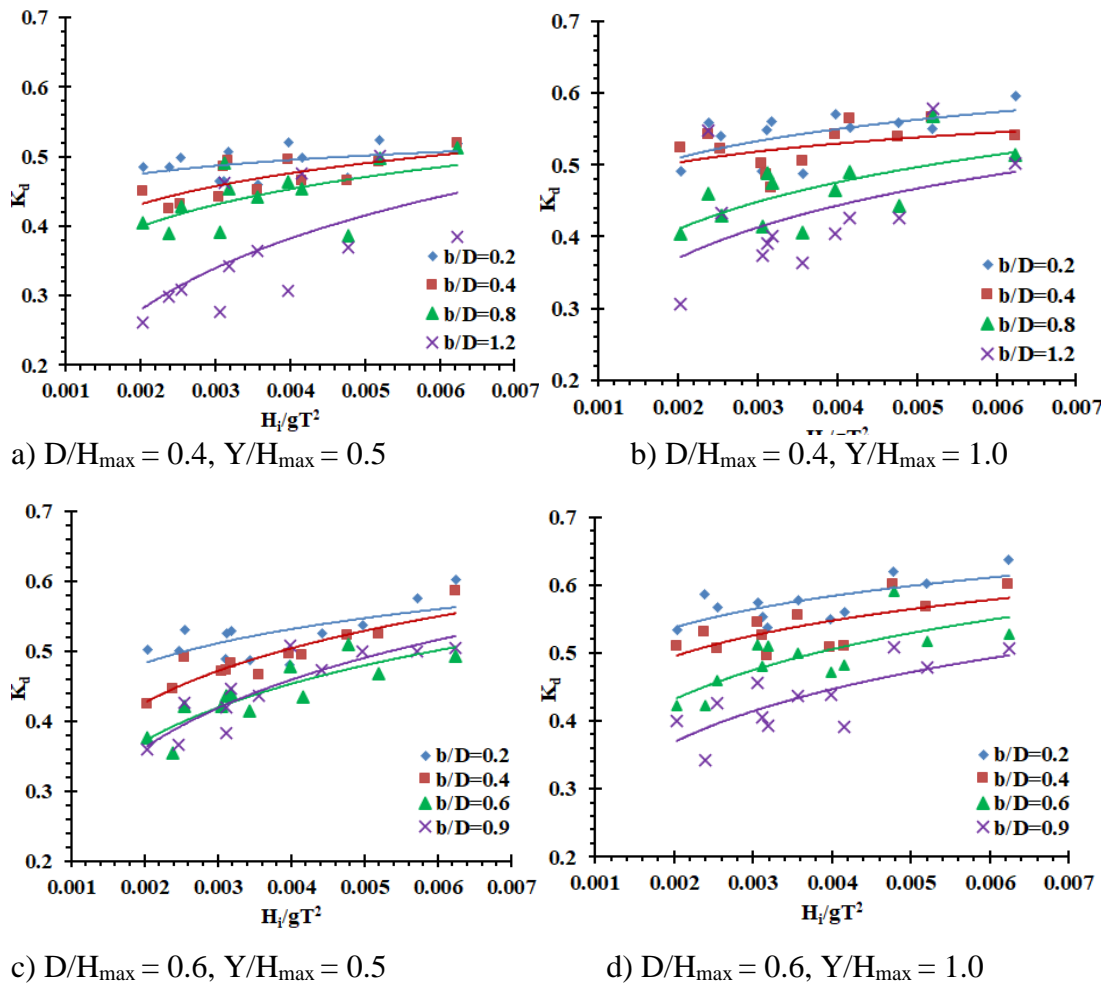


Fig. 4.8 Graphs of K_d versus H_i/gT^2 for varying ratios of b/D , D/H_{\max} and Y/H_{\max} at a water depth of 0.40 m

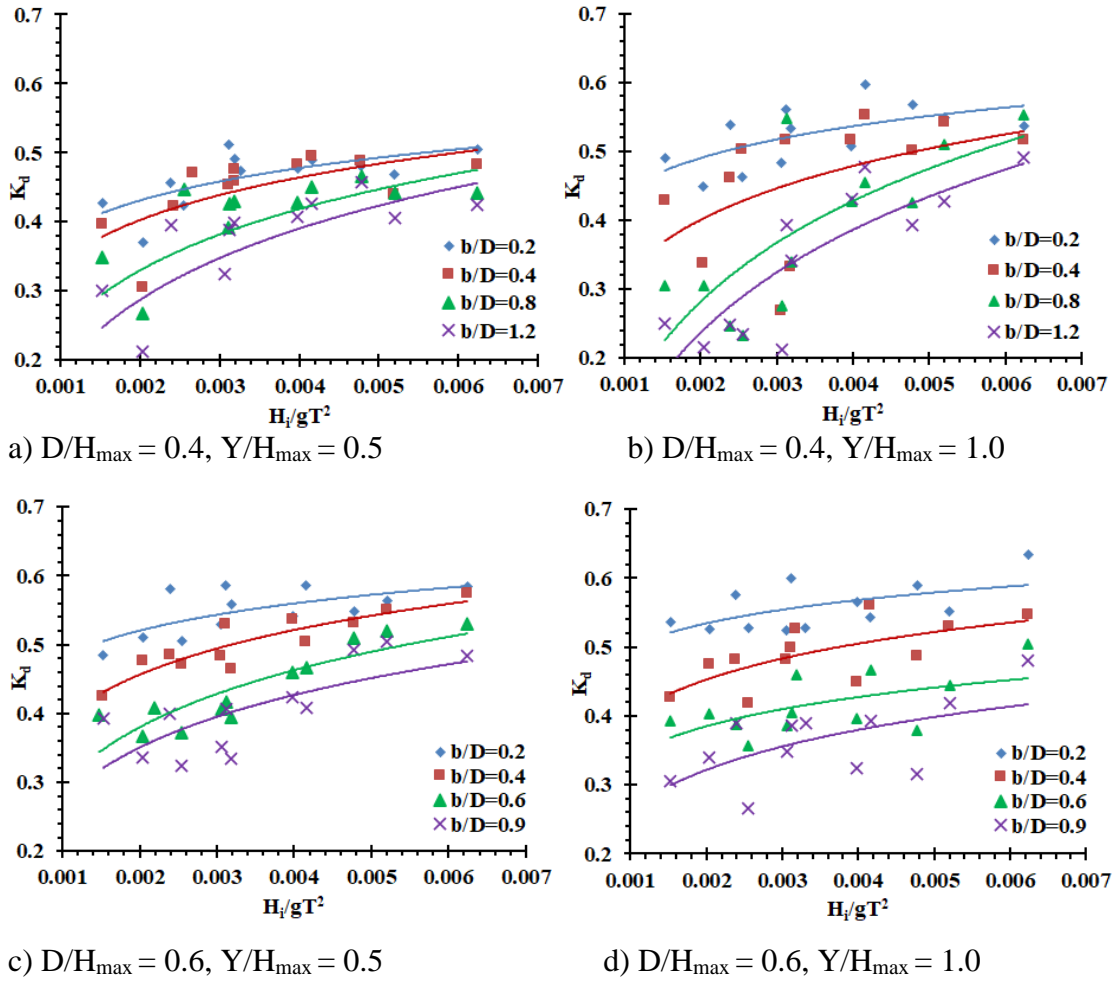


Fig. 4.9 Graphs of K_d versus H_i/gT^2 for varying ratios of b/D , D/H_{\max} and Y/H_{\max} at a water depth of 0.50 m

4.3 IMPACT OF VARYING PILE HEAD CHARACTERISTICS

The geometry of enlarged pile head breakwater has an important role in wave transmission, and this study investigated the effect of increased pile head area attributed by varying the height and diameter in terms of maximum wave height. The height of pile head (Y) is increased from 0.5 times the H_{\max} (i.e. 0.08 m) to 1.0 times the H_{\max} (i.e. 0.16 m) and diameter (D) from $0.4H_{\max}$ (i.e. 0.064 m) to $0.6H_{\max}$ (i.e. 0.096 m). As evident from section 4.2, the relative pile spacing of 0.2 is optimum. Hence, while analysing the effect of pile head characteristics, the spacing between the pile head (b/D) is fixed as 0.2. The graphs are plotted by considering K_t , K_r and K_d versus H_i/gT^2 are as shown in Fig. 4.10 to Fig. 4.12, for three water depths. In Fig. 4.10 to Fig. 4.12, best-fit lines are considered for better visualisation in the analysis of results. The effect of

pile head characteristics is discussed comprehensively in the following sections.

4.3.1 Influence of pile head diameter on

4.3.1.1 Wave transmission

Influence of diameter of pile head is examined by varying the D/H_{\max} from 0.4 to 0.6 (i.e., 0.064 m to 0.096 m) for three depths of water. For 0.3 m water depth (refer Fig. 4.10 a) when $Y/H_{\max} = 0.5$, K_t decreases by 2.8% (i.e., 0.836 to 0.812) at lower wave steepness (0.0020) and 11% (0.798 to 0.710) at higher wave steepness (0.0055). For the same case when Y/H_{\max} is 1.0, K_t decreases by 3.8% (i.e., 0.81 to 0.779) at lower wave steepness and 12.8% (0.741 to 0.646) at higher wave steepness. Referring to Fig. 4.10 b at 0.4 m depth of water, when Y/H_{\max} is 0.5, K_t decreases by 0.22% and 5.95% at the lower and higher wave steepness, respectively. However, when $Y/H_{\max} = 1.0$, K_t decreases by 0.94% at lower wave steepness and 7.61% at higher wave steepness. For the case of 0.5 m depth of water as per Fig. 4.10 c, the value of K_t decreases by 5.20% at lower wave steepness and 7.50% at higher wave steepness for Y/H_{\max} is 0.5. When Y/H_{\max} is increased to 1.0 from 0.5, K_t decreases by 2.63% and 5.09% at lower and higher wave steepness, respectively.

The above analysis concludes that when the ratio of D/H_{\max} increases from 0.4 to 0.6, irrespective of depth of water, the performance of enlarged pile head breakwater increases. The same can also be visualised from Fig. 4.10, where the least value of K_t is obtained for the case of $D/H_{\max} = 0.6$ for all considered depths of water. The probable reason for the increased performance of breakwater with increasing D/H_{\max} ratio is mainly due to the increased projected surface area of the pile for wave-structure interaction. In general, it can be said that, as the projected area of the structure opposing the wave increases, the wave height transmitted should decrease, resulting in more reduced wave disturbance at the lee side of the structure. The whole projected area of the enlarged pile head breakwater at 0.3 m water depth considered in the present study is as tabulated in Table 4.1. The concept breakwater with $D/H_{\max} = 0.4$ has nine numbers of enlarged pile head, whereas, $D/H_{\max} = 0.6$ has six numbers.

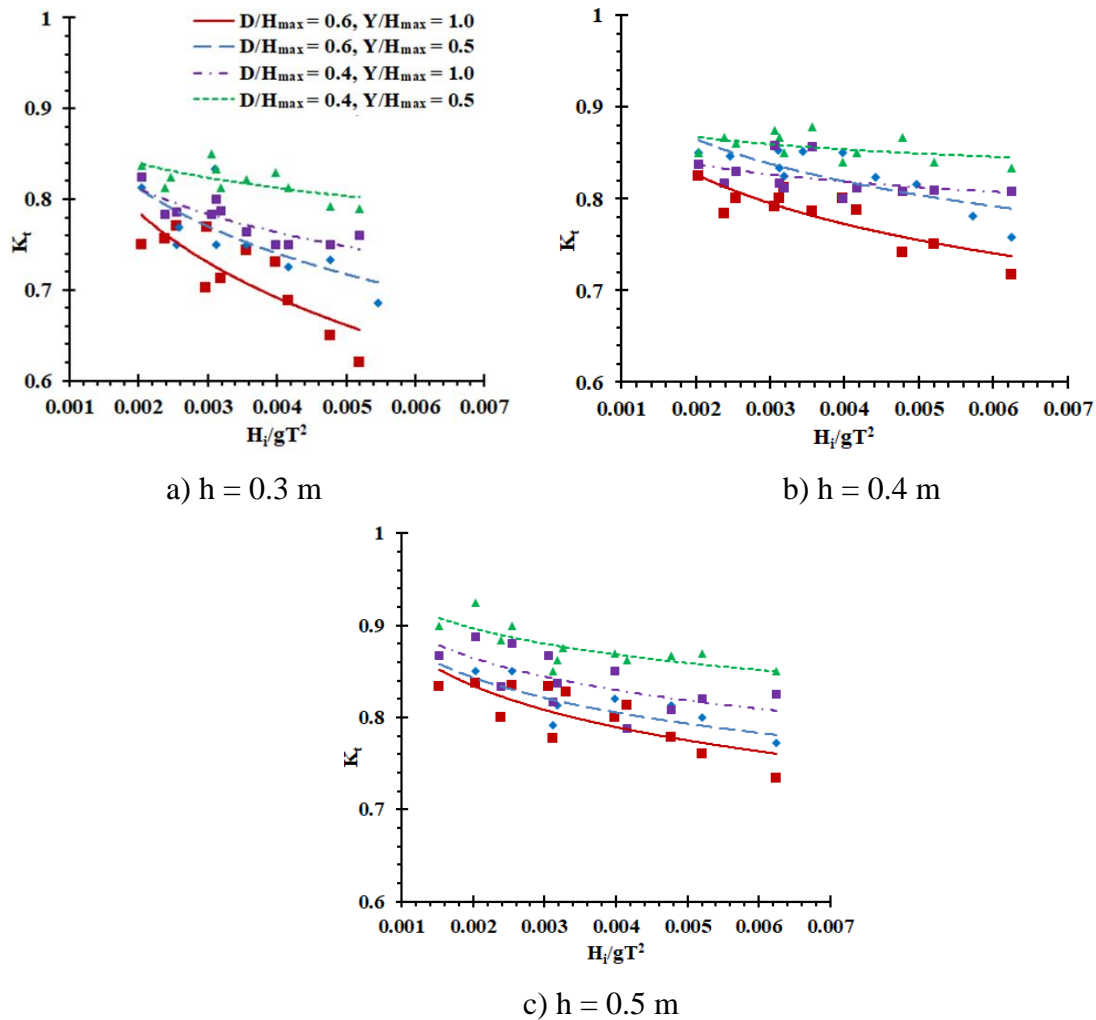


Fig. 4.10 Variation of K_t , with H_i/gT^2 when $b/D = 0.2$ for different h , D/H_{\max} and Y/H_{\max}

Table 4.1 The projected area of the whole structure at 0.3 m water depth

Y/H_{\max}	D/H_{\max}	Projected area of whole Trunk (m^2 per m width) (a)	Projected area of whole Head (m^2 per m width) (b)	Total Projected area (m^2 per m width) $c = a + b$
0.5	0.4	0.132	0.032	0.164
0.5	0.6	0.088	0.032	0.120
1.0	0.4	0.112	0.065	0.177
1.0	0.6	0.074	0.065	0.139

Table 4.1 indicates that $D/H_{\max} = 0.4$ has a more projected area than $D/H_{\max} = 0.6$, but the transmission coefficient is less for the former than the latter, as shown in Fig. 4.10. The reason for the same is visualized by analysing the role of the projected area at the head and trunk portion. The projected area of the pile head is the same for the case of $D/H_{\max} = 0.4$ and 0.6 at $Y/H_{\max} = 0.5$ and also at 1.0 . Hence, the variation in the projected area is observed only at the trunk portion of the enlarged pile head breakwater. Thus, providing more projected area at the trunk portion is ineffective in reducing wave transmission. The reason being exponential decay in velocity components from the free surface and associated wave forces. Hence, providing more area at the trunk portion is not so important than at the surface where more wave force is concentrated. The reason to have less wave transmission in the case of $D/H_{\max} = 0.6$ can be envisioned by considering the wave interaction with individual pile head breakwater on the projected part and the hollowness of the pile head.

Wave interaction on a projected part at the individual pile head: Providing $D/H_{\max} = 0.6$ has a projected area of 0.00768 m^2 and for $D/H_{\max} = 0.4$ is 0.00512 m^2 for the case of $Y/H_{\max}=1.0$. For $D/H_{\max} = 0.6$, 50% more area of the structure interacts with the waves, and also there are more formations of eddies between the piles, which results in a higher loss of wave energy, thus yielding less wave transmission.

Effect of hollow portion of pile head: Increase in the diameter of the pile head by 50% may result in trapping of a portion of the waves by the hollow portion of pile head contributing to an additional loss of wave energy because wave collapsing into the hollow portion while propagating over the structure.

The above reasons make enlarged pile head breakwater more efficient when $D/H_{\max} = 0.6$ for all the considered water depths.

4.3.1.2 Wave reflection

Fig. 4.11 in general indicate that, as the wave steepness increases reflection increases. It is also envisaged from Fig. 4.11 that the reflection coefficient follows reverse order to that of transmission coefficient. The pile head configuration of $D/H_{\max} = 0.6$ with $Y/H_{\max} = 1.0$ shows higher reflection than $D/H_{\max} = 0.4$ with $Y/H_{\max} = 0.5$ and 1.0 for

all considered depths of water. A higher value of reflection is observed at 0.3 m depth of water than the other considered depths of water. For $Y/H_{\max} = 1.0$, change in D/H_{\max} from 0.4 to 0.6 results in, 0.18 to 0.24 and 0.22 to 0.34 increase in K_r at lower and higher wave steepness, respectively at 0.3 m water depth. Hence, for all considered depths of water, K_r increases with increase in pile head diameter. The same is because of the increased wave-structure interaction due to the increased area of structure confronting the wave.

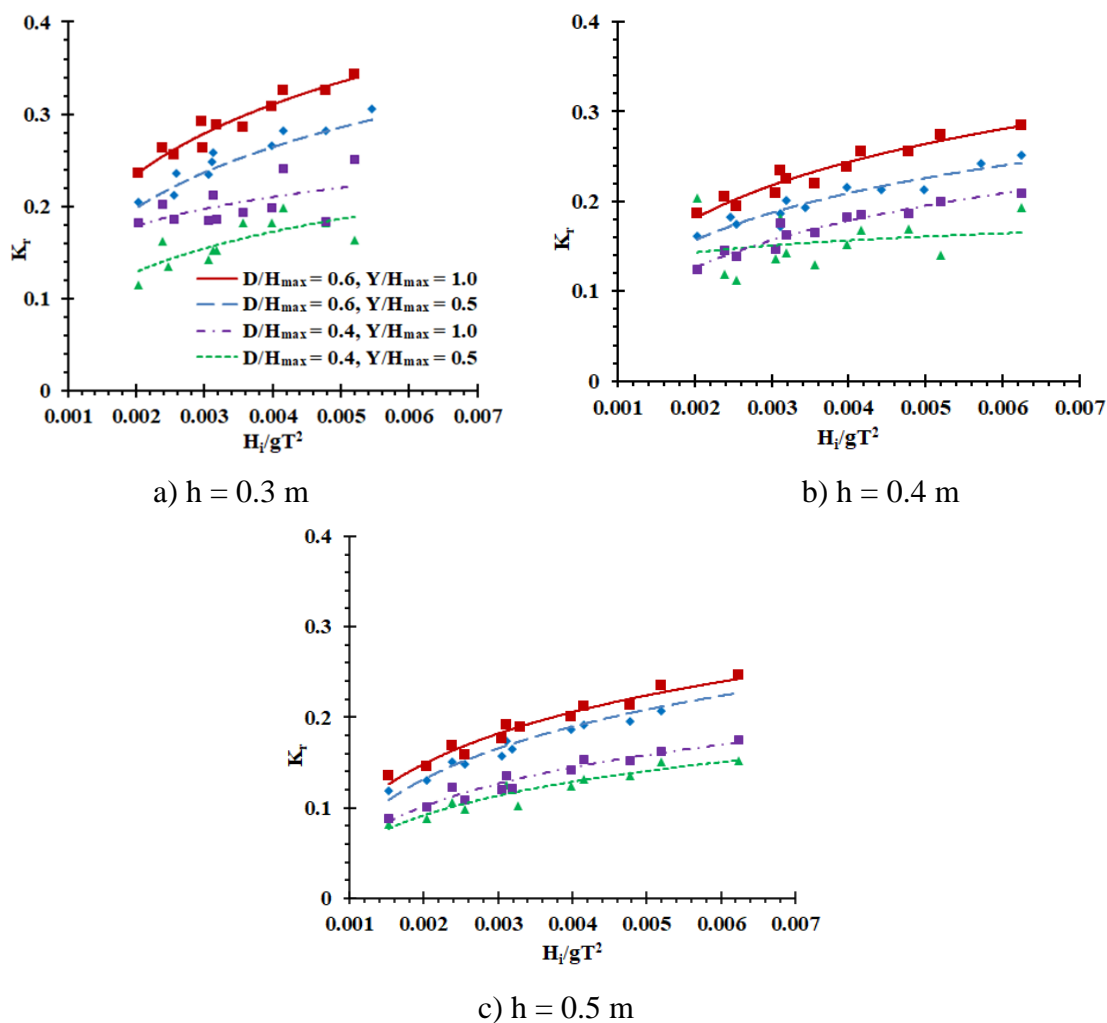


Fig. 4.11 Variation of K_r , with H_i/gT^2 when $b/D = 0.2$ for different h , D/H_{\max} and Y/H_{\max}

4.3.1.3 Wave Energy dissipation

From Fig. 4.12, it can be envisaged that with the increase in wave steepness, wave energy dissipated by the structure increases. Higher dissipation is observed when

$D/H_{\max} = 0.6$ and $Y/H_{\max} = 1.0$ for all considered depths of water. Similarly lower dissipation is observed when $D/H_{\max} = 0.4$ and $Y/H_{\max} = 0.5$. Percentage increase in wave energy dissipation, when D/H_{\max} increases from 0.4 to 0.6 for $Y/H_{\max} = 1.0$ at 0.3 m depth of water is 4.48% at lower wave steepness and 7.03% at higher wave steepness. For 0.4 m water depth, dissipation increases to 5.3% and 6.4% at lower and higher wave steepness, respectively. For a depth of water 0.5 m, dissipation increases to 8.97% at lower wave steepness and 5.2% higher wave steepness. Hence, irrespective of the studied depths of water, the K_d increases with an increase in pile head diameter. This behaviour may be due to the increased wave-structure interaction caused by the higher obstruction area of the structure.

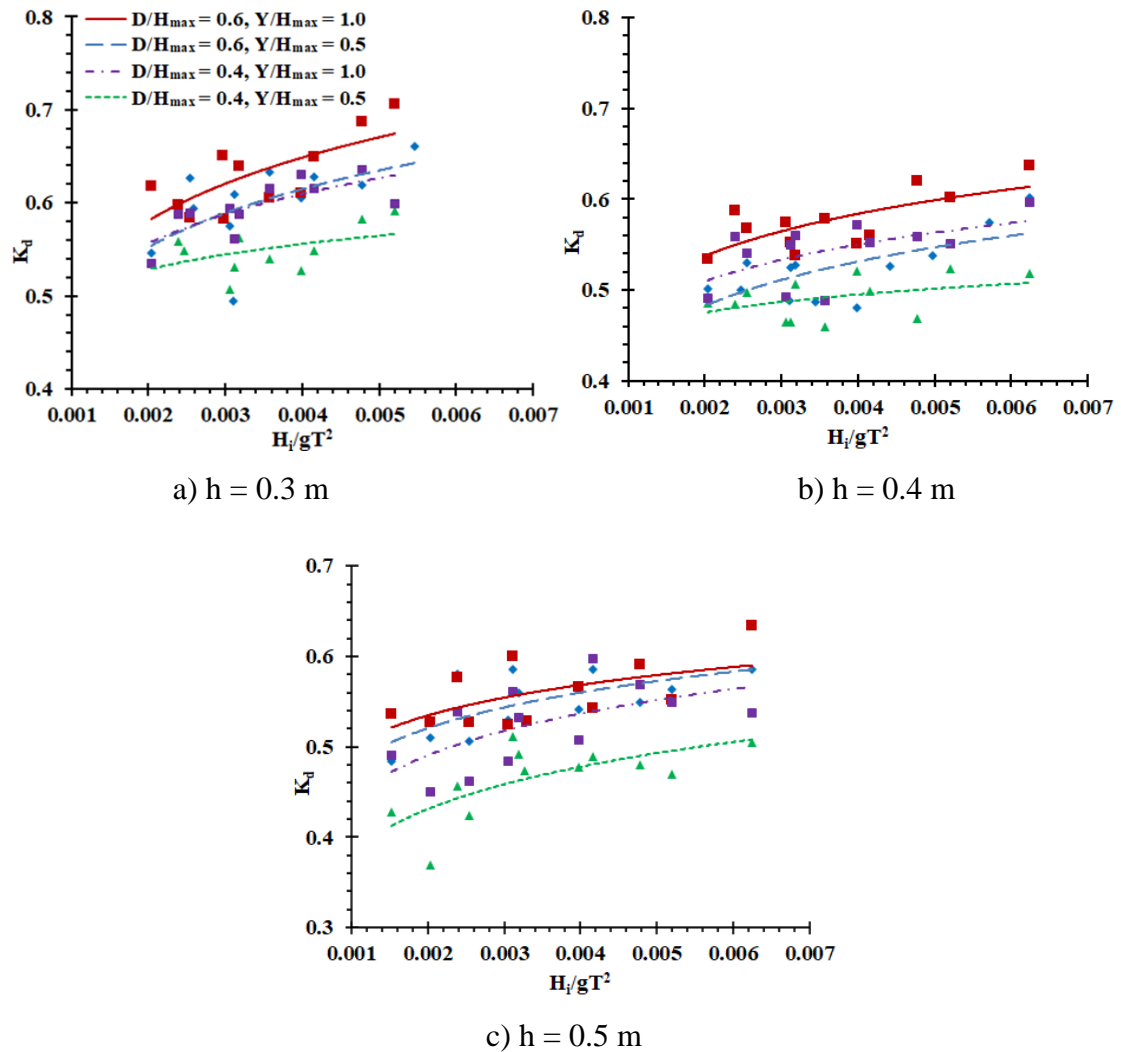


Fig. 4.12 Variation of K_d with H_i/gT^2 when $b/D = 0.2$ for different h , D/H_{\max} and Y/H_{\max}

4.3.2 Influence of pile head height on

The effect of pile head height on the K_t , K_r and K_d are studied by fixing D/H_{\max} to 0.6 and varying Y/H_{\max} from 0.5 to 1.0 for all the considered depths of water. The same is described in detail through the following sections.

4.3.2.1 Wave transmission

According to Fig. 4.13 a , when the relative pile head height (Y/H_{\max}) is varied from 0.5 to 1.0, the transmission coefficient changes from 0.813 to 0.779 (i.e., 4.04% reduction) at lower wave steepness of 0.0021 and from 0.710 to 0.646 (i.e., 8.92% reduction) at higher wave steepness of 0.0052.

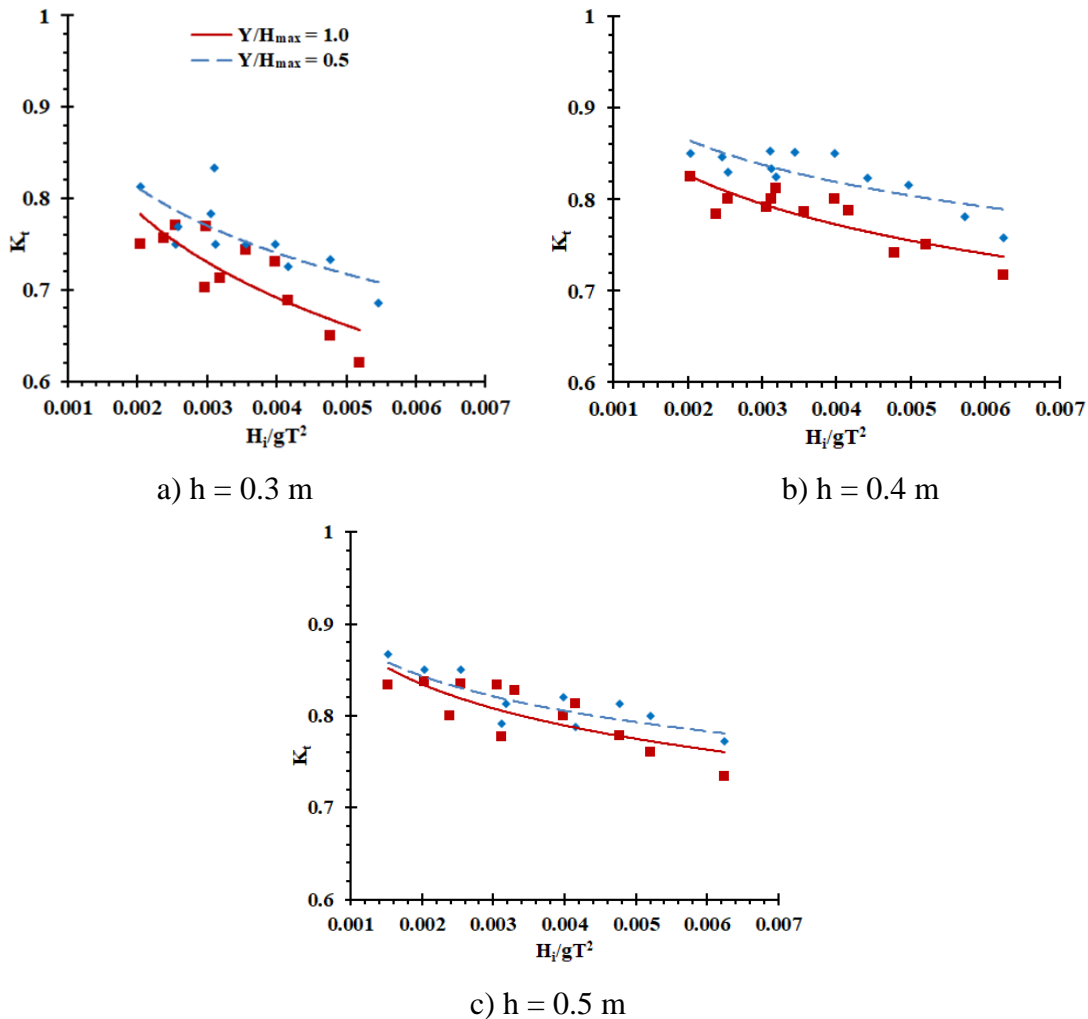


Fig. 4.13 Variation of K_t , with H_i/gT^2 when $b/D = 0.2$ and $D/H_{\max} = 0.6$ for different h , and Y/H_{\max}

For the water depth of 0.4 m (refer Fig. 4.13 b), the percentage reduction of K_t is 4.4% and 6.33% at lower and higher wave steepness, respectively. At 0.5 m depth of water (refer Fig. 4.13 c), percentage reduction of K_t is 0.822% at lower wave steepness and 2.44% at higher wave steepness. The above analysis indicates that for all the water depths considered, the efficiency of the enlarged pile head breakwater increases with the increase in pile head height. The least value of K_t is obtained for the case when $Y/H_{max} = 1.0$. The reason for the same is due to the increased projected area opposing the wave.

4.3.2.2 Wave reflection

Variation of reflection coefficient (K_r) with depths of water is shown in Fig. 4.14.

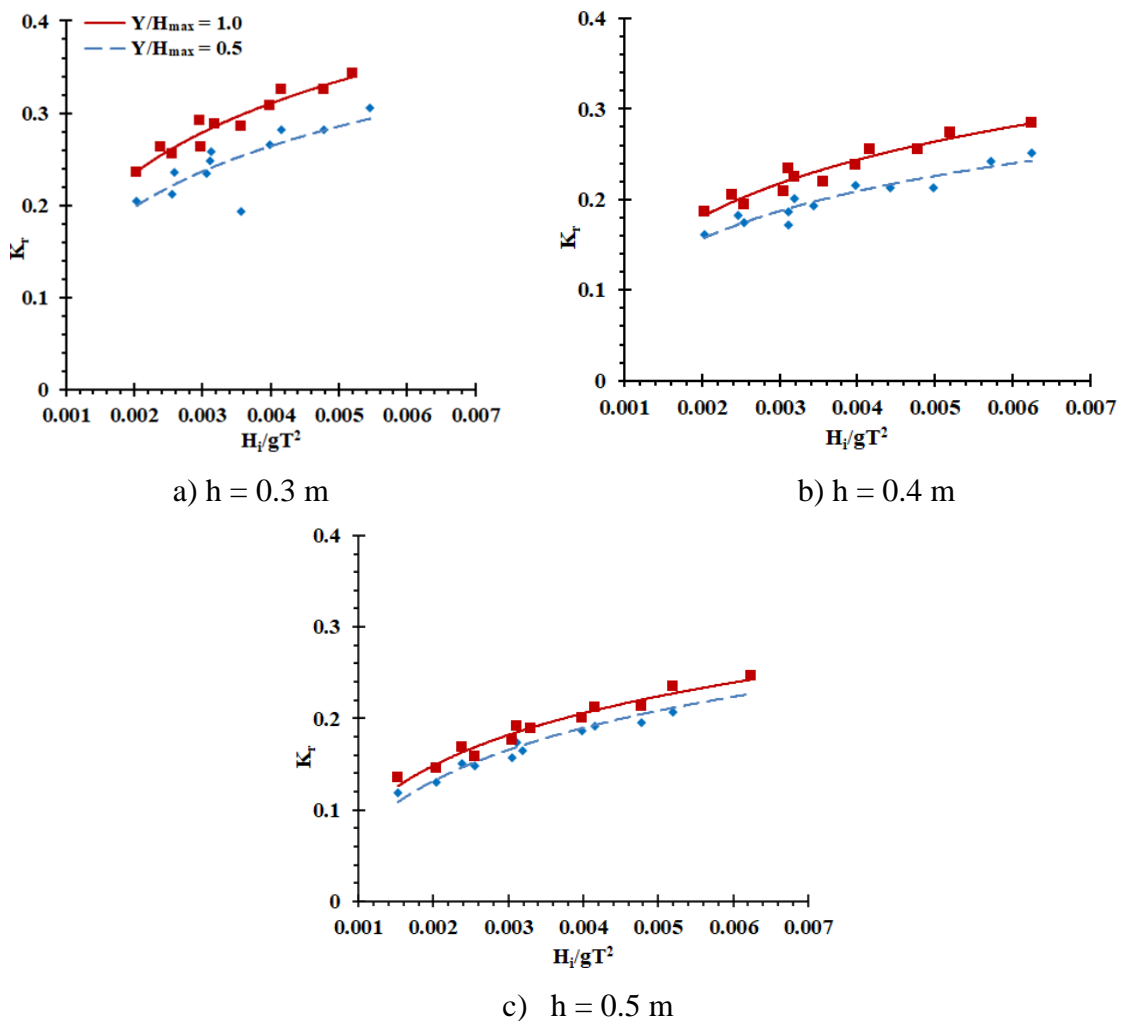


Fig. 4.14 Variation of K_r , with H_i/gT^2 when $b/D = 0.2$ and $D/H_{max} = 0.6$ for different h , and Y/H_{max}

Change in Y/H_{\max} from 0.5 to 1.0 results in an average of 17.9 % change in K_r at 0.3 m depth of water. For 0.4 m depth of water, an average change is 16.43% where as at 0.5 m is observed to be 10.3%.

4.3.2.3 Wave energy dissipation

Variation of energy dissipation coefficient (K_d) with depths of water is shown in Fig. 4.15. Figure indicates that with increase in Y/H_{\max} from 0.5 to 1.0 increases the K_d for all considered depth of water. An average change in K_d is about 5.37%, 10.34% and 1.9% at 0.3 m, 0.4 m and 0.5 m depth of water respectively.

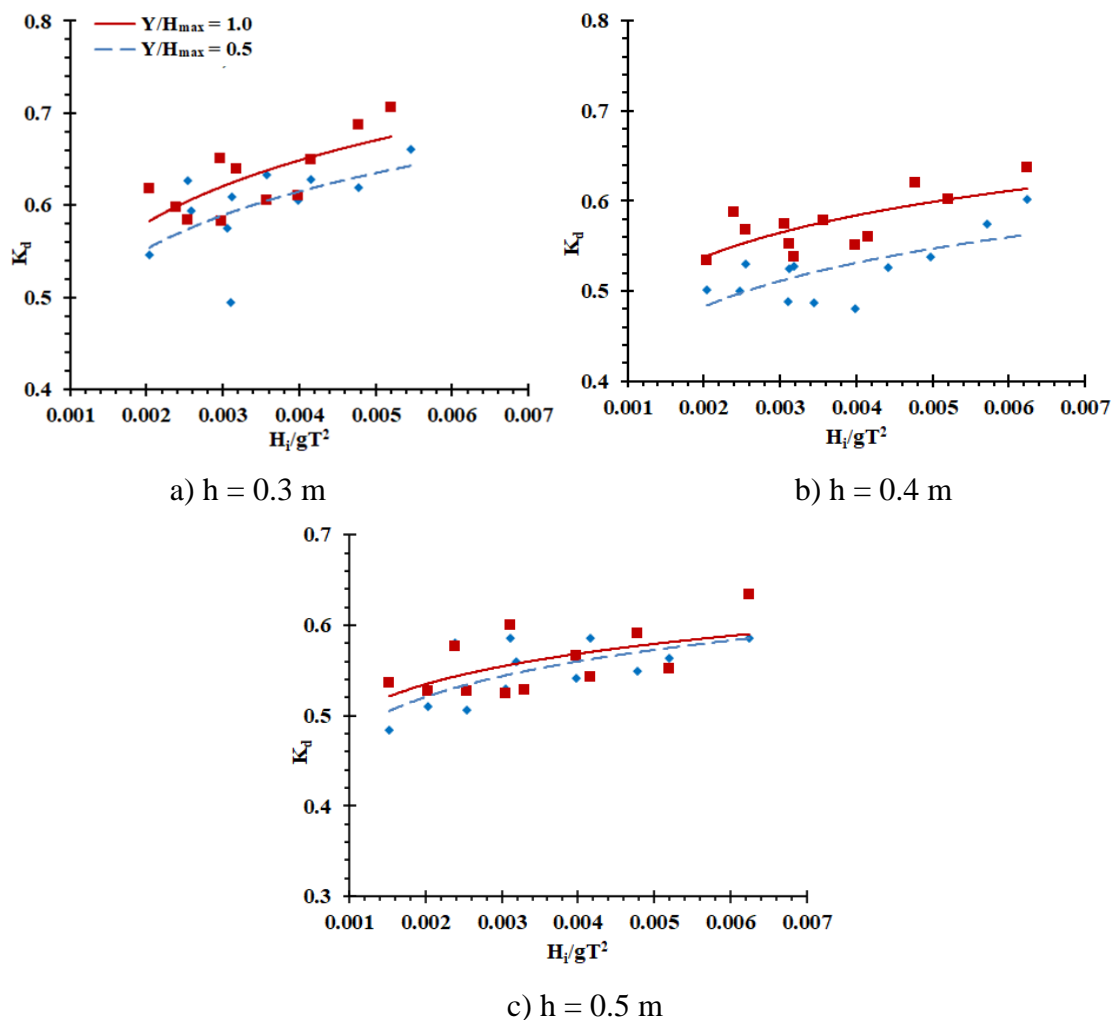


Fig. 4.15 Variation of K_d , with H_i/gT^2 when $b/D = 0.2$ and $D/H_{\max} = 0.6$ for different h , and Y/H_{\max}

4.4 EFFECT OF VARYING RELATIVE SUBMERGENCE OF PILE HEAD AND DEPTH OF WATER

4.4.1 On wave transmission

The effect of Z and h on K_t is depicted in Fig. 4.16. From Fig. 4.16 it is clear that, an increase in Z resulted in decrease in the value of K_t . For the case of $D/H_{\max} = 0.4$ at 0.3 m depth of water, when the pile head submergence is increased by 100% (i.e., 13.333% to 26.667%), the percentage decrease in K_t is 3.11% at lower wave steepness and 6.57% at higher wave steepness, as illustrated in of pile head submergence when the water depth is 0.4 m, K_t decreases by 3.70% and 4.52% at lower and higher wave steepness, respectively. Similarly, when the water depth is 0.5 m, K_t decrease by 3.37% at lower wave steepness and 4.86% at higher wave steepness. Effect of Z when $D/H_{\max} = 0.6$ is same as the case of $D/H_{\max} = 0.4$. An average of 6.8%, 5.45% and 1.76% change in K_t is observed for 0.3 m, 0.4 m, and 0.5 m depth of water respectively. Above analysis indicates that enlarged pile head breakwater is more effective at lower depths of water with relative submergence of 26.667% pile head.

The percentage change in K_t with respect to change in h is provided in Table 4.2 to Table 4.5. The results indicate that, with increase in depth of water, K_t increases. For 25% to 33.33% increases in water depth, resulted in an average of 4% to 6% increase in K_t .

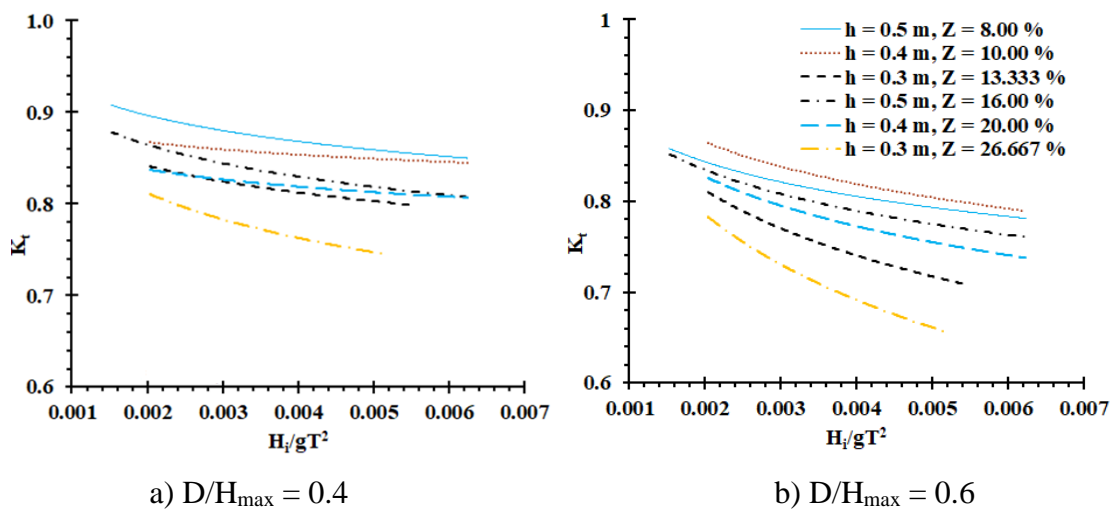


Fig. 4.16 Variation of K_t , with H_i/gT^2 for various h and Z when $b/D = 0.2$

4.4.2 On wave reflection

Fig. 4.17 shows variation in K_r with Z for the D/H_{\max} of 0.4 and 0.6 at three considered depths of water. From the Fig. 4.17, in general it can be concluded that as Z increases K_r increases. A maximum K_r is observed for the case when $Z = 26.667\%$ and $D/H_{\max} = 0.6$ at $h = 0.3$ m.

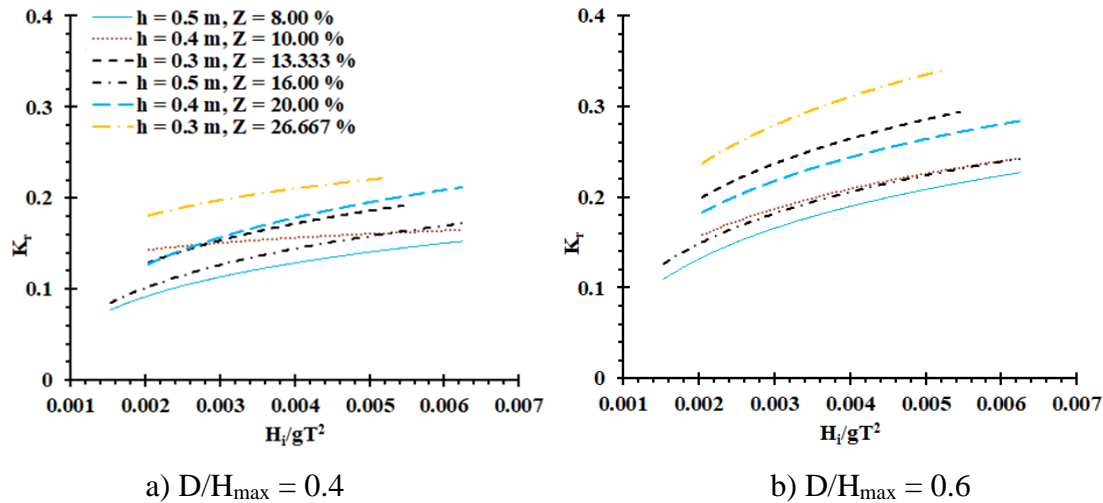


Fig. 4.17 Variation of K_r , with H_i/gT^2 for various h and Z when $b/D = 0.2$

The percentage change in K_r with respect to change in h is provided in Table 4.2 to Table 4.5. The results indicate that, with an increase in depth of water, K_r decreases. For 25% to 33.33% increases in water depth an average of 17% to 19% decrease in K_r is noticed. Hence, it can be said that if the enlarged pile breakwaters are installed near the shore (approximate water depth of 9.0 m), it is more effective in reducing the wave energy approaching the shore.

4.4.3 On wave energy dissipation

Fig. 4.18 shows effect of Z on K_d for D/H_{\max} of 0.4 and 0.6 at three considered depths of water. From the Fig. 4.18, in general it can be concluded that as Z increases K_d increases. A maximum K_d is observed for the case when $Z = 26.667\%$ and $D/H_{\max} = 0.6$ at $h = 0.3$ m.

Table 4.2 to Table 4.5 shows the percentage change in K_d with respect to change in h . The results indicate that, with increase in depth of water, K_d decreases. For 25% to 33.33% increases in water depth, resulted in an average of 7% to 8% decrease in K_d . Hence, from the section 4.4.1 to 4.4.3 it can be stated that if the enlarged pile breakwaters are installed near the shore (approximate water depth of 9.0 m), it is more effective in reducing the wave energy approaching the shore

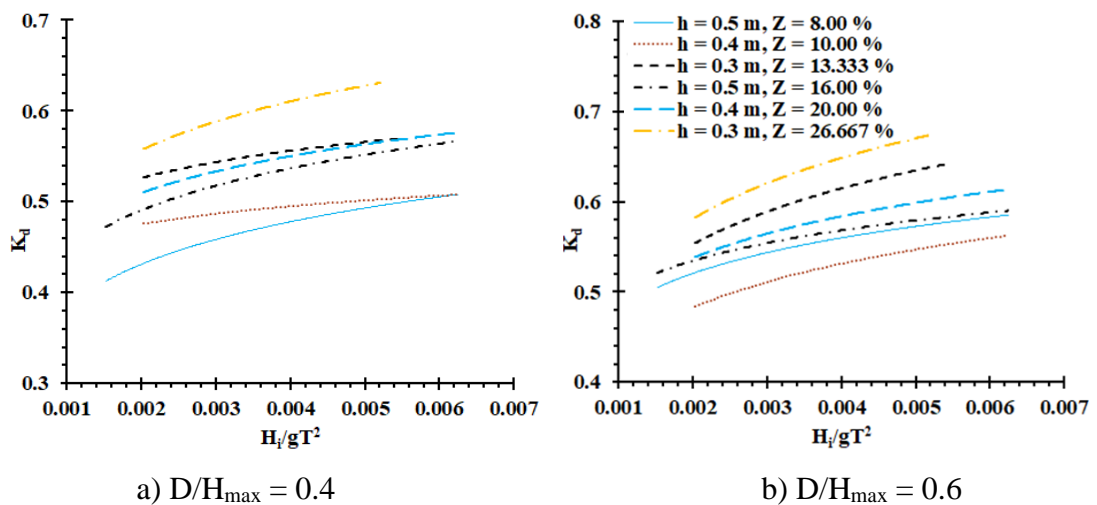


Fig. 4.18 Variation of K_d , with H_i/gT^2 for various h and Z when $b/D = 0.2$

Table 4.2 Percentage variation of K_t , K_r and K_d with water depth for $b/D = 0.2$, $Y/H_{max} = 0.5$ and $D/H_{max} = 0.4$

Water depth variation	0.3 m to 0.4 m		0.4 m to 0.5 m		0.3 m to 0.5 m	
	0.002	0.005	0.002	0.005	0.002	0.005
K_t	+ 3.27	+ 5.94	+ 3.13	+ 0.94	+ 6.50	+ 6.93
K_r	+ 11.79	- 13.65)	- 35.81	- 12.42	- 28.24	- 24.37
K_d	- 9.61	- 11.31	- 9.28	- 1.71	- 18.00	- 12.83

NOTE: “+ “ indicate percentage increase and “ - “ indicate percentage decrease

**Table 4.3 Percentage change in K_t , K_r and K_d with water depth for $b/D = 0.2$,
 $Y/H_{max} = 1.0$ and $D/H_{max} = 0.4$**

Water depth variation	0.3 m to 0.4 m		0.4 m to 0.5 m		0.3 m to 0.5 m	
	0.002	0.005	0.002	0.005	0.002	0.005
K_t	+ 2.66	+ 8.27	+ 3.08	+ 0.57	+ 5.82	+ 8.89
K_r	- 29.79	- 11.23	- 19.51	- 18.89	- 43.49	- 28.00
K_d	- 8.51	- 10.29	- 3.72	- 2.03	- 11.91	- 12.11

**Table 4.4 Percentage change in K_t , K_r and K_d with water depth for $b/D = 0.2$,
 $Y/H_{max} = 0.5$ and $D/H_{max} = 0.6$**

Change in water depth	0.3 m to 0.4 m		0.4 m to 0.5 m		0.3 m to 0.5 m	
	0.002	0.005	0.002	0.005	0.002	0.005
K_t	+ 6.49	+ 12.06	- 2.60	- 1.44	+ 3.72	+ 10.45
K_r	- 21.04	- 20.94	- 16.00	- 7.83	- 33.67	- 27.13
K_d	- 12.56	- 13.76	+ 7.76	+ 4.62	- 5.78	- 9.78

**Table 4.5 Percentage change in K_t , K_r and K_d with water depth for $b/D = 0.2$,
 $Y/H_{max} = 1.0$ and $D/H_{max} = 0.6$**

Change in water depth	0.3 m to 0.4 m		0.4 m to 0.5 m		0.3 m to 0.5 m	
	0.002	0.005	0.002	0.005	0.002	0.005
K_t	+ 6.04	+ 14.97	+ 0.66	+ 2.42	+ 6.75	+ 17.75
K_r	- 22.83	- 21.12	- 18.16	- 15.20	- 36.84	- 33.11
K_d	- 7.46	- 10.66	- 0.58	- 3.29	- 7.99	- 13.60

The reason for the increased efficiency of the structure with decreasing water depth is mainly due to the increase in the projected surface area of the pile head, which may block the entire wave and thus increasing wave attenuation. This behaviour can be explained by considering the case of $D/H_{max} = 0.6$ and $Y/H_{max} = 1.0$. The calculated

percentage blockage area for 0.5 m, 0.4 m and 0.3 m water depths are 64.99, 67.96 and 72.92, respectively. Hence, with decreasing depth of water, the blockage for wave increases and the velocity of the wave approaching also decreases, resulting in increased efficiency.

4.5 VALIDATION OF MODIFIED HYBRID THEORETICAL EQUATION FOR NON-PERFORATED PILE BREAKWATERS

4.5.1 Enlarged pile head breakwater

The present experimental results are compared with the results obtained through the theoretical equation developed by Mei (1989), Kriebel (1992), and Suh et al. (2011). As quoted by Suh et al. (2011), Mei (1989) obtained the transmission and reflection equations by the equations of continuity and motion of small amplitude waves in shallow water. Mei (1989) derived equations as

$$K_t = \frac{U_0}{\sqrt{gk} \left(\frac{H_i}{h} \right)} \quad (4.1)$$

$$K_r = 1 - \frac{\omega U_0}{gkH_i} \quad (4.2)$$

Where $U_0 = \frac{H_i}{h} \sqrt{gk} \frac{\sqrt{1+2\alpha}-1}{\alpha}$, $\alpha = \frac{4}{3\pi} \frac{fH_i}{h}$, f is given by Eq. (3.19).

Kriebel (1992) equation is similar to the Mei (1989) solution and is as follows

$$K_t = \frac{\sqrt{1+4T_t}-1}{2T_t} \quad (4.3)$$

$$K_r = 1 - \frac{\sqrt{1+4T_t}-1}{2T_t} \quad (4.4)$$

$$\text{Where, } T_t = \frac{f}{6} \frac{H_i}{2\pi} \frac{\sinh(2kh)+2kh}{k \sinh^2(kh)} \text{ is the transmission function.} \quad (4.5)$$

The hybrid equations developed by Suh et al. (2011) for the pile breakwater is described through the Eqs. (2.20) to (2.23). About 560 experimental test cases were compared to check the validity of the theoretical equations. The values of K_t , K_r and K_d obtained using the theoretical equations are compared with the experimental results in Fig. 4.19. The equations developed by Mei (1989) and Kriebel (1992) predict the transmission coefficient for pile head breakwater with a variation coefficient (R^2) of 0.542. As shown

in Fig. 4.19 (a) and (b), both the equations underpredict the transmission coefficient and dissipation coefficient but over predict the reflection coefficient. The hybrid theoretical equation developed by Suh et al. (2011) over predicts the transmission coefficient, whereas, reflection and dissipation are underpredicted, as shown in Fig. 4.19 (c). The transmission coefficient obtained by using the hybrid solution developed by Suh et al. (2011) has given an R^2 of 0.480. Fig. 4.19 (d) shows the value of K_t , K_r and K_d predicted by the present modified hybrid equation. The R^2 value for the transmission coefficient for the present hybrid solution is 0.895.

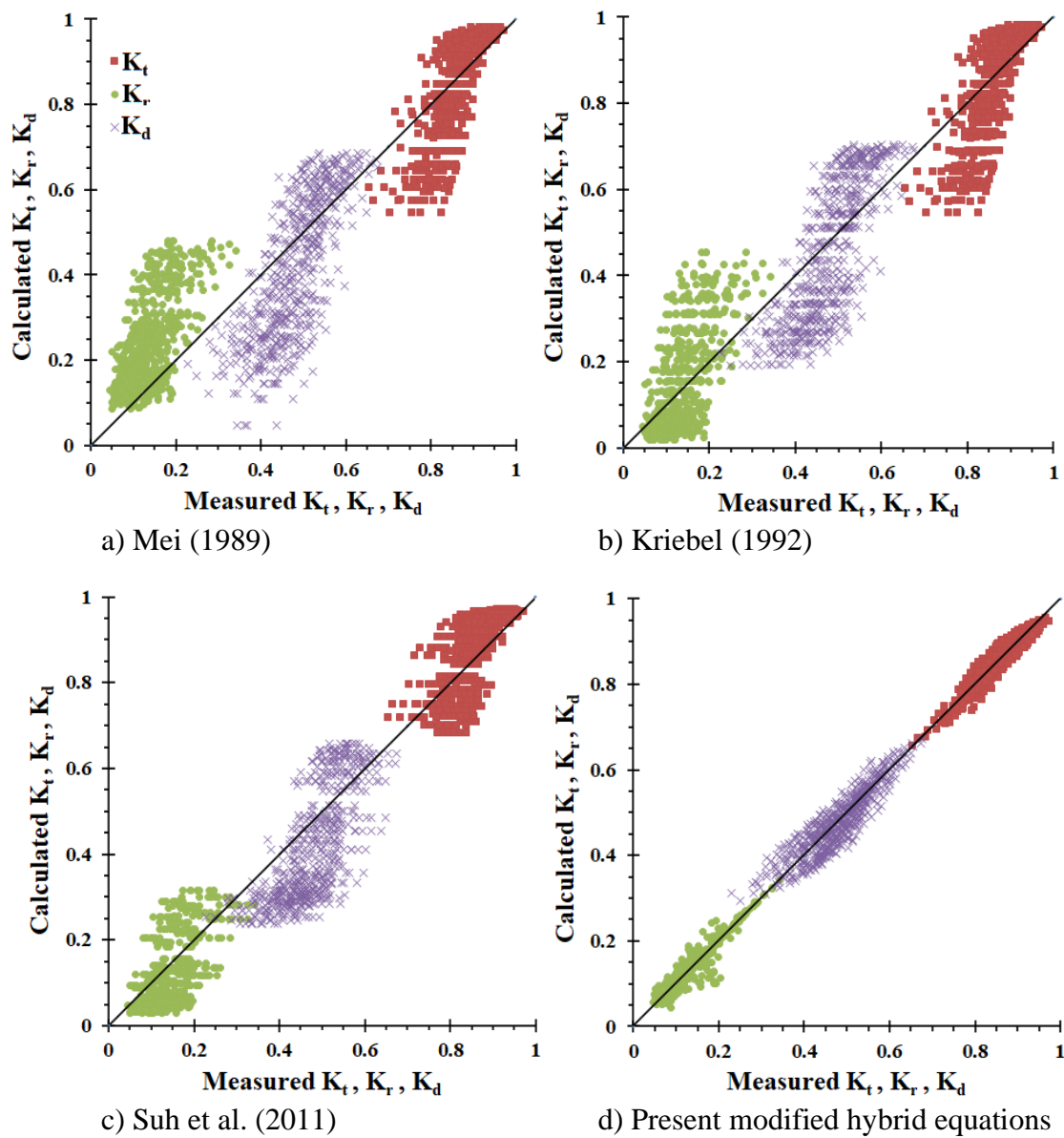


Fig. 4.19 Comparison of theoretical K_t , K_r and K_d with the measured values

Table 4.6 Variation coefficient (R^2) value obtained for different equations for the present experimental data

Reference	Variation Coefficient (R^2)		
	K_t	K_r	K_d
Mei (1989)	0.542	0.456	0.561
Kriebel (1992)	0.542	0.455	0.600
Suh et al. (2011) hybrid solution	0.480	0.421	0.515
Present hybrid solution (Eq. 3.11)	0.895	0.905	0.819

Table 4.7 Scatter index (SI) value obtained for different equations for the present experimental data

Reference	Scatter Index (SI)		
	K_t	K_r	K_d
Mei (1989)	0.104	0.950	0.286
Kriebel (1992)	0.105	0.693	0.241
Suh et al. (2011) hybrid solution	0.076	0.486	0.230
Present hybrid solution (Eq. 3.11)	0.020	0.121	0.070

Table 4.8 Relative root mean square error (RrmsE) value obtained for different equations for the present experimental data

Reference	Relative Root Mean Square Error (RrmsE) in %		
	K_t	K_r	K_d
Mei (1989)	10.393	89.050	28.272
Kriebel (1992)	10.465	64.65	23.824
Suh et al. (2011) hybrid solution	7.556	45.405	22.700
Present hybrid solution (Eq. 3.11)	2.028	11.276	6.800

The R^2 value, scatter index and RrmsE as obtained for the different equations in compared with the present experimental results are shown in Table 4.6 to Table 4.8. Hence, it is evident from Fig. 4.19 (a) to (d) and Table 4.6 to Table 4.8 that, for the enlarged pile head breakwater, the present hybrid equation predicts the better value of

K_t , K_r and K_d than the other compared equations. The present hybrid equation predicts the K_t and K_r with a good accuracy due to the empirically improved γ parameter.

4.5.2 Conventional circular pile breakwater

The present hybrid equation is validated for the non-perforated regular circular pile breakwater using Eq. (3.12). For the present study, the experimental data of Rao (1999) on non-perforated circular pile breakwater is used. Details of the experimental data are shown in Table 4.9.

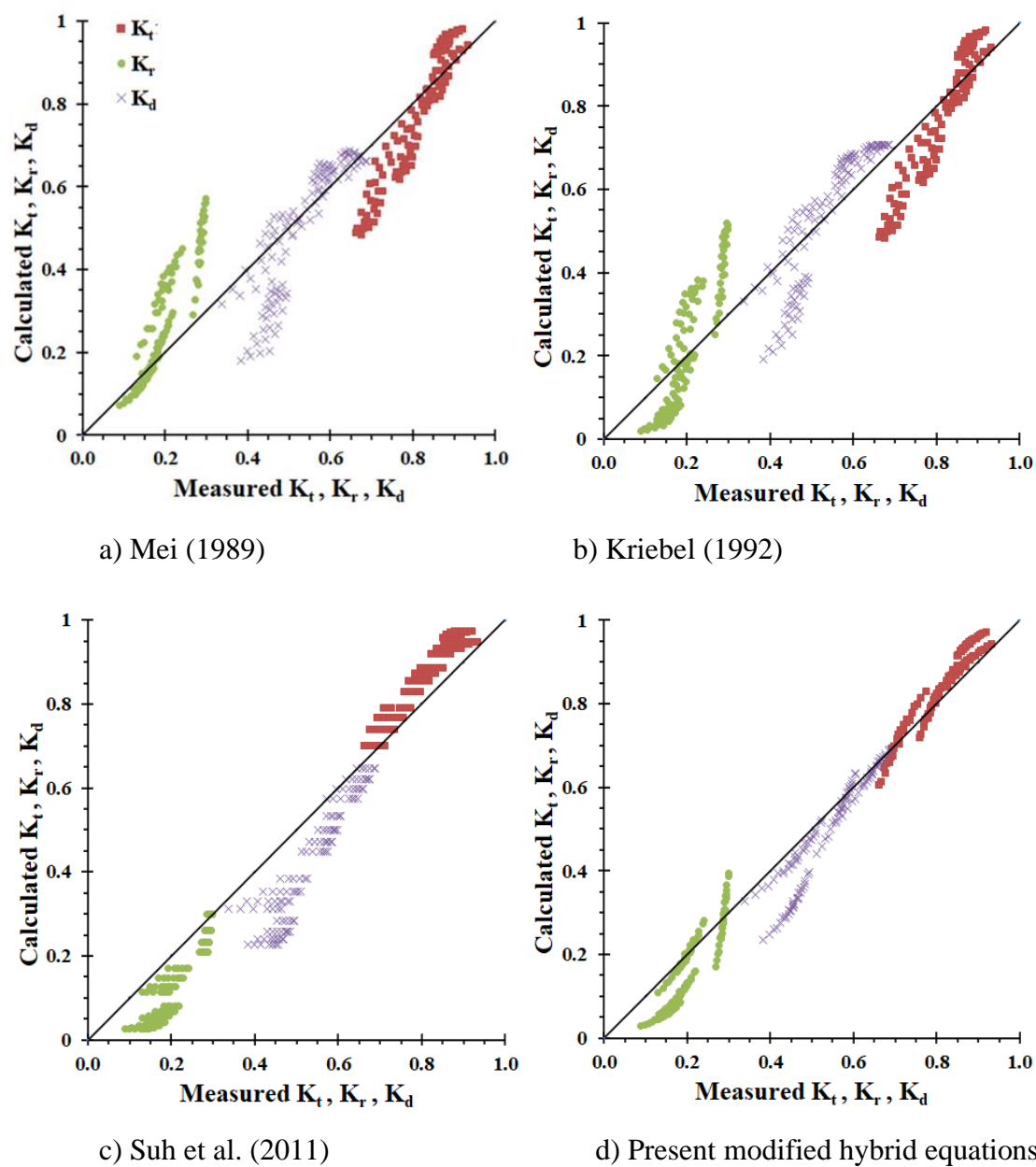


Fig. 4.20 Comparison of theoretical K_t , K_r and K_d with Rao (1999) data

Table 4.9 Experimental parameters, as cited by Rao (1999)

Variable	Expression	Parameter range
Diameter of the pile (m)	d	0.0335
Clear spacing between piles in a row	b/d	0.15, 0.25, 0.5, 1.0
Wave period (s)	T	1.5, 1.75, 2.0, 2.25
Incident wave height (m)	H _i	0.035 to 0.23
Water Depth	h	0.4 m and 0.5 m

Table 4.10 Variation coefficient (R²) value obtained for different equations for Rao (1999) experimental data

Reference	Variation Coefficient (R ²)		
	K _t	K _r	K _d
Mei (1989)	0.920	0.848	0.783
Kriebel (1992)	0.921	0.821	0.807
Suh et al. (2011) hybrid solution	0.923	0.833	0.871
Present hybrid solution (Eq. 3.12)	0.948	0.847	0.897

Table 4.11 Scatter index (SI) value obtained for different equations for Rao (1999) experimental data

Reference	Scatter Index (SI)		
	K _t	K _r	K _d
Mei (1989)	0.111	0.612	0.175
Kriebel (1992)	0.111	0.516	0.165
Suh et al. (2011) hybrid solution	0.086	0.450	0.240
Present hybrid solution (Eq. 3.12)	0.050	0.320	0.133

Transmission, reflection and dissipation coefficients as obtained by Rao (1999) are also compared with the equation proposed by Mei (1989), Kriebel (1992) and Suh et al. (2011). Fig. 4.20, shows the comparison of predicted values of K_t, K_r and K_d with the Rao (1999) experimental data. The value of (R²), SI and RrmsE as obtained for the case K_t, K_r and K_d are shown in Table 4.10 to Table 4.12.

Table 4.12 Relative root mean square error (RrmsE) value as obtained for different equations for Rao (1999) experimental data

Reference	Relative Root Mean Square Error (RrmsE) in %		
	K_t	K_r	K_d
Mei (1989)	11.075	58.862	17.270
Kriebel (1992)	11.154	49.655	16.317
Suh et al. (2011) hybrid solution	8.615	43.286	23.600
Present hybrid solution (Eq. 3.11)	4.924	30.720	13.143

From Fig. 4.20 and Table 4.10 to Table 4.12, it is easily intelligible that the present hybrid solution better predicts the hydraulic characteristics of conventional circular pile breakwater.

4.6 VALIDATION OF NON-PERFORATED ENLARGED PILE HEAD BREAKWATER USING REEF3D

The performance of enlarged pile head breakwater is also investigated using REEF3D under the monochromatic waves. The results are validated with the experimental data described in section 2.4.

Fig. 4.21 compares the results obtained for the case of non-perforated enlarged pile head breakwater with the experimental and theoretical values. The trend lines (K_t , K_r , K_d) obtained from the REEF3D results are in line with the experimental and theoretical results. For gentle waves, REEF3D results for K_t are underpredicted by about 0.5% and steeper waves by 1% with reference to the experimental results. Whereas, K_r is overpredicted by 4% and K_d variation is less than 1%.

As the maximum percentage error is about 4%, it could be concluded that REEF3D may be used to investigate the hydraulic performance of the proposed breakwater structure. Table 4.13 shows the REEF3D quantitative assessment of error using S.I., RrmsE and R^2 indexes compared with the experimental results.

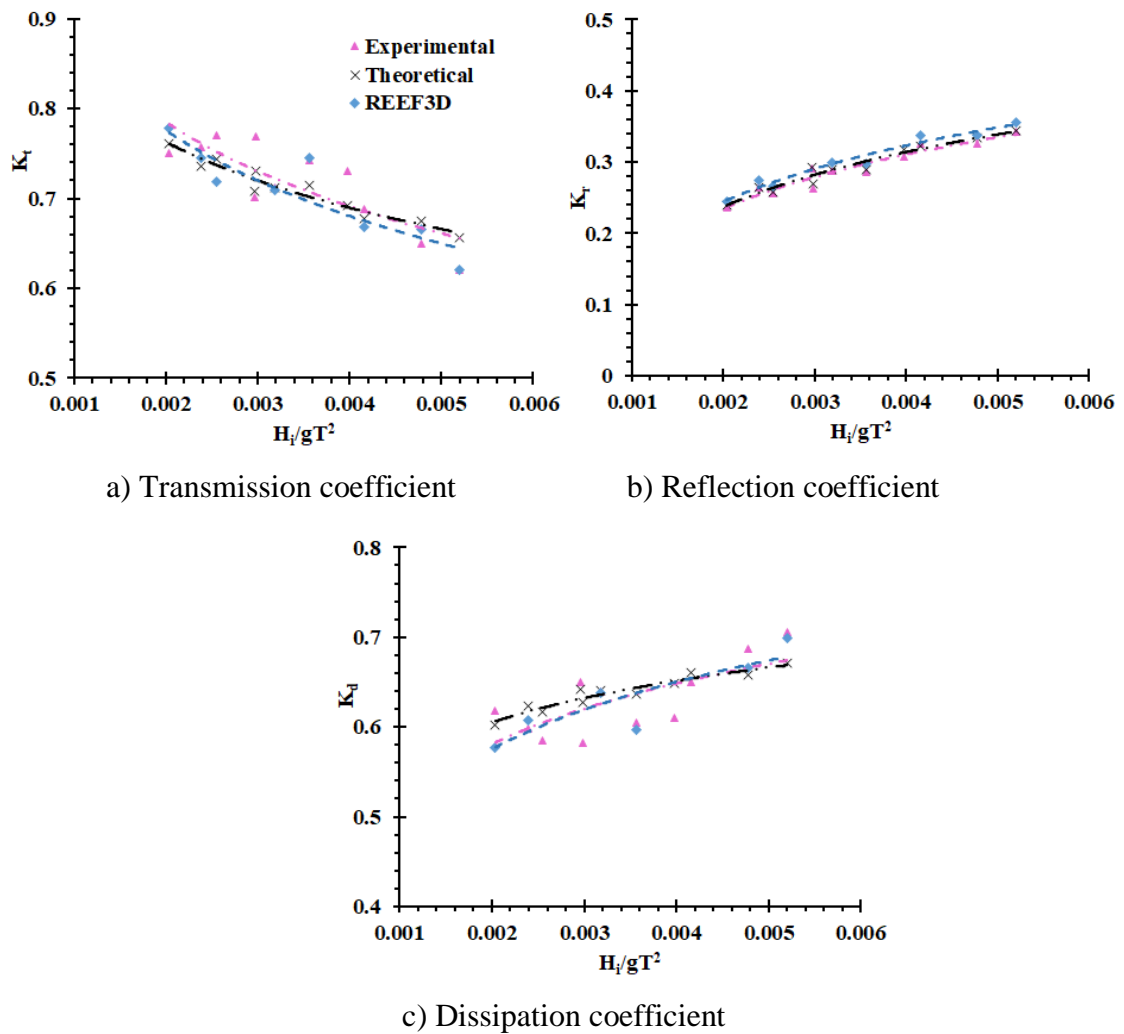


Fig. 4.21 Validation of non-perforated pile head breakwater REEF3D results with experimental and theoretical values

Table 4.13 Quantitative assessment of error using S.I., RrmsE and R² indexes

Model Type	Hydraulic Coefficients	S.I.	RrmsE	R ²
Non-perforated enlarged pile head	K _t	0.017	1.739	0.941
	K _r	0.039	3.940	0.999
	K _d	0.023	2.280	0.880

4.7 COMPARISON OF NON-PERFORATED ENLARGED PILE BREAKWATER PERFORMANCE WITH OTHER RESEARCH WORKS

The hydraulic performance of the present concept model obtained by the physical model test is compared with the available data, wherever possible, as provided by the authors Huang (2007), Rao and Rao (2001, 1999) and Mani and Jayakumar (1995). The test conditions quoted by the respective authors are listed in Table 4.14.

Table 4.14 Test conditions as indicated by the various authors

Reference	Structure Type	Experiment facilities		Structural Parameters		Wave Parameters	
		flume dim. in m	h m	D m	b/D	H m	T s
Rao (1999)	Non-perforated pile	50×0.71×1.1, 1:30 Scale	0.4	0.0335	0.15	0.035 to 0.175	1.5 to 2.25
Rao and Rao (1999, 2001)	Non-perforated suspended pipe	50×0.71×1.1, 1:30 Scale	0.4	0.0335	0.15	0.035 to 0.175	1.5 to 2.25
Huang (2007)	Slotted thin wall	-	0.3	0.019	0.19	0.02 to 0.06	1.1
Mani and Jayakumar (1995)	Non-perforated suspended pipe	30×2.0×1.5	1.0	0.04	0.22	0.06 to 0.24	0.8 to 2.0
Present work	Non-perforated enlarged pile head	50×0.71×1.1, 1:30 Scale	0.3	0.096 and 0.064	0.2	0.06 to 0.16	1.4 to 2.0

The transmission coefficient of enlarged pile head breakwater at gentle waves is higher in the case of Mani and Jayakumar (1995) by 8.36%, and 4.21% in the case of Rao and Rao (2001, 1999), but lower in the case of Rao (1999) by 2.19%, and 1.35% in the case of Huang, (2007). At higher wave steepness, the transmission coefficient is more than 12.5% (Rao and Rao 2001, 1999 and Rao 1999) and 0.834% (Huang 2007) and less

than 0.44% (Mani and Jayakumar 1995).

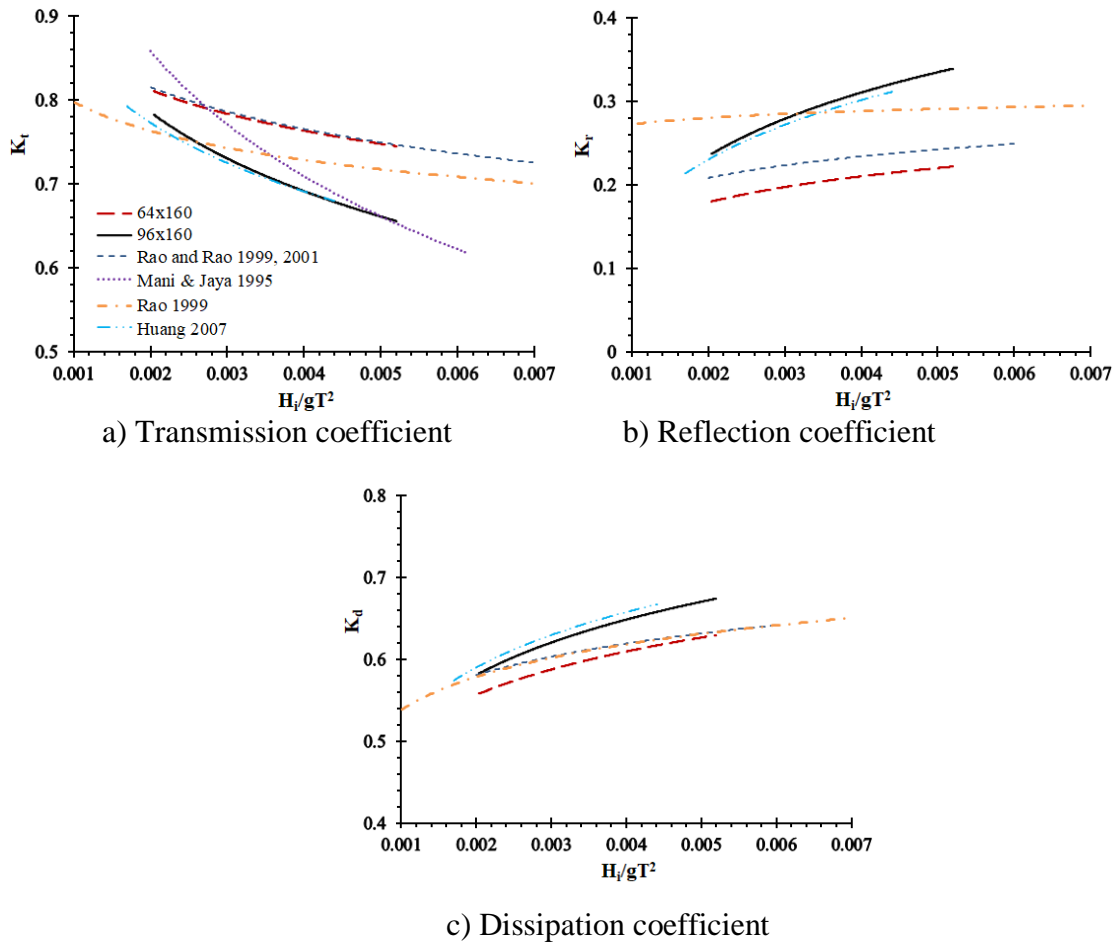


Fig. 4.22 Comparison of K_t , K_r and K_d with different single row pile breakwater models

Fig. 4.22 (b) indicates less reflection for the enlarged pile head breakwater than the compared breakwaters for the case 64×160 . In case of 96×160 , the reflection is more than the Rao and Rao (2001, 1999) by 24%, 5.7% more than Rao (1999) and 6% more than Huang (2007). In terms of the dissipation coefficient, the proposed breakwater is better than Rao and Rao (2001, 1999) and Rao (1999) by 4.43% at lower wave steepness and 16.32% at higher wave steepness. When compared with Huang (2007), it is nearly less than 0.5% at lower and higher wave steepness. It is observed that the trend lines of K_t , K_r and K_d of 96×160 model follows similar trend with that of Huang (2007). Therefore, by considering the above results, it can be stated that the hydraulic

performance of enlarged pile head breakwater with the configuration of $D/H_{\max} = 0.6$, $b/D = 0.2$ and $Y/H_{\max} = 1.0$ is competent with the compared types of breakwaters.

4.8 CONCLUSIONS ON NON-PERFORATED PILE HEAD BREAKWATER

From the experimental studies conducted on the non-perforated enlarged pile head breakwater, the following conclusions are drawn:

- The structural parameters (relative spacing between the piles, the diameter of pile head and the height of pile head), wave parameters (wave height, wave period and wavelength) and depth of water are the important parameters influencing wave transmission, reflection and energy dissipation.
- In general, with an increase in wave steepness (H_i/gT^2) the transmission coefficient (K_t) decreases, reflection coefficient (K_r) increases, and the energy dissipation coefficient (K_d) increases.
- K_t is inversely proportional to Y/H_{\max} , D/H_{\max} , Z and directly proportional to h , b/D . Whereas, K_r and K_d are directly proportional to Y/H_{\max} , D/H_{\max} , Z and inversely proportional to h , b/D .
- The proposed hybrid theoretical equations better predict the hydraulic efficiency of enlarged pile head breakwater, and the estimated values are in line with that of experimental results than the existing compared theoretical equations.
- The results obtained (K_t , K_r , K_d) using REEF3D are inline with the experimental data.
- Wave-structure interaction simulated using REEF3D and physical models are in good agreement.
- Decrease in b/D from 0.9 to 0.2 resulted in a maximum reduction of K_t by 27.73%, increase in K_r by 100% (from 0.17 to 0.34) and increase in K_d by 45% for the case of $D/H_{\max} = 0.6$ with $Y/H_{\max} = 1.0$ at 0.3 m depths of water.
- An increase in D/H_{\max} and Y/H_{\max} resulted in a maximum increase in hydraulic efficiency at 0.3 m water depth than the other considered depth of water.

- Increase in D/H_{\max} from 0.4 to 0.6 resulted in maximum reduction of K_t by 13%, increase of K_r by 54.5% (K_r increase from 0.22 to 0.34) and increase of K_d by 8.97% at higher wave steepness.
- An increase in Y/H_{\max} from 0.5 to 1.0 with $D/H_{\max} = 0.6$ at 0.3m depths of water resulted in maximum decrease in K_t by 9% and correspondingly increase in K_r by 18% and K_d by 8%.
- 25% to 33.33% increases in depth of water results in an average of 4% to 6% increase in K_t , 17% to 19% decrease in K_r and 7% to 8% decrease in K_d .
- The optimum configuration of non-perforated pile head breakwater obtained from the analysis is $D/H_{\max} = 0.6$, $b/D = 0.2$ and $Y/H_{\max} = 1.0$ at 0.3 m depth of water with least K_t value of 0.62.
- For the optimum enlarged pile head breakwater, the K_t obtained is in the range of -8.4% to +12.5% with the compared types of breakwaters.
- The K_r and K_d of enlarged pile head breakwater are in the range of 6% to 24% and -0.56% to 16.3% respectively, than the compared types of breakwaters. Therefor performance of the optimum enlarged pile head breakwater is better when compared with the other pile breakwaters. At this stage, the enlarged pile head breakwater performance shows hope as a solution for protecting the coast against erosion depending on the site conditions
- Based on the present study, friction coefficient (γ), as given by Suh et al. (2011), is modified using the following equations to evaluate the hydraulic characteristics (K_t and K_r) of non-perforated pile head breakwater.
 - The empirically reformed γ equation, using the current set of experimental data is given by

$$\gamma = 1.569 \left(\frac{\bar{\epsilon} \left(\frac{H_i}{h} \right) f \left(\frac{Y}{2h} \right)}{\bar{\epsilon} \bar{\epsilon}} \right)^{0.433}$$

- For the conventional pile breakwater, the developed equation is modified by considering the value of $\frac{Y}{2h} = 1$ and is given by,

$$\gamma = 1.569 \left(\frac{\bar{\epsilon} \left(\frac{H_i}{h} \right) f}{\bar{\epsilon}^{\epsilon}} \right)^{0.433}$$

- The comparison of relationship exhibits improved hydraulic characteristics of conventional and enlarged pile breakwaters due to the empirically improved γ parameter.
- The results of REEF3D and physical model study may vary by 4%.
- An open-source numerical modelling tool REEF3D may be used for modelling and investigating the hydraulic performance of the non-perforated enlarged pile head breakwater.

**INVESTIGATION ON PERFORATED ENLARGED PILE HEAD
BREAKWATER**

**5.1 RESULTS AND DISCUSSION ON PERFORATED ENLARGED
PILE HEAD BREAKWATER**

Decoding the experimental results in general form is very important for real-time applications. Hence, by considering the non-dimensional parameters, the results are presented in graphical form. The results are analysed by considering various parameters like incident wave steepness (H_i/gT^2), size of the pore (S), percentage of perforations (P), distribution of perforations around pile head (p_a), diameter (D) and height of pile head (Y) on wave transmission (K_t), reflection (K_r) and energy dissipation (K_d). The experiments are conducted in three phases. In the first phase, $D/H_{\max} = 0.4$ and $Y/H_{\max} = 0.5$ and 1.0 is considered. For this, the effect of p_a is verified by considering $S = 0.1D$ and $0.15D$, and p_a is varied from 25% to 75%. Verification of the results indicates that p_a of 25% is not effective and K_t decreases with an increase in p_a . Hence, $p_a = 25\%$ is neglected and there is a question, what if p_a is 100%. In the second phase, p_a is varied from 50 to 100% with $S = 0.2D$ and $0.25D$. In the third phase, $D/H_{\max} = 0.6$ and $Y/H_{\max} = 0.5$ & 1.0 is considered. Based on the conclusions drawn from phases 1 and 2, p_a is varied from 50% to 100% with $S = 0.2D$ and $0.25D$. The effect of all the aforesaid parameters is discussed in the following sections.

5.2 EFFECT OF WAVE STEEPNESS

Fig. 5.1, Fig. 5.2, Fig. 5.7, Fig. 5.8, Fig. 5.10, Fig. 5.13, and Fig. 5.16 shows that the transmission coefficient decreases with the increasing incident wave steepness (H_i/gT^2). Increase in H_i/gT^2 from 0.002 to 0.005 results in 9% to 26% reduction in K_t , 40% to 90% increase in K_r and 14% to 28% increase in K_d . The observed behaviour attributes to increased wave steepness, wherein the stable wave structure tends towards instability. The wave at this stage is likely to break and dissipate energy with minimal obstruction. This type of behaviour is similar to the findings of other types of pile

breakwaters as reported by Huang (2007), Koraim (2014), Koraim et al. (2014), Mani and Jayakumar (1995), Rao and Rao (2001, 1999) and Van Weele and Herbich (1972)

5.3 INFLUENCE OF PERFORATIONS ON THE PERFORMANCE CHARACTERISTICS

5.3.1 Effect of distribution of perforation around the pile head when diameter of pile head is 0.064 m on

5.3.1.1 Wave transmission

To understand the influence of distribution of perforation (p_a) around the pile head on K_t , graphs are plotted for K_t versus H_i/gT^2 with p_a as third variable. For the initial phase, the relative pore size of 0.1D and 0.15D are considered. The results are shown in Fig. 5.1 for a relative spacing of 0.2 between piles (b/D) and at 0.3 m depth of water (h). Fig. 5.1 shows that K_t decreases with an increase in p_a for all considered relative size of perforations and Y/H_{max} . Hence, it is evident that an increase in p_a resulted in the increased hydraulic performance of the structure. For the case of $D/H_{max} = 0.4$, $Y/H_{max} = 0.5$ and $S = 0.1D$ increasing p_a from 25% to 50% resulted in average of 1.4% decrease in K_t and for 50% to 75%, it is about 1.2%. When $D/H_{max} = 0.4$, $Y/H_{max} = 0.5$, $S = 0.15D$, change in p_a from 25% to 50%, and 50% to 75% resulted in average of 1.6% and 5.2% decrement of K_t , respectively. Similarly, for $D/H_{max} = 0.4$, $Y/H_{max} = 1.0$ and $S = 0.1D$, average decrease in K_t is found to 3.4% and 1% when p_a is changed from 25% to 50% and 50% to 75% respectively. Since the performance of the structure is better at $p_a = 50\%$ and 75%, $p_a = 25\%$ is ignored for analysing the further cases. But it would be in question that, what if $p_a = 100\%$. This question is addressed in the case when the size of the pore is 0.2D and 0.25D. Fig. 5.2 shows the effect of p_a when the size of perforations is 0.2D and 0.25D at 0.3m water depth.

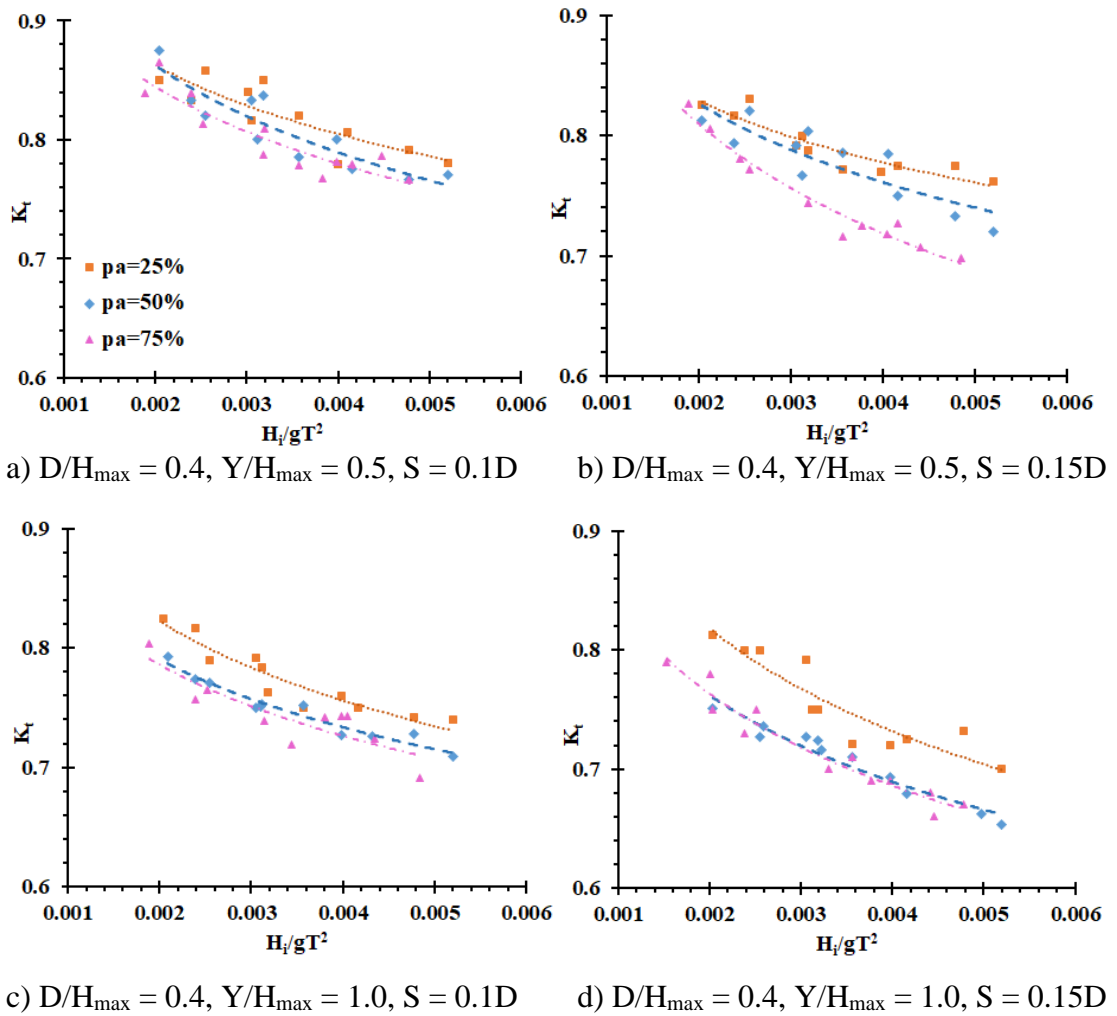


Fig. 5.1 Graphs of K_t versus H_i/gT^2 for various percentage of p_a , $D/H_{\max} = 0.4$, $S = 0.1D$ and $0.15D$ at a water depth of 0.30 m

Fig. 5.1 and Fig. 5.2 show that there is a marginal decrease in K_t with the increase in the percentage of perforation from 50% to 75% for most of the considered cases. Eventually, when the p_a percentage increases to 100% from 75%, K_t is also increased. Hence, an increase in p_a to 100% is not effective in improving the hydraulic efficiency of enlarged pile head structures. The same is depicted well in Fig. 5.2. The increased efficiency is due to an increase in wave-structure interactions. When p_a is 25%, the portion of wave entering the central hollow part of enlarged pile head breakwater through perforations is less than the other cases ($p_a = 50\%$ and 75%), resulting in less wave attenuation. But when p_a is 100%, there is a more chance that wave can simply pass through the perforations from seaside to lee side. Thus, it leads to less hydraulic

efficiency of the pile structure. Thereby $pa = 75\%$ tends to be the better one than the rest.

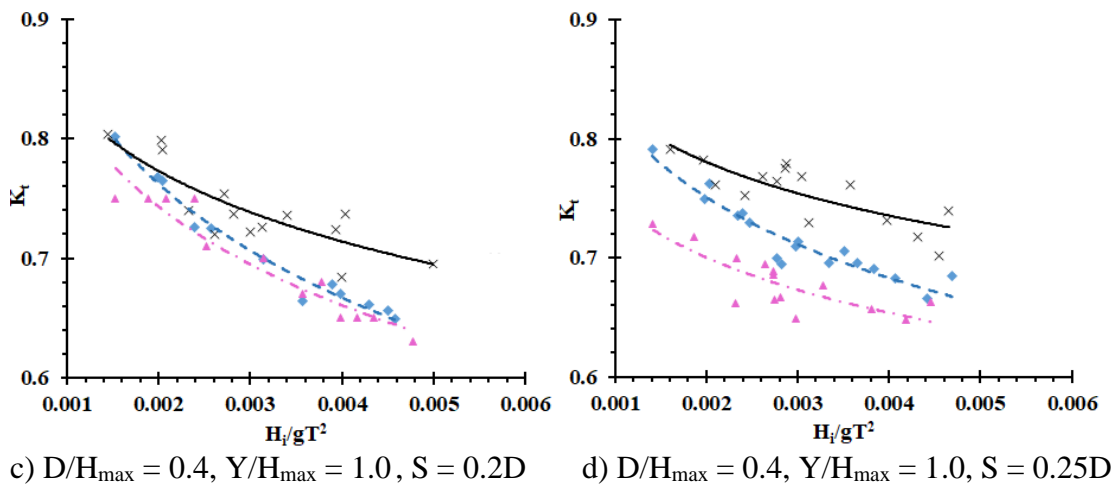
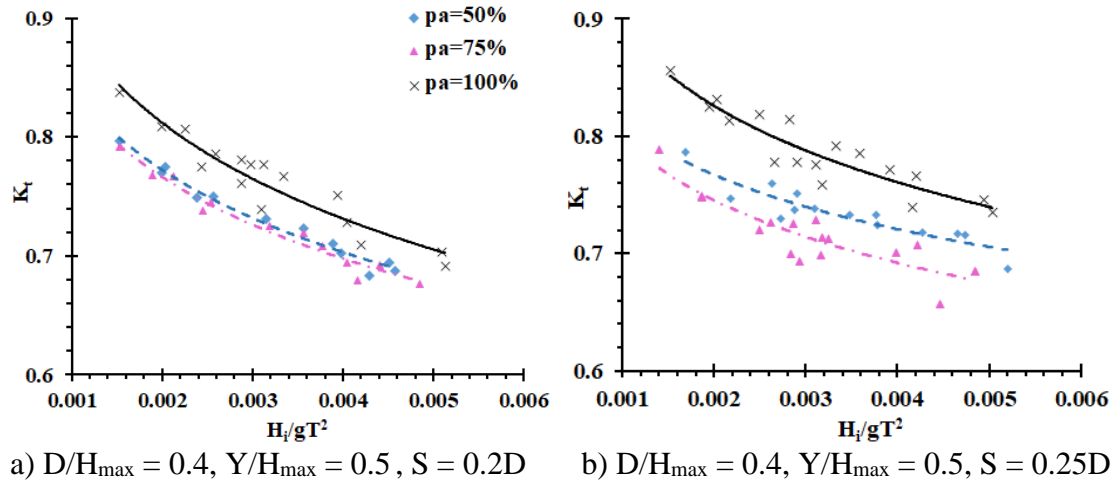
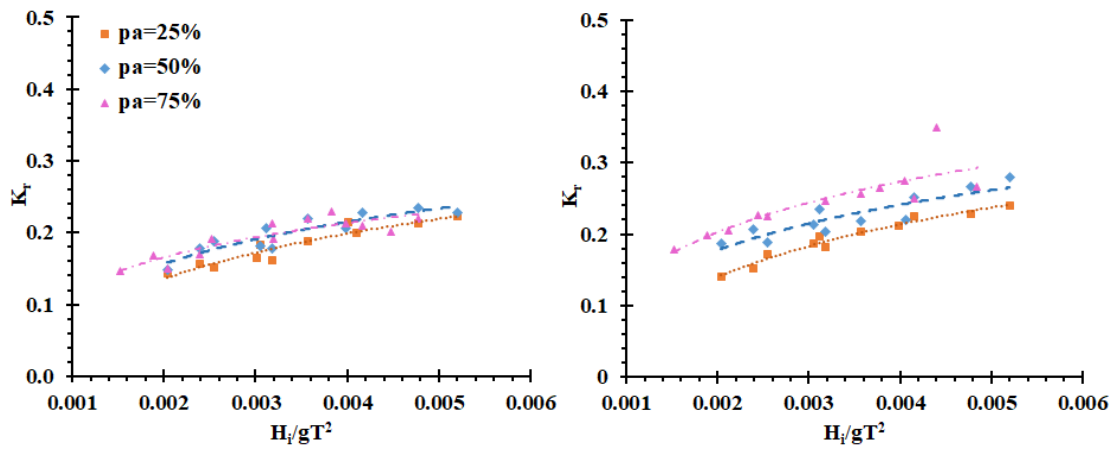


Fig. 5.2 Graphs of K_t versus H_i/gT^2 for various percentage of pa , $D/H_{\max} = 0.4$, $S = 0.2D$ and $0.25D$ at a water depth of 0.30 m

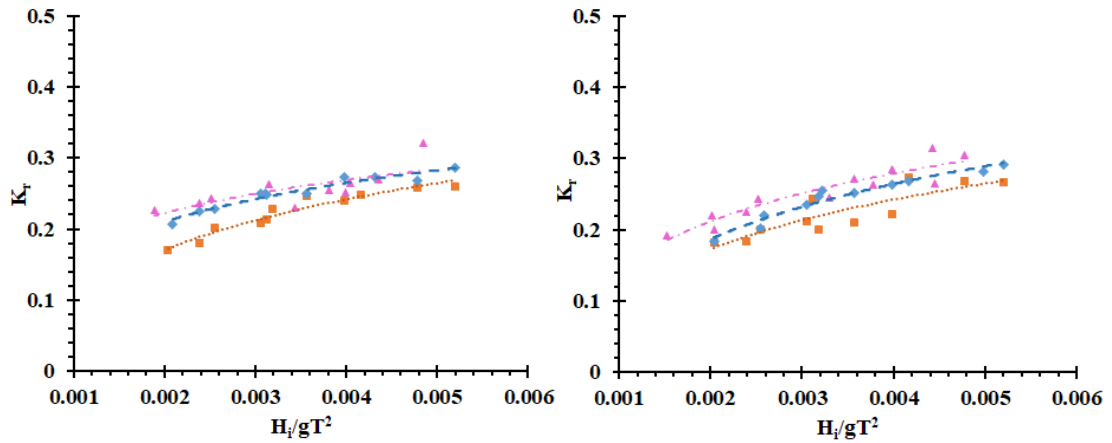
5.3.1.2 Wave reflection

Effect of pa on K_r and K_d is explained through Fig. 5.3 and Fig. 5.4. From Fig. 5.3 and Fig. 5.4, it can be said that with increase in pa from 25% to 75% increases the reflection coefficient (K_r) and increase in pa beyond 75% decreases K_r . The increase in K_r is found to be in the range of 5% to 15%. As pa increases to 100%, wave can pass through the perforation, resulting decrease in K_r .



a) $D/H_{\max} = 0.4$, $Y/H_{\max} = 0.5$, $S = 0.1D$

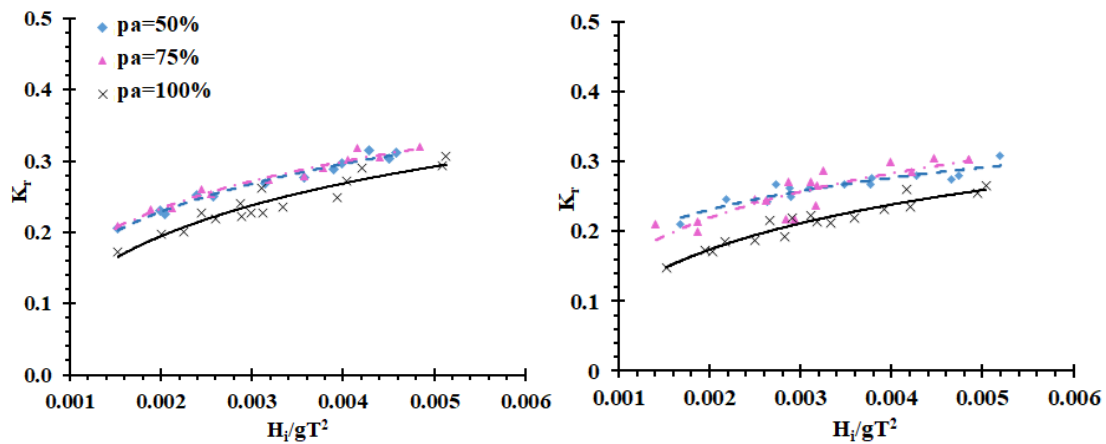
b) $D/H_{\max} = 0.4$, $Y/H_{\max} = 0.5$, $S = 0.15D$



c) $D/H_{\max} = 0.4$, $Y/H_{\max} = 1.0$, $S = 0.1D$

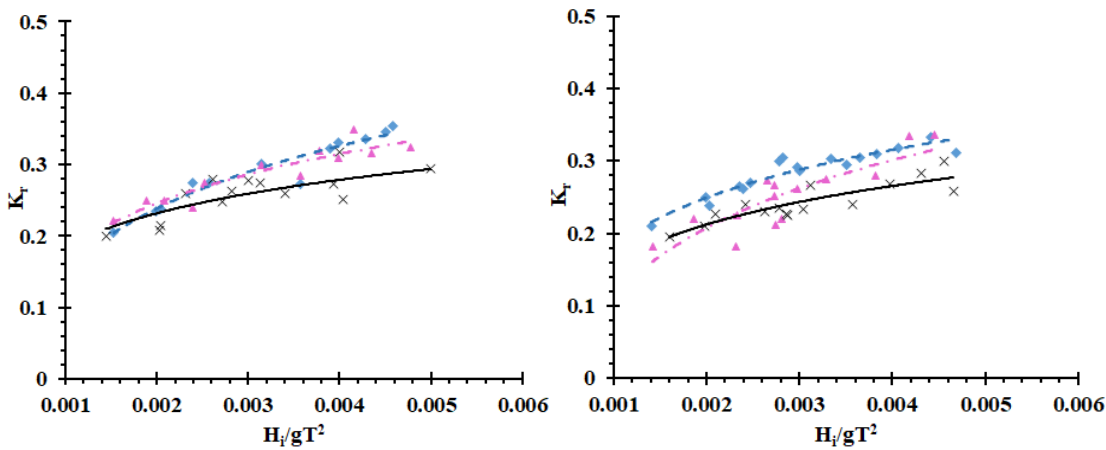
d) $D/H_{\max} = 0.4$, $Y/H_{\max} = 1.0$, $S = 0.15D$

Fig. 5.3 Graphs of K_r versus H_i/gT^2 for various percentage of p_a , $D/H_{\max} = 0.4$, $S = 0.1D$ and $0.15D$ at a water depth of 0.30 m



a) $D/H_{\max} = 0.4, Y/H_{\max} = 0.5, S = 0.2D$

b) $D/H_{\max} = 0.4, Y/H_{\max} = 0.5, S = 0.25D$



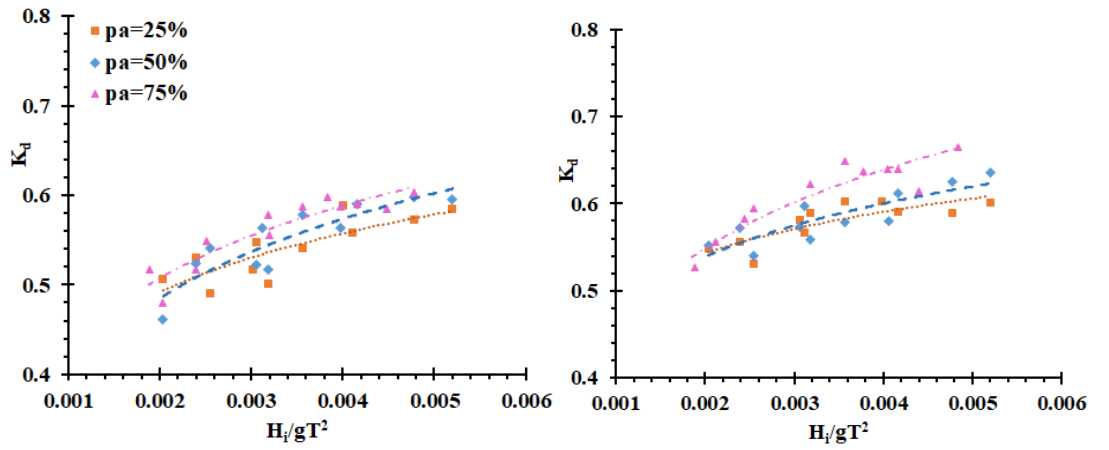
c) $D/H_{\max} = 0.4, Y/H_{\max} = 1.0, S = 0.2D$

d) $D/H_{\max} = 0.4, Y/H_{\max} = 1.0, S = 0.25D$

Fig. 5.4 Graphs of K_r versus H_i/gT^2 for various percentage of p_a , $D/H_{\max} = 0.4$, $S = 0.2D$ and $0.25D$ at a water depth of 0.30 m

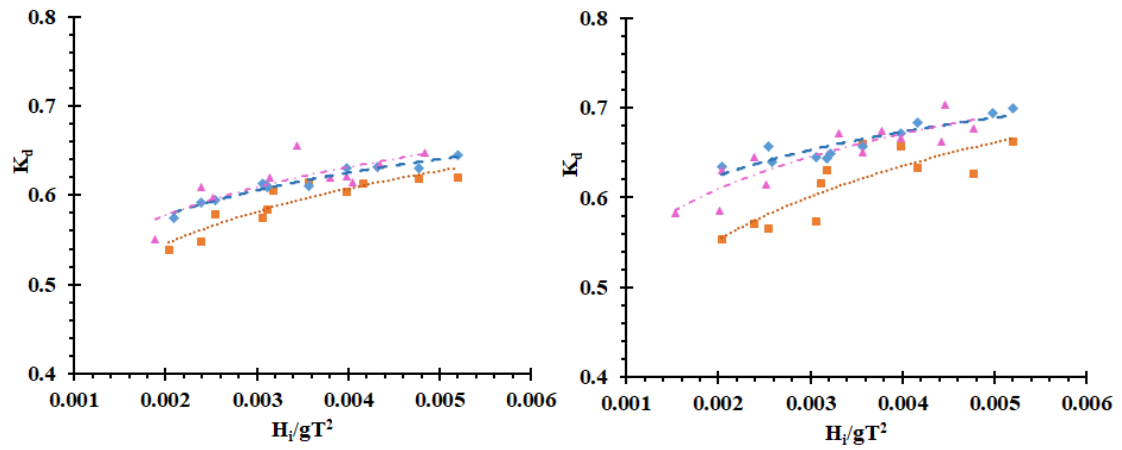
5.3.1.3 Wave Energy dissipation

The effect of p_a on K_d can be visualised through Fig. 5.5 and Fig. 5.6. K_d increases with increase in p_a from 25% to 75% and decreases beyond the value of 75%. As p_a increases to 75% from 25%, a minimum increase in K_d is about 4% for the case of $D/H_{\max} = 0.4, Y/H_{\max} = 0.5$ and $S = 0.1D$ and maximum of 15% when $D/H_{\max} = 0.4, Y/H_{\max} = 0.5$ and $S = 0.15D$.



a) $D/H_{\max} = 0.4, Y/H_{\max} = 0.5, S = 0.1D$

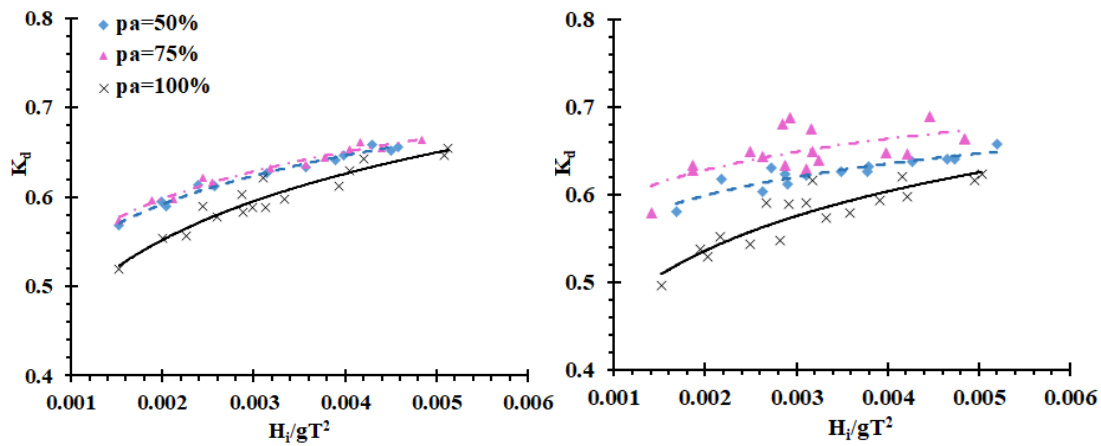
b) $D/H_{\max} = 0.4, Y/H_{\max} = 0.5, S = 0.15D$



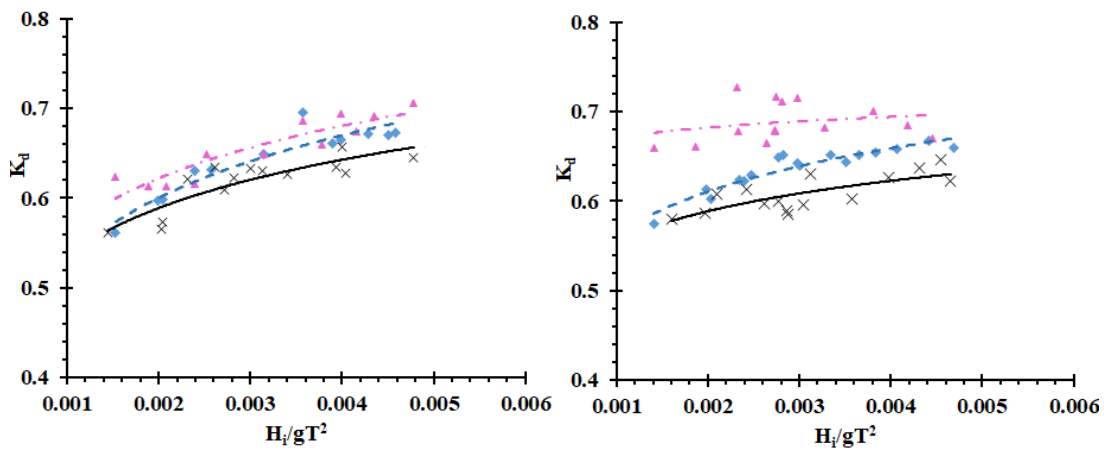
c) $D/H_{\max} = 0.4, Y/H_{\max} = 1.0, S = 0.1D$

d) $D/H_{\max} = 0.4, Y/H_{\max} = 1.0, S = 0.15D$

Fig. 5.5 Graphs of K_d versus H_i/gT^2 for various percentage of p_a with $D/H_{\max} = 0.4, S = 0.1D$ and $S = 0.15D$ at a water depth of 0.30 m



a) $D/H_{\max} = 0.4, Y/H_{\max} = 0.5, S = 0.2D$ b) $D/H_{\max} = 0.4, Y/H_{\max} = 0.5, S = 0.25D$



c) $D/H_{\max} = 0.4, Y/H_{\max} = 1.0, S = 0.2D$ d) $D/H_{\max} = 0.4, Y/H_{\max} = 1.0, S = 0.25D$

Fig. 5.6 Graphs of K_d versus H_i/gT^2 for various percentage of p_a with $D/H_{\max} = 0.4, S = 0.2D$ and $0.25D$ at a water depth of 0.30 m

5.3.2 Effect of relative pore size when diameter of pile head is 0.064 m on

5.3.2.1 Wave transmission

To understand the effect of pore size (S), K_t is plotted against H_i/gT^2 with S and percentage of perforation (P) as third variable and is as shown in Fig. 5.7. From Fig. 5.7, it can be observed that in general, as the pore size and percentage of perforation increases, K_t decreases. Hence, a better value of K_t is obtained for the case when $S = 0.2D$ and $0.25D$. So, it is evident that an increase in pore size with perforations is more important for wave attenuation. Similar findings are reported by Anuar and Sidek (2012). An increase in the pore size highly dominates the wave attenuation than the

increase in perforations with a smaller size of the pore. For instance, as inferred from Fig. 5.7 (a), when S increased by 66.66% (0.15D to 0.25D) and percentage of perforation decreases to 7.41%. The value K_t decreases to 7.5% at lower wave steepness ($H_i/gT^2 = 0.002$) and 4.9% at higher wave steepness ($H_i/gT^2 = 0.005$). A similar trend can also be visualised from Fig. 5.7 (b) to Fig. 5.7 (d). The probable reason for the above observation is that if the pore size is relatively small, even with a higher percentage of perforations is ineffective to create more turbulence to dissipate the wave energy (Rao et al. 1999). In enlarged pile head breakwater, if the pore size is small, wave entering the central hollow part of the structure will also be less. This results in less wave energy dissipation due to less unique wave-structure interaction at the centre hollow part of the enlarged pile head breakwater.

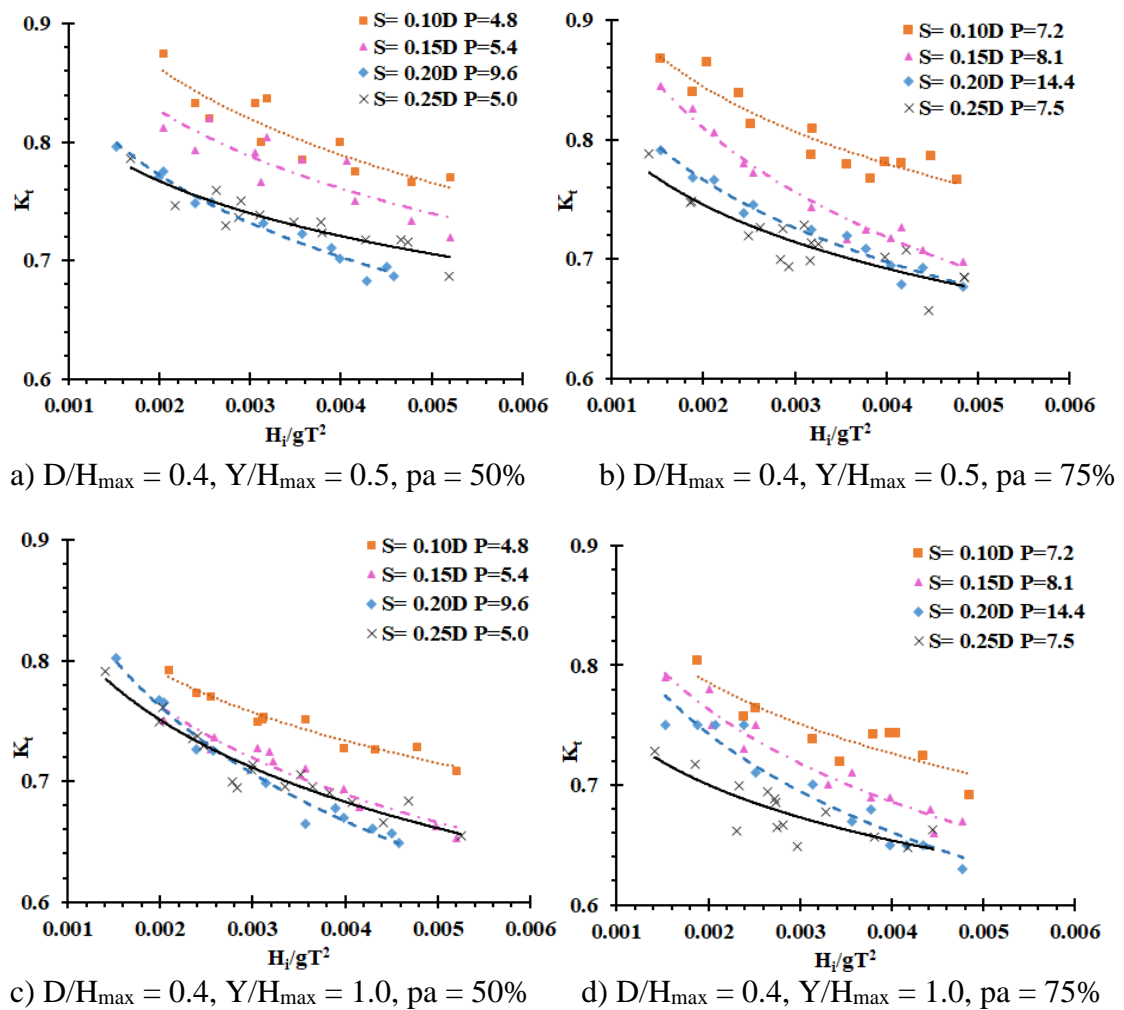


Fig. 5.7 Graphs of K_t versus H_i/gT^2 for $D/H_{max} = 0.4$ for various P and S at 0.3 m water depth

Hence, for the case of pile head breakwater when D/H_{\max} is 0.4 and Y/H_{\max} is 0.5 or 1.0, the best performing model would be when pa is 75% and pore size 0.25D with P equal to 7.5.

5.3.2.2 Wave reflection

Effect of S on K_r is as shown in the Fig. 5.8. For all the considered cases, it is observed that the pile head with smaller pore size has shown less reflection than the larger size of the pore. This observation is in line with the findings of Rao (1999), in which it was reported that the reflection from the small size of perforations is less than the larger size perforations when the range of incident wave steepness is less than 0.004. This may be due to less wave interaction with the structure when the size of the pore is smaller than with the larger size of pores.

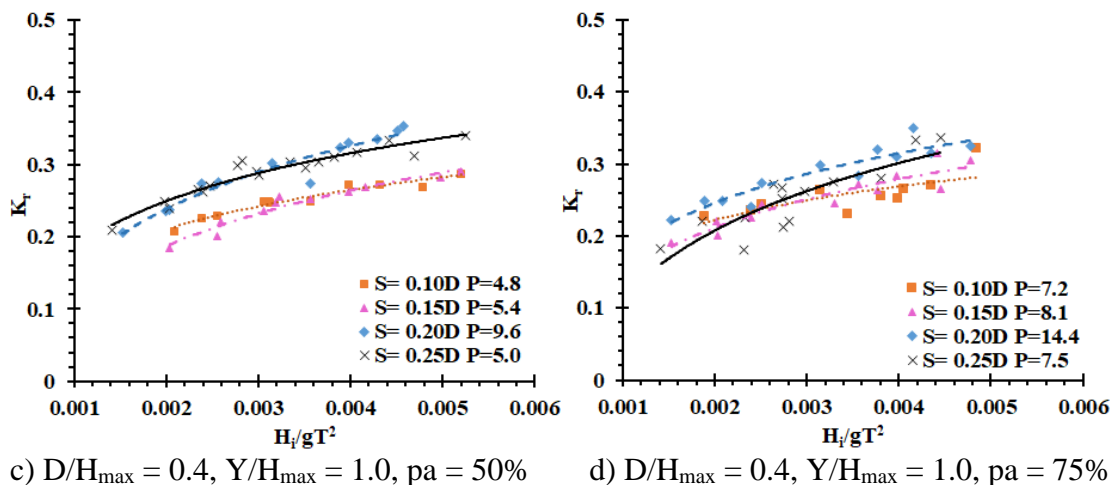
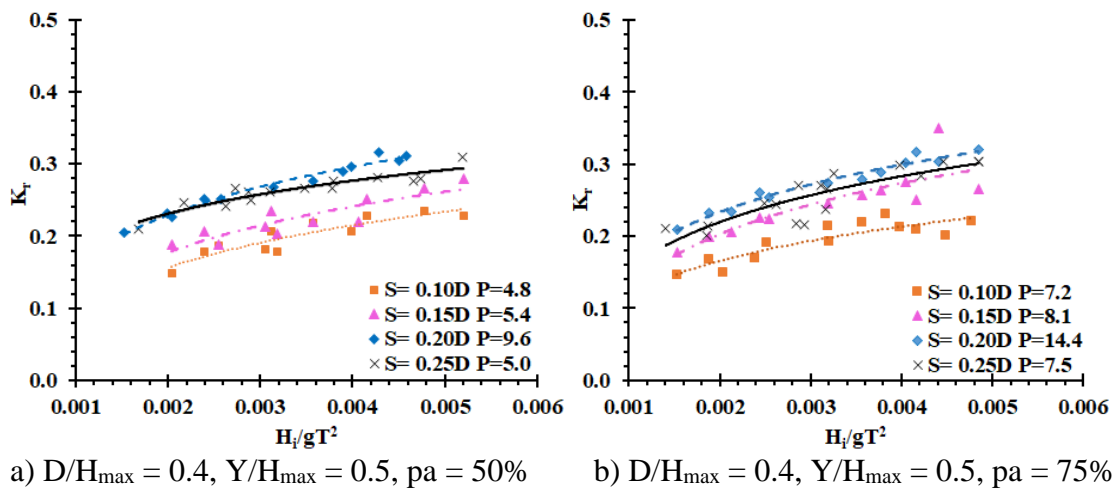


Fig. 5.8 Graphs of K_r versus H_i/gT^2 for $D/H_{\max} = 0.4$ with various percentage of perforation and pore size at 0.3 m water depth

5.3.2.3 Wave energy dissipation

Variation of K_d with S is as shown in Fig. 5.9. From the graph shown, it can be concluded that the larger the pore size, higher will be the wave energy dissipation. For 50% pa, an average of 15% improvement in K_d is observed for $D/H_{\max} = 0.4$ and $Y/H_{\max} = 0.5$ and for the same case when $Y/H_{\max} = 1.0$, an average of 9% improvement in K_d is observed. When $D/H_{\max} = 0.4$, $Y/H_{\max} = 0.5$ and $pa = 75\%$, at lower wave steepness (0.002) about 24% improvement in K_d and at higher wave steepness (0.005), about 10% improvement in K_d is noticeable. Similarly, for $D/H_{\max} = 0.4$, $Y/H_{\max} = 1.0$ and $pa = 75\%$, percentage improvement in K_d is about 19% and 6% at lower and higher wave steepness, respectively achieved.

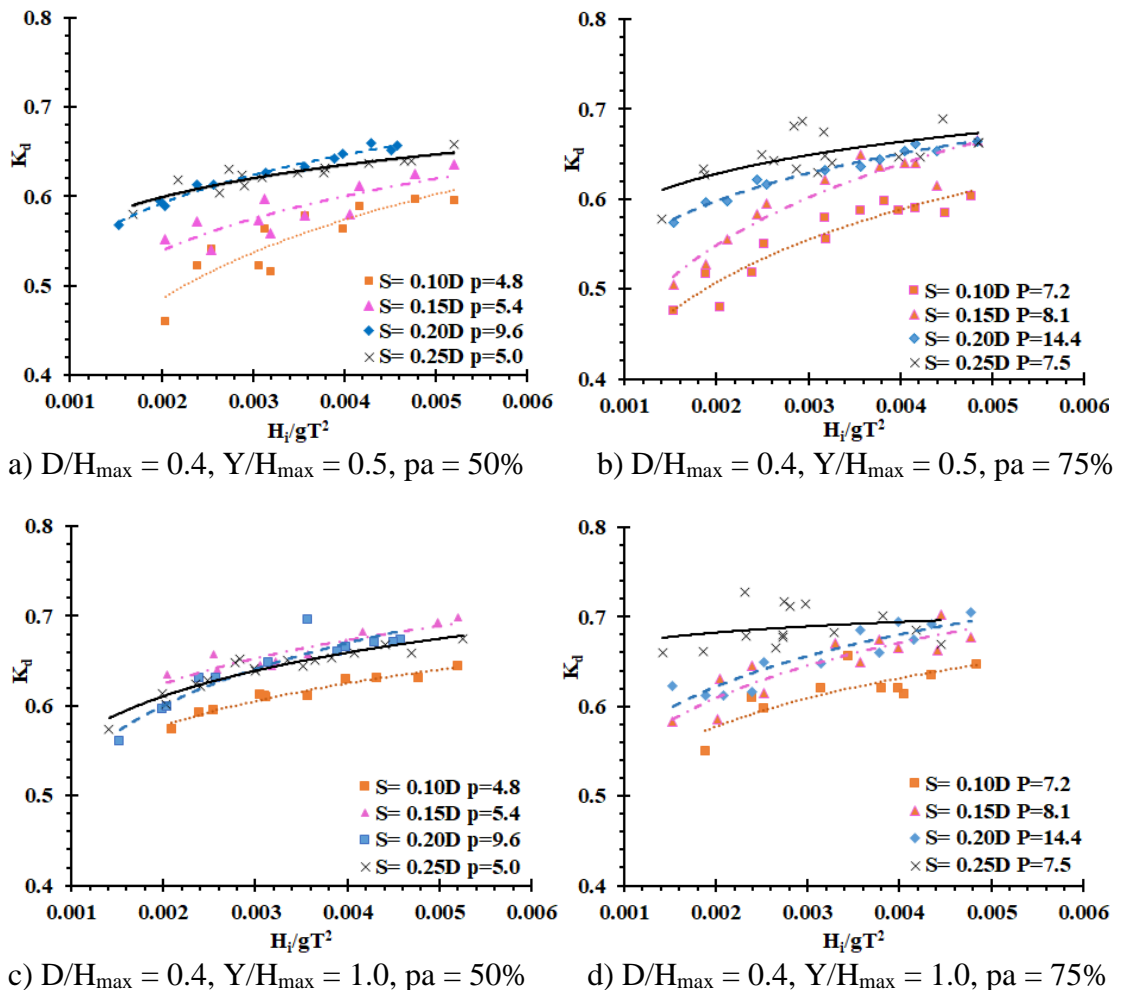


Fig. 5.9 Graphs of K_d versus H_i/gT^2 for $D/H_{\max} = 0.4$ with various P and S at 0.3 m water depth

5.3.3 Effect of distribution of perforation around the pile head when diameter of pile head is 0.096 m on

5.3.3.1 Wave transmission

Effect of distribution of perforations (pa) around pile head on K_t when $D/H_{max} = 0.6$ is shown in Fig. 5.10. As comprehended from the previous section, results obtained for the case of $D/H_{max} = 0.6$ are in line with the results when $D/H_{max} = 0.4$. Hence, the best result for this configuration of pile head breakwater is obtained when S is $0.25D$, P is 22.5 and pa is 75% .

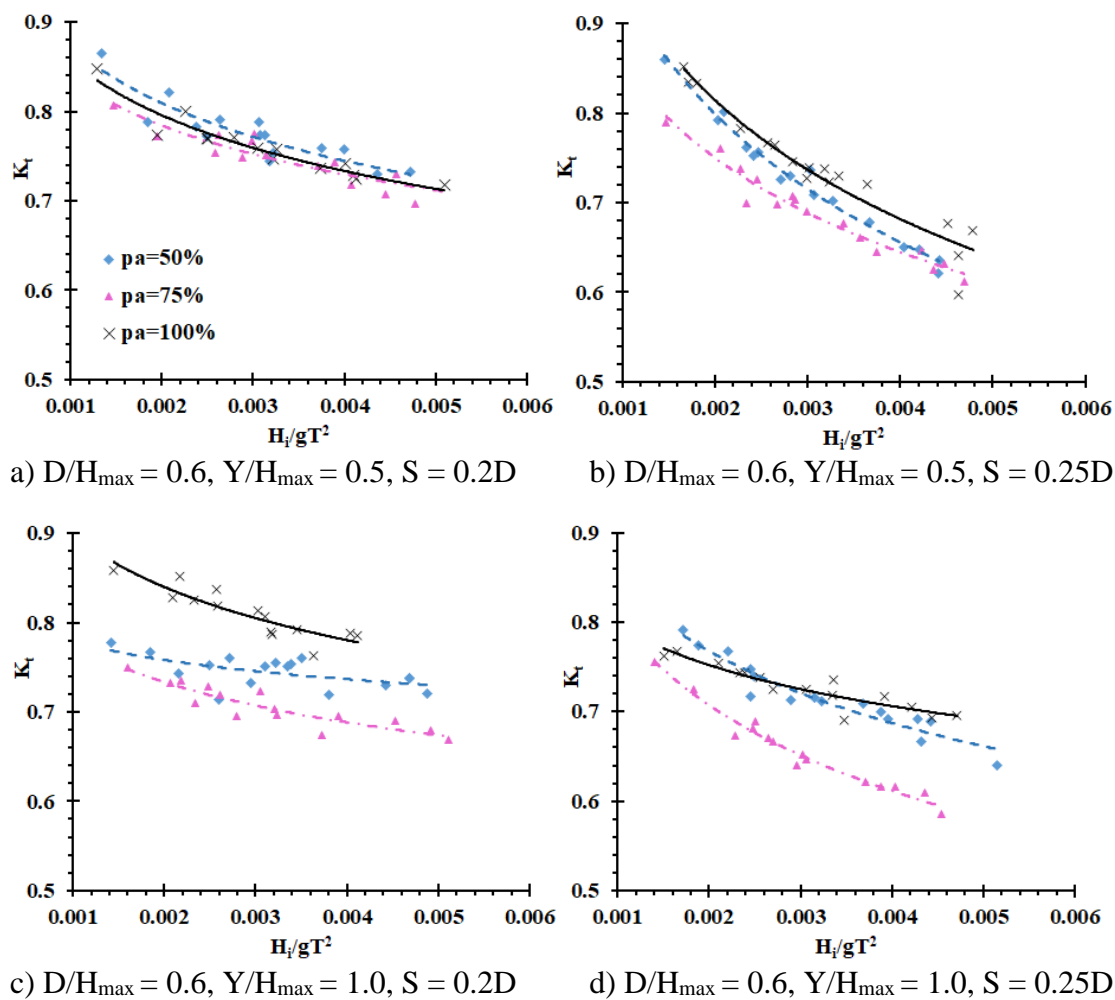


Fig. 5.10 Graphs of K_t versus H_i/gT^2 for various pa , $D/H_{max} = 0.6$, $S = 0.2D$ and $0.25D$ at a water depth of 0.30 m

5.3.3.2 Wave reflection

Variation of K_r for the case when $D/H_{\max} = 0.6$ is as shown in Fig. 5.11. It is observed that the K_r behaviour with pa are reminiscent of the case when $D/H_{\max} = 0.4$.

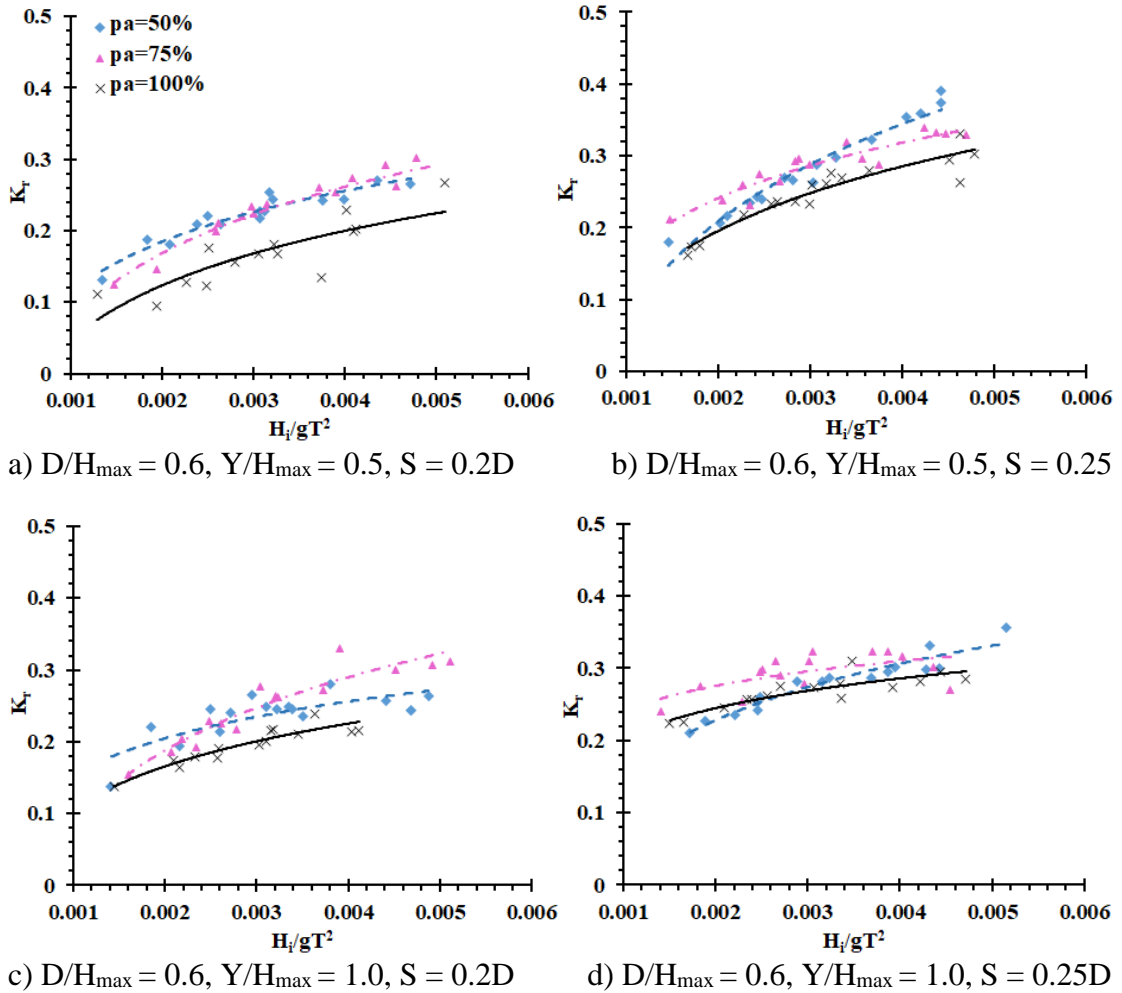


Fig. 5.11 Graphs of K_r versus H_i/gT^2 for various pa , $D/H_{\max} = 0.6$, $S = 0.2D$ and $0.25D$ at a water depth of 0.30 m

5.3.3.3 Wave energy dissipation

Variation of K_d for the case when $D/H_{\max} = 0.6$ is as shown in Fig. 5.12. It is observed that, K_d behaviour with pa are reminiscent of the case when $D/H_{\max} = 0.4$.

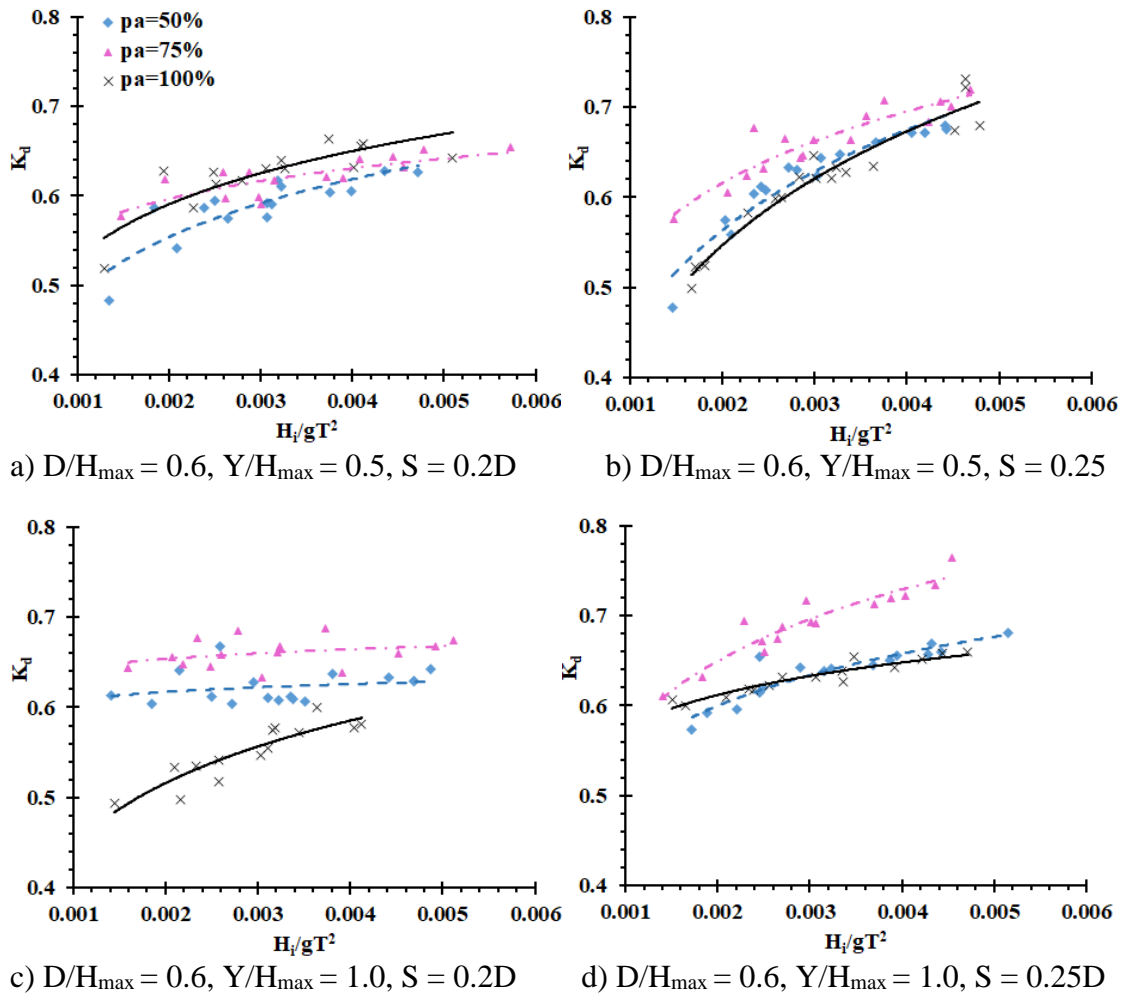


Fig. 5.12 Graphs of K_d versus H_i/gT^2 for various pa , $D/H_{\max} = 0.6$, $S = 0.2D$ and $0.25D$ at a water depth of 0.30 m

5.3.4 Effect of relative pore size when diameter of pile head is 0.096 m on

5.3.4.1 Wave transmission

Fig. 5.13 shows the effect of pore size on the wave attenuation of enlarged pile head breakwater. From Fig. 5.13 (a), it is seen that when the pore size increases from $0.2D$ to $0.25D$ (i.e., 25% increment) percentage of K_t decreases by 4.5% and 16.5% at lower (0.002) and higher wave steepness (0.005), respectively. Similarly, as per Fig. 5.13 (b) K_t decreases by 3.6% at lower wave steepness and 16% at higher wave steepness.

Hence, for pile head breakwater with a configuration of $D/H_{\max} = 0.6$ and $Y/H_{\max} = 0.5$ or 1.0 , the best performing model would be when pa is 75% and pore size is $0.25D$ with P equal to 22.5.

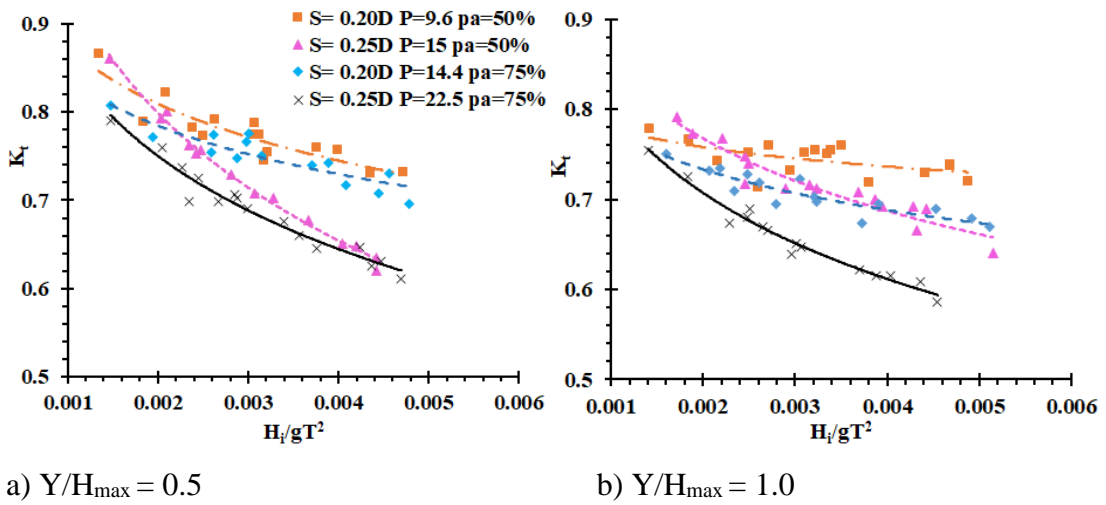


Fig. 5.13 Graphs of K_t versus H_i/gT^2 for $D/H_{\max} = 0.6$, various percentage of perforations and pore size at 0.3 m water depth

5.3.4.2 Wave reflection

The effect of pore size on K_r is shown in Fig. 5.14. As identified from the previous case, larger pore size has higher reflection and more wave energy dissipation than the structure with a smaller pore size.

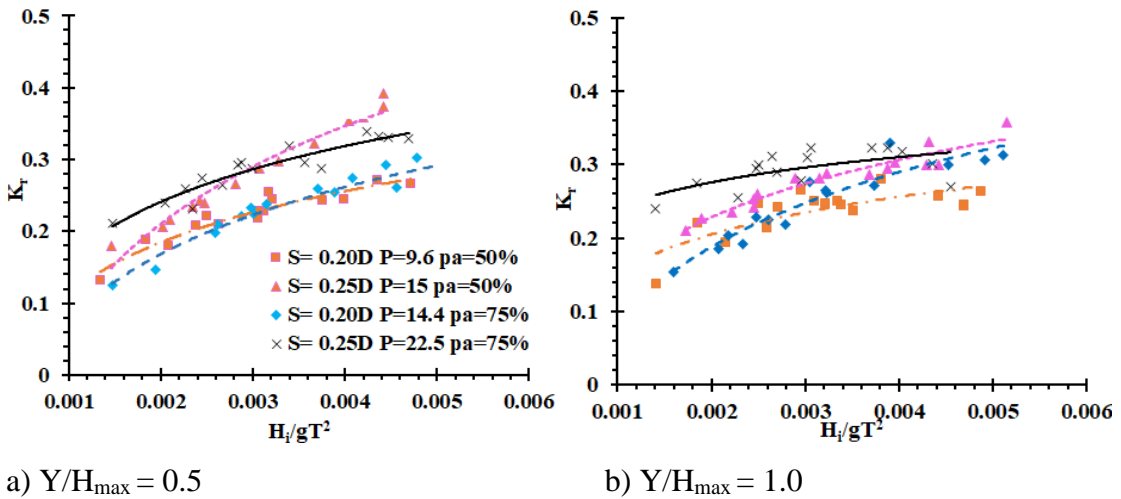


Fig. 5.14 Graphs of K_r versus H_i/gT^2 for $D/H_{\max} = 0.6$, with various P, pa and S at 0.3 m water depth

5.3.4.3 Wave energy dissipation

The effect of pore size on K_r and K_d is shown in Fig. 5.14 and Fig. 5.15. As identified from the previous case, larger pore size has higher reflection and more wave energy dissipation than the structure with a smaller pore size.

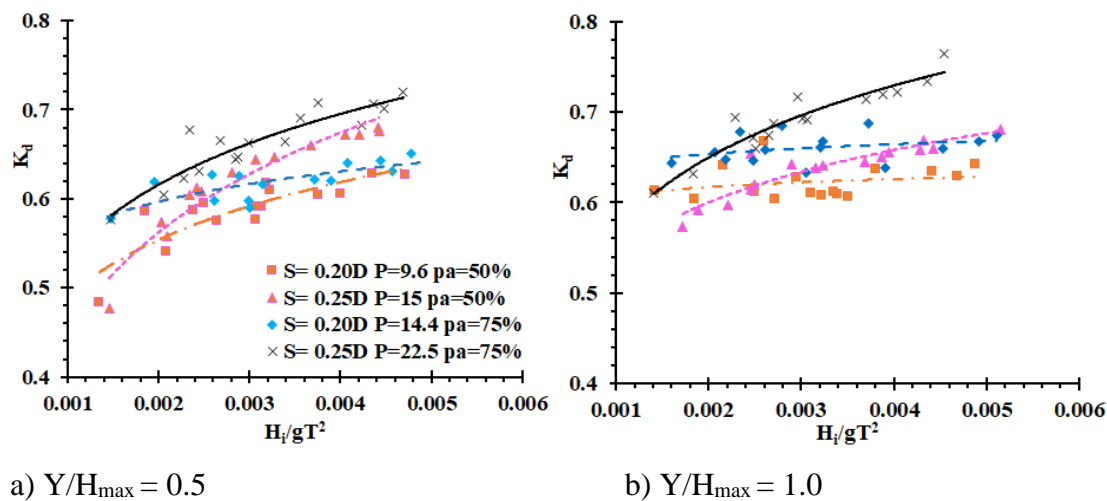


Fig. 5.15 Graphs of K_d versus H_i/gT^2 for $D/H_{max} = 0.6$, with various P , p_a and S at 0.3 m water depth

5.4 COMPARISON OF PERFORATED AND NON-PERFORATED ENLARGED PILE HEAD BREAKWATER

5.4.1 Wave transmission

The effect of perforations on K_t is explained by comparing the perforated and non-perforated cases and the same is shown in Fig. 5.16. It is observed that, providing the perforations of size 0.25D in pile head of configuration of $D/H_{max} = 0.4$ and $Y/H_{max} = 0.5$ at $b/D = 0.2$ with $P = 22.5$ and $p_a = 75\%$, reduces the K_t by 12.3% at lower wave steepness (0.002) and 18.7% at higher wave steepness (0.005). For the same case, when $Y/H_{max} = 1.0$, K_t reduces by 16% and 17.1% at lower and higher wave steepness, respectively. For the case of $D/H_{max} = 0.6$ and $Y/H_{max} = 0.5$, K_t reduces by 8.6% at lower wave steepness and 17.7% at higher wave steepness. Similarly, when $Y/H_{max} = 1.0$, K_t reduces by 10.6% at lower wave steepness and 13.4% at higher wave steepness. Hence, it can be concluded that the perforated structure is better than the non-perforated structure in reducing the wave energy. Overall, perforations of size 0.25D effectively reduce the K_t by about 10% to 18% than the non-perforated pile head breakwater. These

observed results are well matching with results of the perforated conventional pile or pipe breakwater case where about 10% to 14% improvement in K_t is reported (Rao 1999; Rao and Rao 2001).

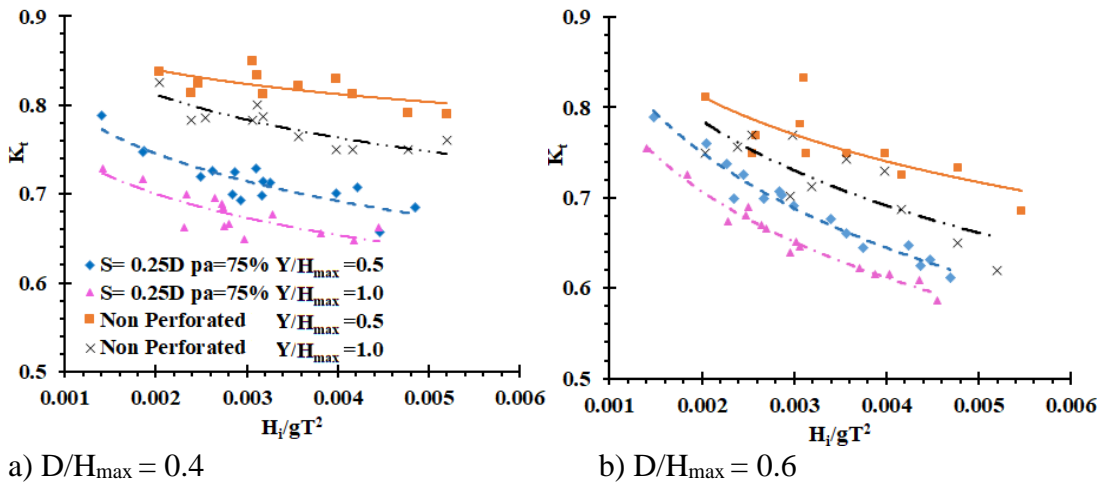


Fig. 5.16 Effect of perforations on K_t for $D/H_{max} = 0.4$ and 0.6 at 0.3 m water depth

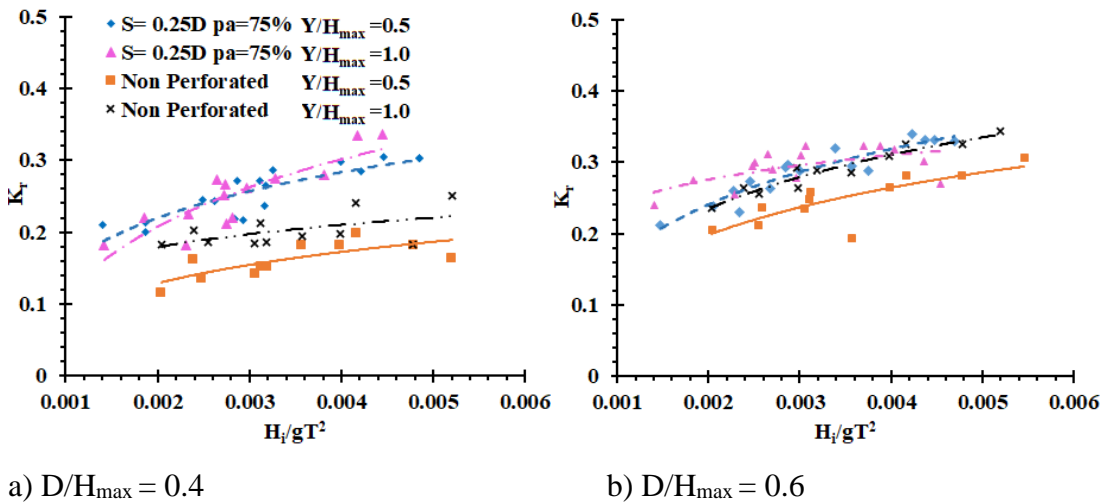


Fig. 5.17 Effect of perforations on K_r for $D/H_{max} = 0.4$ and 0.6 at 0.3 m water depth

5.4.2 Wave reflection

The effect of perforations on K_r is explained by comparing the K_r of perforated with the non-perforated pile head breakwater and the same is shown in Fig. 5.17. Results obtained shows that the perforated structure has more reflection than the non-perforated

structure. These results are opposite to that of Rao et al. (2002b) and Rao and Rao (2001). When $Y/H_{max} = 1.0$ and $D/H_{max} = 0.4$, K_r increases by 16% at lower wave steepness and 50% at higher wave steepness than the non-perforated pile breakwater of similar configurations. However, an opposite trend is observed when $Y/H_{max} = 1.0$ and $D/H_{max} = 0.6$, and K_r increases / decreases by about 17% and 4% respectively at lower / higher wave steepness.

5.4.3 Wave energy dissipation

The dissipation coefficient of perforated and non-perforated enlarged pile head breakwater is compared in Fig. 5.18. Results indicate that the perforated pile head has higher K_d than the non-perforated.

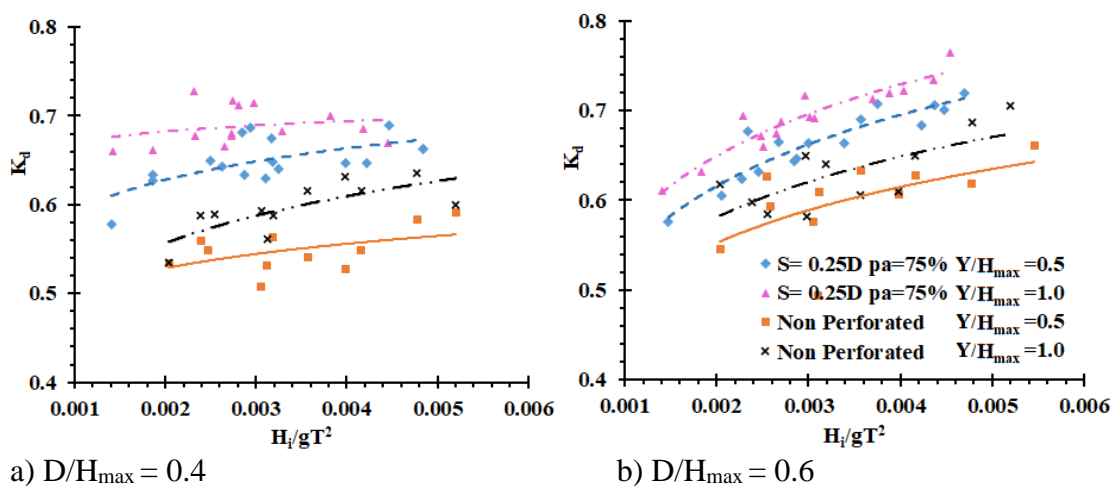


Fig. 5.18 Effect of perforations on K_d for $D/H_{max} = 0.4$ and 0.6 at 0.3 m water depth

K_d increases about 22% at lower wave steepness (0.002) and 11% at higher wave steepness (0.005) when $Y/H_{max} = 1.0$ and $D/H_{max} = 0.4$. Similarly, K_d increases about 12% and 11% at higher and lower wave steepness, respectively, when $Y/H_{max} = 1.0$ and $D/H_{max} = 0.6$.

5.5 PERFORMANCE EVALUATION OF THE BEST MODEL UNDER TIDE

In the prototype conditions, the water depth may vary due to one or a combination of tide, erosion, sea-level rise due to melting of glaciers and storm surge. Therefore,

enlarged pile head breakwater is experimentally investigated for variations in water depths subjected to environmental conditions. For the investigation, three depths of water ranging from 0.25 to 0.35 is considered with an increment of 0.05 m. An incremental water depth of 0.05 m is considered based on the present environmental conditions of Mangaluru coast. For the analysis, the best model from the present experiment is considered. The non-perforated enlarged pile head breakwater with a configuration of $b/D = 0.2$, $Y/H_{\max} = 1.0$, $D/H_{\max} = 0.6$ and perforated breakwater of same configuration as non-perforated with $S = 0.25D$, $P = 22.5$, and $p_a = 75\%$ is selected. To analyse the effect of variation in depth of water, it is assumed that the structure is placed at 0.3 m depth of water, and 0.35 m and 0.25 m are the water depth variations due to environmental conditions.

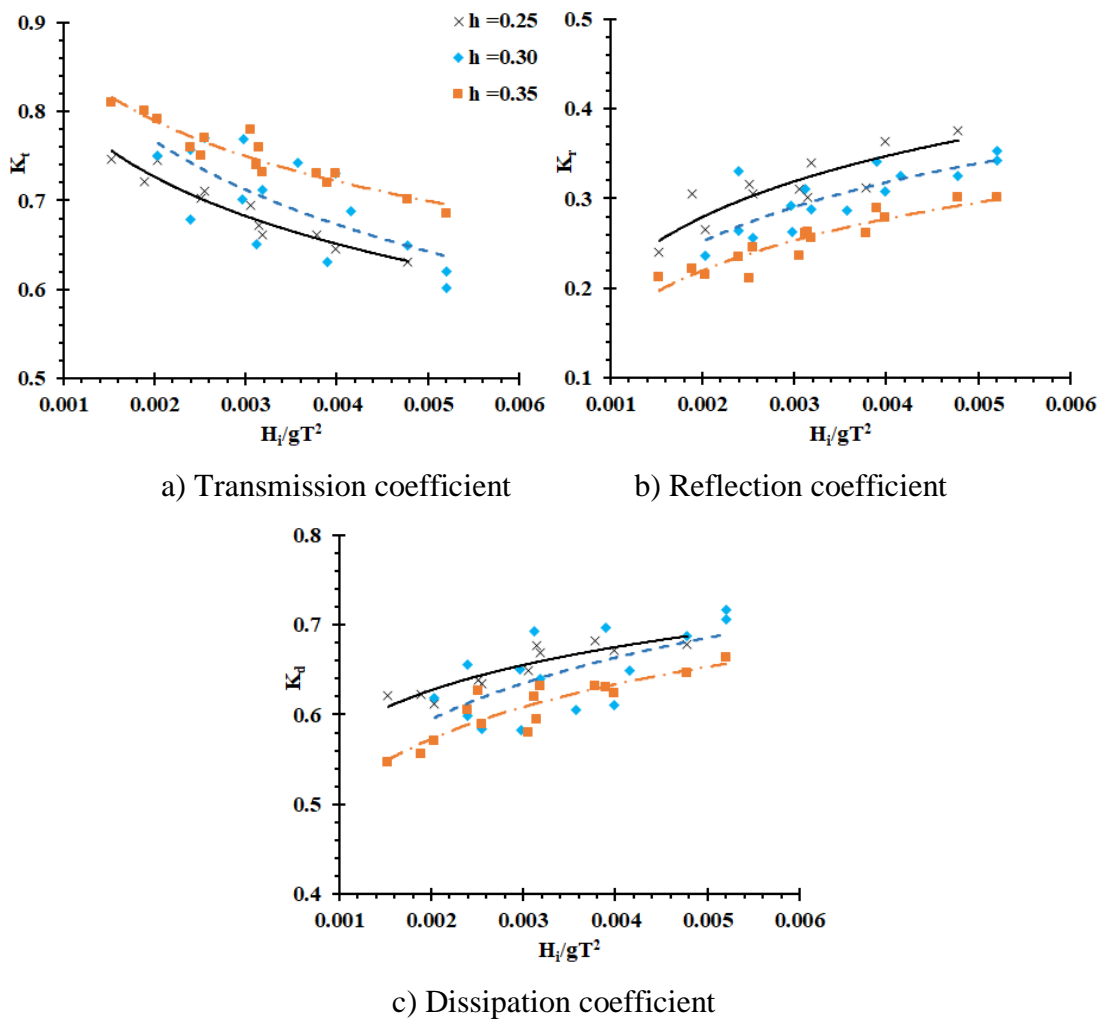


Fig. 5.19 Effect of water level variations on K_t , K_r and K_d for non-perforated pile head breakwater

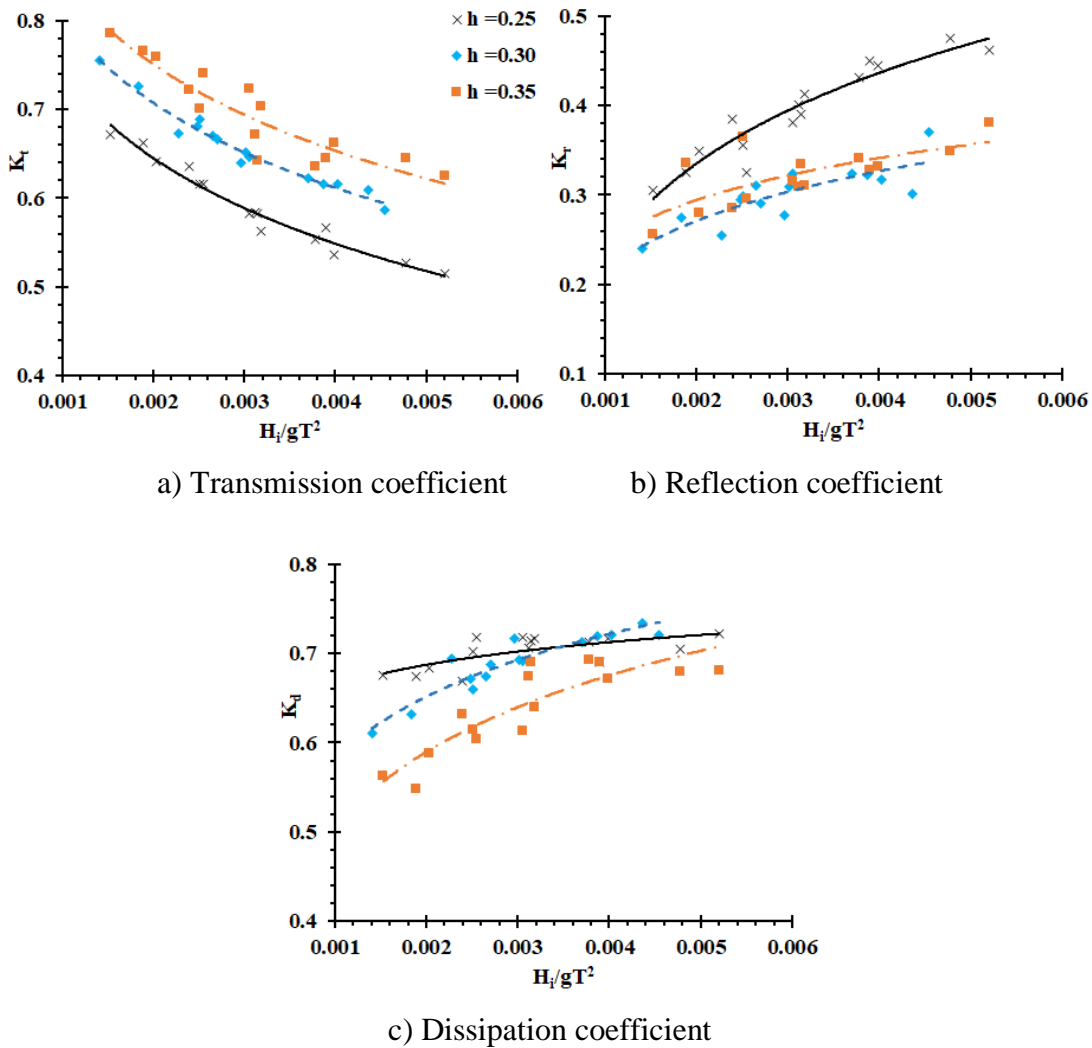


Fig. 5.20 Effect of water level variations on K_t , K_r and K_d for perforated pile head breakwater

Variation of K_t with reference to the depth of water is shown in Fig. 5.19 and Fig. 5.20 for non-perforated and perforated pile head breakwater, respectively. Results indicate that K_t decreases with a decrease in depth of water and vice versa. An average variation in K_t , K_r and K_d observed is shown in Table 5.1.

From the analysis, it can be concluded that placing enlarged pile head breakwater with respect to the average water level or at mean sea level does not make much difference in the hydraulic performance subjected to the variation in the water depth due to changes in environmental conditions.

Table 5.1 An average percentage variation in K_t , K_r and K_d with change in water depth

Type	Change in water depth from 0.3 m to 0.35 m			Change in water depth from 0.3 m to 0.25 m		
	K_t	K_r	K_d	K_t	K_r	K_d
Non-perforated	+ 5.10	- 12.90	- 4.20	- 4.00	+ 9.70	+ 3.10
Perforated	+ 6.2	- 2.70	- 5.80	- 10.00	+ 12.80	+ 5.10

NOTE: “+ “ indicate percentage increase and “ - “ indicate percentage decrease

5.6 VALIDATION OF MODIFIED HYBRID THEORETICAL EQUATION FOR PERFORATED PILE BREAKWATERS

5.6.1 Enlarged pile head breakwater

From literature review it is evident that no theoretical solutions are available to assess the hydraulic performance of perforated enlarged pile breakwater. This motivated the present study to develop hybrid theoretical formulations. About 522 experimental data are compared to check the validity of the theoretical equations. The K_t , K_r and K_d obtained by the theoretical equations are compared with the present experimental data in Fig. 5.21.

The R^2 value for K_t , K_r and K_d obtained for the present hybrid solution is 0.77, 0.81 and 0.62, respectively. The Relative Root Mean Square Error (RrmsE) value obtained for K_t , K_r and K_d is 0.026, 0.026 and 0.03, respectively. From Fig. 5.21, it can be stated that the current hybrid equation for the perforated enlarged pile breakwater predicts K_t , K_r and K_d with a satisfactory level of acceptance.

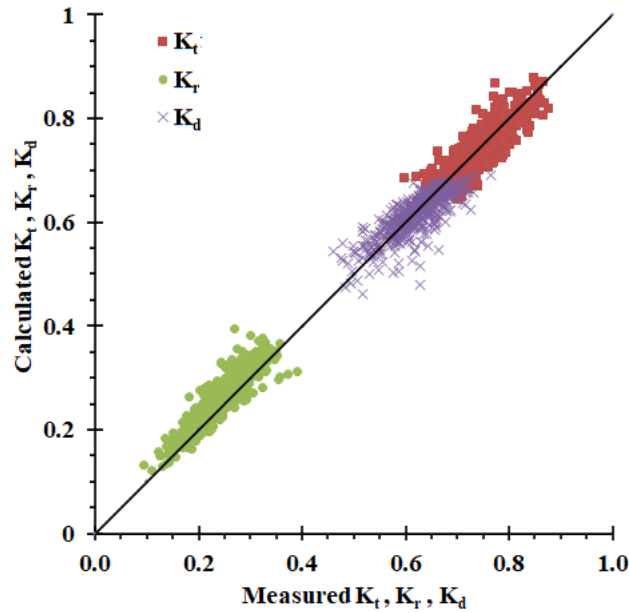


Fig. 5.21 Comparison of theoretical K_t , K_r and K_d with measured values

5.6.2 Conventional circular pile breakwater

The present hybrid equation developed for the perforated enlarged pile head breakwater is also validated for circular hollow perforated pile breakwater. For the present study, Rao (1999) experimental data on perforated circular hollow pile breakwater is used. About 125 data sets are used to compare the theoretical results. Details of the experimental data are shown in Table 5.2. Fig. 5.22 shows the comparison of predicted values of K_t , K_r and K_d with the Rao (1999) experimental data.

Table 5.2 Experimental parameters of perforated pile breakwater (Rao, 1999).

Variable	Expression	Parameter range
Diameter of the pile (m)	d	0.0335
Clear spacing between piles in a row	b/d	0.15
Wave period (s)	T	1.5, 1.75, 2.0, 2.25
Incident wave height (m)	H_i	0.035 to 0.175
Water Depth (m)	h	0.4
Diameter of perforations	S	0.25D, 0.5D
Percentage of perforations (%)	P	6.25, 12.5, 25

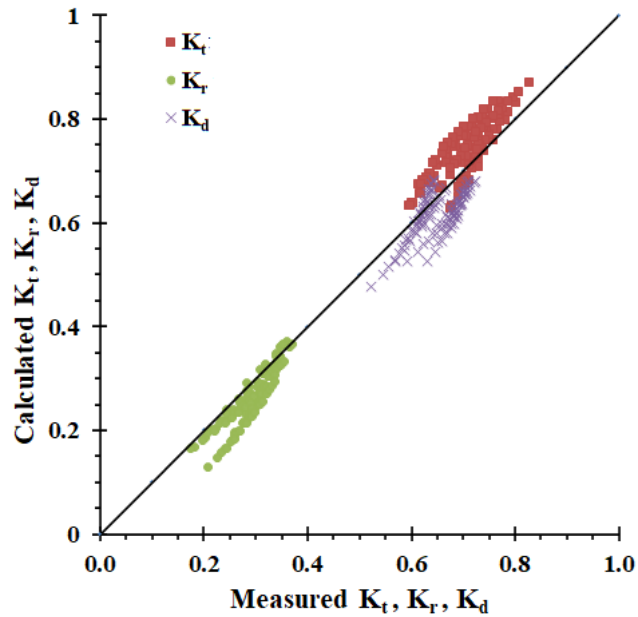


Fig. 5.22 Comparison of theoretical K_t , K_r and K_d with Rao (1999) data

From Fig. 5.22, it can be said that the modified hybrid solution over predicts the K_t and under predicts K_r and K_d . The quantification of the error involved in theoretical prediction is given in Table 5.3.

Table 5.3 Quantitative assessment of error using S.I., RrmsE and R^2 indexes.

Model Type	Hydraulic Coefficients	S.I.	RrmsE	R^2
Perforated enlarged pile head	K_t	0.035	3.46%	0.770
	K_r	0.105	10.30%	0.810
	K_d	0.050	4.84%	0.620
Perforated Regular pile	K_t	0.076	7.56%	0.660
	K_r	0.140	13.82%	0.810
	K_d	0.074	7.40%	0.500

The average value of S.I., RrmsE and R^2 for the current theoretical equation is 0.096, 9.6% and 0.66, respectively. From Fig. 5.21 and Fig. 5.22, it is easily intelligible that the present modified hybrid solution for perforated pile breakwater better predicts the hydraulic characteristics of both enlarged pile head breakwater and conventional circular pile breakwater. The hydraulic coefficients predicted by the hybrid theoretical

equations are acceptable as the predicted values exhibit the RrmsE between 3.48% to 13.8%, which is within the maximum limits (Komen et al. 1994; Nam et al. 2017; Rattanapitikon 2007).

5.7 VALIDATION OF PERFORATED ENLARGED PILE HEAD BREAKWATER USING REEF3D

5.7.1 Comparison of numerical results with the experimental and theoretical data

Fig. 5.23 shows the variations of K_t , K_r and K_d in the case of perforated structure as predicted by the REEF3D compared with the experimental and theoretical results. K_t is underpredicted by about 1% and 3% for gentle and steeper waves respectively, in comparison with the experimental results. For K_r , it is overpredicted by about 11% and in the case of K_d it is underpredicted by 1%. The percentage error observed is more in perforated breakwater than non-perforated breakwater. Since the maximum percentage error is about 11%, it is concluded that the REEF3D software may be employed to investigate the hydraulic performance of enlarged pile head breakwater.

Table 5.4 shows the REEF3D quantitative assessment of error using S.I., RrmsE and R^2 indexes compared with the experimental results.

Table 5.4 Quantitative assessment of error using S.I., RrmsE and R^2 indexes

Model Type	Hydraulic Coefficients	S.I.	RrmsE	R^2
Perforated enlarged pile head	K_t	0.020	2.044	0.992
	K_r	0.143	14.220	0.993
	K_d	0.015	1.497	0.986

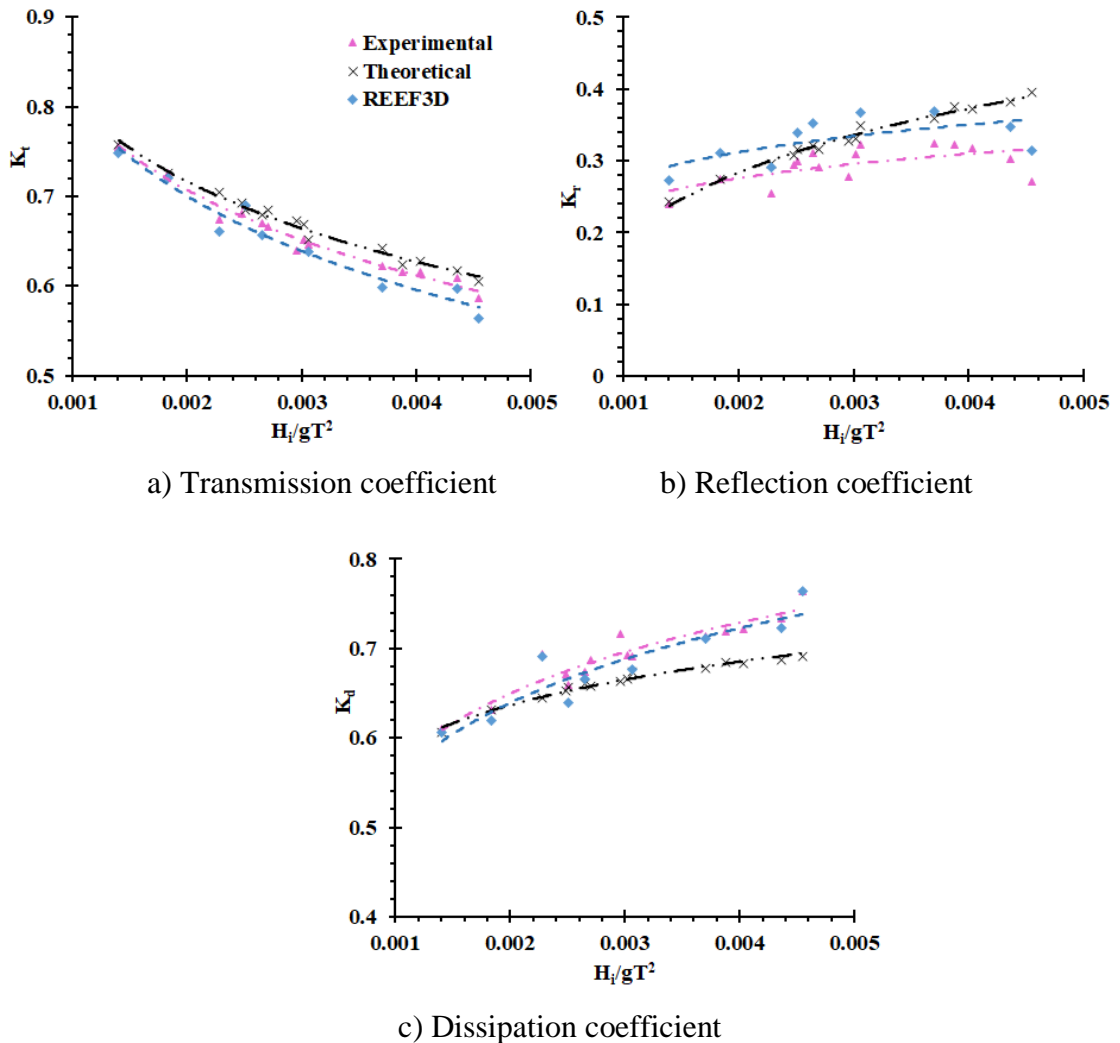


Fig. 5.23 Validation of perforated pile head breakwater REEF3D results with experimental and theoretical values

5.7.2 Effect of perforations

As evident from section 5.4, the perforation is effective in improving the hydraulic performance of enlarged pile head breakwater. The results obtained using REEF3D for the case of non-perforated and perforated enlarged pile head breakwater is shown in Fig. 5.24. As illustrated in Fig. 5.24., the perforation is effective in improving the hydraulic efficiency of the breakwater. It is observed that, providing the perforations of size $0.25D$ in pile head of configuration of $D/H_{\max} = 0.6$ and $Y/H_{\max} = 1.0$ at $b/D = 0.2$ with $p_a = 75\%$, reduces K_t by 12.3% for gentle waves and 16.3% for steeper waves. Hence, it can be concluded that perforations of size $0.25D$ effectively reduce the K_t and K_d by about 12% to 16% than the non-perforated pile head breakwater.

The influence of perforations on K_r is shown Fig. 5.24(b). Results obtained shows that the perforated structure has more reflection than the non-perforated structure. For the compared perforations K_r increases about 4% to 21% for the complete range of wave steepness than the non-perforated pile breakwater of similar configurations. The K_d of perforated and non-perforated enlarged pile head breakwater is also compared in Fig. 5.24(c). Results indicate that the perforated pile head has about 10% higher K_d than the non-perforated.

Since the compared results of the present study on perforated and non-perforated breakwater are in line with the experimental results, it is recommended that REEF3D can be used to model the hydraulic performance of enlarged pile head breakwater.

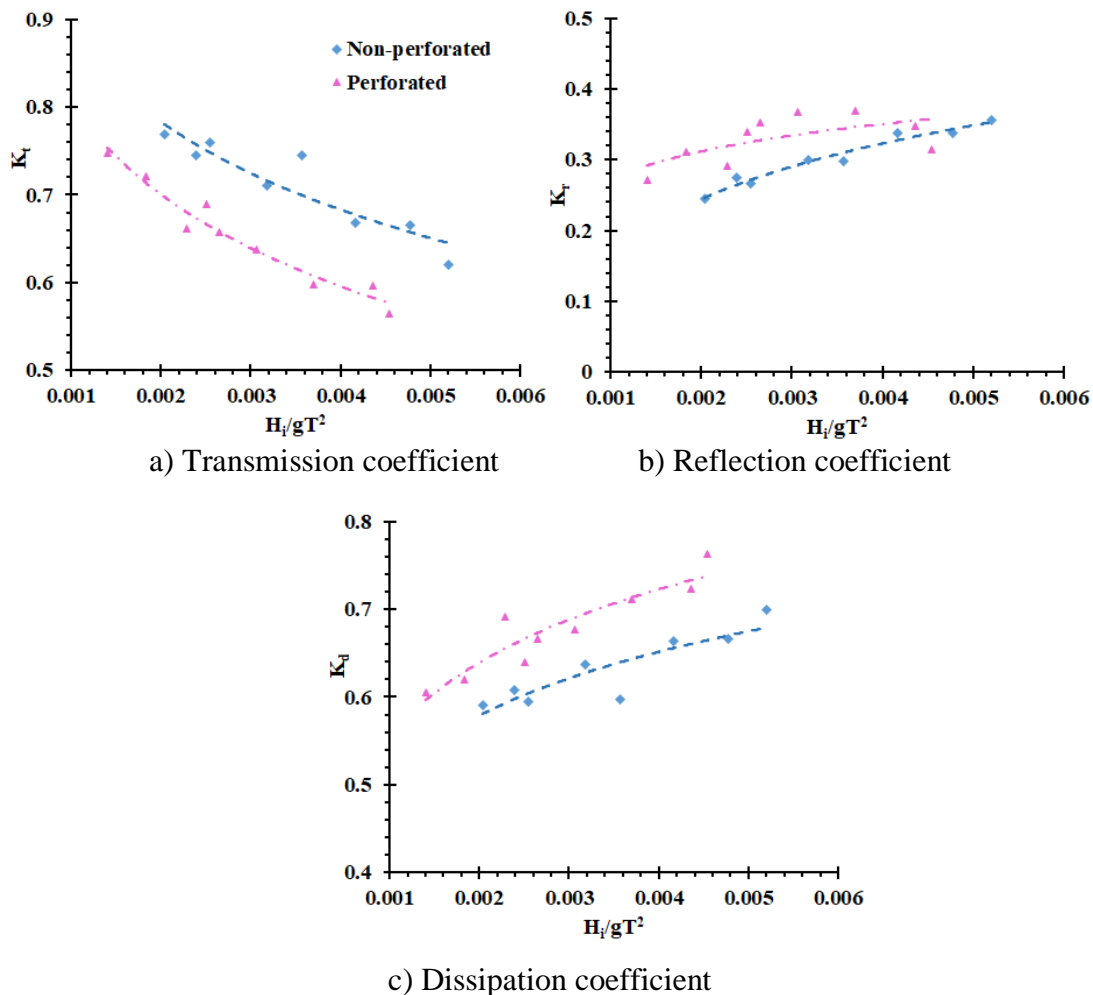


Fig. 5.24 Effect of perforations on K_t , K_r and K_d for $D/H_{max} = 0.6$ at 0.3 m water depth

5.8 COMPARISON OF HYDRAULIC PERFORMANCE OF PERFORATED ENLARGED PILE BREAKWATER WITH OTHER RESEARCH WORKS

The hydraulic performance of the perforated enlarged pile head breakwater obtained through the physical model tests is compared with the other available research works. For the current study, Rao (1999), Huang (2007), Koraim (2014) and Koraim et al. (2014) cases are considered for the comparison. The test conditions quoted by the respective authors are listed in Table 5.5.

Table 5.5 Test conditions as indicated by the various authors

Reference	Structure Type	Experiment facilities		Structural Parameters			Wave Parameters	
		flume dim. in m	h m	D m	b/D	P %	H m	T s
Rao (1999)	Perforated pile	50×0.71×1.1, 1:30 Scale	0.4	0.0335	0.15	25	0.035 to 0.175	1.5 to 2.25
Rao (1999)	Perforated suspended pipe	50×0.71×1.1, 1:30 Scale	0.4	0.0335	0.15	25	0.035 to 0.175	1.5 to 2.25
Huang (2007)	Slotted thin wall	-	0.3	0.0064	1.77	21	0.02 to 0.06	1.1
Koraim (2014)	Pile supported screen type (L shaped bar)	20×2×1.2, 1:10 Scale	0.5	0.05	0.33	25	0.038 to 0.118	0.9 to 1.8
Koraim et al. (2014)	Pile supported screen type (C shaped bar)	20×2×1.2, 1:10 Scale	0.32	0.04	5	50	0.027 to 0.13	1.15 to 2.85
Present work	Perforated enlarged pile head	50×0.71×1.1, 1:30 Scale	0.3	0.096	0.2	22.5	0.06 to 0.16	1.4 to 2.0

Variation of K_t , K_r and K_d with the other type of breakwater is compared, as shown in Fig. 5.25. For the comparison, the best model from the present experiment is considered. Hence, perforated enlarged pile head breakwater with the configuration of $b/D = 0.2$, $Y/H_{max} = 1.0$, $D/H_{max} = 0.6$, $S = 0.25D$, $P = 22.5$, and $p_a = 75\%$ is selected.

The K_t of perforated enlarged pile head breakwater is lower than the other structures. At lower H_i/L (0.02), the present work K_t is less than 4% with respect to perforated pile breakwater (Rao 1999), 16% of perforated pipe breakwater (Rao 1999), 14.6% of slotted breakwater (Huang 2007), 10.4% of pile-supported L shaped screen type breakwater (Koraim 2014) and 11.2% of pile-supported C shaped screen type breakwater (Koraim et al. 2014). At higher H_i/L (0.04), the transmission coefficient is less than 13.7% in analogy to Rao (1999, pile breakwater), 23.8% of Rao (1999, pipe breakwater), 23.6% of Huang (2007), 20.5% of Koraim (2014) and 9.7% of Koraim et al. (2014).

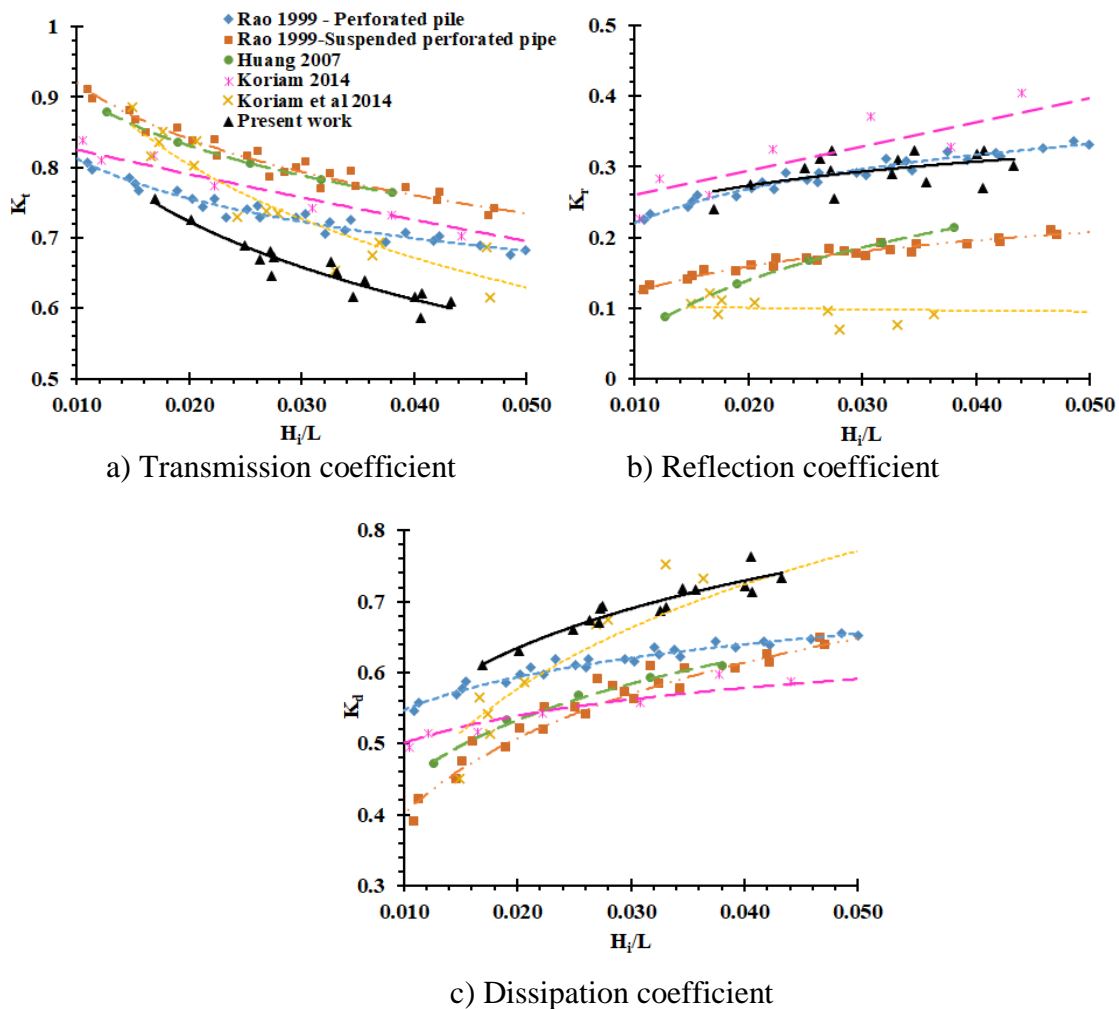


Fig. 5.25 Comparison of K_t , K_r and K_d with different single row pile breakwater models

As shown in Fig. 5.25(b), K_r of the selected model is varying from 0.25 to 0.32 whereas, other studies is in the range of 0.07 to 0.4.

The dissipation coefficient of the proposed breakwater is about 5% to 22% more than the considered type of breakwater, as shown in Fig. 5.25 (c). Hence, it can be concluded that perforated pile head breakwater has less K_t and higher K_d than the other pile type breakwater. This is mainly due to the unique wave-structure interaction from the perforations provided and at the central hollow portion of the structure. Therefore, by considering the above results, it can be stated that the hydraulic performance of perforated enlarged pile head breakwater with $D/H_{\max} = 0.6$, $b/D = 0.2$, $Y/H_{\max} = 1.0$ and $P = 22.5$ is better than other types of breakwaters.

5.9 CONCLUSIONS ON PERFORATED ENLARGED PILE HEAD BREAKWATER

From the experimental studies conducted on the perforated enlarged pile head breakwater, the following conclusions are drawn:

- The structural parameters (size of pile head, percentage distribution of perforations, size of perforations and percentage of perforations), wave parameters (wave period and wavelength) and depth of water are the important parameters influencing the wave transmission, reflection and energy dissipation.
- Wave steepness is inversely proportional to K_t and directly proportional to K_r and K_d .
- An increase in the pore size (S) and the percentage of perforations (P) decreases K_t and increases the K_r and K_d .
- An increase in pore size with perforations is more imperative for wave attenuation. The pore size highly dominates the wave attenuation than the increasing percentage of perforations with the small size of the pore.
- Increase in p_a from 25% to 75% resulted in increased hydraulic efficiency of the structure. But increase in p_a from 75% to 100% resulted in a decrease in efficiency. Hence, a p_a of 75% is found to be optimum.
- The proposed hybrid equation for the perforated pile breakwater predicts more reliable K_t , K_r and K_d values. The proposed hybrid solution can also predict the

hydraulic characteristics of conventional type perforated pile breakwaters subjected to monochromatic waves.

- The results obtained (K_t , K_r , K_d) using an open source CFD tool: REEF3D are in good agreement with the experimental data of perforated enlarged pile head breakwater.
- Wave-structure interaction simulated using REEF3D and physical models are in good agreement.
- Increase in p_a from 50% to 75% results in 1% to 8% decrease in K_t , 5% to 15% increase in K_r and 4% to 15% increase in K_d .
- Increase in S from 0.1D to 0.25D results in 8% to 11% decrease in K_t , 5% to 30% increase in K_r and 12% to 16% increase in K_d .
- An increase in the pore size highly dominates the wave attenuation than the increase in perforations with a smaller size of the pores. When S increased by 66.66% (0.15D to 0.25D) and percentage of perforation decreases to 7.41%. Then the value K_t decreases to 7.5% at lower wave steepness and 4.9% at higher wave steepness.
- Perforations are effective in reducing the K_t of about 10% to 18%, increasing the K_r by 4% to 50% and increasing the K_d by 11% to 22% to that of non-perforated structure.
- Best hydraulic efficiency of the enlarged pile head breakwater structure is obtained when $D/H_{\max} = 0.6$, $Y/H_{\max} = 1.0$, $b/D = 0.2$, $S = 0.25D$, $p_a = 75\%$ and $P = 22.5$ at 0.3 m water depth.
- A 16.7% change in depth of water due to environmental conditions results in an average of 6%, 9% and 5% change in the value of K_t , K_r and K_d , respectively, considering both perforated and non-perforated breakwater.
- The optimum configured perforated enlarged pile breakwater has K_t in the range of 4% to 20.5%, K_r is about -11% to 180% (K_r of present study varies from 0.26 to 0.31 whereas, other studies are in the range of 0.09 to 0.37) and K_d is about 5% to 22%, than compared types of breakwaters.

- Based on the present study, friction coefficient (γ) as given by Suh et al. (2011), is modified using the following equations to evaluate the hydraulic characteristics (K_t and K_r) of perforated enlarged pile head breakwater.

$$\gamma_P = \gamma - X_R$$

$$\gamma = 1.569 \left(\frac{\bar{\epsilon} \left(\frac{H_i}{h} \right) f \left(\frac{Y}{2h} \right)}{\bar{\epsilon} \bar{\epsilon}} \right)^{0.433}$$

X_R is the reduction factor for perforations and is defined as

$$X_R = X_P + \frac{6.391 \times 10^{-4}}{(S-0.0181)} + \frac{H_i}{h}$$

In which S = size of perforation, and

$$X_P = 0.0117P' + \frac{0.027}{(P'-3.24)} + \frac{0.0282}{(6.79-P')} - \frac{0.0473}{(P'-10.12)}, \text{ where } P' = \frac{100}{P}$$

- Based on R^2 , R_{rmsE} and SI index it can be concluded that the present hybrid equations developed for the perforated enlarged pile head and conventional perforated pile head breakwater can predict hydraulic coefficients with a satisfactory level of acceptance.
- A least value of $K_t = 0.58$ is obtained for the enlarged perforated pile breakwater structure with the structural configuration of $b/D = 0.2$, $D/H_{max} = 0.6$, $Y/H_{max} = 1.0$, $S = 0.25D$, $p_a = 75\%$ and $P = 22.5$ along with $K_r = 0.36$ and $K_d = 0.73$. Hence, depending on the site conditions the present concept may be considered as a solution for the protection of coast against erosion.
- The results of REEF3D and physical model study for perforated pile head breakwater is vary by 11%.

6.1 BACKGROUND

Coastal erosion of beaches has been a common problem around the world. One of the eco-friendly control measures for coastal erosion is to dissipate the energy of waves impinging on the shores by constructing offshore breakwater. Pile breakwater is one such type of offshore breakwater that consists of a number of closely spaced piles. Construction of piles at closer spacing is highly challenging and expensive. This problem can be addressed by reducing the number of piles and modifying the pile with an enlarged head in the vicinity of the water surface, where wave energy is concentrated.

In the present study, an experimental investigation on the hydraulic performance of enlarged pile head breakwater is conducted in a wave flume. The concept breakwater is subjected to monochromatic waves of varying wave heights and wave periods generated in different depths of water. The experiments are conducted on non-perforated and perforated breakwater. Observed K_t , K_r and K_d in this study are in line with the similar type of pile breakwaters. Experimental results indicate that the pore size highly dominates the wave attenuation than the increasing percentage of small size of perforations. The present experimental data is also validated with the available theoretical solution. Since the results are not in good agreement, a hybrid theoretical model is modified and reconstructed based on the present study for prediction of transmission, reflection and dissipation coefficients. In addition, the predicted results obtained from the proposed solutions are found to be in good agreement with the conventional pile breakwater models.

The detailed conclusions derived from the experiments conducted on different cases of enlarged pile head breakwater are presented in the following sections, whereas, a summary of these conclusions, along with the recommendations and the scope for further research, is included in the end.

6.2 GENERAL CONCLUSIONS

From the physical model studies conducted herein on the non-perforated and perforated enlarged pile head breakwater, the following general conclusions are drawn:

1. The structural parameters (relative spacing between the pile, the diameter of pile head, the height of pile head, percentage distribution of perforations, size of perforations and percentage of perforations), wave parameters (wave height, wave period and wavelength) and depth of water are the important parameters influencing wave transmission, reflection and energy dissipations.
2. In general, with an increase in wave steepness (H_i/gT^2) the transmission coefficient (K_t) decreases, reflection coefficient (K_r) increases, and the energy dissipation coefficient (K_d) increases.
3. K_t is inversely proportional to Y/H_{max} , D/H_{max} , Z and directly proportional to h , b/D . Whereas, K_r and K_d are directly proportional to Y/H_{max} , D/H_{max} , Z and inversely proportional to h , b/D .
4. Up to 75% increase in percentage distribution of perforations around the pile head, K_t decreases and K_r and K_d increases. However, increasing the pa beyond 75% change the trends in opposite way.
5. The pore size highly dominates the wave attenuation than the increasing percentage of perforations with the small size of the pore.
6. The perforated structure is better than the non-perforated structure in enhancing the wave attenuation.
7. The hydraulic performance of non-perforated and perforated enlarged pile head breakwater is better than the other types of breakwaters such as pile breakwater, pipe breakwater, pile supported C and L shaped screen breakwater.
8. The results of experimental and REEF3D model studies are in good agreements.
9. The proposed equation predicts the performance (K_t , K_r , K_d) of enlarged pile head breakwater in line with the experimental results than the existing theoretical equations.
10. The proposed hybrid solution may be used not only for the perforated and non-perforated pile breakwaters but also to estimate the performance of conventional pile breakwaters.

The key findings derived from the studies are listed in the following sections:

6.3 CONCLUSIONS ON NON-PERFORATED ENLARGED PILE HEAD BREAKWATER

1. Decrease in b/D from 0.9 to 0.2 resulted in a maximum reduction of K_t by 27.73%, increase in K_r by 100% (from 0.17 to 0.34) and increase in K_d by 45% for the case of $D/H_{\max} = 0.6$ with $Y/H_{\max} = 1.0$ at 0.3 m depths of water.
2. Increase in D/H_{\max} from 0.4 to 0.6 resulted in maximum reduction of K_t by 13%, increase of K_r by 54.5% (K_r increase from 0.22 to 0.34) and increase of K_d by 8.97% at higher wave steepness.
3. 25% to 33.33% increases in depth of water results in an average of 4% to 6% increase in K_t , 17% to 19% decrease in K_r and 7% to 8% decrease in K_d .
4. The optimum configuration of non-perforated pile head breakwater obtained from the analysis is $D/H_{\max} = 0.6$, $b/D = 0.2$ and $Y/H_{\max} = 1.0$ at 0.3 m depth of water with least K_t value of 0.62.
5. For the optimum enlarged pile head breakwater, the K_t obtained is in the range of -8.4% to 12.5%, K_r in the range of 6% to 24% and K_d in the range of -0.56% to 16.3% with the compared types of breakwaters.
6. Based on the present study, friction coefficient (γ), as given by Suh et al. (2011), is modified using the following equations to evaluate the hydraulic characteristics (K_t and K_r) of non-perforated pile head breakwater.

The empirically reformed γ equation, using the current set of experimental data is given by

$$\gamma = 1.569 \left(\frac{\bar{\epsilon} \left(\frac{H_i}{h} \right) f \left(\frac{Y}{2h} \right)}{\bar{\epsilon} \bar{\epsilon}} \right)^{0.433}$$

7. The comparison of relationship exhibits improved hydraulic characteristics of conventional and enlarged pile breakwaters due to the empirically improved γ parameter.

6.4 CONCLUSIONS ON PERFORATED ENLARGED PILE HEAD BREAKWATER

1. Increase in p_a from 50% to 75% results in 1% to 8% decrease in K_t , 5% to 15% increase in K_r and 4% to 15% increase in K_d .
2. Increase in S from 0.1D to 0.25D results in 8% to 11% decrease in K_t , 5% to 30% increase in K_r and 12% to 16% increase in K_d .
3. An increase in the pore size highly dominates the wave attenuation than the increase in perforations with a smaller size of the pores. When S increased by 66.66% (0.15D to 0.25D) and percentage of perforation decreases to 7.41%. Then the value K_t decreases to 7.5% at lower wave steepness and 4.9% at higher wave steepness.
4. Perforations are effective in reducing the K_t of about 10% to 18%, increasing the K_r by 4% to 50% and increasing the K_d by 11% to 22% to that of non-perforated structure.
5. Best hydraulic efficiency of the enlarged pile head breakwater structure is obtained when $D/H_{\max} = 0.6$, $Y/H_{\max} = 1.0$, $b/D = 0.2$, $S = 0.25D$, $p_a = 75\%$ and $P = 22.5$ at 0.3 m water depth.
6. A 16.7% change in depth of water due to environmental conditions results in an average of 6%, 9% and 5% change in the value of K_t , K_r and K_d , respectively, considering both perforated and non-perforated breakwater.
7. The optimum configured perforated enlarged pile breakwater has K_t in the range of 4% to 20.5%, K_r is about -11% to 180% (K_r of present study varies from 0.26 to 0.31 whereas, other studies are in the range of 0.09 to 0.37) and K_d is about 5% to 22%, than compared types of breakwaters.
8. Based on the present study, friction coefficient (γ) as given by Suh et al. (2011), is modified using the following equations to evaluate the hydraulic characteristics (K_t and K_r) of perforated enlarged pile head breakwater.

$$\gamma_P = \gamma - X_R$$

$$\gamma = 1.569 \left(\frac{\bar{\epsilon} \left(\frac{H_1}{h} \right) f \left(\frac{Y}{2h} \right)}{\bar{\epsilon} \bar{\epsilon}} \right)^{0.433}$$

X_R is the reduction factor for perforations and is defined as

$$X_R = X_P + \frac{6.391 \times 10^{-4}}{(S-0.0181)} + \frac{H_i}{h}$$

In which S = size of perforation, and

$$X_P = 0.0117P' + \frac{0.027}{(P'-3.24)} + \frac{0.0282}{(6.79-P')} - \frac{0.0473}{(P'-10.12)}, \text{ where } P' = \frac{100}{P}$$

9. Based on R^2 , R_{rmsE} and SI index it can be concluded that the present hybrid equations developed for the perforated enlarged pile head and conventional perforated pile head breakwater can predict hydraulic coefficients with a satisfactory level of acceptance.
10. A least value of $K_t = 0.58$ is obtained for the enlarged perforated pile breakwater structure with the structural configuration of $b/D = 0.2$, $D/H_{max} = 0.6$, $Y/H_{max} = 1.0$, $S = 0.25D$, $p_a = 75\%$ and $P = 22.5$ along with $K_r = 0.36$ and $K_d = 0.73$. Hence, depending on the site conditions the present concept may be considered as a solution for the protection of coast against erosion.
11. The results of REEF3D and physical model study vary by a maximum of 4% and 11% for non-perforated and perforated pile head breakwater, respectively.
12. An open-source numerical modelling tool REEF3D may be used for modelling and investigating the hydraulic performance of the non-perforated enlarged pile head breakwater.

6.5 SUMMARY OF CONCLUSIONS

From the present experimental investigations, the following summary of conclusions are drawn.

1. The transmission coefficient (K_t) is directly proportional to relative pile spacing (b/D) and depth of water (h) whereas, the K_r and K_d are inversely proportional.
2. K_t is inversely proportional to H_i/gT^2 , Y/H_{max} , D/H_{max} , Z , S and P , whereas, K_r and K_d follow the opposite trend.
3. The optimum configuration of single row non-perforated enlarged pile head breakwater is $b/D = 0.2$, $D/H_{max} = 0.6$, $Y/H_{max} = 1.0$ at 0.3 m depth of water.
4. The optimum configuration of single row perforated enlarged pile head breakwater is $b/D = 0.2$, $D/H_{max} = 0.6$, $Y/H_{max} = 1.0$, $S = 0.25D$, $p_a = 75\%$ and $P = 22.5$ at 0.3 m depth of water.

5. Perforated enlarged pile head breakwater performs 10% to 18% better with respect to the non-perforated pile head structure.
6. The REEF3D predicts the performance of non-perforated as well as perforated structure to the tune of -1 to 4% and -1 to 11%, respectively. Therefore, it can be said that REEF3D numerical model may be used for simulating enlarged pile head breakwater structures.
7. The modified empirical parameter (γ) of the equation (Suh et al 2011)
 - a) For non-perforated structure is

$$\gamma = 1.569 \left(\frac{\bar{\epsilon} \left(\frac{H_i}{h} \right) f \left(\frac{Y}{2h} \right)}{\bar{\epsilon}^{\bar{\epsilon}}} \right)^{0.433}$$

- b) For perforated structure is

$$\gamma_P = \gamma - X_R$$

X_R is the reduction factor for perforations and is defined as

$$X_R = X_P + \frac{6.391 \times 10^{-4}}{(S-0.0181)} + \frac{H_i}{h}$$

In which S = size of perforation (m), and

$$X_P = 0.0117P' + \frac{0.027}{(P'-3.24)} + \frac{0.0282}{(6.79-P')} - \frac{0.0473}{(P'-10.12)}, \text{ where } P' = \frac{100}{P}$$

6.6 SCOPE FOR FURTHER RESEARCH

Some of the boulevards of further research could be investigations of the optimum perforated pile head structure with

- Varying patterns of perforations like horizontal or vertical slit openings.
- Different shapes of enlarged pile head, such as rectangular or conical.

AI-1 GENERAL

Reynolds number Re is defined as (Sarpkaya (1976), Zhong et al. (2020), Sheng et al. (2014), Viviano et al. (2018))

$$Re = \frac{UD}{\nu}$$

Where, U is the characteristic speed and is defined by employing the maximum water particle velocity from small-amplitude water wave theory (Dean and Dalrymple 1991)

$$U = \omega A_w$$

Where, $\omega = \frac{2\pi}{T}$ and T is the wave period in s

ν is the kinematic viscosity = $1.004 \times 10^{-6} \text{ m}^2/\text{s}$, A_w is the wave amplitude = $\frac{H}{2}$

D is the diameter of the enlarged pile head (characteristic length of the system)

For the current case Re is between 8×10^3 to 3×10^4

Depth of water, h	Wave period T	Wave height, H	Wave amplitude, A_w	Diameter of pile head, D	Reynolds number, Re
m	s	m	m	m	
0.3	1.4	0.06	0.03	0.064	8.583E+03
0.3	1.4	0.1	0.05	0.064	1.430E+04
0.3	2	0.08	0.04	0.064	8.010E+03
0.3	2	0.14	0.07	0.064	1.402E+04
0.4	1.4	0.06	0.03	0.064	8.583E+03
0.4	1.4	0.12	0.06	0.064	1.717E+04
0.4	2	0.08	0.04	0.064	8.010E+03
0.4	2	0.14	0.07	0.064	1.402E+04
0.5	1.4	0.08	0.04	0.064	1.144E+04
0.5	1.4	0.16	0.08	0.064	2.289E+04
0.5	2	0.08	0.04	0.064	8.010E+03
0.5	2	0.16	0.08	0.064	1.602E+04
0.3	1.4	0.06	0.03	0.096	1.287E+04
0.3	1.4	0.1	0.05	0.096	2.146E+04
0.3	2	0.08	0.04	0.096	1.202E+04
0.3	2	0.14	0.07	0.096	2.103E+04
0.4	1.4	0.06	0.03	0.096	1.287E+04
0.4	1.4	0.12	0.06	0.096	2.575E+04
0.4	2	0.08	0.04	0.096	1.202E+04
0.4	2	0.14	0.07	0.096	2.103E+04
0.5	1.4	0.08	0.04	0.096	1.717E+04
0.5	1.4	0.14	0.07	0.096	3.004E+04
0.5	2	0.08	0.04	0.096	1.202E+04
0.5	2	0.16	0.08	0.096	2.403E+04

UNCERTAINTY ANALYSIS

AII-1 GENERAL

The hydrodynamic test facilities differ from one another with regard to facilities, instrumentation, experimental procedures and scale. Hence, it becomes necessary for a test facility to provide with possible lower and upper margins, which can be adopted with a fair confidence level. Such a study for an experimental test procedure in a particular facility is termed as uncertainty analysis. Uncertainty describes the degree of goodness of a measurement or experimentally determined result. It is an estimate of experimental error. It is possible to conduct experiments in a scientific manner and predict the accuracy of the result (Misra, 2001) with the help of uncertainty analysis. Experimental error sources should be identified and the error (δ) should be determined from manufactures brochures, from calibration and conducting simple experiments respectively (Kline, 1985). The use of uncertainty analysis is indispensable in physical model studies. There is no single way to describe uncertainty in measurements and there are many different situations that demand somewhat differing description. The distribution of uncertainty between precision and bias is arbitrary. Whatever may the method used for calculating uncertainty, but the method used should be reported in some appropriate way and that the report includes the method employed (Kline, 1985). It is also generally agreed that the inaccuracies can be appropriately expressed by an “uncertainty” and these values could be obtained by an “Uncertainty analysis”. The confidence interval gives an estimated range of values, which is likely to include an unknown population parameter. From a given set of observations the estimated range is calculated. The 95% confidence interval limits must always be estimated and this concept of confidence level is fundamental to uncertainty analysis (Misra, 2001).

The Indian coastline is about 7516.6 km long, 5422.6 km spread along the mainland and around 2094 km along the coast of the archipelago of Andaman and Nicobar, and Lakshadweep. The coastline comprises a myriad of coastal features such as headlands, promontories, rocky shores, sandy spits, barrier beaches, open beaches, embayment,

estuaries, inlets, bays, marshy land and islands etc. According to the naval hydrographic charts, the Indian mainland consists of nearly 43% sandy beaches, 11% rocky coasts with cliffs and 46% mudflats and marshy coasts.

AII-2 PROCEDURE FOR UNCERTAINTY ANALYSIS

A best-fit curve can include both 95% confidence band and the 95% prediction band. Confidence band tells about 95% sure that the true best fit curve (if an infinite number of data points are available) lies within the confidence band. The prediction band tells about the scatter of the data. If data points are considered, 95% points are expected to fall within the prediction band. Since the prediction band has to an account for uncertainty in the curve itself as well as scatters around the curve, it is much wider than the confidence band. Fig. AI-1 shown below, confidence bands contain a minority of data points. The confidence bands shown have a 95% chance of containing the true best fit curve and the dashed prediction bands include 95% of the data points. Also the 95% confidence and prediction bands have been accepted to be reliable enough for usage under the adoption of uncertainty analysis.

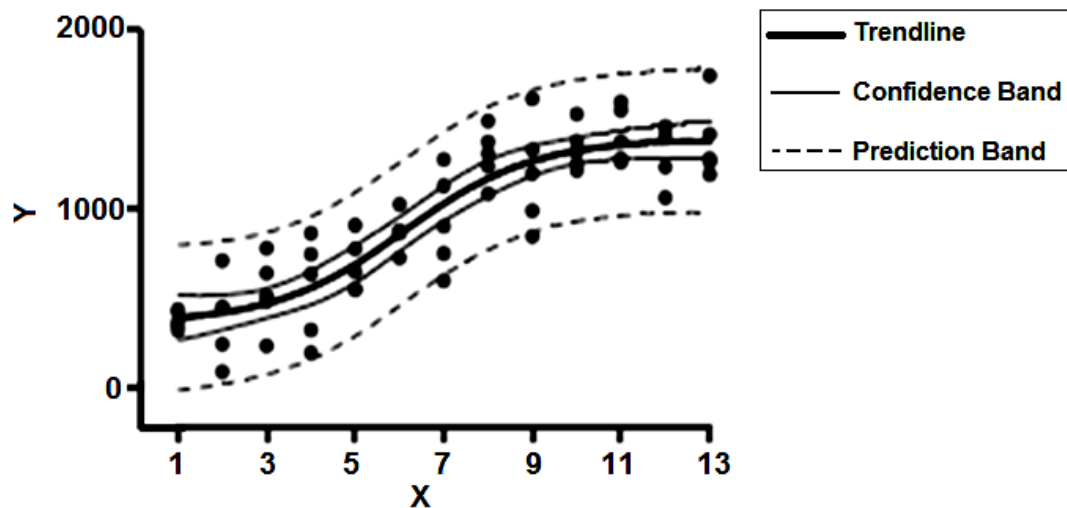


Fig. AI-1 Graph example for 95% confidence and prediction band

A $100(1-\alpha)$ percent confidence interval about the mean response at the value of $x = X_1$, say Y_1 is given by Montgomery and Runger (1999) as follows:

$$Y_1 = Y_0 + t_{(\alpha/2, n-2)} \sqrt{\sigma^2 \left[\frac{1}{n} + \frac{(x_0 - \bar{x})^2}{S_{xx}} \right]}$$

Where $Y_0 = \beta_0 + \beta_1 X_0$ computed from regression model, α = significance level used to compute the confidence level, σ^2 = variance, n = sample size, \bar{x} = sample mean, x = variable, S_{xx} = standard deviation, $t(\alpha/2, n-2)$ = t-distribution values for $n-2$ degrees of freedom.

A $100(1-\alpha)$ percent prediction interval on a feature observation Y_0 at given value x_0 is given by:

$$Y_1 = Y_0 + t_{(\alpha/2, n-2)} \sqrt{\sigma^2 \left[1 + \frac{1}{n} + \frac{(x_0 - \bar{x})^2}{S_{xx}} \right]}$$

AII-3 CONFIDENCE AND PREDICTION INTERVAL FOR TRANSMISSION COEFFICIENT

The 95% confidence and prediction band for the variation of transmission coefficient (K_t) with incident wave steepness H_i/gT^2 for enlarged pile head (non-perforated and perforated) breakwater models tested with $T = 1.4$ s to 2.0 s, $H = 0.06$ m to 0.16 m and $h = 0.30$ is shown in Fig. AI-2. For the analysis, the best performing model configuration having least K_t and Large K_d is considered. The non-perforated enlarged pile head breakwater with a configuration of $b/D = 0.2$, $Y/H_{\max} = 1.0$, $D/H_{\max} = 0.6$ and perforated breakwater of same configuration as non-perforated with $S = 0.25D$, $P = 22.5$, and $pa = 75\%$ is selected.

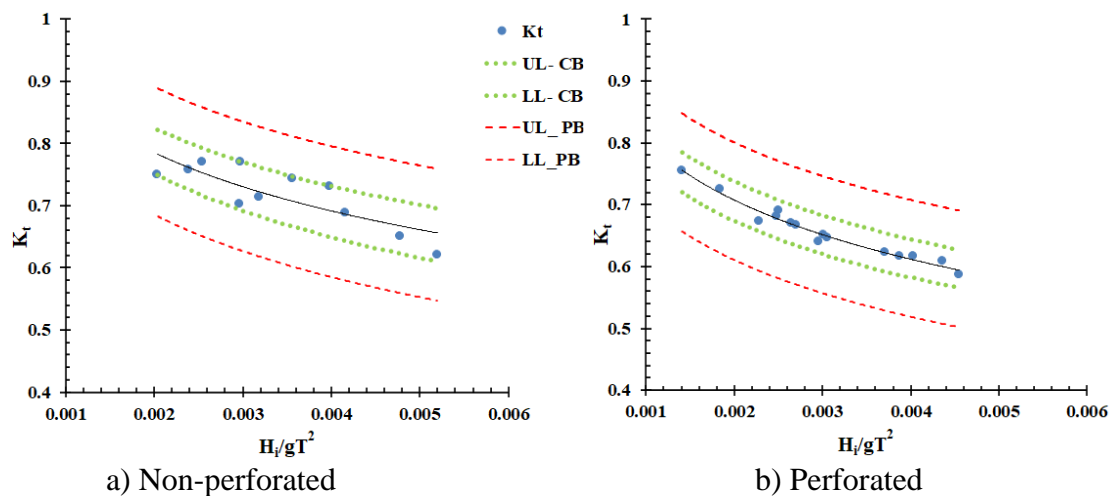


Fig. AI-2 Plot of 95% confidence and prediction bands for variation of K_t

It is observed that an average of 90% of experimental data for K_t lie within the 95% confidence bands. The trend line for the graph drawn on variation of K_t with H_i/gT^2 lie within 95% confidence bands and data points lie within the 95% prediction bands drawn. Therefore, the results obtained are so far reliable.

AII-4 CONFIDENCE AND PREDICTION INTERVAL FOR REFLECTION COEFFICIENT

The 95% confidence and prediction band for variation of K_r with H_i/gT^2 for enlarged non-perforated and perforated breakwater models tested with $T = 1.4$ to 2.0 s, $H = 0.06$ m to 0.16 m and $h = 0.30$ m is shown in Fig. AI-3. From the Fig. AI-3 it can be observed that the 80% of the data lie within 95% confidence and prediction bands drawn.

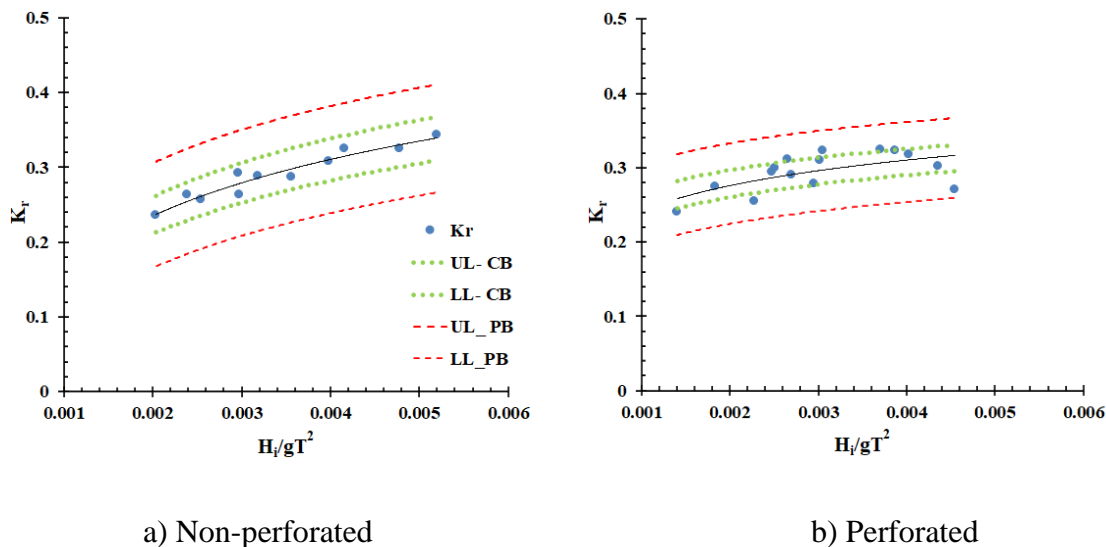


Fig. AI-3 Plot of 95% confidence and prediction bands for variation of K_r

AII-5 AI-3 CONFIDENCE AND PREDICTION INTERVAL FOR REFLECTION COEFFICIENT

The 95% confidence and prediction band for variation of K_d with H_i/gT^2 for enlarged non-perforated and perforated breakwater models tested with $T = 1.4$ to 2.0 s, $H =$

0.06 m to 0.16 m and $h = 0.30$ m is shown in Fig. AI-4. From the Fig. AI-4 it can be observed that the 84% of the data lie within 95% confidence and prediction bands drawn.

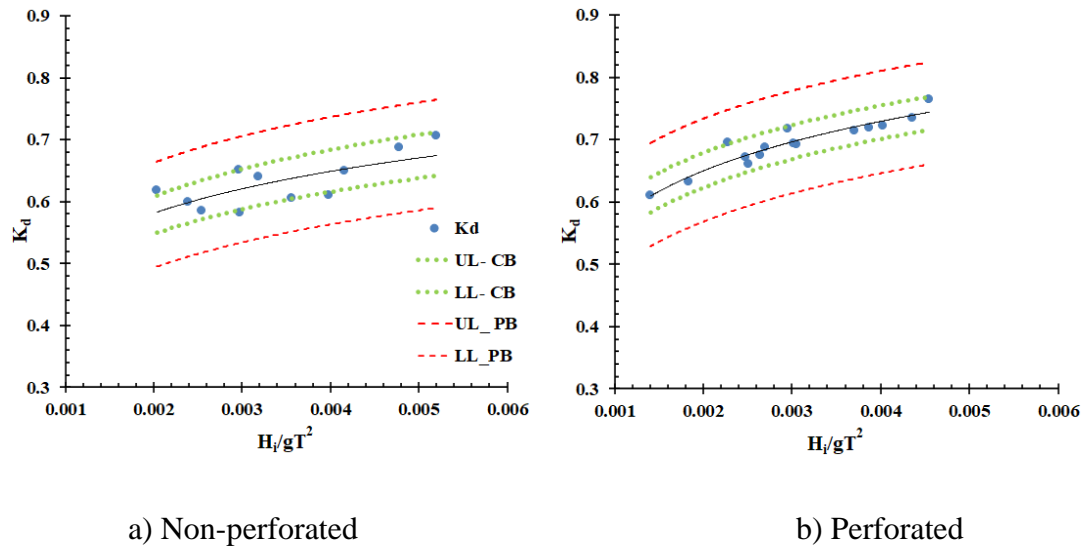


Fig. AI-4 Plot of 95% confidence and prediction bands for variation of K_d .

REFERENCES

- Afshar, M.A. (2010). "Numerical wave generation in OpenFOAM®." Master's thesis, Department of Shipping and Marine Technology, Chalmers University of Technology Gothenburg, Sweden.
- Aggarwal Ankit, Csaba Pákozdi, Hans Bihs, Dag Myrhaug and Mayilvahanan Alagan Chella (2018). "Free surface reconstruction for phase accurate irregular wave generation." *Journal of Marine Science and Engineering*, 6 (105), 1-23.
- Aggarwal Ankit, Hans Bihs, Seimur Shirinov and Dag Myrhaug (2019). "Estimation of breaking wave properties and their interaction with a jacket structure." *Journal of Fluids and Structures*, 91, 1–36.
- Aggarwal Ankit, Mayilvahanan Alagan Chellaa, Arun Kamath, Hans Bihs and Øivind Asgeir Arntsena (2016). "Irregular wave forces on a large vertical circular cylinder." *13th Deep Sea Offshore Wind R&D Conference*, EERA DeepWind'2016, , Trondheim, Norway, Energy Procedia 94 (2016) 504 – 516.
- Ahmad Nadeem, Hans Bihs, Dag Myrhaug, Arun Kamath, Øivind A. Arntsen (2019). "Numerical modeling of breaking wave induced seawall scour." *Coastal Engineering*, 150, 108-120.
- Anuar, N. M., and Sidek, F. J. (2012). "Wave characteristics around perforated piles in a two rows arrangement." *Malaysian Journal of Civil Engineering*, 24, 48-66.
- Bihs Hans and Arun Kamath (2017). "A combined level set/ghost cell immersed boundary representation for floating body simulations." *International Journal for Numerical Methods in Fluids*, 83(12), 905–916.
- Bihs Hans, Arun Kamath, Mayilvahanan Alagan Chella and Arntsen, Øivind A. (2016). "Breaking-wave interaction with tandem cylinders under different impact scenarios." *Journal of Waterway, Port, Coastal, and Ocean Engineering*, 142(5), 4016005–4016014.

Bihs Hans, Arun Kamath, Mayilvahanan Alagan Chella and Arntsen, Øivind A. (2019). "Extreme wave generation, breaking and impact simulations with REEF3D." *Proceedings of the ASME 2017 36th International Conference on Ocean, Offshore and Arctic Engineering (OMAE, 2017) June 25-30, Trondheim, Norway* 141(4), 41802–41807.

Bihs Hans, Mayilvahanan Alagan Chella, Arun Kamath and Arntsen, Øivind A. (2017). "Numerical investigation of focused waves and their interaction with a vertical cylinder using REEF3D." *Journal of Offshore Mechanics and Arctic Engineering*, 139, 41101–41108.

Bovin, R. (1964). "Comments on vertical breakwaters with low coefficients of reflection." *Dock and Harbour Authority*, London, Vol. 45, 56-61.

Chandramohan, P., Sanil Kumar V., Nayak B. U. and Raju N. S. N. (1994). "Surf zone dynamics along the South Karnataka coast between Bhatkal and Ullal, west coast of India." *Indian Journal of Marine Sciences*, 23, 189-194.

Chorin, A. J. (1968). "Numerical solution of the Navier-Stokes." *Mathematics of Computation*, 22 (104), 745-762.

Coastal Regulation Zone Notification (2019) *Ministry of Environment, Forest and Climate Change*, New Delhi, India

Dattatri, J., N. B. S. Rao, Nagendra Kumar B., Subba Rao and Dwarakish G. S. (1997). "Coastal erosion along Dakshina Kannada coast, Karnataka, India." *Proc. National seminar on "Coastal zone environment management: An appraisal of the contemporary research and development"*, Dept. of Marine Geology, Mangalore University, Mangalagangothri, India.

Davidson, P. A. (2015). "Turbulence: An introduction for scientists and engineers." *Oxford university press*.

Elsharnouby, B., Soliman, A., Elnaggar, M., and Elshahat, M. (2012). "Study of environment friendly porous suspended breakwater for the Egyptian Northwestern Coast." *Ocean Engineering*, 48, 47–58.

Ergin, A. and Pora, S. (1971). "Irregular Wave Action on Rubble-Mound Breakwaters." *Journal of Waterway, Harbour, Coastal. Engineering Division*, 97, 279–293

Gardner, J. D., Townend, I. H., and Fleming, C. A. (1986). "The design of a slotted vertical screen breakwater." *20th International Conference on Coastal Engineering*, 138, 1881–1893.

Goda, Y., and Suzuki, Y. (1976). "Estimation of incident and reflected waves in random wave experiments." *15th International Conference, Coastal Engineering*, 828–845.

Griggs, G.B., Tait, J.F., Scott, K., and Plant, N. (1991). "The interaction of seawalls and beaches: Four years of field monitoring, Monterey bay, California.", *Conference on coastal sediments, Coastal Sediments '91*, ASCE, 1871-1885.

Günaydin, K., and Kabdaşlı, M. S. (2004). "Performance of solid and perforated U-type breakwaters under regular and irregular waves." *Ocean Engineering*, 31, 1377–1405.

Hagiwara, K. (1984). "Analysis of upright structure for wave dissipation using integral equation." *Proc. 19th coastal engineering conference, Houston, Texas*, ASCE, New York, N.Y., 2810- 2826.

Hayashi, T., Hattori, M. Kano, T. and Shirai, M. (1966). "Hydraulic research on the closely spaced pile breakwater." *Proc. 10th coastal engineering conference, Tokyo, Japan*, ASCE, New York, N.Y, 873-884.

Hayashi, T., Hattori, M., and Shirai, M. (1968). "Closely spaced pile breakwater as a protection structure against beach erosion." *Coastal Engineering in Japan*, Japan Society of Civil Engineers, Tokyo, Japan, 11, 149-160.

Herbich, J.B. (1990). "Pile and offshore breakwaters." *Handbook of coastal and ocean engineering*, Edited by Herbich J.B., Gulf Publishing Company, 895-904.

Herbich, J.B., and Douglas, B. (1988). "Wave transmission through a double row of pile breakwater." *Proc. 21st Coastal Engineering Conference*, Torremolinos, Spain, ASCE, New York, N. Y., 2229-2241.

Hildebrandt, A., and Sriram, V. (2014). "Pressure distribution and vortex shedding around a cylinder due to a steep wave at the onset of breaking from physical and numerical modeling." *Proceedings of the International Offshore and Polar Engineering Conference*, (January), 405–410.

Huang, Z. (2007). "Wave interaction with one or two rows of closely spaced rectangular cylinders." *Ocean Engineering*, 34(11–12), 1584–1591.

Huang, Z., Li, Y., and Liu, Y. (2011). "Hydraulic performance and wave loadings of perforated/slotted coastal structures: A review." *Ocean Engineering*, 38(10), 1031–1053.

Hughes, S. A. (1993). Physical models and laboratory techniques in coastal engineering. *Advanced Series in Ocean Engineering*, World Scientific, Singapore.

Hutchinson, P.S. and Raudkivi, A.J. (1984). "Case history of a spaced pile breakwater at Halfmoon bay marina, Auckland, New-Zealand." *Proc. 19th Coastal Engineering Conference*, Houston, Texas, ASCE, New York, N.Y., 2530-2535.

Isaacson, M. (1991). "Measurement of regular wave reflection." *Journal of Waterway, Port, Coastal, and Ocean Engineering*, 117(6), 553–569.

Isaacson, M., Premasiro, S., and Yang, G. (1998). "Wave interaction with vertical slotted barrier." *Journal of Waterway, Port, Coastal, and Ocean Engineering*, 124, 118–126.

Jeya, T.J., Sriram, V. and Sundar, V. (2021). "Hydrodynamic characteristics of vertical and quadrant face pile supported breakwater under oblique waves."

Proceedings of the Institution of Mechanical Engineers, Part M: Journal of Engineering for the Maritime Environment, 236(1), 62-73..

Jiang, G. S., and Shu, C. W. (1996). "Efficient implementation of weighted ENO schemes." *Journal of Computational Physics*, 126(1), 202–228.

John, E.J. (1988). "Coastal erosion and protection along the west coast of India." Technical Report, Dept. of Applied Mechanics and Hydraulics, KREC., Surathkal, submitted to the Ministry of Surface Transport, Govt. of India.

Kakuno, S. and Liu, P.L.F. (1993). "Scattering of water waves by vertical cylinders." *Journal of Waterway, Port, Coastal, and Ocean Engineering*, 119(3), 302 - 322.

Kamath A. (2012). "Wave forces on structures using REEF3D". Master thesis, Norwegian University of Science and Technology, Trondheim, Norway.

Kamath, A., Bihs, H., Alagan Chella, M., and Arntsen, Ø. A. (2016). "Upstream-Cylinder and Downstream-Cylinder Influence on the Hydrodynamics of a Four-Cylinder Group." *Journal of Waterway, Port, Coastal, and Ocean Engineering*, 142(4), 4016002–4016012.

Kamath, A., Bihs, H., Chella, M. A., and Arntsen, Ø. A. (2015). "CFD simulations to determine wave forces on a row of cylinders." *Procedia Eng.*, 116(1), 623–630.

Kamath, A., Chella, M. A., Bihs, H., and Arntsen, Ø. A. (2015a). "Evaluating wave forces on groups of three and nine cylinders using a 3D numerical wave tank." *Engineering Applications of Computational Fluid Mechanics*, 9(1), 343–354.

Kamphuis, J. W. (1991). "Physical Modelling." *Handbook of Coastal and Ocean Engineering*. (E. J. B. Herbich, ed.), Gulf Publishing Company, Houston, Texas.

Kankara, R. S., Ramana Murthy M. V., and Rajeevan M. (2018). "National assessment of shoreline changes along Indian coast - A status report for 1990–2016." *National Centre for Coastal Research*, Chennai, India.

Karnataka Engineering Research Station, (1989). "Booklet on Sea Erosion studies conducted at Ullal Sea Erosion Site, Mangalore Taluk, D. K. District," KERS, Krishnarajasagara, Govt. of Karnataka.

Kim, B. H. (1998). "Interactions of waves, seabed and structures." PhD thesis, Seoul National University, Seoul, South Korea.

Komen, G. j., Cavaleri, L., Donelan, M., Hasselmann, K., Hasselmann, S., and Janssen, P. a. e. m. (1994). Dynamics and modelling of ocean waves.

Kondo, H. and Toma, S. (1972). "Reflection and transmission for a porous structure." *Proc. 13th Coastal Engineering Conference*, Vancouver, B.C., Canada. ASCE, New York, N.Y., 1847-1866.

Koraim, A. S., Iskander, M. M. and Elsayed, W. R. (2014). "Hydrodynamic performance of double rows of piles suspending horizontal C shaped bars." *Coastal Engineering*, 84, 81-96.

Koraim, A.S. (2014). "Hydraulic characteristics of pile supported L-shaped bars used as a screen breakwater." *Ocean Engineering*, 83, 36–51.

KREC Study Team (1994). "Study on Coastal Erosion (Dakshina Kannada District), Input to Environmental Master Plan Study, Danida-DEE-Mangalore." KREC, Surathkal.

Kriebel, D. L. (1992). "Vertical wave barriers: wave transmission and wave forces." *Proc. 23rd Int. Conf. on Coastal Engineering*, 1313–1326.

Krishnakumar, C., Sundar, V., and Sannasiraj, S. A. (2010). "Hydrodynamic performance of single- and double-wave screens." *Journal of Waterway, Port, Coastal, and Ocean Engineering*, ASCE, 136, 59–65

Laju, K., Sundar, V., and Sundaravadivelu, R. (2005). "Studies on pile supported skirt breakwater." *Proc. 1st Int. Conf. on Coastal Zone Management and Engineering Middle East*, Dubai, United Arab Emirates, 1-12.

- Laju, K., Sundar, V., and Sundaravadivelu, R. (2011). "Hydrodynamic characteristics of pile supported skirt breakwater models." *Applied Ocean Research*, 33(1), 12-22.
- Langhaar, H. L. (1951). *Dimensional Analysis and Theory of Models*, John Wiley & Sons, New York.
- Liu, H., Ghidaoui, M. S., Huang, Z., Yuan, Z., and Wang, J. (2011). "Numerical investigation of the interactions between solitary waves and pile breakwaters using BGK-based methods." *Computers & Mathematics with Applications*, 61(12), 3668–3677.
- Mani, J. S. (2009). "Experimental and numerical investigations on zigzag porous screen breakwater." *Natural Hazards*, 49(2), 401–409.
- Mani, J. S., and Jayakumar, S. (1995). "Wave transmission by suspended pipe breakwater." *Journal of Waterway, Port, Coastal, and Ocean Engineering*, ASCE, 121 (6), 335-338.
- Martin, T., and Bihs, H. (2021). "A non-linear implicit approach for modelling the dynamics of porous tensile structures interacting with fluids." *Journal of Fluids and Structures*, 100(1), 1–31.
- Martin, T., Kamath, A., and Bihs, H. (2020). "A Lagrangian approach for the coupled simulation of fixed net structures in a Eulerian fluid model." *Journal of Fluids and Structures*, 94, 102962.
- Mei, C. C. (1989). *The Applied Dynamics of Ocean Surface Waves*. World Scientific, Singapore.
- Miquel, A., Kamath, A., Alagan Chella, M., Archetti, R., and Bihs, H. (2018). "Analysis of different methods for wave generation and absorption in a CFD-based numerical wave tank." *Journal of Marine Science and Engineering*, 6(2), 1–20.
- Misra, S.C. (2001). "Uncertainty analysis in hydrodynamic tests." *Proc. Int. Conf. Ocean Engineering*, 1, 207–214.

Mojtahedi, A., Beiragh, M. S., Farajpour, I., and Mohammadian, M. (2020). “Investigation on hydrodynamic performance of an environmentally friendly pile breakwater.” *Ocean Engineering*, 217, 107942.

Nadeem Ahmada, Hans Bihsa, Dag Myrhaugb, Arun Kamatha and Øivind A. Arntsen (2019). “Numerical modeling of breaking wave induced seawall scour.” *Coastal Engineering*, 150, 108–120.

Nagai, S. (1966). “Researches on Steel-Pipe Breakwaters.” *Coastal Engineering 1966*, New York, American Society of Civil Engineers, Chapter 49, 850–872.

Nam, P. T., Larson, M., Hanson, H., and Oumeraci, H. (2017). “Model of nearshore random wave transformation: Validation against laboratory and field data.” *Ocean Engineering*, 135, 183–193.

Neelamani, S., and Rajendran, R. (2002). “Wave interaction with T-type breakwaters.” *Ocean Engineering*, 29(2), 151–175.

Neelamani, S., and Vedagiri, M. (2002). “Wave interaction with partially immersed twin vertical barriers.” *Ocean Engineering*, 29(2), 215–238.

Osher, S., and Sethian, J. A. (1988). “Fronts propagating with curvature-dependent speed: Algorithms based on Hamilton-Jacobi formulations.” *Journal of Computational Physics*, 79, 12–49.

Park, W. S., Kim, B. H., Suh, K. D., and Lee, K. S. (2000). “Scattering of irregular waves by vertical cylinders.” *Coastal Engineering*, 42(2), 253–271.

Peng, D., Merriman, B., Osher, S., Zhao, H., and Kang, M. (1999). “A PDE-based fast local level set method.” *Journal of Computational Physics*, 155, 410–438.

Rageh, O. S., and Koraim, A. S. (2010). “Hydraulic performance of vertical walls with horizontal slots used as breakwater.” *Coastal Engineering*, 57(8), 745–756.

Ramnarayan, S. K., Sannasiraj, S. A., and Sundar, V. (2020). “Hydrodynamic characteristics of curved and vertical front face pile-supported breakwaters in regular waves.” *Ocean Engineering*, 216, 108105.

Rao Subba and N. B. S. Rao (2001). “Laboratory investigation on wave transmission through suspended perforated pipes.” *ISH Journal of Hydraulic Engineering*, 7(1), 23 – 32.

Rao Subba and N.B.S. Rao, (1999). “Laboratory investigation on wave reflection characteristics of suspended perforated pipe breakwater.” *ISH Journal of Hydraulic Engineering*, 5(1), 22 – 32.

Rao Subba and Pramod Ch., (2003). “Beach profile studies along KREC beach of Karnataka Coast.” *NITK Research Bulletin*, National Institute of Technology Karnataka, Surathkal, Dec, 12(2), 24 – 31.

Rao Subba, (2002). “Study of coastal erosion along Karnataka coast.” *ISH Journal of Hydraulic Engineering*, 8(2), 23- 33.

Rao Subba, Kiran G Shirlal, Praveen Suvarna, B.R. Subramanian and R.S. Kankara (2007). “Modelling of coastal process around Gurupur–Netravathi river mouth using Mike-21.” *4th Indian National Conference on Harbour and Ocean Engineering (INCHOE-07)*, NITK., Surathkal, 1, 392-401.

Rao Subba, Kiran G. Shirlal and Habeeb Khan P., (2002a). “Sediment trend matrix analysis of beach sand along Dakshina Kannada coast.” *KREC Research Bulletin*, Karnataka Regional Engineering College, Surathkal, 11(1), 17 - 23.

Rao Subba, Kiran G. Shirlal and N. B. S. Rao, (2003). “Sediment Trend Matrix Analysis Normal to Shore near Surathkal Beach, Karnataka.” *Journal of Geological Society of India*, Bangalore, 61, 215 – 219.

Rao Subba, Kiran G. Shirlal, Radheshyam B. and Mahaganisha K., (2004). “Study of littoral transport along D.K. Coast, Karnataka.” *3rd Indian National Conference on*

Harbour and Ocean Engineering (INCHOE-04), National Institute of Oceanography (NIO), GOA, 1, 89 - 95.

Rao Subba, Kiran G. Shirlal, Subramanian, B. R., Radheshyam B, Govindaraja K. R. and Praveen Suvarna, (2006). "On modelling the sediment dynamics using MIKE-21 ST off Gurupur-Netravathi river mouth." *Proc. National Conference on Hydraulics and Water Resources (HYDRO-06)*, ISH and Bharati Vidyapeeth University, Pune, 467 - 474.

Rao Subba, Kiran. G. Shirlal and Habeeb Khan P, (2001). "An interpretation of sediment trends along D.K. Coast." *ISH Journal of Hydraulic Engineering*, The Indian Society for Hydraulics, CWPRS, Pune., 7(1), 33 - 39.

Rao Subba, N. B. S. Rao, and Sathyanarayana, V.S. (1999). "Laboratory investigation on wave transmission through two rows of perforated hollow piles." *Ocean Engineering*, 26(7), 675–699.

Rao Subba, Kiran. G. Shirlal, and Rao, N. B. S. (2002b). "Wave transmission and reflection for two rows of perforated hollow piles." *Indian Journal of Marine Sciences*, 31(4), 283–289.

Rao, Subba (1999). "Studies on the performance of perforated pile breakwaters." PhD thesis, Submitted to Mangalore University, Mangalore, Karnataka, India.

Rattanapitikon, W. (2007). "Calibration and modification of energy dissipation models for irregular wave breaking." *Ocean Engineering*, 34(11–12), 1592–1601.

Reedijk, B., and Muttray, M. (2009). "Pile row breakwaters at Langkawi, Malaysia, 10 years of beach development." *Coastal Structures 2007*, World Scientific Publishing Company, Singapore, 562–573.

Salmon, J. E., Holthuijsen, L. H., Zijlema, M., Vledder, G. P. van, and Pietrzak, J. D. (2015). "Scaling depth-induced wave-breaking in two-dimensional spectral wave models." *Ocean Modelling*, 87, 30–47.

Sasikumar, A., Kamath, A., and Bihs, H. (2020). “Modeling porous coastal structures using a level set method based VRANS-solver on staggered grids.” *Coastal Engineering Journal*, 62(2), 198–216.

Shetty, A., Jayappa, K. S., and Mitra, D. (2015). “Shoreline change analysis of Mangalore coast and morphometric analysis of Netravathi-Gurupur and Mulky-Pavanje spits.” *International conference on water resources, coastal and ocean engineering (ICWRCOE 2015)*, Aquatic Procedia, 4, 182–189.

Shu, C. W., and Osher, S. (1988). “Efficient Implementation of Essentially Non-oscillatory Shock-Capturing Schemes.” *Journal of Computational Physics*, 77, 439–471.

Subrahmanya K. R., and Rao B. R. J., (1991). “Marine geological aspects of Dakshina Kannada coast.” *Perspective on Dakshina Kannada and Kodagu*, Mangalore University Decennial Volume, Mangalore, 201-220.

Suh, K. D. D., Shin, S. and Cox, D. T. (2006). “Hydrodynamic characteristics of pile-supported vertical wall breakwaters.” *Journal of Waterway, Port, Coastal, and Ocean Engineering*, 132(2), 83-96.

Suh, K. D., Son, S. Y. Lee, J. I., and Lee, T. H. (2002). “Calculation of irregular wave reflection from perforated-wall caisson breakwaters using a regular wave model.” *28th International Conference on Coastal Engineering*, Cardiff, Wales, 1709–1721.

Suh, K., Ji, C. and Kim, B. H. (2011). “Closed-form solutions for wave reflection and transmission by vertical slotted barrier,” *Coastal Engineering*, 58(12), 1089-1096.

Suh, K., Jung, H. Y. and Chong, K. P. (2007). “Wave reflection and transmission by curtainwall – pile breakwaters using circular piles.” *Ocean Engineering*, 34, 2100–2106.

Sundar, V. and Subbarao, B. V. V. (2002). “Hydrodynamic performance characteristics of quadrant front-face pile-supported breakwater.” *Journal of Waterway, Port, Coastal and Ocean Engineering*, 129(1), 22–33.

Terrett, F. L., Osorio, J. D. C., and Lean, G. H. (1968). "Model studies of a perforated breakwater." *Coastal Engineering Proceedings*, (11), 1104-1120.

Truitt, C. L. and Herbich, J. B. (1987). "Transmission of random waves through pile breakwaters." *Proc. 20th Coastal Engineering Conference*, Taipei, Taiwan, ASCE, New York, N. Y., 2303-2313.

U.S. Army Corporation of Engineers. (1984). "Shore Protection Manual (SPM)." *Coastal Engineering Research Centre*, U.S. Government Printing Office, Washington, D.C.

USBR (1980). "Hydraulic laboratory techniques." *US Department of the Interior, Water and Power Resources Service*, Denver, Colorado.

Van der Vorst, H. A. (1992). "Bi-gstab: A fast and smoothly converging variant of Bi-CG for the solution of nonsymmetric linear systems." *SIAM Journal on scientific and Statistical Computing*, 13(2), 631-644.

Van Weele, J. and Herbich, J. B. (1972). "Wave reflection and transmission for pile arrays." *Proc. 13th Coastal Engineering Conference*, Vancouver, B.C., Canada. ASCE, New York, N.Y., 1935-1953.

Wang, G., Ren, B. and Wang, Y. (2016). "Experimental study on hydrodynamic performance of arc plate breakwater." *Ocean Engineering*, 111, 593–601.

Wang, W., Kamath, A., Martin, T., Pákozdi, C. and Bihs, H. (2020). "A comparison of different wave modelling techniques in an open-source hydrodynamic framework." *Journal of Marine Science and Engineering*, 8 (7), 526-553.

Whillock, A.F. and Price, W.A. (1976). "Armour blocks as slope protection." *15th International Conference on Coastal Engineering*, Honolulu, Hawaii, United States, 2564–2571.

Wilcox, D. C. (1994). *Turbulence Modelling for CFD*. DCW Ind. Inc, La Canada, California. 2, 103-217

Wroniszewski, P. A., Verschaeve, J. C. G. and Pedersen, G. K. (2014). "Benchmarking of Navier-Stokes codes for free surface simulations by means of a solitary wave." *Coastal Engineering*, 91, 1-17.

Xuan, T. Le, Tran Ba, H., Manh, H. Le, Van, D. Do, Minh Nguyen, N., Wright, D. P., Bui, V. H., Mai, S. T. and Tran Anh, D. (2020). "Hydraulic performance and wave transmission through pile-rock breakwaters." *Ocean Engineering*, 218, 108229.

Yagci, O., Kirca, V. S. O., Kabdasli, M. S., Celik, A. O., Unal, N. E., and Aydingakko, A. (2006). "An experimental model application of wave screen: Dynamic pressure, water particle velocity, and wave measurements." *Ocean Engineering*, 33(10), 1299-1321.

Zhu, D.T. (2011). "Hydrodynamic characteristics of a single row pile breakwater." *Coastal Engineering*, 58(5), 446–451.

Zhu, D.T. (2013). "Full wave solution for hydrodynamic behaviours of pile breakwater." *China Ocean Engineering*, 27(3), 323–334.

PUBLICATIONS

JOURNAL PAPERS

Praveen S. Suvarna, Arunakumar Hunasanahally Sathyanarayana, Pruthviraj Umesh, Kiran G. Shirlal. (2021). “Hydraulic performance of perforated enlarged pile head breakwaters through laboratory investigation” *Ocean Engineering.*, 241 (2021), 110089. DOI <https://doi.org/10.1016/j.oceaneng.2021.110089>

Praveen S. Suvarna, Arunakumar Hunasanahally Sathyanarayana, Pruthviraj Umesh, Kiran G. Shirlal. (2020). “Laboratory investigation on hydraulic performance of enlarged pile head breakwater.” *Ocean Engineering.*, 217 (2020), 107989. DOI <https://doi.org/10.1016/j.oceaneng.2020.107989>

CONFERENCE PAPERS

Praveen S. Suvarna, Arunakumar H S, Shery Mathew, Pruthviraj U and Kiran G. Shirlal (2018). “Numerical investigation of hydrodynamic performance on pile breakwater.” *6th Natl. Conf. Coastal, Harbour, Ocean Engineering INCHOE 26th to 28th Sept. 2018*, 1017–1027.

RESUME

NAME : **PRAVEEN SUVARNA S**
Date of Birth : 14-10-1983
Mobile : 09886108169
Email : civilsuvarna@gmail.com
Permanent Address : Devi Prasad House
Cross Padavu, Permude Village
MRPL Road, Bajpe
Mangalore, Karnataka- 574509
Qualifications : B.Tech (Civil Engineering),
M.Tech (Marine Structure)
Publications : International journals - 3
International conferences - 3

